2009

TISSUE ENGINEERING CELLULARIZED SILK-BASED LIGAMENT ANALOGUES

Scott Sell
Virginia Commonwealth University

TISSUE ENGINEERING CELLULARIZED SILK-BASED LIGAMENT ANALOGUES

A Dissertation submitted in partial fulfillment of the requirements for the degree of Doctor of Philosophy in Biomedical Engineering at Virginia Commonwealth University.

by

SCOTT ALLEN SELL
B.S. Virginia Commonwealth University, 2003
M.S. Virginia Commonwealth University, 2006

Director: Gary L. Bowlin, Ph.D.
Professor, Department of Biomedical Engineering

Virginia Commonwealth University
Richmond, Virginia
August 2009

Acknowledgement

Writing the acknowledgement section for my Master's thesis six years ago, I commented on how long the journey had been. Well, I can scarcely remember that journey anymore thanks to the odyssey that has been my Ph.D. Throughout it all I have had the support and backing of a large group of people; a group that I owe a large part of my success in life to. First, I would like to take this opportunity to thank the members of my committee: Gary Bowlin, David Simpson, Hu Yang, Tom Haas, and Matt Beckman. You provided wisdom and guidance throughout the duration of my stay at VCU.

Gary, looking back, I realize that I have known you for more than a third of my life. In that time, not only were you my mentor, you were my friend and confidant. Heck, I'll just say it man… you're my idol. Be forewarned, even as I prepare to move on and eventually make my own way, you will still be the first person I call when I need someone to bail me out! Hopefully, there will be many more revolving doors for us to share in the future.

Dave, I have trouble describing in print the experiences that I have had talking to you or visiting with you in your lab. Words simply can't do that insanity justice. The world just needs to know that you have always been uplifting, informative, and full of good ideas, while your disregard for any and all OSHA and OEHS regulations only adds to your mystique. I fear that if I mention details you might get shut down.

To my labmates past and present, you guys were great. I'm not going to list names (I've been here for 10 years, that'd be a long list!) but you know who you are. I couldn't have made it through without you guys. You were the people whom I bombarded with stupid questions, and reciprocated by providing mostly wrong answers. Hopefully I didn't screw anybody's research up too badly. In any case, it was fun. I will always remember the good times we had moving labs (multiple times!), blowing stuff up (the near death experience in particular), and absorbing as much "science" as possible at conferences. Mmmmm science.

Finally I have to thank my family, and especially my wife. I could probably write another 300 pages on how you carried, drug, and pushed me through this ordeal. When people say that I am "internally motivated" what they are really saying is that I am "Tracy motivated." You have been nose to the grindstone for the past six years so that I could focus on my (ever)continuing education. The time has come for all YOUR hard work to pay off, and when it does… I'm taking you on vacation!

Table of Contents

List of Tables

Page

List of Figures

Page

List of Abbreviations

AAMI	Association for the Advancement of Medical Instrumentation
ACL	Anterior cruciate ligament
AM	Anteromedial bundle
ANOVA	Analysis of variance
ANSI	American National Standards Institute
BMP	Bone morphogenetic protein
BSM	Bladder smooth muscle cells
CA	Carbonated apatites
CHD	Coronary heart disease
CVD	Cardiovascular disease
DI	De-ionized water
DMEM	Dulbecco's modified eagle medium
DMF	Dimethylformamide
EBP	Elastin binding protein
ECM	Extracellular matrix
EC	Endothelial cells
EDC	1-ethyl-3-(3-dimethylaminopropyl)carbodiimide hydrochloride
e-PTFE	Expanded polytetrafluoroethylene
FB	Fibroblasts
FBS	Fetal bovine serum
FFT	Fast Fourier transform
FGF	Fibroblast growth factor
fHA	Fluoridated apatite
FTIR	Fourier transform infrared spectroscopy
GFP	Green fluorescent protein
GLUT	Glutaraldehyde
H&E	Hematoxylin and eosin staining
HA	Hydroxyapatite
hAEC	Human aortic endothelial cells
hCA	Human coronary artery
hEPM	Human embryonic palatal mesenchymal cells
HFP	1,1,1,3,3,3 hexafluoro-2-propanol
hLF	Human ligament fibroblasts
HMDI	1,6-diisocyanatohexane
hSV	Human saphenous vein
hTERT	Human telomerase reverse transcriptase
hUVEC	Human umbilical vascular endothelial cells
IGF-1	Insulin-like growth factor-1
IGFBP-3	Insulin-like growth factor binding protein-3
IL	Interleukin
ITEMS	Intelligent Tissue Engineering via Mechanical Stimulation
LCL	Lateral collateral ligament

MAP	Mean arterial pressure
MCL	Medial collateral ligament
MEM	Minimal essential medium
MSC	Mesenchymal stem cells
NGF	Nerve growth factor
NHS	N-hydroxysuccinimide
NRK	Normal rat kidney cells
OA	Osteoarthritis
PBS	Phosphate buffered saline
PCL	Polycaprolactone
PCL	Posterior cruciate ligament
PDO	Polydioxanone
PDS	Polydioxanone suture
PEG	Poly(ethylene glycol)
PEO	Poly(ethylene oxide)
PEUU	Polyester urethane urea
PET	Polyethylene terephthalate
PGA	Poly(glycolic acid)
PLA	Poly(lactic acid)
PLGA	Poly(lactide-co-glycolide)
PM	Posterolateral bundle
PPO	Poly(propylene oxide)
PU	Polyurethane
RPM	Revolutions per minute
RWVB	Rotary wall vessel bioreactor
SEM	Scanning electron microscopy
SF	Silk fibroin
SIS	Subintestinal submucosa
SMC	Smooth muscle cells
SPCL	Silk fibroin blended with polycaprolactone
SPDO	Silk fibroin blended with polydioxanone
TFE	Trifluoroethanol
TGF-β	Transforming growth factor- β
THF	Tetrahydrofuran
TNBS	2,4,6-trinitrobensenesulfonic acid
VEGF	Vascular endothelial growth factor

Abstract

TISSUE ENGINEERING CELLULARIZED SILK-BASED LIGAMENT ANALOGUES

By Scott Allen Sell, M.S.

A Dissertation submitted in partial fulfillment of the requirements for the degree of Doctor of Philosophy in Biomedical Engineering at Virginia Commonwealth University.

Virginia Commonwealth University, 2009

Director: Gary L. Bowlin, Ph.D.
Professor, Department of Biomedical Engineering

The resurgence, and eventual rise to prominence in the field of tissue engineering, that electrospinning has experienced over the last decade speaks to the simplicity and adaptability of the process. Electrospinning has been used for the fabrication of tissue engineering scaffolds intended for use in nearly every part of the human body: blood vessel, cartilage, bone, skin, nerve, connective tissue, etc. Diverse as the aforementioned tissues are in both form and function, electrospinning has found a niche in the repair of each due to its capacity to consistently create non-woven structures of fibers ranging from nano-to-micron size in diameter. These structures have had success in tissue engineering applications because of their ability to mimic the body's natural structural framework, the extracellular matrix. In this study we examine a number of different

techniques for altering scaffold properties (i.e. mechanical strength, degradation rate, permeability, and bioactivity) to create electrospun structures tailored to unique tissue specific applications; the end goal being the creation of a cellularized tissue engineering ligament analogue. To alter the mechanical properties of electrospun structures while maintaining high levels of bioactivity, synthetic polymers such as polydioxanone were blended in solution with naturally occurring proteins like elastin and fibrinogen prior to electrospinning. Cross-linking of electrospun structures, using glutaraldehyde, carbodiimide hydrochloride, and genipin, was also investigated as a means to both improve the mechanical stability and slow the rate of degradation of the structures. Fiber orientation and scaffold anisotropy were controlled through varying fabrication parameters, and proved effective in altering the mechanical properties of the structures. Finally, major changes in the structure of electrospun scaffolds were achieved through the implementation of air-gap electrospinning. Scaffolds created through air-gap electrospinning exhibited higher porosity's than their traditionally fabricated counterparts, allowing for greater cell penetration into the scaffold. Overall, this collection of results provides insight into the diversity of electrospinning and reveals innumerous options, both pre and post fabrication, for the tissue engineer to create site-specific engineering scaffolds capable of mimicking both the form and function of native tissue.

CHAPTER 1 Tissue Engineering of the Extracellular Matrix

INTRODUCTION

Tissue engineering is an interdisciplinary field aimed at the application of the principles and methods of engineering and the life sciences toward the fundamental understanding of structure-function relationships in normal and pathological mammalian tissues and the development of biological substitutes to restore, maintain, or improve tissue functions [1-6]. Typically this involves collaborative efforts between materials scientists, cell and molecular biologists, immunologists, surgeons, and engineers to create replacement tissues that will be accepted by the body and promote native extracellular matrix (ECM) production. This requires the use of materials that do not activate catabolic pathways in the body, ultimately leading to fibrous encapsulation or destruction of the material [5-8].

Natural and synthetic ECM analogues have played a vital role in the field of tissue engineering since the early 1980s [1, 9, 10]. Improvements in the fabrication process as well as scaffold structure continue to occur in hopes of finding an ideal scaffold for each specific tissue engineering application. The overall function of the biodegradable scaffold is to create a 3D microenvironment that will provide the necessary support for transplanted or host cells to induce normal physiologic regeneration and function.

Ideally, the scaffold should mimic the native ECM it is going to replace. In order for this to happen, several design considerations should be taken into account including fabrication, structure, biocompatibility, and biodegradability [9]. Many different materials have been used to create scaffolds for different tissue engineering applications, each one offering different features and characteristics. More information will be given later in this chapter about these design considerations and the different materials used to fabricate various ECM analogues.

Fabrication techniques for scaffolds range from traditional engineering methods such as solvent casting and particulate leaching, to computer aided design technologies consisting of techniques such as 3-D printing and solid free form fabrication. Other processes include textile techniques such as electrospinning and weaving, and decellularization of tissues [11]. The process of electrospinning to create tissue engineered ECM analogues will be discussed extensively later in this text.

TISSUE ENGINERING

The use of isolated cells or cell substitutes is the most direct tissue engineering approach, typically using autologous or allogenic cells as therapeutic agents. This allows for the replacement of cells in areas of damaged tissue, ultimately using the cell's ability for replication to promote tissue repair and resumed function [4, 5]. These cells can be differentiated and tissue specific (i.e. injecting chondrocytes into cartilage [12]) or can be undifferentiated, generic stem cells that could be injected into areas of damaged tissue

and allowed to differentiate as needed [8, 13]. The upside of such an approach is the avoidance of surgery, as well as the ability to manipulate cells as needed *in vitro* prior to their implantation into the body. However, the major drawback of this approach is the time required to culture a usable number of cells. Without the presence of a large universal cell bank, cells must be taken from a donor and cultured to a usable number prior to implantation in their eventual recipient [4, 8].

Another approach to tissue engineering is the use of either pre-cellularized or acellular ECM analogues. The use of matrix analogues may be the most challenging, albeit potentially the most beneficial, approach to tissue engineering. The ultimate goal of this approach to tissue engineering is to enhance the body's ability to heal and repair itself by introducing a scaffold that the body recognizes and incorporates directly into the reparative process of the tissue. These systems are meant to mimic the native extracellular ECM and can serve as a structural framework for both cells and signaling molecules using the body as a bioreactor, exerting normal physiologic biomechanical and biochemical signals upon the scaffold. The idea being that the ECM analogue will induce cells to more accurately reproduce their normal physiological behavior, thereby improving tissue regeneration and repair [1, 14, 15]. A number of tissue-inducing signaling molecules have been incorporated into ECM analogue scaffolds to aid this process. These signaling molecules can include a wide number of cytokines and chemokines to promote cell growth, instruct differentiation, and promote cellular migration [5]. Since they are open to immunological attack, much research has been done on the material composition of these matrix analogue systems in order to produce

matrices that elicit little to no immune response and most closely mimic both the structure and function of native ECM.

Native ECM. Mammalian tissue is composed of two major components: cells (both parenchymal and mesenchymal) and ECM. A large majority of tissue volume is composed of the ECM component, which also provides much of a tissue's geometric shape. From a structural standpoint, the ECM is a complex arrangement of proteins and polysaccharides such as collagen, hyaluronic acid, proteoglycans, glycosaminoglycans, and elastin. These ECM components are constantly being synthesized, secreted, oriented, and modified by the cellular components that they support. Historically, the function of native ECM was only believed to be as a structural framework for tissues. However, it is now understood that the ECM, through interaction with receptors on the surfaces of cells, directly takes part in promoting cell adhesion, migration, growth, differentiation, and apoptosis. The ECM also plays a role in cytokine activity and intracellular signaling. Growth factors and signaling molecules can be stored within ECM to preserve against their degradation, or they can attach to the surface of the ECM to present themselves more efficiently to cell receptors [5, 7, 16].

Table 1.1. Some major ECM components, their function, and location. Adapted from [5].

Component	Function	Location
Collagen	Tissue architecture, tensile strength, cell-matrix interaction, matrix-matrix interaction	Widely distributed
Elastin	Tissue architecture, elasticity	Tissues requiring elasticity (lung, blood vessel, skin)
Proteoglycans	Cell-matrix interaction, matrix-matrix interaction, cell proliferation, cell migration	Widely distributed
Hyaluronan	Cell-matrix interaction, matrix-matrix interaction, cell proliferation, cell migration	Widely distributed
Laminin	Basement membrane component, cell migration	Basement membranes
Fibronectin	Tissue architecture, cell-matrix interaction, matrix-matrix interaction, cell proliferation, cell migration	Widely distributed
Fibrinogen	Cell proliferation, cell migration, hemostasis	Blood, wound healing

Interactions between cells and the ECM are complex and dynamic, and play critical roles during development, wound healing, and environmental maintenance (figure 1.1). During development, cell-ECM interaction is responsible for pattern formation, morphogenesis, and phenotype acquisition and maintenance. During wound healing clot formation, inflammation, formation of granulation tissue, and remodeling are all mediated by cell-ECM interaction. Initial attraction and adhesion of cells to the ECM is induced by multiple, low affinity charge and hydrophobic interactions. During the spreading phase of adhesion, heterodimeric transmembrane proteins known as integrins

on the cell surface bind to specific small peptide fragment sequences on the ECM molecules. This allows for cells to bind to the ECM, through focal adhesions, and promote direct communication between the two. Integrin binding is both specific and reversible and allows cells to differentiate, secrete and absorb matrix, and transmit signals [7]. Signals are sent from the ECM across the cell membrane to soluble molecules in the cytoplasm and through direct connections with the cytoskeleton and into the cell nucleus, evoking a cellular response, termed "outside-in" signaling. This direct contact allows for stronger, more specific signaling than through the release of diffusible signaling molecules. Cell-ECM interactions can also be of an "inside-out" nature, when changes within the cell feed back to alter the activity of surface receptors, ultimately creating changes in the integrin and non-integrin receptors in focal adhesions [7]. In what is known as dynamic reciprocity, the cellular response to the ECM signaling can often alter the state of the ECM. For example cells may release matrix metalloproteases to break down an overly dense ECM to allow for their migration or proliferation [5, 16].

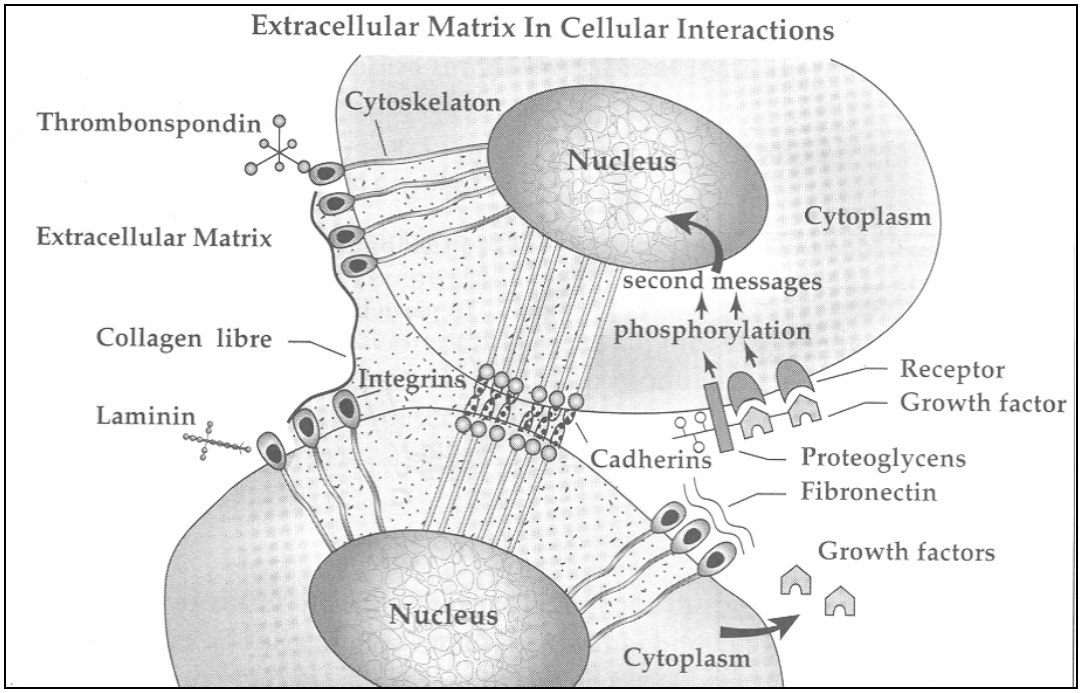

Figure 1.1. ECM-cell interaction depicting integrin receptors. Reprinted from [5].

ECM Analogue Scaffolds. As complex a structure as the native ECM has been revealed to be, it should be no surprise that the creation of a successful engineered ECM analogue has proven to be extremely challenging. Ideally, one would like to mimic both the fibrillar form and the complex function of the native ECM [11, 17, 18]. To attain a successful ECM analogue scaffold, there are several design and material criteria that must be met. First and foremost, the scaffolding material should be subjected to the same standards as any other biomaterial implanted in the body, namely, the scaffold should not initiate any adverse tissue or immune reactions. For many applications, scaffolding materials should be biodegradable or bioabsorbable at a rate that will allow for their gradual incorporation into the surrounding tissue without any fibrous encapsulation or

residual evidence of their presence [6, 10, 11, 17]. ECM analogue scaffolds have been fabricated from an extensive array of materials through a number of different fabrication techniques. A wide number of different polymers, both synthetic and natural in origin, have been used as ECM analogues. The most common matrix materials in use today are polymers such as poly(glycolic acid) (PGA), poly(lactic acid) (PLA), and their copolymer poly(lactide-co-glycolide) (PLGA). However there has also been extensive work done with polycaprolactone (PCL) and polydioxanone (PDO), as well as some polyanhydrides, polyorthoesters, polycarbonates, and polyfumarates [6, 17]. As for ECM analogues engineered from natural materials, collagens [19], elastin [20], fibrinogen [21], and silk [22] have been used. ECM substitutes of this variety have the potential for a greater upside than their synthetic counterparts due to the fact that they are constructed from native ECM materials and may be expected to retain some of their biologic behavior [6, 23]. Inorganic materials such as hydroxyapatite (HA), tricalciumphosphate, ceramics, and glass have also been used [6, 24]. Both the materials and their fabrication techniques will be discussed in detail later in this text.

The architecture of the scaffold is every bit as important as the material from which it is fabricated. As previously stated, an ECM analogue should mimic the form of the native ECM. To be ideal, this ECM analogue would need to mimic the topographical features and geometry on the macro-scale, micro-scale, and even nano-scale levels, as each influences cell response to the scaffold [25]. Native ECM is composed of nanoscale fibers that can provide structural integrity to tissues. Recent advances in fabrication techniques (self-assembly, phase separation, and electrospinning) have made the creation

of consistently nanofibrous scaffolds possible. The use of nanofibrous scaffolds creates structures with a very high surface area to volume ratio to support cell growth and infiltration [10, 18, 26]. In addition, the morphological similarities between the nanofibrous structures and the native ECM are believed to improve cellular response and overall biocompatibility [18].

Success as a tissue-engineering scaffold in many applications is ultimately dependant upon the ability for cells to infiltrate the ECM analogue, migrate throughout its thickness, proliferate, and restore normal physiologic function [27, 28]. The scaffold's porous structure, a combination of microporous (pore diameters < 2 nm), mesoporous (pores with diameter 2 nm – 50 nm), or macroporous (pore diameters > 50 nm) void spaces, plays a major role in cellular penetration [23, 29]. As yet there has been no concrete claim to an ideal pore diameter, but it has been documented that pores with a small diameter, yet larger than the diameter of a cell, are favorable [10]. Not only do the pores of an ECM analogue scaffold need to be of a sufficient size for tissue growth to occur, but they also need to be open and interconnected. Interconnectivity refers to the extent of which pores are connected with their neighboring pores, and has a large effect on nutrient and waste diffusion, cell migration, and overall scaffold permeability [6, 30, 31]. The terms porosity and permeability are often incorrectly used interchangeably in the realm of tissue engineering and in the consideration of ECM analogue scaffolds. By definition, porosity is the amount of void space contained within a structure, while permeability is a measure of the ease of which a fluid can move through the structure. Matrix permeability ultimately depends on the combination of scaffold porosity, pore size

and distribution, pore interconnectivity, and pore orientation and scaffold porosity to determine the hydraulic permeability of an ECM analogue scaffold [30, 31].

While not commonly reported for tissue engineered scaffolds, permeability and porosity are extremely important to ECM analogue success. Healthy, living tissue *in vivo* relies on the microvasculature to distribute blood and exchange metabolites through a combination of diffusion over short distances and flow-limited exchange. There are currently no tissue engineered products that contain their own pre-vascularised capillary bed to provide nutrients to the structure, chaining their initial effectiveness to the limits of passive diffusion [32]. The limitations of diffusion based nutrient transport restrict the maximum thickness of avascular tissue engineered constructs to less than 2 mm [33]. Scaffolds with increased porosity and permeability help to promote the diffusion of nutrients to cellular constituents, while promoting the diffusion of metabolic waste away from the cells. An increase in nutrient penetration distance will promote cell migration away from the scaffold periphery, and the presence of interconnected macropores will augment their ability to migrate [30, 31]. The degradation behavior of synthetic polymer based scaffolds is also controlled in part by the permeability of the ECM analogue. Low porosity and permeability scaffolds made of poly(α-hydroxy acids) have exhibited increased rates of degradation due to an increase in autocatalytic activity. Essentially, as the polymers breakdown via hydrolysis, the acidic byproducts become trapped within the scaffold and lower the local pH. This reduced pH then accelerates the degradation of the polymer from the inside out resulting in a rapid loss of mechanical stability [30, 34].

SYNTHETIC SCAFFOLDS

Synthetic scaffolds, as mentioned above, have been used as ECM analogues and offer many advantages over natural polymers, as well as limitations. For one, the material properties of synthetic polymers can be controlled to suit specific functions, and therefore, can be more beneficial as a scaffold for multiple tissue engineering applications. In addition, many synthetic polymers are bioresorbable and have a known degradation rate, mechanical strength, and are readily available, and therefore, degradation time should not vary significantly between hosts [11]. Synthetic scaffolds provide many positive characteristics for their use as scaffolding materials, and almost seem to be the answer for ideal tissue engineering scaffolds, but the key dilemma is they lack one of the major requirements of an ECM analog. Although the surface and structural characteristics of synthetic polymers can be controlled, they are synthetic, as their name implies, and therefore, are deficient in the biological component of the native ECM [1, 35]. Another disadvantage is that the degradation products of these polymers can be toxic products, mostly weak acids, which can cause an adverse reaction if they accumulate locally [10].

Biodegradable synthetic polymers have been the primary focus for tissue engineered scaffolds, with most belonging to the polyester family. Some of the most commonly used polymers will be more specifically outlined in the following paragraphs. A brief overview of the polymers' characteristics is displayed in table 1.2 [10, 11, 36, 37].

Table 1.2. Properties of degradable synthetic polymers used for tissue engineering scaffolds.

Polymer	Degradation method	Degradation time	Primary Degradation Products	Bulk Mechanical Stiffness: E-modulus (GPa)	Tissue Engineering Applications
PGA	Ester Hydrolysis	1 to ~12 months	Glycolic acid	5-7	Skin, cartilage, bone, ligament, tendon, vessels, nerve, bladder, liver
PLA	Ester Hydrolysis	5 to ~60 months	Lactic acid	2-3	
PLGA	Ester Hydrolysis	1 to ~12 months	Lactic acid and glycolic acid	2-7	
PDO	Ester Hydrolysis	3 weeks to 6 months	Hydroxy-ethoxyacetic acid	0.002-0.04	Orthopedics, drug delivery, bone, vessels
PCL	Ester hydrolysis	1 to 3 years	Caproic acid	0.4	Skin, cartilage, bone, ligament, tendon, vessels, nerve
PEG/PEO	Nondegradable	Not applicable	Not applicable	0.1-5	Drug delivery, cartilage

Poly(glycolic acid). PGA is a biodegradable, linear, aliphatic polyester that possesses a compact, repeating structural unit [10, 35, 38] (table 1.2, figure 1.2). It is currently used in a variety of medical applications, but was initially developed as a commercially available suture in the 1970s because of its superior biocompatibility and reproducible mechanical properties [1, 39]. PGA is formed from the ring opening

polymerization of glycolide and produces high molecular weight materials [40]. Some characteristics of PGA include a high crystallinity (46-55%), a high melting point (185-225ºC), a glass transition temperature of 35-40ºC, and a low solubility in organic solvents [10, 36, 38-40]. The glass transition temperature of PGA is very close to physiological temperature (35-40ºC), and thus, water infiltration and loss of mechanical strength may occur more easily after implantation. Mechanical properties of PGA sutures include a tensile strength of 106 Kpsi, an elongation of 24%, and a knot retention of 65 Kpsi [1, 35]. Due to its hydrophilic nature, PGA degrades into glycolic acid over a period of 2-4 weeks *in vivo.* The predictable bioabsorption of this polymer and the fact that its degradation product is metabolized in the body makes it an attractive option for many tissue engineering applications. More specifically, for applications where an initially tough, but fast degrading material is desired, this polymer is a superior choice, as 60% of its strength is lost by hydrolytic degradation during the first 2 weeks.

PGA scaffolds have previously been formed by traditional extrusion methods [41], electrospinning [42], and solvent casting or particulate leaching [36]. Extrusion methods produce fibers with a minimum diameter above 10µm which is a highly unfavorable size compared to native ECM analogs. Electrospinning methods have produced fibers of 200nm-1.5µm, depending upon polymer concentration. During an *in vitro* biocompatibility study, PGA scaffolds that were pretreated with hydrochloric acid demonstrated the ability to increase rates of proliferation of cardiac fibroblasts (FBs) compared to cells on tissue culture plastic. *In vivo* studies with the same scaffolds resulted in full incorporation of the scaffolds into the hind leg tissue of rats [38]. Freed et

al. demonstrated PGA nonwoven mesh scaffolds seeded with chondrocytes have the ability to aid in cellular attachment and proliferation and the regeneration of cartilaginous matrix [39].

Poly(lactic acid). Another biodegradable, aliphatic polyester commonly used in clinical applications is PLA [1] (table 1.2, figure 1.2). Formed from the polymerization of lactide, this polymer is present in two isoforms: d(-) for dexorotary, l(+) for levorotary, and the synthetic blend, dL for racimic [40]. P(l)LA and P(d)LA are semi-crystalline solids, and P(dL)LA is amorphous. The difference in the polymer's crystallinity has an effect on its clinical application. P(dL)LA is usually used in drug delivery applications because of its low tensile strength, high elongation and rapid degradation time, while the semicrystalline PLA is preferred for load-bearing applications such as orthopedic fixations and sutures because of its higher tensile strength and modulus and lower elongation [35, 40]. Because of the extra methyl group in the monomer, PLA is more hydrophobic than PGA. The chemical structure of PLA contains an ester bond, which makes it less likely to undergo hydrolysis. Because of this, it degrades much slower than PGA (typically 30-50 weeks) and has a higher solubility in organic solvents. Since the degradation of PLA yields L-lactic acid, for most tissue engineering applications, P(l)LA is chosen over P(d)LA because lactic acid is naturally present and metabolized in the body [1, 10, 35, 36]. Other characteristics of PLA include 37% crystallinity, a melting point of 96-185ºC, and a glass transition temperature of 57-65ºC [35, 40]. It is important to mention that caution should be taken when sterilizing this polymer via gamma-

radiation because this may cause chain separation, cross-linking, and a decrease in crystallinity.

PLA scaffolds have been processed using traditional fiber extrusion methods, similar to PGA, and have resulted in fiber diameters on the micro-scale. Electrospun PLA scaffolds produce fibers with diameters ranging from 100nm-10μm, depending upon solvent and concentration. *In vitro* experiments done by Yang, et al. demonstrate neural stem cell elongation and outgrowth is parallel to the direction of P(l)LA fibers and higher cell differentiation for P(l)LA nanofibers versus microfibers [43]. Human articular chondrocytes cultured on PLA scaffolds formed from a spin-casting method revealed cellular attachment was increased on P(dL)LA scaffolds versus P(l)LA scaffolds. In contrast, cellular proliferation was greater on P(l)LA scaffolds as compared to P(dL)LA scaffolds. This is most likely due to the differences in crystallinity of the two polymers, which could cause a difference in the amount of serum proteins that are absorbed [44].

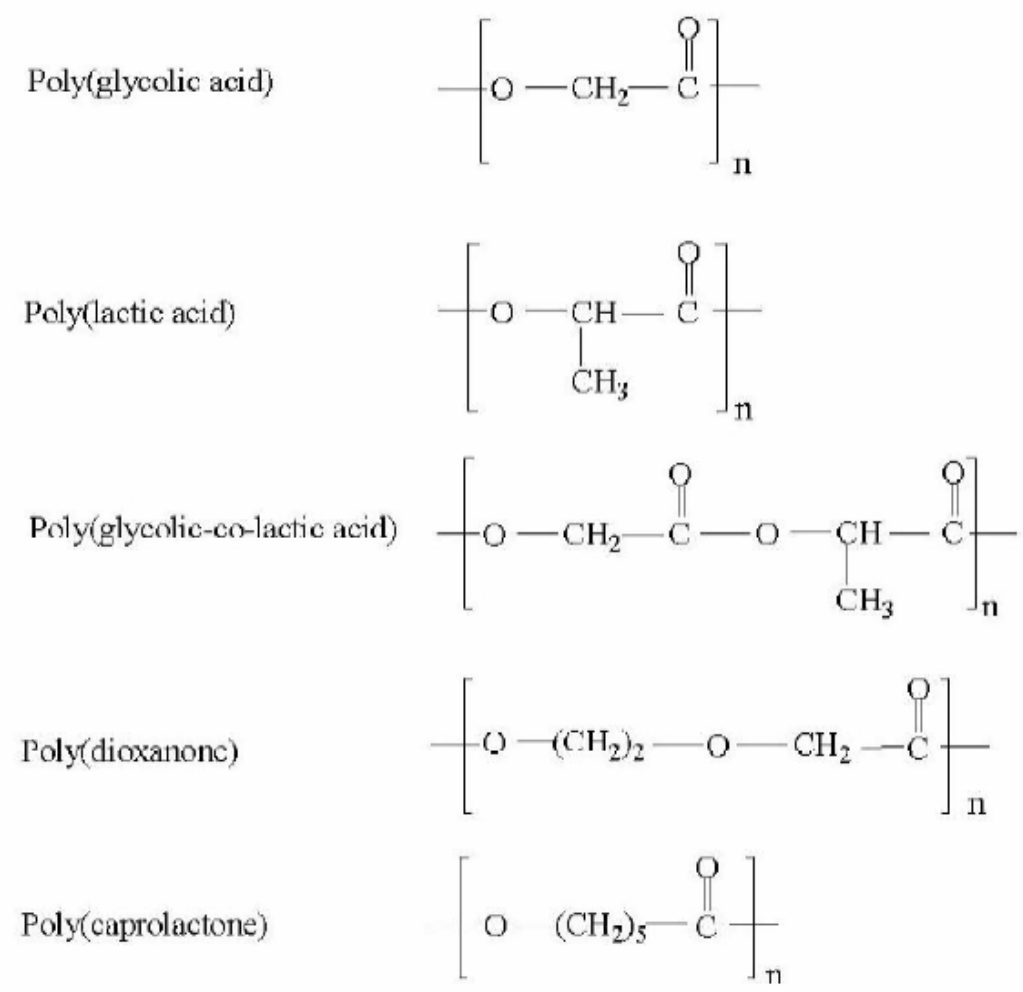

Figure 1.2. Chemical structures of commonly used biodegradable synthetic polymers. Reprinted from [36].

Poly(lactide-co-glycolide). PLGA (table 1.2, figure 1.2) is the copolymer formed by PGA and PLA. Unlike each individual homopolymer, this copolymer is amorphous when either monomer is present under 70mol% because of the disruption of the regularity of the polymer chain by the other monomer [40]. This characteristic results in a decrease in degradation rates and mechanical strength [10, 35, 45]. If either homopolymer is present above 70mol%, the copolymer exhibits some crystallinity. PLGA also exhibits

lower crystallinity and melting temperature compared to PGA or PLA. This copolymer degrades in bulk by ester hydrolysis (Table 1.1), and the rate of degradation can be altered by adjusting the ratio of PLA/PGA.

PLGA has been used for many medical and tissue engineering applications such as surgical sutures, cardiac tissue regeneration, and drug delivery because it is biodegradable and biocompatible [1, 45, 46]. Bone formation on PLGA foams fabricated by solvent casting/particulate leaching (to be discussed later) by mesenchymal stem cell (MSC) -derived osteoblasts has also been reported [47]. PLGA scaffolds have also been shown to support the cell growth and function of a variety of other cell types including FBs, chondrocytes, and smooth muscle cells [10, 46].

Polydioxanone. PDO is a biodegradable polyester formed from the ring opening polymerization of monomer paradioxanone [40, 48] (table 1.2, figure 1.2). Originally this polymer was developed for use as a suture because of its superior degradation rate of 6-12 months, falling in between PGA and PLA. PDO exhibits a high crystallinity of 55% and a glass transition temperature of -10-0ºC. Another attractive property is its excellent flexibility because of an ester oxygen group in the backbone structure [1, 40, 48]. In addition, PDO has shown no acute or toxic effects upon implantation. A negative aspect of the polymer when used as a suture is its shape memory. Because of the suture's ability to retain its spooled shape, knot retention becomes very difficult. Although this may prevent PDO from being an ideal suture material, shape memory may be a positive aspect for tissue engineering applications. For example, if used in a vascular graft, it can

provide rebound and kink resistance [1, 40, 48]. Also, the degradation rate of PDO sutures can be a negative aspect because it may be too rapid to allow for a durable closure for wounds and may cause abnormal healing.

Electrospinning of PDO has been performed and has resulted in fiber diameters of 180nm-1.4μm, depending upon solution concentration, and exhibits material properties within the same range as the major structural components of the native vascular ECM (collagen and elastin). As fiber diameter decreases, it has been shown that cell interaction improves and immune response is reduced [1, 48]. PDO scaffolds have also been used in other applications including orthopedics, plastic surgery, drug delivery, cardiovascular and bone repair [48].

Polycaprolactone. PCL is another linear aliphatic polyester that has demonstrated good biocompatibility, favorable mechanical properties and a slow degradation rate of 1-3 years [1, 36, 37] (table 1.2, figure 1.2). Prepared by the ring opening polymerization of the cyclic monomer ε-caprolactone, PCL is a repeating unit of one ester group and five methylene groups. This semi-crystalline polymer is highly soluble and exhibits a low melting point of 58-64ºC and a glass transition temperature of -60ºC [10, 36, 40]. Degradation of PCL occurs by bulk or surface hydrolysis of the ester linkages, producing a byproduct of caproic acid [10]. To increase its degradation rate, PCL has been easily copolymerized with a variety of polymers including collagen, PGA, PLA, and poly(ethylene oxide) (PEO) [1, 10, 36, 40].

Electrospun scaffolds of PCL that were seeded with MSC-derived osteoblasts promoted cellular penetration as well as ECM formation [47]. Other studies have shown PCL scaffolds support human osteoblast and dermal FB cell viability and the proliferation of human biliary epithelial cells [10]. PCL scaffolds have also been used for tissue engineering applications such as cartilage [49] and vascular [50].

Poly(ethylene glycol)/Poly(ethylene oxide). Poly(ethylene glycol) (PEG) is a linear-chained polymer consisting of an ethylene oxide repeating unit (Table 1.2). PEO has the same backbone as PEG, but a higher molecular weight because of its longer chain length [10]. PEG and PEO are both hydrophilic and are synthesized by anionic or cationic polymerization of ethylene oxide [10, 51]. They have the ability to act as swelling polymers, which has led to their use as a hydrogel, and makes them excellent polymers for medical applications such as drug delivery [52]. Another attractive property for their use in tissue engineering is their low toxicity and biocompatibility [51]. A limitation of PEG and PEO is their inability to naturally degrade, but if they are copolymerized with a hydrolytically or enzymatically degradable polymer, they can be made degradable [10, 51, 53]. PEO-based copolymers, such as the triblock copolymer with poly(propylene oxide) (PPO), PEO-PPO-PEO, could be designed to form gels at body temperature by forming a liquid crystalline phase, and have been mainly used in drug delivery applications where they have been known to enhance drug penetration [51]. Riley et al. cultured chondrocytes on PEG-based hydrogel scaffolds and found the

scaffolds supported the survival of the cells and the deposition of a cartilage-like matrix [54].

NATURAL SCAFFOLDS

To overcome the disadvantage that synthetic polymers have of lacking the biological component, natural polymers are widely used, either by themselves, or as a blend with synthetics. Derived from renewable resources such as plants, animals and microorganisms, natural polymers used in scaffolds offer an advantage because of their excellent biocompatibility and biodegradability [55]. They are biologically similar to the native ECM, which allows cells to interact with these polymers in a natural manner through receptors and signals, and also aids in the correct functioning of cells such as attachment, proliferation and differentiation. Disadvantages of natural polymers include variations in degradation rates, batch to batch inconsistency, and poor mechanical strength [1, 9, 10]. Another important disadvantage to consider is the ability of these polymers to induce a negative immune response due to the presence of impurities and endotoxins, depending on their source [55]. A detailed description of some of the most widely used natural polymers in tissue engineering is discussed below.

Collagen. Collagen is the most abundant protein found in the body. It functions to provide the overall structure and strength to tissues and is the principal component of the native ECM. In addition, the collagen structure provides cells with the appropriate

microenvironment for embryologic development, organogenesis, cell growth, and wound repair and also stores and releases important cell mediators such as growth factors [1, 55]. Currently, there are over 20 different kinds of collagen that have been identified, with the basic structure composed of three polypeptide chains, coiled around each other to form a triple helix (figure 1.3).

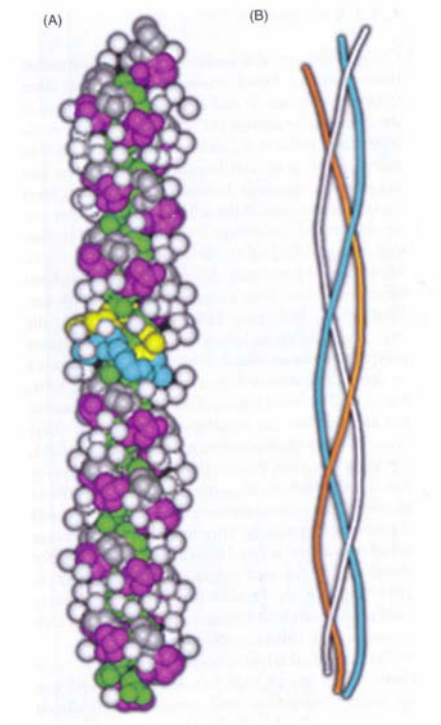

Figure 1.3. Picture depicts triple-helical collagen structure. (A) Model of collagen peptide where Gly is green, Pro is grey, and Hyp is shown in magenta. (B) The schematic of the triple helix. Reprinted from [55].

The most common triple helix of collagen is formed by the peptides Proline, Hydroxyproline, and Glycine in the sequence Pro-Hyp-Gly. The individual triple helices arrange to form collagen fibrils, which account for the structural integrity of the tissue.

Collagen fibril formation is an extracellular process, which occurs through the cleavage of terminal procollagen peptides by specific procollagen metalloproteinases. The different types of collagen are found in different areas of the body depending upon the role and makeup of the tissue. Type I collagen is the most common type, found in dermis, bone, tendon, fasciae, sclera, organ capsules, and fibrous cartilage, and is a major component of mature scar tissue. Type II collagen is mostly found in hyaline and elastic cartilage, the developing cornea, and in the vitreous body of the eye. The wall of blood vessels and hollow intestinal organs consist mostly of type III collagen, which also co-polymerizes with type I. Types V and XI are less abundant and mostly occur co-polymerized with type V and type XI [56]. One reason for collagen's wide use in tissue engineering applications is because it can be isolated from many different sources and is relatively non-immunogenic. The primary sources of collagen is animal tissues (porcine and calf skin, bovine tendon, rat tail) in which it is purified from the tissues using an enzymatic treatment and salt/acid extraction. Deriving this polymer from animals, although an easily accessible source, does pose some problems as its use as a scaffold because of the possibility of the transmission of infectious agents and of rejection from the host tissue. Fortunately, many new attempts have been made to derive collagen from safer sources, such as jellyfish [57], and to produce human recombinant collagen [58]. These alternatives provide a more reliable and predictable source of collagen that is free of animal components.

One feature that is necessary for all types of collagen for their use in tissue engineering applications is chemical cross-linking. Although this process can be a

disadvantage for this natural polymer's use in tissue engineering applications because of the addition of toxic solvents, this is necessary to stabilize the polymer in order to control the mechanical properties. Cross-linking can be achieved in various ways, including chemically (glutaraldehyde, 1-ethyl-3-(3-dimethylaminopropyl) carbodiimide hydrochloride (EDC), genipin), physically (freeze drying, UV radiation, heating), and enzymatically [55, 56].

Degradation of collagen is done naturally by matrix metalloproteinases, specifically collagenase and serine proteases [56], which also provides an advantage for its use in tissue engineering. It is used in various medical applications, such as wound dressings and artificial skin, and collagen scaffolds have also been used in a variety of tissue engineering applications, such as vascular grafts [59], tendon/ligament [60, 61], cartilage [62], and breast tissue [63].

Some drawbacks of collagen for tissue engineering applications include the polymer's low mechanical properties, the need for cross-linking (mentioned above), risk of viral infection, increased antigenicity potential and an extremely fast biodegradation rate [56].

Gelatin. Gelatin is obtained by a controlled hydrolysis of collagen and is a natural polymer that is of interest in tissue engineering because of its excellent biocompatibility and biodegradability, and cost efficiency. Generally speaking, there are two types of gelatin: Type A and Type B. Type A is extracted from collagens, and processed by an acidic pretreatment, and Type B is obtained by an alkaline pretreatment,

which causes it to have higher carboxylic acid content than Type A. For many years it has been used as a vascular prosthetic sealant, a dressing for wounds and a carrier for drug delivery, and recently it has gained interest for its use as a scaffold for tissue engineering applications [1, 64]. One drawback of gelatin is that it dissolves as colloidal sol at temperatures at or above 37ºC, and gels at lower temperatures around room temperature. However, when combined with other synthetic polymers, or cross-linked, this limitation can be reduced.

In a study done by Zhang et al., a mixture of gelatin and PCL solutions were electrospun to produce fibrous scaffolds. These scaffolds proved to have excellent biocompatibility with bone marrow stromal cells and also aided in the process of cellular migration, proliferation, and penetration [65]. Gelatin scaffolds have also been used for nerve [66], hepatic [67], and cartilage [68] tissue engineering applications.

Elastin. Elastin is the most linearly elastic biosolid known and is a key structural protein found in the native ECM of connective tissues where elasticity and recoil are critical parameters (figure 1.4). Elastin consists of several repetitive amino acid sequences, including VPGVG, APGVGV, VPGFGVGAG and VPGG [55]. Mature elastin is formed from tropoelastin, a 70-kDa protein consisting of alternating hydrophobic regions (responsible for the elasticity) and cross-linking domains. Additionally, it ends with a hydrophilic carboxy-terminal sequence containing its only two cysteine residues [69]. A highly insoluble protein, elastin constitutes walls of arteries and veins, ligaments, lung parenchyma, skin, and intestines.

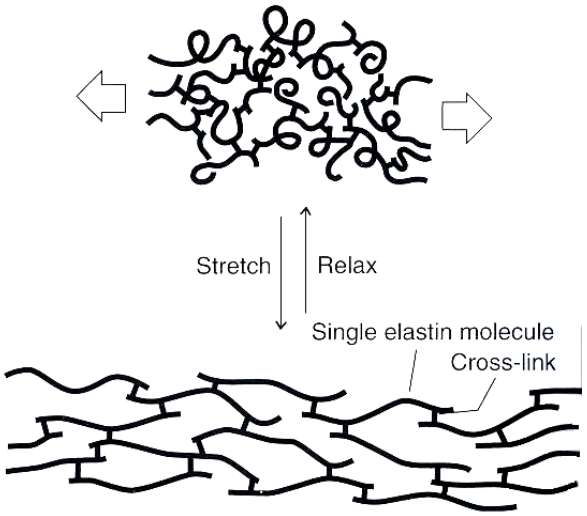

Figure 1.4. Elastin structure reprinted from [55].

There are some drawbacks of elastin that have limited its use as a biomaterial. Upon implantation, elastin preparations have a strong tendency to calcify. This may be due to microfibrillar components, such as calcium-binding fibrillin, within the elastic fiber that are difficult to remove, although there have been studies that disprove this theory. Another limitation of elastin is the complexity of its purification process [70]. Similar to collagen, pure elastin scaffolds need to be cross-linked to improve their mechanical integrity, which also presents a limitation [71].

Elastin scaffolds have mostly been fabricated by electrospinning [20], but others have used insoluble elastin in gels [72] and elastin-like polypeptide block copolymers [73]. In previous studies, electrospun elastin scaffolds have been shown to regulate proliferation, migration, and differentiation of smooth muscle cells (SMCs) as well as reduce the vascular proliferative response to arterial injury in vivo [59, 70]. Several other

studies have been performed using elastin scaffolds for cardiovascular tissue engineering purposes [74-76].

Fibrinogen. Fibrinogen is a naturally occurring plasma protein (340kDA) that plays an important role in blood clotting, fibrinolysis, cellular and matrix interactions, inflammation, wound healing, and neoplasia [77-79]. Fibrinogen molecules are elongated 45-nm structures consisting of two outer D domains, each connected by a coiled-coil segment to a central E domain (figure 1.5).

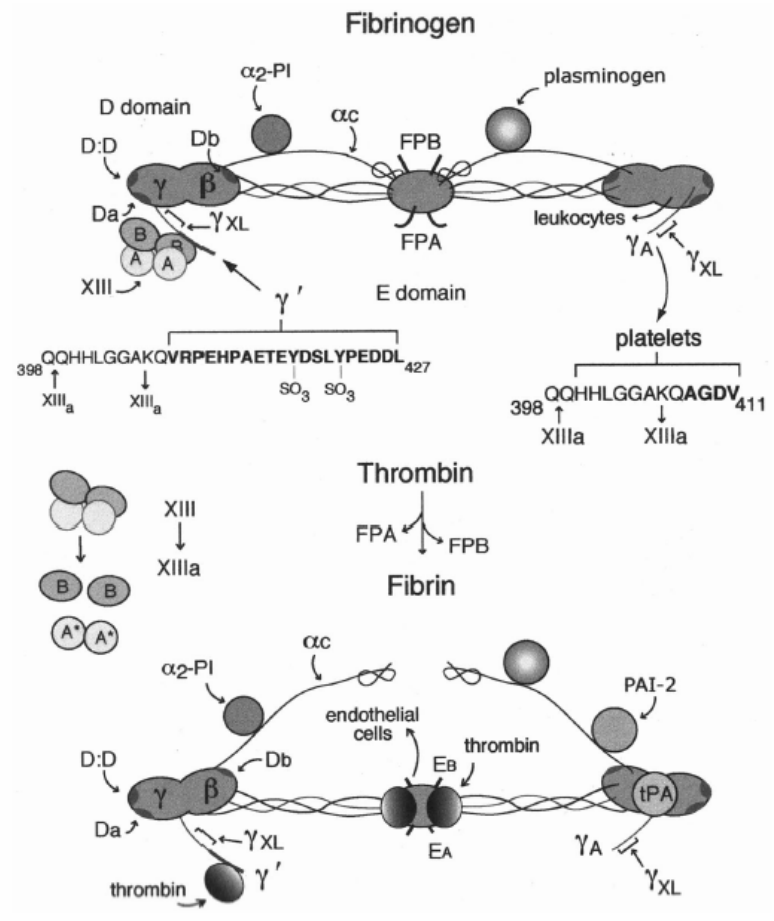

Figure 1.5. Schematic diagram representing the major structural features of fibrinogen and its cleavage to fibrin. Reprinted from [79].

These molecules consist of six polypeptide chains: two Aα, two Bβ, and two γ, and when fibrinogen reacts with thrombin, two peptides are cleaved to produce fibrin monomers. In the presence of calcium and factor XIII, fibrous clots and other fibrous structures are formed by the fibrin monomers. These structures play a role in the wound healing process, serving as a provisional matrix on which tissues rebuild and repair themselves. For this reason, fibrinogen is an attractive protein for its use in tissue engineering applications.

Another advantage of fibrinogen is that it has two integrin binding sites, RGDF and RGDS, in which many cellular interactions occur through binding to these sites. Cells that have receptors for these binding sites include platelets, endothelial cells (EC), melanoma cells, FBs, and monocytes, neutrophils [79].

Fibrin-based scaffolds have been developed previously in the form of fibrin gels and wet extrusion fibronectin-fibrinogen cables. Although these gels were easily degradable, non-immunogenic, and promoted cell migration, they lack the structural integrity needed for practical use in a tissue. The limitation of the wet extruded cables is their resulting large fiber size; 200-250μm in diameter is many orders of magnitude larger than the native fibers of the ECM, resulting in an unfavorable environment for cells to correctly function. Electrospun fibrinogen has also been accomplished and has shown excellent cellular interaction as well as mechanical properties similar to those of native tissue [77, 78].

Silk Fibroin. Silk is an extremely common fibrous protein that has been used as a medical grade suture for centuries. More recently silk has become a material of interest in the creation of tissue engineering scaffolds due to its unique blend of material characteristics. Silk exhibits excellent biocompatibility with a foreign body response comparable to other degradable sutures, hemocompatibility, and oxygen and water permeability. Although it is classified as a non-degradable suture, it has been shown that silk will break down through proteolytic degradation and will be slowly absorbed *in vivo* as biocompatible amino acids. The rate of degradation varies based upon implantation site and the size of the implanted fibers, but has been reported to lose the majority of its tensile strength between 6 weeks and one year after implantation. Silk also possesses remarkable mechanical properties not seen in other naturally occurring proteins [22, 80, 81]. It has been reported that natural silk fibers have tensile strength and yield at fracture values comparable to synthetic fibers such as Kevlar [82].

Silk is produced in nature by a wide variety of insects and spiders, with the silk from *Bombyx mori* silkworm cocoons being the most commonly harvested. Natural silk is composed of two distinct proteins: a glue-like sericin protein, which serves to hold fibers together, and a fibroin filament component which acts as the mechanical backbone. As sericin has proven to elicit an adverse immune response inside the body, it is the degummed silk fibroin (SF) that is used in medical applications such as braided suture. This 325 kDa protein consists of repetitive hydrophobic blocks, which form crystalline β-sheets through hydrogen bonding, and amorphous hydrophilic regions. The β-sheets

provide the structure with its tensile strength, while the amorphous regions provide elasticity and toughness [22, 81, 82]. SF fibers have been used as both knitted constructs [83-85] and as electrospun scaffolds of reconstituted SF [86-94]. It has been well documented that reconstituted fibers of SF are almost completely amorphous in their structure and must be annealed in a methanol or ethanol solution to create β-sheet crystallization [86-88, 90, 91, 93, 95, 96]. Despite this annealing process, reconstituted SF scaffolds have proven to be highly conducive to cell seeding, with literature reporting successful proliferation of FBs [22, 84, 86, 91], osteoblast-like cells [22], keratinocytes [91], and bone marrow stem cells [22, 80, 81, 83, 85, 88].

Acellular Matrix and Submucosa. Another natural-based material that has been used as a successful scaffold for tissue engineering applications is decellularized ECM. As mentioned before, nearly all tissues are comprised of ECM that consists of structural proteins, polysaccharides, cytokines, and growth factors. While this process of decellularization aims at completely removing all cellular and nuclear material from the tissues, the bulk composition, mechanical properties, and biological activity are still in tact [97]. Using this type of scaffold eliminates some of the drawbacks and limitations of techniques that will be mentioned later, such as insufficient mechanical strength and possible undesirable inflammatory responses, but still has other disadvantages, including rapid degradation rates and calcification production. Native ECM structures are advantageous for their use as tissue engineered scaffolds because they induce a positive

host response that promotes cell infiltration, rapid scaffold degradation, formation of host derived neomatrix, and tissue remodeling with a minimum amount of scarring [98].

Briefly, decellularization is the process by which cells are removed from an ECM through a series of mechanical, chemical or enzymatic steps, leaving an acellular matrix that can serve as a tissue engineering scaffold. The main components of the native ECM that are left after the decellularization process are collagen and elastin [11]. ECMs that have been successfully processed this way include urinary bladder, the dermis of the skin, small intestine, pericardium, basement membrane and stroma of the decellularized liver, and decellularized Achilles tendon [98].

The submucosa is the layer of tissue beneath a mucous membrane or the layer of connective tissue beneath the tunica mucosa. Similar to the decellularized ECM described above, subintestinal submucosa (SIS) is an attractive material for tissue engineering scaffolds because of the structural and biological factors present in the tissue [99-102]. *In vivo* studies done with a bladder submucosa confirm this tissue can contribute to bladder tissue regeneration. Normal cellular organization and phenotype were demonstrated, along with the presence of nerve fibers [103]. Two drawbacks of both decellularized ECM and SIS are that they exhibit a rapid rate of degradation *in vivo*, and may elicit calcification. This former problem is especially prevalent in submucosal tissue, while native ECM tissue also has problems with scaffold shrinkage *in vivo*.

OVERVIEW

This study examines the tissue engineer's ability to create tissue specific scaffolds through the process of electrospinning. The inherent flexibility of the electrospinning process, through the use of various polymers, polymer blends, and solvents, can create structures that exhibit a wide array of mechanical and bioactive properties. Altering process control variables such as mandrel rotational speed and charging voltage can dramatically change the structure of the finished fibrous scaffold. Further modification of electrospun scaffolds can occur post-process through the application of a number of different cross-linking agents to modify scaffold mechanical properties and rates of degradation. When one considers the seemingly infinite number of iterations available to the tissue engineer for controlling electrospun scaffold properties, it is easy to recognize that the electrospinning process has the potential to create tailor-made structures for almost any part of the human body. The following chapters of this text provide insight into the alteration of scaffold properties and their use in a number of different applications:

- Electrospinning of Biopolymers for Cardiovascular Applications (currently in press for publication in *Advanced Drug Delivery Reviews, 2009*)
- Creation of Electrospun ECM Analogues (published in *Polymer International, 2007, volume 56, pages 1349-1360*)
- Electrospinning PDO and Elastin Blends (published in *Biomedical Materials, 2006, volume 1, pages 72-80*)

- Electrospinning PDO and Fibrinogen Blends (published in the *Journal of Engineered Fibers and Fabrics, 2008, volume 3, pages 12-21*)
- Cross-linking Electrospun Fibrinogen to Tailor Scaffold Properties (published in *Biomedical Materials, 2008, volume 3, EPUB*)
- Creation of Aligned Silk Scaffolds for Tissue Engineering (in review for publication in *Biomedical Materials, 2009*)
- Creating Cellularized Ligament Analogues

The first two chapters are reviews of the current use of electrospinning in tissue engineering; one for cardiovascular specific applications and the other providing information on electrospinning's use in creating scaffolds for a number of different tissues in the body. Next, two chapters detailing the use of PDO blended with the natural polymers elastin and fibrinogen. These polymers were blended in a number of different ratios in an attempt to combine the inherent strength of the synthetic PDO polymer with the high level of bioactivity native to the natural polymers. PDO and elastin solutions were blended together, while PDO and fibrinogen were introduced at the point of fiber formation through a specially designed nozzle. The following chapter investigates the use of a number of different cross-linking agents to modify the degradation rate and mechanical properties of electrospun fibrinogen structures. The subsequent chapter looks at fiber orientation in terms of its effect on scaffold mechanical properties when used as either ligament or vascular grafts. Finally, the last chapter utilizes the method of air-gap electrospinning to create cellularized ligament analogue structures. While seemingly disjoint on the surface, the results discussed in this text are

intended to emphasize the flexibility of the electrospinning process with regards to tissue engineering, and to highlight the ability of the tissue engineer to create tailor-made tissue specific scaffolds.

CHAPTER 2 Electrospinning of Biopolymers for Cardiovascular Applications

Preface: The following manuscript is currently in press for publication in Advanced Drug Delivery Reviews, 2009 [104]. The work included is a review article which explores the process of electrospinning with an emphasis on the electrospinning of an array of biopolymers for cardiovascular specific applications.

Electrospinning of Collagen / Biopolymers for Regenerative Medicine and Cardiovascular Tissue Engineering

Scott A. Sell, Michael J. McClure, Koyal Garg, Patricia S. Wolfe, and Gary L. Bowlin

Department of Biomedical Engineering
Virginia Commonwealth University
Richmond, VA 23284

ABSTRACT

The process of electrospinning has seen a resurgence of interest in the last few decades which has lead to a rapid increase in the amount of research devoted to its use in tissue engineering applications. Of this research, the area of cardiovascular tissue engineering makes up a large percentage, with substantial resources going towards the creation of bioresorbable vascular grafts composed of electrospun nanofibers of collagen and other biopolymers. These bioresorbable grafts have compositions that allow for the *in situ* remodeling of the structure, with the eventual replacement of the graft with completely autologous tissue. This review will highlight some of the work done in the field of electrospinning for cardiovascular applications, with an emphasis on the use of biopolymers such as collagens, elastin, gelatin, fibrinogen, and silk fibroin, as well as biopolymers used in combination with resorbable synthetic polymers.

INTRODUCTION

Cardiovascular disease (CVD), specifically coronary heart disease (CHD) resulting from arteriosclerosis, remains the leading cause of death in the United States and has been so virtually every year since 1900 [105]. Arteriosclerosis is a vascular disease characterized by thickening of the arterial wall and a subsequent decrease in the arterial lumen leading to an eventual decrease or loss of circulation distal to the disease site. Once blood flow is compromised, vascular bypass is an option to restore blood flow

to tissues distal to the restriction or blockage [59]. In 2005 there were 469,000 bypass procedures performed due to CHD [105], which typically involve the replacement of a coronary artery with a patients own saphenous vein or internal mammary artery. While these autologous replacement grafts have an acceptable patency rate, they are not always a viable option as the patient may also suffer from peripheral vascular disease; affecting upwards of 8 million Americans and up to 20% of those 65 years of age or older [105]. Further complicating the use of autologous vessels is the fact that they are limited in number and a previous bypass operation may have already required the vessel's use [106]. Currently available commercial alternatives to the autologous vessel gold standard are limited to synthetic vessels made of expanded polytetrafluoroethylene (e-PTFE) and woven or knitted polyethylene terephthalate (PET) fibers (Dacron®). These materials have been used with moderate success as medium (6-10 mm internal diameter, ID) and large (> 10 mm ID) diameter prosthetics, but their efficacy is severely limited when used as small diameter vessels (< 6 mm ID). Larger diameter vessels experience higher flows and less resistance than small diameter vessels, such as the popliteal or coronary arteries, where low blood flow and high shear makes the synthetic graft more prone to thrombus formation and intimal hyperplasia [59, 106-116]. Dacron® and e-PTFE grafts are non-degradable and lack the ability to promote native tissue regeneration, making them a permanent fixture in the body. As a permanent fixture, the graft is constantly threatened with attack from the patient's own foreign body response as well as bacterial graft infection [113, 115, 117]. The electrospinning of biopolymers holds the potential to create bioresorbable vascular prosthetics that not only mimic the structure and function of

native vessel, but also have the ability to degrade over time and become replaced with autologous tissue.

Native Vascular Physiology. Native artery is an extremely complex multi-layered tissue composed of a number of different proteins and cell types, which each plays an integral role in the mechanical behavior of the structure (figure 2.1). In order to withstand the high flow rate, high pressure, and pulsatile nature of blood flow, artery is comprised of three distinct layers: intima, media, and adventitia. Each of these layers has a different composition and plays a different physiological role. The intimal layer is the innermost layer of the vessel wall and is made up of a single layer of ECs on a thin basal lamina and a subendothelial layer made of collagen type IV and elastin. This layer contacts the bloodstream and therefore provides a critical barrier to platelet activation. The thick medial layer is composed of several layers of SMC in a matrix of collagen types I and III, elastin, and proteoglycans. The outermost adventitial layer is made of FB and randomly arranged collagen type I [59, 118, 119]. The major protein components of native artery, collagen and elastin, provide tensile support and prevent vessel rupture, and confer elasticity to the vessel, providing the ability to recover from pulsatile deformation, respectively [120, 121]. It is the elastic nature of elastin that dominates the low-strain mechanical response of the vessel to blood flow and prevents pulsatile energy from being dissipated as heat [122, 123].

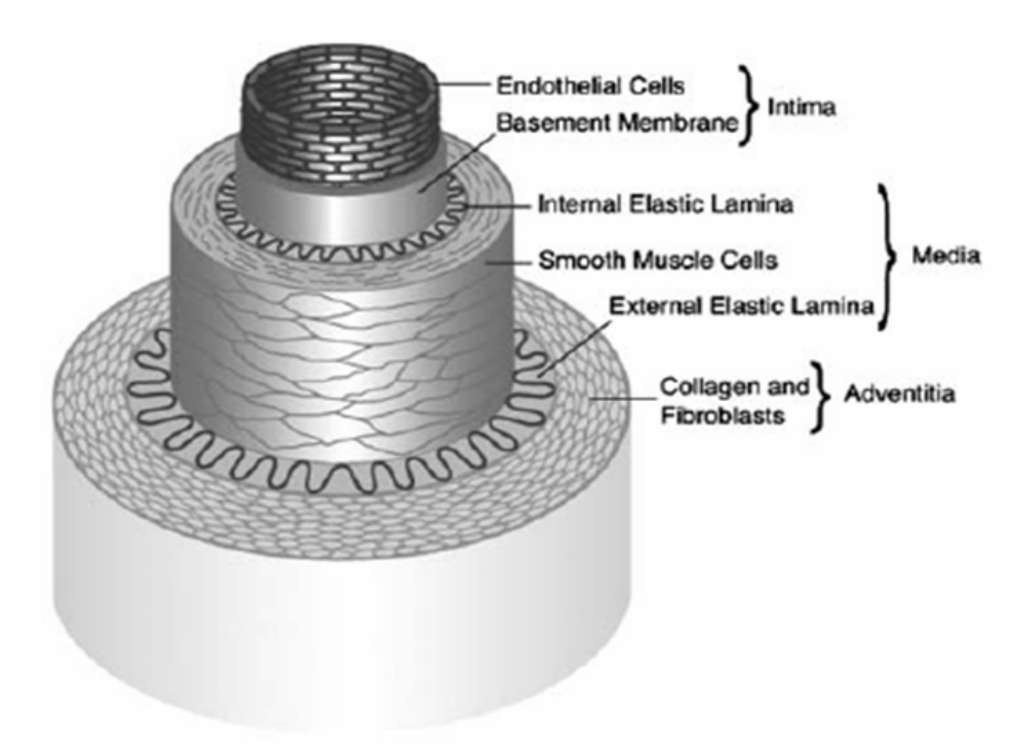

Figure 2.1. Drawing of arterial wall depicting the native tissue's three primary layers: intima, media, and adventitia. Reprinted from [111].

Bioresorbable Vascular Grafts. Bioresorbable grafts are advantageous when compared to their non-resorbable counterparts due to the fact that a resorbable vascular prosthetic with adequate mechanical properties can be implanted and degraded gradually over a period of time, leaving behind no permanent synthetic materials to initiate a chronic foreign-body reaction [115]. Through the years, there have been many different approaches to the creation of a vascular graft that can be gradually degraded over time and replaced with native tissue. Wesolowski et al. first introduced the concept of a bioresorbable vascular prosthetic in the early 1960s. These first bioresorbable incarnations were composed of a variety of Dacron® yarns, collagen coatings, and

collagen fibers. The permanent Dacron® provided mechanical stability, while the collagen added bioactivity to the structure and promoted the ingrowth of native tissue as it was degraded and remodeled [124, 125]. The 1970s, and '80s saw the advent of a number of different aliphatic polyesters (PLA, PGA, PDO, etc.). These polymers breakdown through hydrolysis in the body, and can have their rate of degradation tailored by altering their structures [115, 126-130]. While this preliminary work failed to result in a successful commercially available graft, it laid the foundation for current research in bioresorbable prosthetics and demonstrated the possibilities of *in situ* tissue engineering.

The creation of an off-the-shelf bioresorbable vascular graft designed to be remodeled *in situ* would use a patient's own body as a bioreactor and the host's own cells to populate and modify the scaffold. The challenge of creating such a prosthetic is to tailor the graft to resorb at a rate comparable to the rate of natural tissue regeneration. This is necessary to prevent loss of the prosthetic mechanical backbone prior to the formation of autologous tissue substantial enough to withstand the rigors of the vascular system and prevent rupture or aneurysm formation. The eventual absence of foreign material would reduce both the host's foreign body response and the risk of graft infection, while increasing the patency of the prosthetic [50, 115, 131].

Aside from being bioresorbable, a tissue engineered vascular graft needs to meet several other criteria to be considered ideal. From an implantation standpoint, the graft would need to be easy for surgeons to handle with excellent suture retention, and resistant to kinking while remaining flexible. The graft must be leak resistant, yet have sufficient porosity to allow for the ingrowth of autologous tissue. The graft must also have

compliance similar to that of native artery to prevent intimal hyperplasia, but must be strong enough to prevent the formation of aneurysm. Manufacturing concerns also play a role in creating an ideal vascular graft, as the structure must be easy to produce, sterilize, and store, as well as be economical and available off-the-shelf in a variety of sizes [50, 113].

Electrospinning. The resurgent interest in electrospinning in recent years has helped to rejuvenate the research of bioresorbable vascular grafts. One of the main attractions of electrospinning is the fact that it is a simple process requiring little specialized equipment. A standard electrospinning setup consists of a high voltage power supply, syringe pump, grounded target, and a spinneret (typically a syringe fitted with a blunt tip needle, figure 2.2). The process itself can be easily performed in a laboratory setting or scaled up for large-scale production with little modification. In brief, a polymer solution is drawn into the spinneret and charged with a large electric potential in the range of several kilovolts. A grounded target is placed a set distance from the charged polymer solution to create a static electric field. When the electric potential reaches a critical level, the electrostatic repulsion of the polymer solution overcomes the surface tension at the tip of the spinneret, and a fine jet of entangled polymer chains is drawn out. This jet whips through the air toward the grounded target, creating a dry fiber through the evaporation of the polymer's solvent. The electrospinning process has the capacity to produce fibers that range from 50 nm to 10 μm in diameter, collected on the

grounded target, dependant upon the processing conditions of the polymer solution/solvent used [11, 25, 48, 132-134].

Apart from the simplicity of its setup, the versatility of the electrospinning process has also made it ideal for tissue engineering. The process is compatible with a wide array of polymers, both natural and synthetic in origin, as well as the combination of any number of different polymers. A large number of biopolymers have been electrospun in our lab and others, and will be discussed in detail in this manuscript: collagens, elastin, fibrinogen, hemoglobin and myoglobin [135], and SF. Polymer solutions can be combined in a single reservoir, spun side by side from separate spinnerets, or layered sequentially to provide a large number of options for altering scaffold properties. In addition, electrospun scaffolds can be created in nearly any shape required, and can consist of fibers in an assortment of orientations [132]. Electrospinning provides researchers with the ability to create, not only flat sheets, but also the seamless tubes required for vascular applications. These tubes can be created in any diameter to fit the specifications of any vascular conduit.

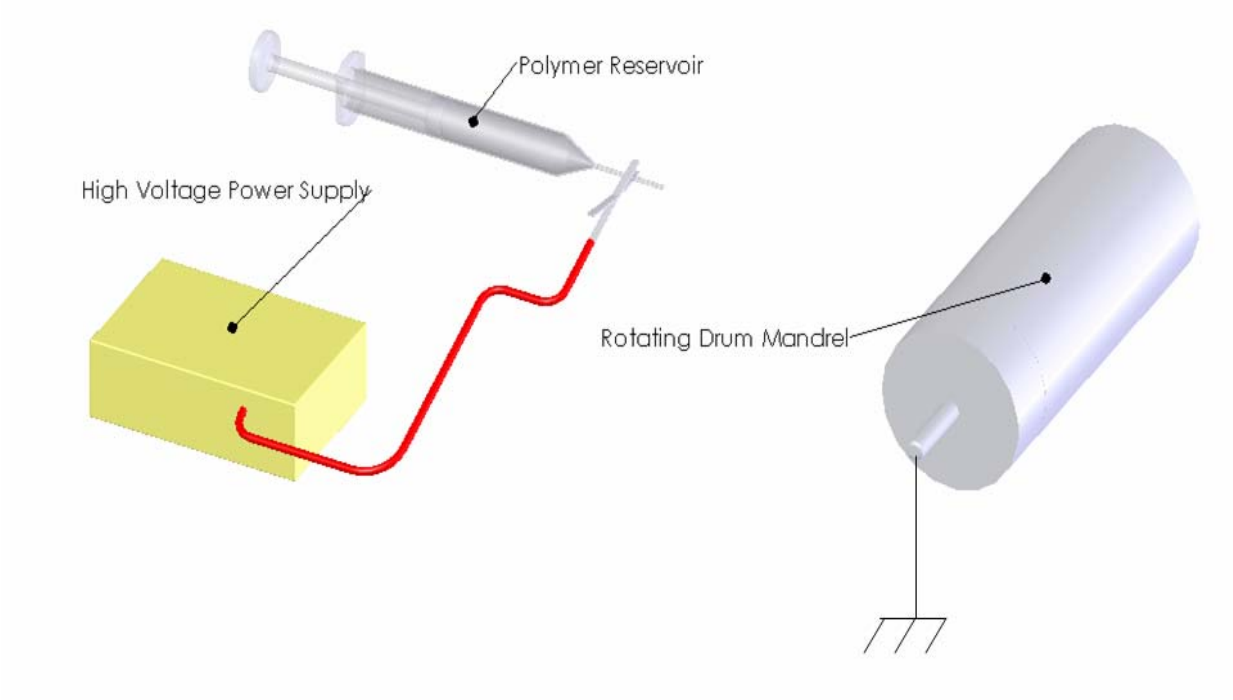

Figure 2.2. Schematic representation of a simple electrospinning setup utilizing a grounded rotating drum as a collection mandrel.

ELECTROSPUN BIOPOLYMERS

Collagen. Collagen is the most abundant protein in the human body, a key element of the ECM, and imparts structural integrity and tensile strength to tissues. Tissue disruption following injury requires collagen for the repair and restoration of structure and function. Excessive collagen deposition at a wound site results in loss of anatomical structure, function and fibrosis. Conversely, if insufficient amounts of collagen are deposited, the wound is weak and may rupture [136].

The collagen super family includes over 30 different gene products that assemble into at least 20 genetically different collagen types, which may be homotrimeric or

heterotrimeric in nature. All of the collagens share the triple helical molecular structure. The collagens most involved in forming fibrillar structures include types I, II, III, V and XI, with the fibril forming collagens type I, II, III being the most abundant [1]. The underlying α chains that form these polymers are arranged into a repeating motif that forms a coiled structure, exhibiting a 67 nm interval that imparts a characteristic banding pattern to the collagen structure. The main collagens of interest to cardiovascular engineering are collagens I, III, and IV. Collagen type I consists of two αI chains and one α2 chain forming fibrils of 50 nm in diameter, and is present in bone, skin, dentin, cornea, blood vessels, fibrocartilage and tendon. Type III collagen is present in our skin as well as in ligaments, blood vessels and internal organs, and is composed of three α1(III) chains resulting in fibrils ranging from 30 to 130 nm in diameter [19]. Type III collagen also contributes to the flexibility of blood vessels and is expressed during the initial period of wound healing. Collagen type IV, which is a major structural element of the basal lamina and basement membranes, is a nonfibrillar collagen. These collagens associate with fibrillar collagens to form microfibrils and network structures.

Collagen has been used in a variety of tissue engineering applications because of its predominance in the ECM, non-immunogenicity and available methods of isolation from a variety of sources. However, the typical procedures used to isolate and reprocess this natural scaffolding into an engineered material may compromise many of its biological and structural properties [1]. Collagen fibers also possess some unique structural properties important for tissue engineering: they transmit forces, dissipate energy, prevent premature mechanical failure and provide biological signals to adjacent

cells that regulate functional responses. Additionally, collagen is resorbable, has high water affinity, low antigenicity, very good cell compatibility and ability to promote tissue regeneration [19]. These factors combine to make collagen one of the most ideal biopolymers available for tissue engineering applications.

Electrospinning of Collagen. Collagen is one of the most plentiful proteins found in native blood vessel, and along with SMCs, collagen confers wall strength and resistance to vessel rupture in a harsh *in situ* environment [120]. Our laboratory has worked extensively on the electrospinning and characterization of many of the structural collagens that play significant roles in native vascular tissue: types I [19], III [137], and IV [1] (figure 2.3). This work has demonstrated that the electrospinning process has the potential to produce collagen fibers that closely mimic, and at some point may even fully reproduce, the structural and biological properties of the natural collagen ECM. Electrospun fibers of type I collagen dissolved in 1,1,1,3,3,3 hexafluoro-2-propanol (HFP) exhibited a linear relationship between polymer concentration and fiber diameter. Electrospun collagen solutions ranged in concentration from 0.03 to 0.10 g/ml of HFP, and resulted in scaffolds composed of 100 nm to 5 μm diameter fibers [19]. The electrospinning of collagen type III, like collagen type I, demonstrated a linear relationship between solution concentration and fiber diameter for collagen concentrations between 20 and 80 mg/ml. Over this range of concentrations, fiber diameter increased from 115 to 612 nm. It was found that for concentrations higher than 80 mg/ml, the electrospun collagen type III resulted in small fragments of fibers as well

as some ribbon like fibers [137]. Our laboratory has also done some preliminary work with the electrospinning of the basement membrane forming collagen type IV from HFP, to form fibers with diameters ranging from 100 nm to 2 μm [1].

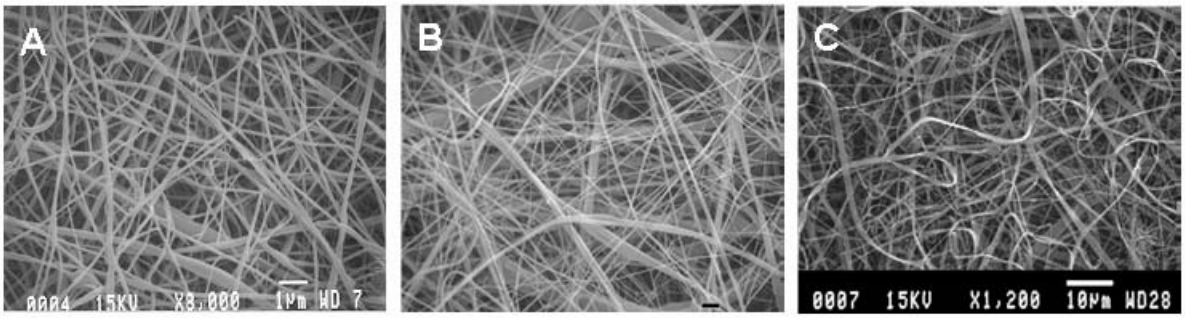

Figure 2.3. Scanning electron micrographs of (A) electrospun type I collagen (8,000x, scale bar 1.0 μm), (B) electrospun type III collagen (4,300x, scale bar 1.0 μm), and (C) electrospun collagen type IV collagen (1,200x, scale bar 10 μm). (A) reprinted from [59]. (B) and (C) reprinted from [1].

As HFP is a strong organic solvent, it has been suggested that electrospinning of collagen from HFP may result in structures composed of gelatin fibers [138]. However, there has been research conducted which demonstrates differences between collagen and gelatin electrospun from HFP [28], as well as research that demonstrates only minor differences between structures of collagen electrospun from HFP and structures of collagen electrospun from phosphate buffered saline (PBS) based solutions [139].

Telemeco et al. [28] have shown a number of morphological characteristics which differ between scaffolds of electrospun collagen and gelatin. First, the pore size of electrospun gelatin matrix is smaller (approx. 2000-6000 nm^2) than the average pore dimension of electrospun collagen (approx. 1500-4000 nm^2). Second, electrophoretic analysis has shown that samples of electrospun gelatin are composed of fragments of type

I collagen. In contrast, samples of electrospun collagen appear to be composed of intact monomers. Finally, fibrils of collagen exhibit a 67 nm repeat banding pattern that is thought to expose a binding site in the native collagen fibril that enhances cell adhesion and migration. However, electrospun gelatin fibrils exhibit a non-descript amorphous structure and lack this 67 nm repeat pattern

In vivo behavior of the two structures is also markedly different. Electrospun cylindrical constructs of collagen type I and gelatin were implanted into the belly of the vastus lateralis of the rat and recovered after seven days for microscopic evaluations. It was found that constructs composed of electrospun type I collagen were fully infiltrated with interstitial cells and were well integrated with the surrounding muscle tissue of the host. The implant was free from fibrotic encapsulation and there was a smooth continuum of cells from the host tissue into the electrospun collagen. Also, functional capillaries were present throughout the walls of these implants. Electrospun constructs of gelatin on the other hand delaminated from the host tissue after seven days *in vivo*. It was revealed by microscopic examination that these implants developed fibrotic capsules, were poorly infiltrated with interstitial cells, and appeared to be infiltrated by lymphocytes [28].

Dong et al. [139] recently published a study on the electrospinning of collagen from a simple binary mixture of PBS and ethanol. They found that pore sizes are similar between collagen scaffolds electrospun from either HFP or PBS/ethanol solutions. Fourier transform infrared spectroscopy (FTIR) data revealed that the triple helical structure of type I collagen remained intact after electrospinning from the PBS/ethanol

mixtures. By comparison, there were only minor differences observed in the amide I and amide II bands of structures electrospun from HFP and the PBS/ethanol solutions.

Electrospinning Collagen and Synthetic Polymer Blends. Collagen, while a structural protein *in vivo*, lacks mechanical integrity upon hydration in an electrospun form. Without sufficient cross-linking of the electrospun structure it does not have the strength to withstand arterial forces. Previously established methods of cross-linking with glutaraldehyde (GLUT), successful in increasing the strength of the electrospun structures, also carry an enhanced risk of cytotoxicity and calcification when used *in vivo*. To circumvent this problem our laboratory has published a technique for the cross-linking of electrospun collagen with EDC in ethanol [140]. Another method for improving the mechanical stability of an electrospun collagen scaffold is to incorporate biodegradable synthetic polymers into the structure to impart immediate strength to the scaffolds while maintaining a high level of bioactivity through the presence of collagen.

Blends of collagen with synthetic polymers have been used to tailor mechanical and bioactive properties of the electrospun scaffolds. Collagen in the native ECM serves as an adhesion protein that enhances cell attachment and proliferation through specific interactions between RGD domains in collagen molecules and integrin receptors in the cell membrane. Thus, the presence of collagen in the scaffolds would aid in increasing the biocompatibility of the scaffolds. Other methods for introducing proteins into nanofibrous structure such as coating or grafting, lead to slow mass transfer of the proteins into the three dimensional porous materials. Electrospinning of a blended

collagen mixture is much simpler because it avoids the slow mass transfer process and also uses lesser amounts of chemical reagents. Moreover, the existence of collagen on the surface and inside the structure provides sustained cell recognition signals with polymer degradation, which is crucial for cell function and development [141].

Stitzel et al. [142] used a combination of collagen fibers and PLA to create a scaffold for vascular engineering. Collagen fibers were wound with a novel winding apparatus with variable pitch to mimic the SMC structure in an artery. Biodegradable PLA was spun around the collagen fibers for SMC seeding and to hold the fibers in place during tissue regeneration. The collagen fiber and matrix was designed to create a residual stress environment similar to that found in native arteries, which encourages SMC orientation along the principal stress directions of an artery. A distinct regularity in alignment of the SMCs along the direction of the large collagen fiber was observed, demonstrating that one can positively influence the alignment of SMCs before implantation and can thus improve the speed with which the graft can be incorporated into the vasculature.

Segmented polyurethanes (SPU) have also been used to create synthetic/biopolymer-blended scaffolds. A tri-layered electrospun mesh composed of type I collagen, styrenated gelatin (ST-gelatin), and SPU was created in which individual fiber meshes were deposited layer by layer by sequential electrospinning. Confocal laser scanning micrographs of the scaffolds revealed the SPU, ST-gelatin, and collagen layers to be segregated and hierarchically positioned in the order of the vertical direction of the meshes. Using this approach, a bi-layered electrospun tube composed of a collagen mesh

cell-adhesive inner layer and an SPU structural outer layer was constructed as a prototype small diameter vascular graft. The authors speculated that such hierarchically designed artificial grafts may provide compliance matching that of native arteries, cell and tissue ingrowth, and transient antithrombogenicity in the early phase of implantation [143].

PCL is a bioresorbable polymer with excellent mechanical properties that has recently seen a marked increase in its usage as a tissue engineering scaffold. A PCL/collagen type I composite scaffold with the ability to resist high degrees of pressurized flow over long term, while still providing a favorable environment for the growth of vascular cells was developed by Lee et al. [144]. The PCL/collagen composite scaffolds, with fiber diameters of approximately 520 nm (figure 2.4), possessed appropriate tensile strength (4.0 ± 0.4 MPa) and adequate elasticity (2.7 ± 1.2 MPa). The burst pressure of the composite scaffolds (4912 ± 155 mmHg) was much larger than that of the PCL scaffolds alone (914 ± 130 mmHg), as well as exceeding the burst strength of native vessels. The composite constructs were seeded with bovine ECs and SMCs, and showed the formation of a confluent layer of ECs on the lumen and SMCs on the outer surface of the scaffold.

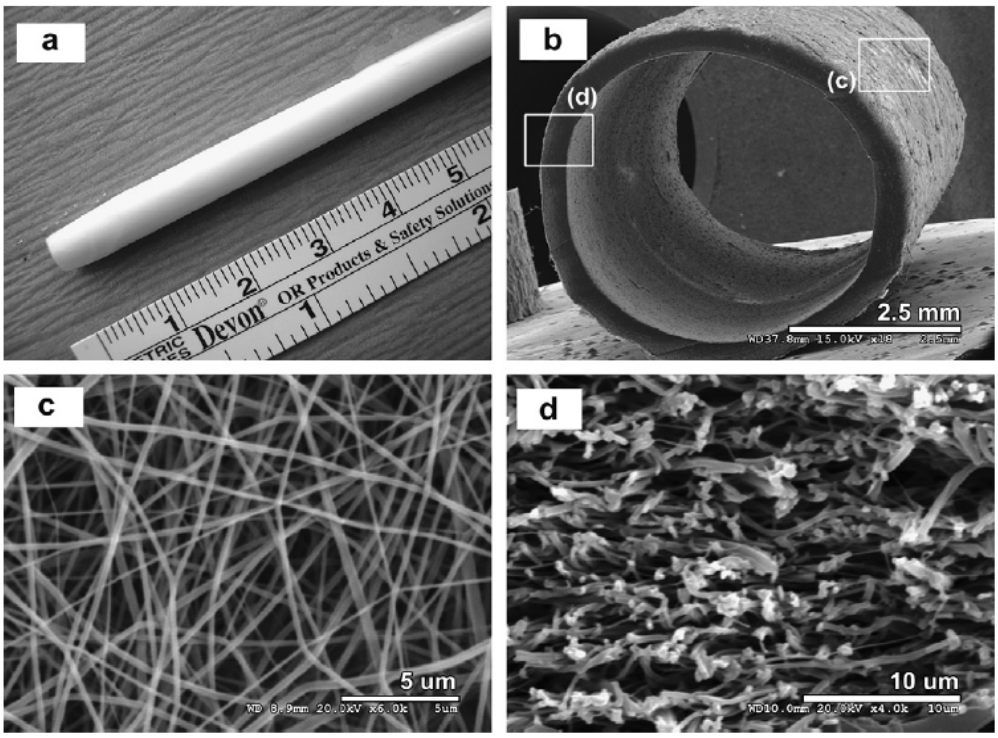

Figure 2.4. The gross appearance (a), and SEM images of electrospun PCL/collagen composite scaffolds: (b) entire scaffold (18x), (c) surface (6,000x), and (d) cross-sectional (4,000x) morphologies. Reprinted from [144].

These PCL/collagen electrospun scaffolds were also investigated for their *in vivo* stability in a rabbit aortoiliac bypass model. It was observed that endothelialized grafts resisted adherence of platelets when exposed to blood. Also, it was demonstrated by serial ultrasonography that these scaffolds were able to retain their structural integrity over 1 month of implantation. Moreover, these scaffolds continued to maintain biomechanical strength at retrieval that was comparable to native artery [145].

In a study by Venugopal et al. [146], PCL and collagen types I and III were blended and electrospun to create nanofibers with a diameter of 210–225 nm. The tensile modulus of the structures was 18 MPa with a tensile strength of 7.79 MPa, appropriate

for a blood vessel conduit. SMCs were seeded on the scaffolds and their proliferation was quantified. Proliferation was significantly increased up to 63%, 73% and 82% in PCL/collagen nanofiber scaffolds compared to PCL nanofiber scaffolds after 2, 4 and 6 days, respectively. He et al. [141] fabricated collagen type I blended poly (L-lactic acid)-co-poly(ε-caprolactone) [P(LLA-CL), 70:30] biohybrid scaffolds by electrospinning, and tested for the growth of ECs. Scanning electron microscopy (SEM) analysis revealed a smooth nanofiber surface and a narrow fiber diameter distribution between 100-200 nm. It was demonstrated that collagen blended polymer nanofibers could enhance the viability, spreading and attachment of human coronary artery endothelial cells (hCAECs) and preserve their phenotype.

PDO is a polymer used commonly as a commercially available suture that has been shown to exhibit excellent mechanical properties, shape memory, a low inflammatory response, and a slower rate of degradation than other resorbable suture materials [48]. Electrospun scaffolds of PDO/collagen have been successfully created that, when hydrated, exhibited mean peak stresses between 4.6 and 6.7 MPa, mean tangential moduli between 7.6 and 18.0 MPa and mean strain to failure values between 56.5% and 186.4% (table 2.1). It is to be noted that as with other composite materials, these results were not just the average of the component contributions. It has been speculated by the authors that an as yet unexplained interaction has taken place between the polymers. These preliminary data seem to indicate that blends of PDO and collagen may mimic the mechanical and morphological requirements of a blood vessel's microenvironment [137].

Table 2.1. Results of uniaxial tensile testing of electrospun blends of PDO and collagen types I and III compared to native saphenous vein, femoral artery, and e-PTFE (30 mm internodal distance). Modified from [137]

Composition	Peak Stress (MPa)		Tangential Modulus (MPa)		Strain At Break (%)	
	Dry	Wet	Dry	Wet	Dry	Wet
100:0 PDO	5.8 ± 0.7	4.8 ± 0.6	13.2 ± 3.1	10.4 ± 3.8	185.8 ± 93.4	229.8 ± 117.2
90:10 PDO:CI	6.3 ± 0.7	5.7 ± 1.1	25.7 ± 3.0	11.2 ± 1.8	57.5 ± 4.8	89.2 ± 4.6
80:20 PDO:CI	6.4 ± 1.0	5.9 ± 1.1	48.3 ± 12.5	15.8 ± 3.7	40.4 ± 8.0	72.8 ± 11.1
70:30 PDO:CI	6.7 ± 0.4	4.9 ± 0.5	68.3 ± 6.1	18.0 ± 2.7	27.5 ± 4.7	56.5 ± 11.8
90:10 PDO:CIII	5.1 ± 0.9	5.2 ± 0.9	19.1 ± 5.5	8.9 ± 2.6	63.0 ± 8.9	100.1 ± 18.7
80:20 PDO:CIII	6.6 ± 0.5	6.1 ± 0.7	22.3 ± 2.9	8.5 ± 1.5	115.6 ± 6.4	153.5 ± 21.3
70:30 PDO:CIII	5.8 ± 1.1	6.7 ± 0.8	26.7 ± 4.3	7.6 ± 1.8	110.7 ± 21.4	186.4 ± 18.0
90:10 PDO:CI/CIII	4.6 ± 1.3	4.6 ± 1.0	14.1 ± 4.8	7.7 ± 2.7	64.9 ± 11.3	101.1 ± 12.5
80:20 PDO:CI/CIII	5.5 ± 0.8	5.0 ± 0.4	27.0 ± 6.2	10.1 ± 1.2	54.4 ± 10.1	88.2 ± 7.6
70:30 PDO:CI/CIII	6.2 ± 1.0	4.6 ± 0.8	37.6 ± 11.9	9.0 ± 2.3	53.8 ± 13.8	98.3 ± 18.1
e-PTFE	6 – 15		42 – 60		20 – 30	
Saphenous Vein	3		43		11	
Femoral Artery	1 – 2		9 – 12		63 – 76	

Elastin. *In vivo*, elastin is a chemically inert, highly insoluble polymer composed of covalently cross-linked molecules of its precursor, tropoelastin, a soluble, non-glycosylated and highly hydrophobic protein. Tropoelastin expression and subsequent elastin synthesis typically occurs in FBs, vascular SMCs, ECs, and chondrocytes [147]. During the process of elastogenesis, tropoelastin is synthesized, preventing its premature intracellular aggregation and protecting it from proteolytic degradation by binding a 67 kDa galactoectin (elastin binding protein, EBP). This association lasts until the complex is excreted into the extracellular space. EBP then interacts with galactosugars of the

microfibrils, dramatically decreasing its own affinity for tropoelastin. In order for proper elastogenesis to occur, the interaction of the N-terminal part of the microfibrillar-associated glycoprotein with the C-terminal end of tropoelastin is required. Once aligned, lysyl oxidase deaminates and oxidizes the lysyl residues to allysine following the action of Cu^{2+}. Cross-links are then formed by the reaction of the allysines with themselves or with an unmodified lysine [147-149].

As a biomaterial, elastin is becoming more and more popular for tissue engineering applications as one of the main structural components of the vascular ECM. The incorporation of elastin into biomaterials has been used in several different forms, including insoluble elastin occurring in autografts, allografts, xenografts, decellularized ECM, and in purified elastin preparations where the insoluble elastin is hydrolyzed to a soluble form of α, β, and κ elastin [150]. Although insoluble elastin in its different graft forms could be considered a more "natural state," there is an advantage to its solubility which makes handling and analysis of the material more straightforward. Additionally, elastin peptides influence signaling, chemotaxis, proliferation, and protease release via the elastin receptor [151]. Daamen et al. not only found that solubilized elastin induced angiogenesis, but also increased elastic fiber synthesis and displayed no signs of calcification when compared to grafts containing its insoluble form [152]. This is one of many studies that have proven soluble elastin to be an advantageous biopolymer.

Electrospinning of Elastin. In low flow environments, such as small diameter blood vessels, it is essential to match the mechanical forces of a vascular graft with the

native artery for proper graft functionality. To elicit these specific properties, the proper choice of polymers and fabrication must be made. As stated previously, tropoelastin provides the necessary building blocks to form native elastin *in vivo*. If tropoelastin were processed into a vascular graft this could prove to be a major advantage in cardiovascular tissue engineering. Li et al. demonstrated that recombinant human tropoelastin could be electrospun to form both nanofibers and microfibers, depending on the delivery rate [153]. In their study, both tropoelastin and solubilized α-elastin were electrospun. The parameters were optimized and the final products were compared through microscopy, mechanical tensile moduli, and cellular activity with human embryonic palatal mesenchymal (hEPM) cells. Mechanically, elastin allows for distension and recoil *in vivo*. It was determined that the elasticity of tropoelastin far exceeded that of soluble elastin, which could prove to be advantageous, allowing for the creation of grafts with compliance matching native artery.

Electrospinning Elastin and Synthetic Polymer Blends. Much like electrospun collagen, one of the limitations that pure electrospun soluble elastin has is its inherently poor mechanical properties. It has also been shown that electrospun elastin dissolves in water instantaneously if uncross-linked; however, blending with synthetic polymers will help to maintain the structural integrity of the scaffold and thereby retain elastin. A study done by McClure et al. [71] using weight sampling, SEM characterization, uniaxial tensile testing, and a 2,4,6-trinitrobensenesulfonic acid (TNBS) assay discovered that elastin, when blended with PDO, dissolved over time (figure 2.5). As the percentage of

synthetic was increased, the time to dissolve elastin from the scaffold increased as well, likely due to more elastin becoming entrapped within the PDO fibers. Scaffolds containing large amounts of elastin experienced almost instantaneous weight loss, while scaffolds containing larger amounts of PDO lost weight at a much slower rate with some elastin remaining after 1440 minutes in solution. This weight loss was corroborated by uniaxial tensile testing, which revealed differences between samples of varying elastin percentage over the time course. However, when the electrospun structures were cross-linked with either EDC or genipin, elastin containing scaffolds retained their original weight throughout the time course, but experienced slightly altered mechanical properties. Most studies involving elastin use some form of cross-linking whether it be GLUT, EDC, or 1,6-diisocyanatohexane (HMDI) in order to retain the electrospun biopolymer.

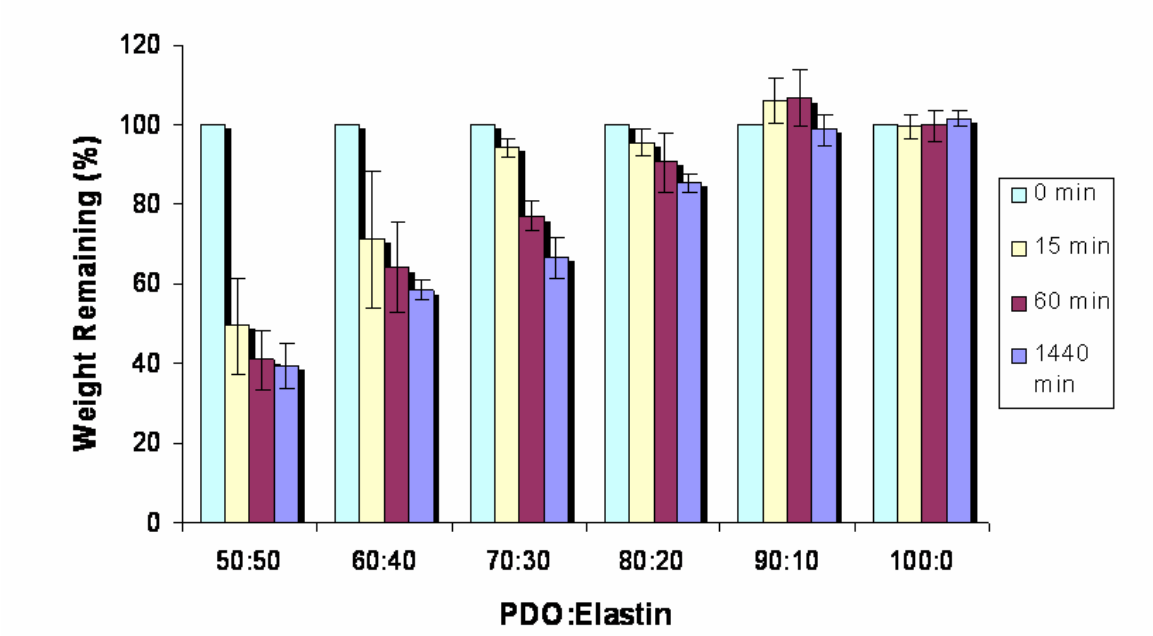

Figure 2.5. Percent of scaffold weight remaining after t = 0, 15, 60, and 1440 minutes, respectively in PBS. Modified from [71].

Since compliance mismatch between the graft and native artery is one of the major causes of graft failure, the authors of this manuscript have tested several combinations of PDO and elastin in order to determine its mechanical behavior *in vitro* [20]. A difference in this study, compared to other publications of vascular graft compliance, was that compliance was determined under dynamic conditions mimicking physiological parameters (figure 2.6), therefore providing a lucid interpretation as to how the graft should perform in the body. In this study, it was determined that certain PDO/elastin blends closely matched those of native artery.

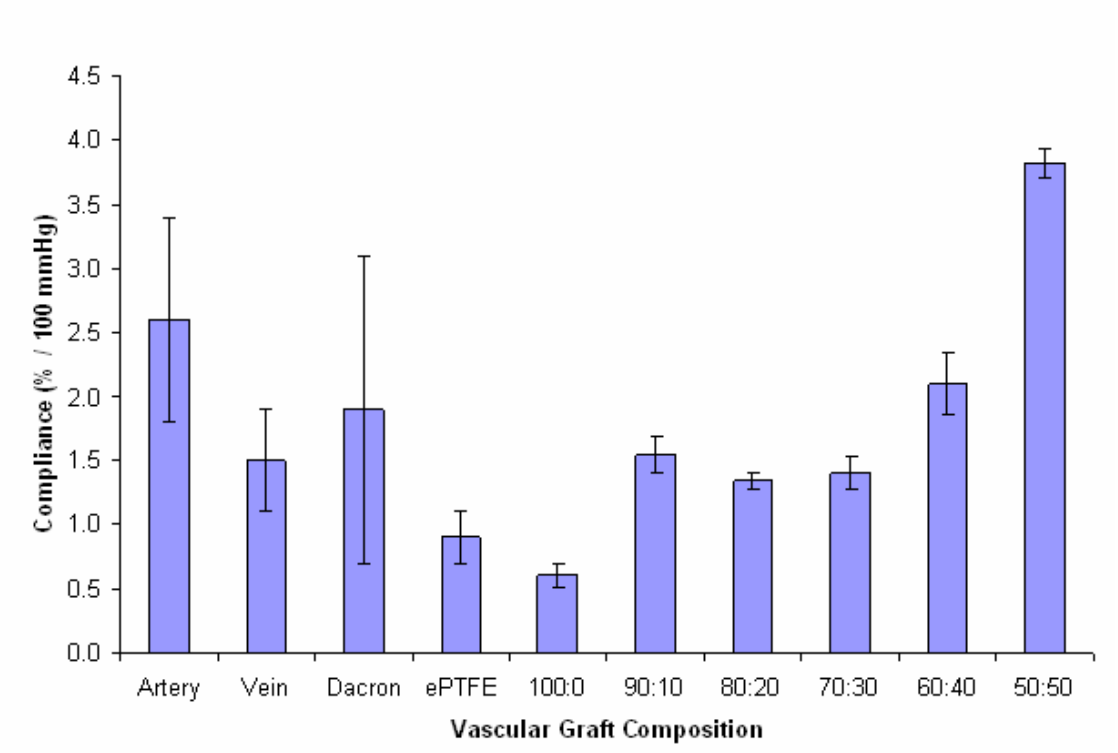

Figure 2.6. Compliance determined for 120/80 mmHg pressure level for native artery and vein, current synthetic prosthetics, and electrospun blends of PDO and elastin (PDO:elastin). Modified from [20].

This led to a subsequent study performed by Smith et al. [154] in which small diameter grafts composed of PDO and elastin, 1.9 mm inner diameter, were electrospun with a double or single layer of degradable suture reinforcement. Grafts were initially electrospun with a single layer of PDO/elastin and then wound with 6-0 polydioxanone monofilament suture (PDS^{TM} II) to provide additional mechanical strength, maintaining a spacing of 1 mm and a pitch of 9^{o}. Four separate groups, double layered suture, single layered suture, and two groups containing no suture reinforcement (double layered polymer and single layered polymer), were mechanically characterized through dynamic

compliance and burst strength. When suture was added to the scaffold structure, it provided higher bursting strength but lower compliance. If suture was removed from the structure completely, the graft displayed higher compliance but lower burst strength, where double layered polymer exhibited higher mechanical strength and lower compliance than that of single layered polymer. The addition or subtraction of suture allowed these vascular conduits to be mechanically tailored as necessary, a major benefit to biodegradable conduits. These PDO/elastin grafts displayed mechanical characteristics within the range of native artery further proving the benefits of elastin's use as a biopolymer, and demonstrated the potential of a multi-layered structure in replicating the mechanical properties of the native vasculature.

Another study involving the use of a elastin/synthetic polymer multi-layered structure was published by Thomas et al. [155], creating a tri-layered gelatin, elastin, and Maxon® blended graft, with each layer containing a different blend of polymers. The innermost layer contained purely gelatin and elastin, the middle layer contained gelatin, elastin, and Maxon, and the outer layer contained gelatin and Maxon. Each layer provided the scaffold with different mechanical properties contributing to the overall behavior of the graft. Slightly changing the parameters in one layer subsequently changed the overall material properties of the graft. A different way of approaching this aspect of vascular tissue engineering has been done by El-Kurdi et al. [156]. This group utilized a porcine internal jugular vein with an outer electrospun polymer wrap providing resistance against aneurysm formation. These outer polymer wraps contained poly(ester

urethane) urea (PEUU), collagen, and elastin to provide the necessary mechanical strength while encouraging cellular infiltration.

There have been many studies published on the material properties and mechanical response of electrospun vascular grafts, which are extremely important for the prediction of a grafts behavior *in vivo*. However, another important aspect of vascular regenerative medicine, which has not yet been studied extensively, is the initial host response produced when a graft is implanted. One such study was done by measuring the immunomodulatory nature of PDO/elastin scaffolds [157]. Results indicated that both PDO and elastin acted as immunosuppressive agents. The effect of these materials immunosuppresive nature is not yet fully understood. This result could prove to be detrimental, as patients requiring a vascular graft would most likely be in poor health and already somewhat immunocompromised. However, local immunosuppresion could be a benefit if it was required for cells to be seeded onto the graft; cells contained within the graft would be protected to some degree from attack by the immune system upon implantation. *In situ* evaluation would be needed to completely evaluate the body's response to the graft.

Collagen and Elastin Blends. As collagen and elastin are two of the most prevalent protein constituents in native vessel, it is only logical that they are often used in concert as tissue engineering scaffolds for vascular applications. Boland et al. [59], in an attempt to create a biomimicking layered vascular structure, first electrospun an 80/20 collagen type I/elastin tube on a 4 mm diameter mandrel. This tube was subsequently

seeded with both FBs and SMCs. Another tubular scaffold of 30/70 collagen type I/elastin was electrospun on a 2 mm diameter mandrel. This electrospun scaffold was then inserted into the 4 mm diameter scaffold and the lumen was filled with a SMC suspension. After 3 days in culture, a suspension of human umbilical vascular endothelial cells (hUVECs) was injected into the lumen, and the entire construct was cultured for 2 more days. Histological examination revealed complete cellular infiltration into the three-layered construct after 21 days, as shown in a cross-sectional cut of the tubular scaffold in figure 2.7. The artificial intima was covered by morphologically mature ECs and SMCs were present throughout the media, and had begun to align circumferentially around the axis of the scaffold. The FBs and SMCs in the adventitia created a dense population throughout the outermost wall. This study proved that an electrospun scaffold that mimics the native ECM is highly beneficial in the field of vascular tissue engineering. However, the lack of synthetic polymers in the tubular structures did not allow for sustained mechanical viability.

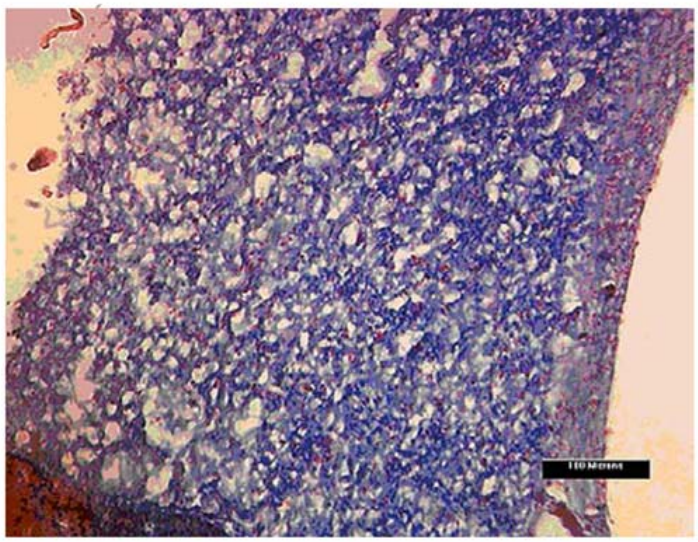

Figure 2.7. Electrospun collagen/elastin scaffold after 21 days in culture, showing extensive SMC infiltration, and a dense distribution of cells across the cross-section of the scaffold. Reprinted with permission from [59].

In a study by Buttafoco et al. [120], soluble collagen type I from calf skin and soluble elastin from bovine neck ligament were electrospun from aqueous acidic solutions in order to avoid the use of organic solvents. To ensure continuous and homogenous fibers, PEO and sodium chloride (NaCl) was added. Meshes composed of fibers with diameters ranging from 220 to 600 nm were obtained by spinning the collagen/elastin solutions. Scaffolds completely devoid of PEO and NaCl were obtained by cross-linking with EDC and N-hydroxysuccinimide (NHS). SMCs were successfully cultured on cross-linked scaffolds and a confluent layer of cells was observed after 14 days on the surface of the different scaffolds.

Combinations of collagen and elastin with synthetic polymers have also been used in order to create scaffolds with desirable mechanical properties, bioactivity, and

sustained mechanical integrity. Nanofiber scaffolds were fabricated using a mixture of 40% collagen type I, 15% elastin and 45% PLGA by weight electrospun onto a 4.75 mm diameter cylindrical mandrel. Collagen type I and movat staining were used to demonstrate a uniform distribution of collagen and elastin throughout the scaffold wall. Compliance testing results showed that the diameter change was approximately 9% for native vessels and 12–14% for electrospun scaffolds under a physiologic pressure range. *In vitro* cell proliferation of SMCs and ECs was determined by mitochondrial metabolic activity assay (MTT) and showed an average of 82% of SMCs and 72% of ECs survived on the scaffolds. Scaffolds were also implanted subcutaneously in mice to demonstrate the biocompatibility of the electrospun vascular scaffolds *in vivo*. No behavioral or visible changes of physical impairment indicating systemic or neurological toxicity were observed during the post-operative examinations or at the time of sacrifice. During the entire study period, complete blood count of the implanted animals was within normal limits. No significant lesions or evidence of particle migration in any of the major organs was observed. Histology revealed an initial minimal inflammatory response, which subsided over time [158].

In a similar study, an array of synthetic materials with 45% collagen, 15 % elastin, and 40% biodegradable synthetic (PLGA, PLLA, PCL, and poly(D,L-lactide-*co*-ε-caprolactone) (PLCL)) were electrospun. Tubular scaffolds were characterized through SEM, uniaxial tensile testing, and biocompatibility. Once again it was demonstrated that scaffold mechanical properties were improved with the addition of synthetic polymers. An interesting result of this study was the dimensional stability of the synthetic

containing scaffolds after 56 days in culture medium at 37°C, where collagen/elastin blends were completely dissolved after 28 days in medium. This demonstrated that in order for a graft to remain patent when using biopolymers such as collagen and elastin, the addition of a synthetic is necessary for sustained stability [159].

Gelatin. Gelatin is a derivative of collagen, acquired by denaturing the triple-helix structure [1, 10]. There are two types of gelatin extracted from collagenous tissue: type A, processed by an acidic pretreatment, and type B, processed by an alkaline pretreatment. The main difference between the two is that type B has higher carboxylic acid content than type A. Due to the similarities between gelatin and collagen and its natural origin, it has become an attractive polymer for tissue engineering applications. Li et al. [160] have demonstrated that the average diameter of electrospun gelatin and collagen fibers were similar, and could be scaled down to 200–500 nm. The mechanical properties of the two were also similar, with tensile strengths of 8–12 MPa, and ultimate elongations of 0.08–0.1 mm/mm. However, gelatin exhibited a higher tensile modulus than collagen fibers. In addition to similar mechanical properties to collagen, gelatin exhibits excellent biodegradability, non-antigenicity, and cost efficiency [1, 64, 65, 75]. One drawback of gelatin is that it dissolves as a colloidal sol at temperatures at or above 37ºC, and gels at lower temperatures around room temperature. However, when cross-linked, or combined with synthetic polymers, this limitation can be significantly reduced [65].

Gelatin nanofibers have been electrospun from the organic solvents HFP and trifluoroethanol (TFE), as well as formic acid, acetic acid, and water. Gelatin scaffolds, as well as gelatin/synthetic polymer scaffolds, have been gaining interest as a tissue engineering scaffold, and there have been several studies detailing their efficacy [64, 65, 67, 75, 153, 161-163]. Electrospun gelatin scaffolds have been used for applications such as wound healing [164], nerve [66], cartilage, bone [165], and dermal tissue engineering applications [166]. For vascular applications, much of the work with gelatin has been centered around its use as sealant or coating to enhance the biological properties of synthetic scaffolds. Gelatin containing grafts have displayed better biointegration than non-coated grafts, as well as excellent cellular biocompatibility and antithrombogenicity [167-170].

Much of the work published on gelatin scaffolds has been directed towards use in cardiac tissue engineering applications. Li et al. [171] electrospun gelatin with a conductive polymer, polyanaline. Pure gelatin scaffolds (8% w/v) were fabricated with fiber diameters of 800 nm, tensile strength of 5.7 MPa, modulus of 499 MPa, and an elongation of 96%. The addition of polyanaline (3% w/v at ratios of 15:85, 30:70, 45:55, and 60:40 polyanaline:gelatin) at increasing concentrations caused a decrease in the fiber diameter and an increase in the mechanical integrity of the scaffolds. Cell culture analysis done with H9c2 rat cardiac myoblasts resulted in attachment, spreading, migration and proliferation to confluence on the scaffolds. In a similar study, PLGA, gelatin, and elastin were co-electrospun at 10%, 8%, and 20% (w/v) respectively at ratios of 3:1:2 and 2:2:2 (PLGA:gelatin:elastin). These scaffolds exhibited high mechanical

properties, with moduli of 254 MPa (3:1:2 ratio) and 122 MPa (2:2:2 ratio). These scaffolds also facilitated excellent cell proliferation, morphology and penetration of H9c2 rat cardiac myoblasts and neonatal rat bone marrow stromal cells showing their ability to be used in cardiovascular tissue engineering applications [172].

Gelatin (5%, 7% and 10% w/v) has also been electrospun with PCL (1%, 7%, 5%, and 10% w/v) to create scaffolds that avoid the need for post-fabrication cross-linking. Fiber sizes were recorded at diameters ranging from 640 nm to 880 nm depending on the amount of gelatin and PCL, where an increase in the percentage of gelatin and PCL resulted in higher fiber diameters. Pore sizes of the scaffolds were measured to be 24-79 μm^2 with a tensile strength of 6.14-11.17 MPa, and a Young's modulus of 57-138 MPa. Human adipose derived stem cells were cultured on the electrospun gelatin/PCL scaffolds and demonstrated extensive cell attachment, excellent cell migration, and confluent coverage over the entire scaffold [75]. In a study done by Zhang et al. [65], a mixture of gelatin (10% w/v) and PCL (10% w/v) solutions (50:50 ratio) were electrospun to produce fibrous scaffolds with fiber diameters that ranged from 10 nm to 1 μm (figure 2.8). Mechanical testing of the gelatin/PCL scaffolds resulted in tensile strengths of 1.29 MPa, a Young's modulus of 30.8 MPa, and an elongation of 138%. These scaffolds proved to have excellent biocompatibility with bone marrow stromal cells and also aided in the process of cellular migration, proliferation, and penetration.

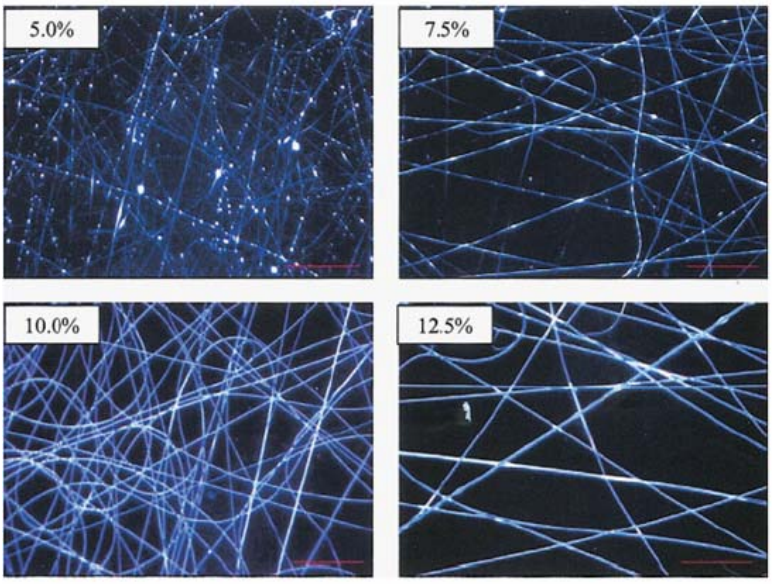

Figure 2.8. Optical microscope images of electrospun gelatin at different concentrations. Reprinted from [65].

Heydarkhan-Hagvall et al. [75] blended PCL with collagen, elastin, and gelatin biopolymers. It was observed that with increasing protein and polymer concentrations, fiber size increased proportionally but pore size decreased. In terms of mechanical properties, electrospun gelatin/PCL scaffolds displayed a higher tensile strength when compared to collagen/elastin/PCL scaffolds. All hybrid scaffolds were seeded with adipose-derived stem cells. SEM and nuclei staining of cell-seeded scaffolds showed complete cell attachment to the surfaces of both hybrid scaffolds, but cell migration into the scaffold was mainly seen in the gelatin/PCL hybrid scaffold.

An interesting alternative to bovine and porcine derived gelatin has also recently been published by Songchotikunpan et al. [163] which may prove to be beneficial as a scaffolding material for tissue engineering. Gelatin extracted from Nile tilapia was

electrospun from an acetic acid solvent or a formic acid solvent and resulted in fiber diameters ranging from 161 to 761 nm for acetic acid and 109 to 302 nm for formic acid. Mechanical properties for the pure gelatin fiber mats included a tensile strength of 2.4-4.2 MPa, Young's modulus in the range of 118-194 MPa, and the elongation of 3.3-37.6%. Gelatin scaffolds were cross-linked, which caused the mats to become stiffer, with tensile strength increasing to 4.9-10.6 MPa, Young's modulus being 366-570 MPa, and the elongation ranging from 3.3-25.7%.

Fibrinogen . Fibrinogen is a 340 kDa glycoprotein, synthesized by the liver and found freely circulating in the bloodstream which plays a major role in clotting. During the coagulation cascade, more specifically the common pathway, fibrinogen is cleaved by thrombin to cause spontaneous polymerization of fibrin monomers. Fibrin then forms lateral protofibril associations, which result in the formation of a loosely assembled clot, subsequently stabilized by covalent cross-links created by plasma transglutaminase (factor XIIIa). This stable clot not only plays a haemostatic role, but also acts as an initial scaffold for tissue regeneration, serving as a platform for cell migration and proliferation [79, 173-175].

As a protein critical to the coagulation of blood, fibrinogen is not generally thought about as a scaffold for cardiovascular engineering, but more commonly as a haemostatic agent or wound dressing. However, the effectiveness of fibrinogen as a tissue engineering scaffold has the potential to extend beyond its primary role in clotting; it is a protein with the capacity to bind a wide array of molecules that could be beneficial

from a vascular prosthetic engineering standpoint. Fibrinogen has been shown to contain RGD integrin binding sites which commonly bind FBs and ECs. Additionally, fibrinogen has demonstrated the ability to bind with high affinity to functional vascular endothelial growth factor (VEGF), fibroblast growth factor (FGF), and a number of other cytokines [79, 176-178].

The electrospinning of fibrinogen nanofibers was first published by Wnek et al. [21], and has since been demonstrated as a tissue engineering scaffold with great potential. Preliminary *in vitro* cell culture with neonatal rat cardiac FBs proved the electrospun fibrinogen scaffolds to be extremely bioactive, with cardiac FBs readily migrating through the scaffolds and depositing native collagen [78]. A similar study done with human bladder smooth muscle cells (hBSMs) also demonstrated the ability of electrospun fibrinogen scaffolds to be degraded and remodeled over a short time course, with nearly complete remodeling taking place by day 14 (figure 2.9) [179]. Similar to electrospun collagen, electrospun fibrinogen lacks the mechanical integrity to serve as a tissue engineering scaffold on its own for long periods of time [77]. However, its mechanical properties can be altered by combining fibrinogen with synthetic polymers such as PDO [180], as well as cross-linking of the scaffolds with EDC and genipin [181]. Due to the important part fibrinogen plays in the clotting cascade, its role in cardiovascular tissue engineering has yet to be determined; blood material interaction studies are needed to establish how electrospun fibrinogen scaffolds behave in contact with blood, with *in situ* evaluation required to fully understand their interaction.

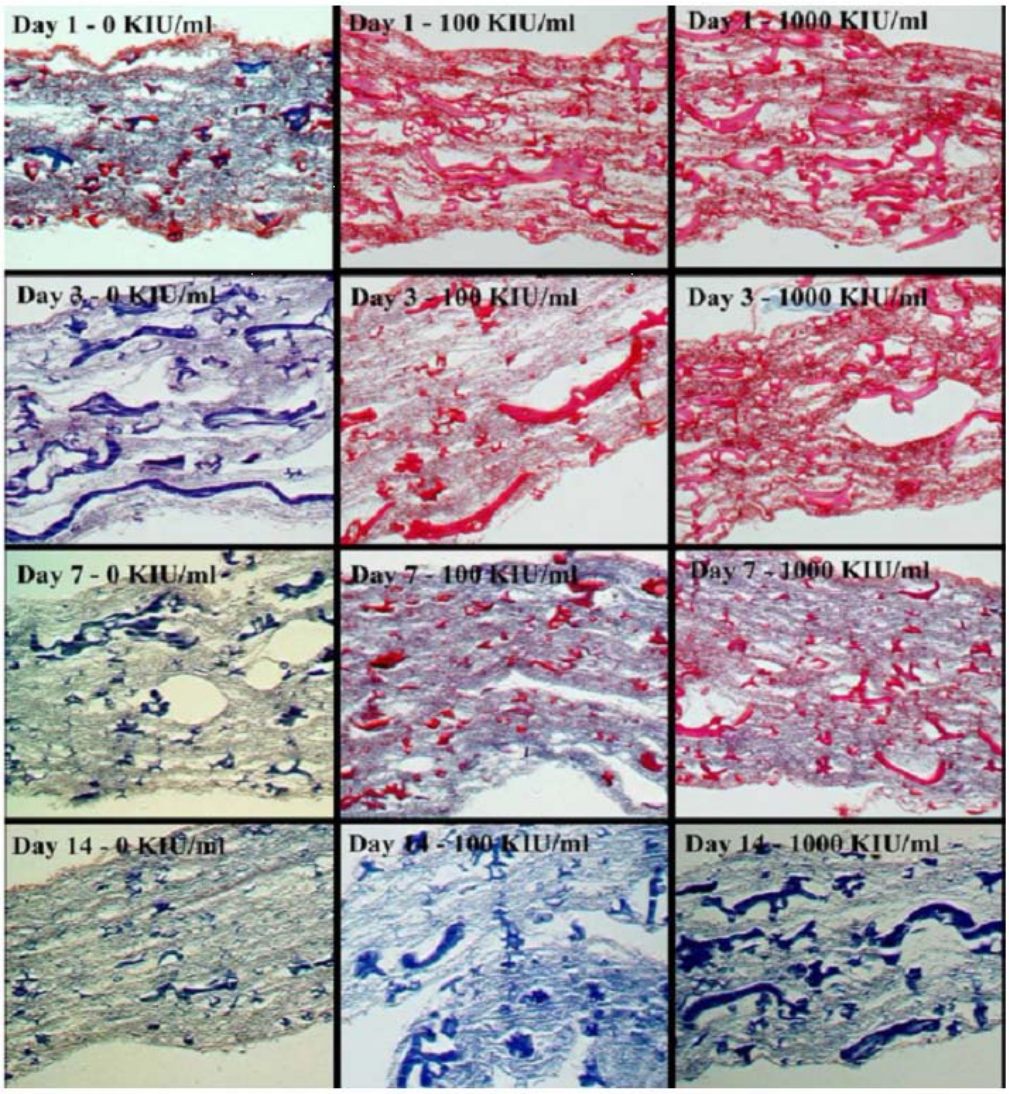

Figure 2.9. Histological evaluation of electrospun fibrinogen scaffolds seeded with hBSMs and stained with Masson's Trichrome to demonstrate the production of new collagen matrix (blue) and remodeling of fibrinogen (red). Scaffolds contained increasing amounts of aprotinin from left to right. Images at 20x. Reproduced from [179].

Silk Fibroin. Silk is an intriguing natural protein, used for centuries as a medical grade suture, which is gaining momentum as a tissue engineering scaffold due to its

unique blend of material characteristics and bioactivity. Silk exhibits excellent biocompatibility with a foreign body response comparable to other degradable sutures, hemocompatibility, and oxygen and water permeability. Silk has also been shown to break down through proteolytic degradation and be slowly absorbed *in vivo* as biocompatible amino acids, despite the fact it is listed as a non-degradable suture due to the length of time over which it degrades. The rate of degradation varies based upon implantation site and the size of the implanted fibers, but has been reported to lose the majority of its tensile strength between 6 weeks and one year after implantation. Silk also possesses remarkable mechanical properties not seen in other naturally occurring proteins [22, 80, 81]. It has been reported that natural silk fibers have tensile strength and yield at fracture values comparable to synthetic fibers such as Kevlar [82].

The use of silk fibers in tissue engineering typically refers to the use of SF. Silk, which is produced in nature by a wide variety of insects and spiders, is composed of two distinct proteins: a glue-like sericin protein, which serves to hold fibers together, and a 325 kDa fibroin filament component which acts as the mechanical backbone. The sericin protein has proven to elicit an adverse immune response inside the body, making its removal necessary for tissue engineering applications [22, 81, 82].

Historically, tissue engineering with SF has been reserved for ligament engineering applications, as both knitted constructs [83-85] and as electrospun scaffolds of reconstituted SF [86, 88-94]. These studies have demonstrated the bioactivity of SF when seeded with FBs [22, 84, 86, 91], osteoblast-like cells [22], keratinocytes [91], and bone marrow stem cells [22, 80, 81, 83, 85, 88]. However, SF has also been recently

utilized in the creation of electrospun bioresorbable vascular grafts with promising results. Zhang et al. successfully seeded electrospun SF with both human aortic endothelial cells (hAEC) and human coronary artery smooth muscle cells (hCASMC) [182]. Both hAECs and hCASMCs demonstrated an affinity for the electrospun SF. hCASMCs were shown to elongate and align themselves with SF fibers as well as produce native collagen ECM. By 7 days in cultures hAECs exhibited an interconnecting network of capillary tubes with an identifiable lumen (figure 2.10 C, D). Soffer et al. electrospun tubular SF constructs and performed tensile, creep, and burst strength studies to determine their mechanical properties [183]. SF vascular grafts demonstrated the ability to withstand native arterial pressures while behaving in a similar manner to native vessels during creep testing. While much is yet to be determined with electrospun SF vascular grafts, these two studies reveal great potential for the use of SF in the future of cardiovascular engineering.

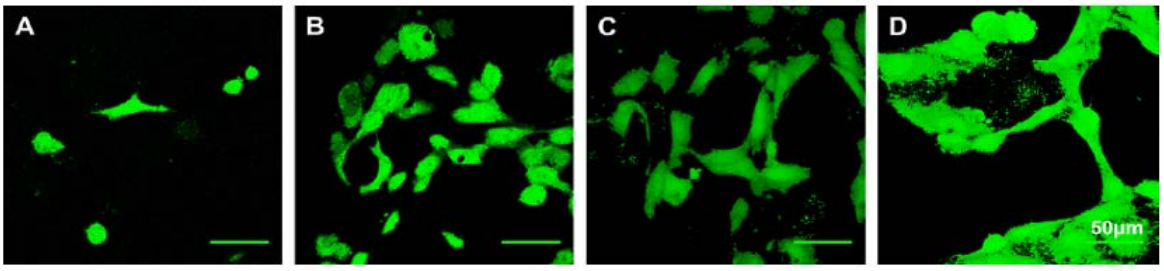

Figure 2.10. hAECs seeded on electrospun SF scaffolds. Cell viability was determined through live/dead assay at days 1, 4, 7, and 14 (A, B, C, and D, respectively). Scale bar is 50 µm. Reprinted from [182].

CHALLENGES TO BE MET

There are still many challenges that have to be met prior to the creation of an ideal vascular substitute. To date, there has not been an ideal electrospun scaffold created for use as a bioresorbable vascular substitute. Electrospinning, which does an excellent job of mimicking the architecture of the native ECM, retains many aspects that make it more of an art than a science when it comes to creating tissue engineering structures. While there is much potential in the electrospinning of biopolymers, researchers need to fine-tune the process to create reproducible scaffolds with ideal fiber and pore sizes. Our knowledge of polymers has allowed us to create electrospun structures that can be both bioactive and display sufficient mechanical properties for vascular success in a laboratory setting. However, more research is necessary to understand the *in vivo* behavior of these materials; their rate of degradation and remodeling *in situ*, as well as their inflammatory and immune responses need to be understood before they make the leap from benchtop to bedside. Finally, while our knowledge of vascular biology is growing on an almost daily basis, there is still much that needs to be done with respect to regulating the remodeling that takes place *in vivo*. We have to promote remodeling and integration of an electrospun graft at an accelerated pace, while preventing fibrosis or a chronic inflammatory response, or the premature degradation of the electrospun structure.

CONCLUSION

Despite the fact that there are still many obstacles that must be overcome in the creation of a successful electrospun biopolymer vascular graft, research from the last ten years has exponentially increased our knowledge and understanding of what is required of a vascular substitute. A decade ago the biopolymers that constitute native vessel, such as collagen and elastin, had yet to be electrospun, limiting vascular prosthetics to synthetic polymers that failed to replicate the structure or function of the native vasculature. The creation of structures made from these nanofiber biopolymers has the potential to not only mimic the structure of native artery, but also mimic the mechanical properties and behavior of native artery, thereby enhancing the success of vascular prosthetics as a whole.

CHAPTER 3 Creation of Electrospun ECM Analogues

Preface: The following manuscript appeared in Polymer International, 2007, volume 56, pages 1349-1360 [24]. The work included is a review article which provides insight into the versatility of the electrospinning process, allowing it to create ECM analogues made from a wide range of natural and synthetic polymers that have applications in nearly every part of the human body.

Extracellular Matrix Regenerated: Tissue Engineering via Electrospun Biomimetic Nanofibers

Scott Sell[1], Catherine Barnes[1], Matthew Smith[1], Michael McClure[1], Parthasarathy Madurantakam[1], Joshua Grant[2], Michael McManus[3], and Gary Bowlin[1]

[1]Department of Biomedical Engineering
Virginia Commonwealth University
Richmond, VA 23284

[2]Department of Physiology
Virginia Commonwealth University
Richmond, VA 23298

[3]Department of Urologic Surgery
Virginia Commonwealth University
Richmond, VA 23298

ABSTRACT

While electrospinning had seen intermittent use in the textile industry since the early twentieth century, it took the explosion of the field of tissue engineering, and its pursuit of biomimetic ECM structures, to create an electrospinning renaissance. Over the past decade, a growing number of researchers in the tissue engineering community have embraced electrospinning as a polymer processing technique that effectively and routinely produces non-woven structures of nano-scale fibers (sizes of 80 nm to 1.5 microns). These nano-fibers are of physiological significance as they closely resemble the structure and size scale of the native ECM (fiber diameters of 50 to 500 nm). Attempts to replicate the many roles of the native ECM have led to the electrospinning of a wide array of polymers, both synthetic (poly(glycolic acid), poly(lactic acid), polydioxanone, polycaprolactone, etc.) and natural (collagen, fibrinogen, elastin, etc.) in origin, for a multitude of different tissue applications. With various compositions, fiber dimensions, and fiber orientations, the biological, chemical, and mechanical properties of the electrospun materials can be tailored. In this review we highlight the role of electrospinning in the engineering of different tissues and applications (skin/wound healing, cartilage, bone, vascular tissue, urological tissues, nerve, and ligament), as well as discuss its potential role in future work.

INTRODUCTION

Significant tissue engineering research is based on the creation of scaffolds that simulate the body's native ECM. [184, 185] The ECM is a complex arrangement of proteins and polysaccharides such as collagen, hyaluronic acid, proteoglycans, glycosaminoglycans, and elastin. These ECM components are constantly synthesized, secreted, oriented, and modified by the cellular components that they support. Classically, the function of native ECM was only believed to be as a structural framework for tissues. However the ECM, through interaction with receptors on the surfaces of cells, directly takes part in promoting cell adhesion, migration, growth, differentiation, and apoptosis. The ECM also plays a role in cytokine activity and intracellular signaling, both of which serve numerous functions in cell regulation and activation. [5, 16]

Ideally, to create a tissue engineered scaffold capable of the regeneration of fully functional tissue, one would like to mimic both the fibrillar form and the complex function of the native ECM. [11, 17, 18] To attain a successful ECM analogue scaffold, there are several design and material criteria that must be met. First and foremost, the scaffolding material should be subjected to the same standards as any other biomaterial implanted in the body, namely, the scaffold should not initiate any adverse tissue or immune reactions. For many applications, scaffolding materials should be biodegradable or bioabsorbable at a rate that will allow for their gradual incorporation into the surrounding tissue without any fibrous encapsulation or residual evidence of their

presence. [11, 17] To be ideal, this ECM analogue would need to mimic the topographical features and geometry on the macro-, micro-, and even nano-scale levels, as each influences cell response to the scaffold. [25] Native ECM is composed of nano-scale fibers that offer structural integrity to tissues. Electrospinning (figure 3.1) allows for the creation of ECM analogue scaffolds composed of nano-scale fibers, which creates a very high surface area to volume ratio to support cell growth and infiltration. [18, 186] In addition, the morphological similarities between the nanofibrous structures and the native ECM are believed to improve cellular response and overall biocompatibility. [16, 18] A study by Sanders et al. showed that electrospun scaffolds composed of micro-scale and smaller diameter fibers resulted in little to no fibrous encapsulation when compared to larger diameter fibers. [187]

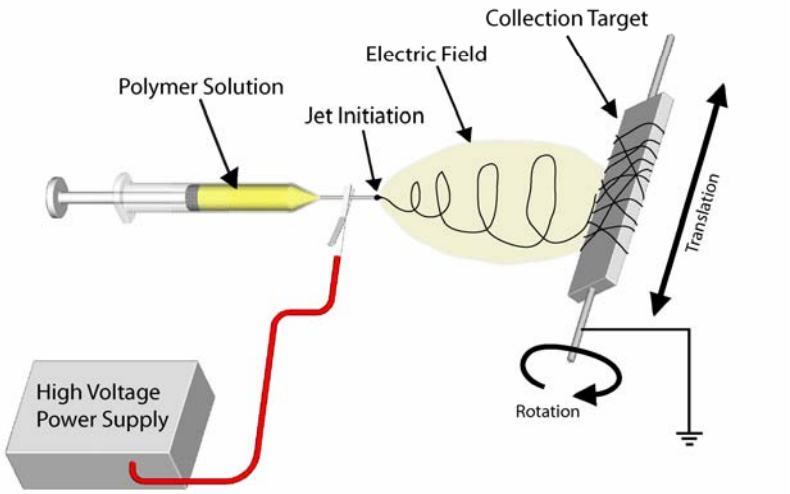

Figure 3.1. Generic electrospinning setup depicting the major components of the electrospinning process, including a high voltage power supply, polymer solution, and grounded collection target.

APPLICATIONS FOR ELECTROSPINNING IN TISSUE ENGINEERING

Skin / Wound Healing. Skin is the body's largest organ, and functions foremost as a barrier, preventing pathogens from entering the body. It is also a sensory organ and a regulator, gauging water retention and heat loss. Skin is composed of two layers, the epidermis and dermis (figure 3.2). [188] The epidermis is composed of five strata, with the most proximal layer, the strata germinativum, providing germinal cells for regeneration of the four other layers. The regeneration of this layer is of extreme importance in understanding and promoting wound healing. The underlying dermis is composed of two regions, the papillary dermis and the deeper reticular dermis. These layers are composed primarily of FBs, which secrete ECM proteins such as collagen and elastin, however macrophages and lymphocytes are also present. [189, 190] It is this unique structure that gives skin its distinctive biomechanical properties.

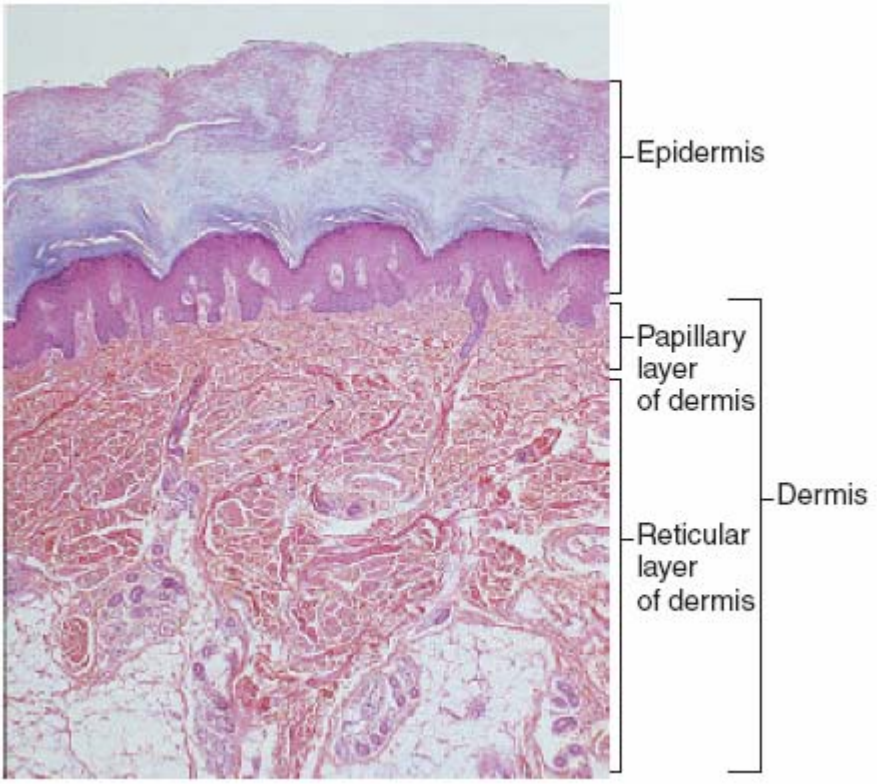

Figure 3.2. Picture of histology demonstrating the main layers of skin, the dermis and epidermis. Reprinted from [191].

Severe burns, pressure ulcers, and other chronic ulcerations pose hurdles to caregivers and are costly to treat. Healing tissue undergoes several stages: hemostasis, inflammation, proliferation, and remodeling. [192] Although tissue engineered aids to wound healing can be applied to a variety of dermal maladies, they do not replace the stages of wound healing. Rather, they aid endogenous wound healing, and are ultimately replaced by native tissue. [193]

Tissue engineering of skin poses many challenges to researchers. Autografts and allografts are effective, but their use is limited due to their inherent limited supply and

cost. Current wound dressings use material from a variety of natural and synthetic sources. Many successful skin grafts utilize natural ECM proteins. Collagen, in particular, has been used extensively in many successful wound dressings. Alloderm™ is an autograft that uses acellular matrix cultivated from cadavers. Integra™ is a temporary dressing composed of type I collagen and glycosaminoglycans (chondroitin-6-sulfate). Dermagraft™ and TransCyte™ both use cultured neonatal foreskin FBs on synthetic polyglactin and nylon fiber, respectively. Apligraft™ and Orcel™ are both skin equivalents made from bovine collagen. Despite their successes, many of these treatments are still expensive, and they do not fully replace damaged skin, thus new inroads to the resolution of these problems must be made [188, 190, 194].

Electrospinning has great potential for contributing to the field of skin tissue engineering. This process produces scaffolds that are highly conducive to cell infiltration, attachment, and activity while also providing structural support for regenerating tissues. [185] Electrospinning allows for the control of pore size and polymer diameter and thus provides a greater degree of control over cell infiltration. [28, 195] This makes electrospinning relevant to wound healing, as these properties are highly desirable in the development of wound dressings. [190] Electrospun synthetic materials, such as polyurethane membranes, already demonstrate effectiveness as wound dressings [21]. In addition, electrospun polystyrene scaffolds were found to promote natural FB and keratinocyte self-organization in the absence of any external cues. [196]

Several natural polymers that are important considerations for inclusion in wound dressings have been electrospun, including collagen, fibrinogen, and hemoglobin. [19, 21,

135] Recently in our laboratory, the globular proteins hemoglobin and myoglobin were successfully electrospun into fibrous mats (figure 3.3). The significance of this achievement, with regard to wound dressings and skin regeneration, is that the inclusion of hemoglobin in wound dressings may help to deliver oxygen directly to the healing tissues. Made possible by the high surface area-to-volume ratio of electrospun scaffolds, electrospun hemoglobin contains approximately the same number of hemoglobin molecules per unit volume as a red blood cell (based on the concentrations of hemoglobin electrospun, i.e. 150 mg/mL and 225 mg/mL); thus electrospun hemoglobin mats have the potential to supply approximately the same oxygen per unit volume as a functional red blood cell. [135]

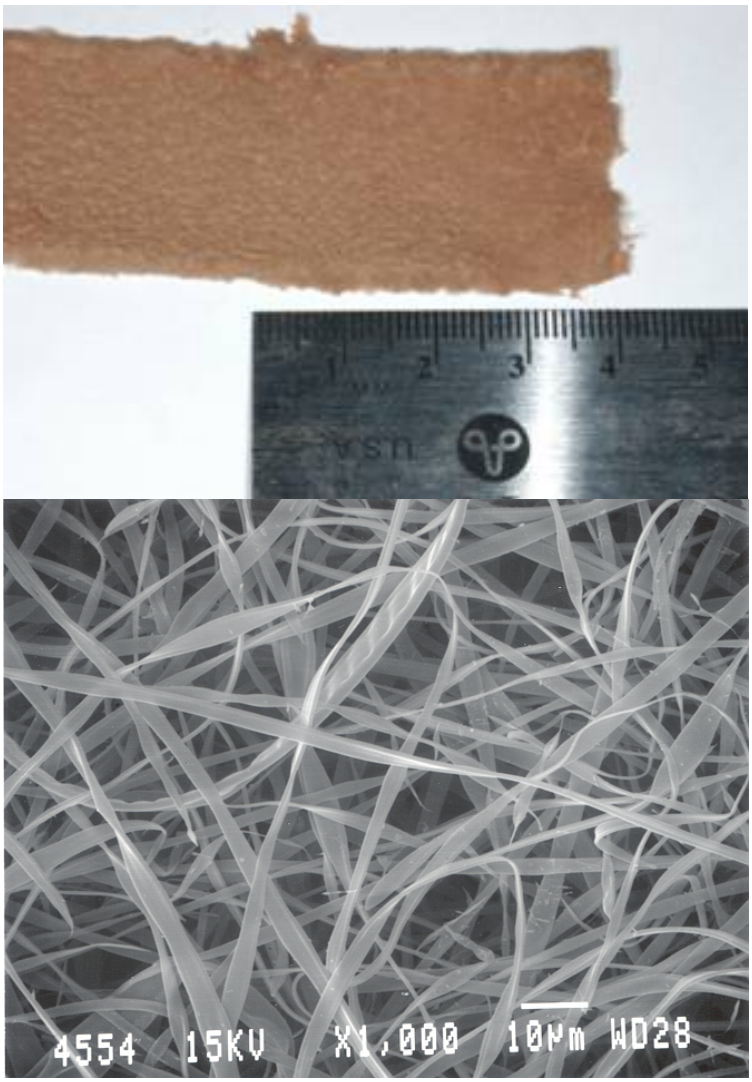

Figure 3.3. Photograph (top) and scanning electron micrograph (bottom) of a hemoglobin scaffold electrospun from a 175 mg/ml solution.

Blends of natural and synthetic polymers have also been successfully electrospun and proven applicable for use in dermal substitutes. [197] Additionally, electrospun materials offer added benefits of drug delivery and controlled release. [198] Future work in this area should focus on combinations of these desirable components into multifunctional scaffolds, including incorporation of analgesics for pain relief,

hemoglobin for increasing oxygen delivery to healing tissues, and fibrinogen for hemostasis and adhesion, and synthetic materials for additional mechanical integrity.

Cartilage. Articular cartilage is a thin layer of connective tissue covering synovial joint surfaces. In normal physiologic conditions, articular cartilage is porous and highly hydrated. Articular cartilage functions to absorb energy, distribute loads uniformly between bones, and provide low-friction articulation. [199] Cartilage can be considered a fiber-reinforced composite material, that is both non-homogeneous and anisotropic, consisting of two major structural macromolecules (collagen, mainly type II, and proteoglycans), cells, water, and solutes including ions and nutrients. [200, 201] Collagen and proteoglycan macromolecules are intertwined to form a solid structure that is anchored to the subchondral bone and through which water and solutes move freely in and out of the tissue to provide nourishment to the thinly dispersed cells (known as chondrocytes) as well as mechanical support and lubrication to the joint. For normal human articular cartilage the compressive modulus is 0.79 MPa and the tensile modulus ranges from 0.32 to 10.2 MPa depending upon direction and location (i.e. depth) of testing. [200, 202, 203]

Mature articular cartilage is aneural, avascular, and alymphatic. [204] Hence, articular cartilage has a limited capacity for repair and regeneration, and in situations of trauma, overuse, or misuse, degenerative changes may occur that can eventually lead to the development of osteoarthritis (OA). [205] Early changes seen in OA include a disruption in the collagen fiber network (such as loosening), changes in proteoglycan

properties (such as disaggregation or swelling), and changes in the collagen-proteoglycan interactions. [200] There are numerous autologous and allogeneic therapies and tissue grafts/transplantations that have been investigated for the therapeutic treatment of articular cartilage defects, all of which have had varying results. [201, 205-213]

Because of the inability of cartilage to regenerate when injured, tissue engineering holds much promise in the repair of larger cartilage defects. The tissue engineering of articular cartilage commonly involves using a three-dimensional scaffold onto which articular chondrocytes or their precursor cells are seeded (sometimes with the addition of growth factors) in order to grow a three-dimensional tissue that can be implanted into the joint defect. The goal is *in vitro* chondrogenesis within the cell-electrospun scaffold construct that matches native *in vivo* chondrogenesis. Such *in vitro* chondrogenesis is dependent upon cell type, initial cell density, scaffold characteristics, and culture conditions.

There are a number of natural materials utilized in scaffold materials to fill cartilage defects, including fibrin, agarose and alginate hydrogels, collagen (gels, sponges, and fibrous scaffolds), chitosan hydrogels and molded porous structures, and hyaluronan. [206, 208-210, 214] Of the synthetic materials utilized as scaffolds for articular cartilage tissue engineering, the most widely used are PLA, PGA, and their copolymers. [202, 206, 208-210, 213, 214] These scaffolds can be produced in the forms of foams, hydrogels, woven and nonwoven fiber meshes, or multi-phase structures. [206, 215] Though the choice of scaffold has not been agreed upon, there is consensus that mechanical stimuli are necessary in the tissue engineering of articular cartilage. [208,

216, 217] Bioreactors have become quite popular since they allow the control of *in vitro* culture conditions (including biochemical factors in the growth medium) and provide low-shear mechanical stimuli to cells (figure 3.4). [201, 208, 213, 218]

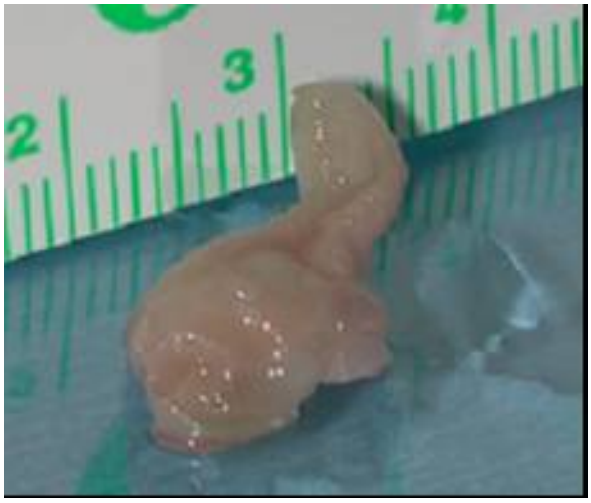

Figure 3.4. Articular cartilage sample developed from normal human chondrocytes and electrospun collagen type II in a slow turning lateral vessel bioreactor.

Thus far, many scaffolds tested have not resulted in regenerated tissue with the biomechanical or morphological properties native to that of normal articular cartilage. [206] Due to limited availability of suitable donor tissue and the desire to match the mechanical properties of the implant with the mechanical requirements *in vivo*, investigators have recently become interested in designing electrospun scaffolds for the tissue engineering of articular cartilage. Type II collagen was first electrospun for potential use in cartilage tissue engineering by Matthews et al. using HFP as the solvent to produce fibrous scaffolds (with mean fiber diameters of 110 and 1750 nm). Following

cross-linking in GLUT vapors, seeding with normal human articular chondrocytes, and two weeks in a rotary cell culture system, there was a nearly confluent layer of cells on the external seeded surface with some observable degree of remodeling of the matrix. [219] Shields et al. electrospun type II collagen in HFP; the scaffolds were cross-linked with GLUT vapor and seeded with adult human articular chondrocytes (statically cultured for 7 days). Chondrocytes adhere and proliferate throughout the thickness of the scaffolds [220]. Our laboratory has recently electrospun type II collagen (extracted from fetal bovine articular cartilage) at concentrations between 60 mg/ml and 120 mg/ml in HFP resulting in mean fiber diameters ranging from 107 to 446 nm (unpublished data), as shown in figure 3.5. The lower end of these average fiber diameters approach the 80 nm fibers that make up native articular cartilage.

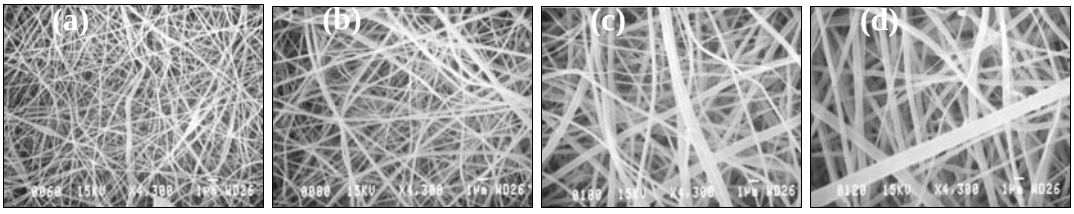

Figure 3.5. Scanning electron micrographs of electrospun type II collagen at (a) 60 mg/ml, (b) 80 mg/ml, (c) 100 mg/ml, and (d) 120 mg/ml (1 μm scale bar, 4300X magnification).

Several other materials have also been electrospun for the tissue engineering of cartilage. Bhattatai et al. electrospun alginate-PEO in water solutions to create scaffolds with mechanical properties within the range of articular cartilage following cross-linking with calcium chloride. Cellular compatibility was investigated (3 days) with

chondrocytes and resulted in the cells attaching well, forming clusters, and maintaining their round morphology. [221] Li et al. electrospun PCL in tetrahydrofuran (THF) and dimethylformamide (DMF) (producing 700 nm diameter fibers) to investigate the responses of fetal bovine chondrocytes *in vitro*; the cells appeared round, adhered to and extended along the fibers, and expressed cartilage-associated ECM genes. [109] In another study, Li et al. seeded electrospun PCL scaffolds with human bone marrow derived MSCs and maintained these in medium supplemented with recombinant human transforming growth factor-β1 (TGF-β1) prepared to promote chondrogenesis. In the presence of TGF-β1, the PCL scaffold induced greater expression of sulfated glycosaminoglycan synthesis and collagen types II and IX were up-regulated; the cell count remained constant after 21 days. [108] Recently, Li et al. electrospun different poly(α-hydroxy ester) polymers, including PGA, PLA, copolymers of the two, and PCL. For the PLLA and PCL scaffolds, which had the lowest Young's moduli (uniaxial tensile testing) of the polymers investigated and maintained their fibrous structure following a 42 day degradation analysis, the seeded chondrocytes adhered to the fibers and began migrating through pores during the 7 days of incubation. [222] Shin et al. electrospun the copolymer PLGA in DMF and THF (producing a mean fiber diameter of 550 nm and a porosity of 81 %). Tensile testing of dry samples revealed a mean tensile modulus of 95.5 MPa, a mean ultimate tensile stress of 3.1 MPa, and a mean ultimate tensile strain of 79 %; there was little degradation of this scaffold even after 7 weeks of incubation. [223] Chitosan was mixed with a small amount of PEO in an undisclosed solvent and electrospun by Subramanian et al. Tensile testing of wet samples gave results of 2.3 MPa

for the modulus and 0.6 MPa for the ultimate tensile strength. Following cell seeding, canine chondrocytes attached to the fibers of the scaffold; cell growth was not inhibited by the electrospinning reagents or process. [224]

Bone. The skeletal system provides structure to the body, protects internal organs and acts as a reservoir of calcium and phosphate. In spite of its perceived inert role of providing rigid structural support, it is extremely plastic in its ability to adapt to ever changing loading conditions, and its remarkable ability to regenerate without scar formation in adults following injury makes it unique. However, the intrinsic ability of bone to regenerate is limited by the size of the defect. Early studies established a threshold-critical sized defect, beyond which regeneration is limited and fibrous ingrowth occurs. Numerous instances (birth defects, comminuted and non-union fractures, tumor resections) occur in clinical practice when the threshold is surpassed and external intervention in some form becomes necessary. [225-227]

The replacement of lost bone tissue has taken a variety of forms: metals, ceramics, polymers and bone itself, none of which has proven to be ideal. Inadequate supply and risk of disease transmission limits the use of autografts and allografts. Metals and ceramics replace only the structural function of the lost bone tissue and lack the ability to be resorbed, therefore needing to be removed at a later date. Tissue engineered solutions containing cellular components and resorbable electrospun scaffolds offers enormous promise to restore tissue function without a need for removal. Electrospun scaffolds are economical, easy to produce and can be fabricated into highly

interconnected porous scaffolds that permit cellular infiltration and vascular ingrowth. The diversity electrospinning affords has resulted in scaffolds created from both ceramics and polymers, and various composites of the two. [228]

Bioactive glasses are an interesting class of ceramics that can form chemical bonds with the host bone at the interface. Such materials are used in bone replacement therapies; predominantly in bulk form. In one study, a precursor solution containing calcium and phosphate was mixed with a high molecular weight polymer (undefined by author) and electrospun. Subsequent heat treatment and calcination decomposed the polymer to yield pure HA fibers. [229] Kim et al., electrospun sol-gel precursor solution mixed with polyvinyl butyral to generate nanofibers of HA and fluoridated apatite (fHA). The fibers were heated to remove any polymer components and to induce crystallization of HA and fHA. [230] Subsequently, they developed a novel composite by hybridizing heat treated electrospun bioactive glass nanofibers with reconstituted type I collagen solution. The sol was processed differently and lyophilized to yield either membranes or thick scaffolds. Incubation of these scaffolds in simulated body fluid for 7 days resulted in formation of nanocrystalline carbonated apatites (CA) that were chemically bonded to the scaffolds. Osteoblasts cultured on bioactive scaffolds showed enhanced function (alkaline phosphatase assay) compared to those cultured on collagen scaffolds. [231] Other ceramics with potential for tissue engineering are the bioinert Alumina and stabilized Zirconia, which have been used for total hip replacements because of their superior mechanical properties and excellent biocompatibility. A recent study proved the possibility of electrospinning zirconia (2-30 wt%) from an aqueous based suspension of

PEO:PEG (1:2 weight ratio), and it would be interesting to observe if the results could be exploited in tissue engineering. [232]

A number of different polymers have been electrospun for use in bone engineering, both synthetic and natural in origin. PCL has been one of the most popular synthetic polymers used for bone engineering scaffolds because of its biocompatibility, slow degradation, and the ease of electrospinning from a variety of solvents. MSCs from rats cultured on electrospun PCL scaffolds, supplemented with osteogenic media for 4 weeks, showed complete penetration of the scaffolds with the formation of multilayers. Mineralization and type I collagen were detected by the von Kossa protocol and immunostaining, respectively. [47] Incorporation of calcium carbonate and HA powders to the polymer solution have resulted in slight increases in the mechanical properties and fiber diameters but have not affected the biocompatibility. [233]

Another class of synthetic polymers recently electrospun is phosphazenes, which were first introduced for tissue engineering applications in the early nineties. [234] Laurencin et al., successfully electrospun a solution of polyphosphazene that was loaded 50-90% w/w with nano-crystalline HA and concluded that incorporation of nano HA (nHA) was maximal with a theoretical loading of 50%. [235]

Chitin is the planet's second most abundant carbohydrate; chitin and its deacetylated product chitosan have been long recognized for their antifungal properties and ability to induce protease inhibitors in plants.[236] Recent evidence points to the role of chitin in the induction of interleukins (IL), FBs, and angiogenesis, [237] suggesting a role in immunity. Blends of chitosan and PEO from acetic acid solutions

have been successfully electrospun. [238, 239] A preliminary investigation into a 90:10 PEO:chitosan blend showed that the scaffold was non-toxic and osteoblast spreading in culture was optimal, as evaluated by SEM after 5 days. The cells developed discrete filopodia and exhibited long microvilli on their surfaces, which attached to and grew along the polymer nanofibers. The authors concluded that the cells adhered to and maintained characteristic morphology indicative of phenotype. [240]

Electrospinning of SF solutions blended with PEO was first reported by Jin et al., for the generation of submicron sized fibers. [88, 89] In a later study, SF-PEO based blends were electrospun with or without bone morphogenetic protein 2 (BMP-2) and nHA, seeded with human MSCs, and cultured for 4 weeks. Significantly higher levels of calcium deposition, DNA content, and elevated levels of mRNA bone marker transcripts were observed in silk:PEO scaffolds functionalized with BMP-2 and HA. These findings suggest electrospun silk-based scaffolds can be used as delivery systems for cytokines and growth factors. [241]

Vascular Tissue. The capabilities of electrospinning to mimic the microenvironment of a cell are especially important when dealing with vascular grafts. The dynamic situation of a blood vessel creates a complicated sequence of events in which the walls are stretched and the inner lumen is sheared. A microenvironment capable of withstanding these forces with minimal energy loss is essential for proper blood vessel functioning. Electrospinning of polymer fibers into a vascular conduit has

been demonstrated to be a potential technique that not only creates scaffolds simulating the ECM, but also contributes tailorable mechanical properties (figure 3.6).

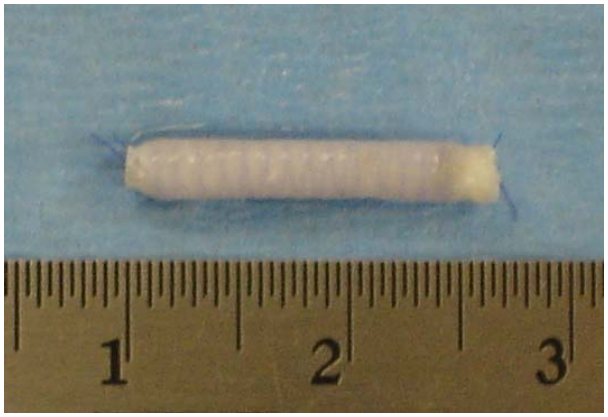

Figure 3.6. 1.8 mm I.D. reinforced PDO-elastin tube with imbedded PDS-II suture windings for possible use as a small-diameter vascular graft.

Currently, the most common vascular materials are Dacron (PET) and e-PTFE. Dacron is widely known for its use in aortic and iliac grafts. Its success in these areas of the body is due mainly to larger diameters and flow rates, which are not conducive to thrombus formation and the subsequent decrease in luminal diameter. However, for a small diameter graft of 5 mm or less, the following properties must be attained for successful grafting to occur: biocompatibility, lack of chemical reactivity, very low thrombogenicity, porosity, and mechanical strength, including compliance matching that of native artery and resistance to aneurysm formation. [59, 242, 243]

Inner luminal wall thickening and subsequent occlusion and loss of blood flow in vascular grafts is one of the most critical concerns when designing a vascular prosthetic. Mechanical problems such as compliance mismatch between the natural vessel and

prosthetic contribute to this effect, and are a key component to the creation of a successful vascular graft. Recently, our laboratory performed compliance testing of electrospun PDO and elastin in an effort to match natural arterial compliance. Various ratios of PDO:Elastin were electrospun and tested in a bioreactor with internal pressures changing cyclically from 120 mmHg to 80 mmHg at 60 Hz, where a blend of 50:50 showed particular promise (figure 3.7) [20]. Vaz et al. selected two different polymers to be electrospun together, PCL and PLA, and characterized their properties through uniaxial tensile testing. [244] Testing of the circumferential dilation of electrospun segmented polyurethane (SPU) scaffolds by Matsuda et al. demonstrated the dependence of scaffold compliance on mandrel rotation, as scaffolds created with a high degree of rotation were less compliant. [245] Enhancement of the mechanical properties of electrospun PLLA was demonstrated by Lee et al. This unique approach to biomaterial production involved adding a small quantity of nano-sized montmorillonite (MMT) platelets to increase mechanical and physical properties. [246]

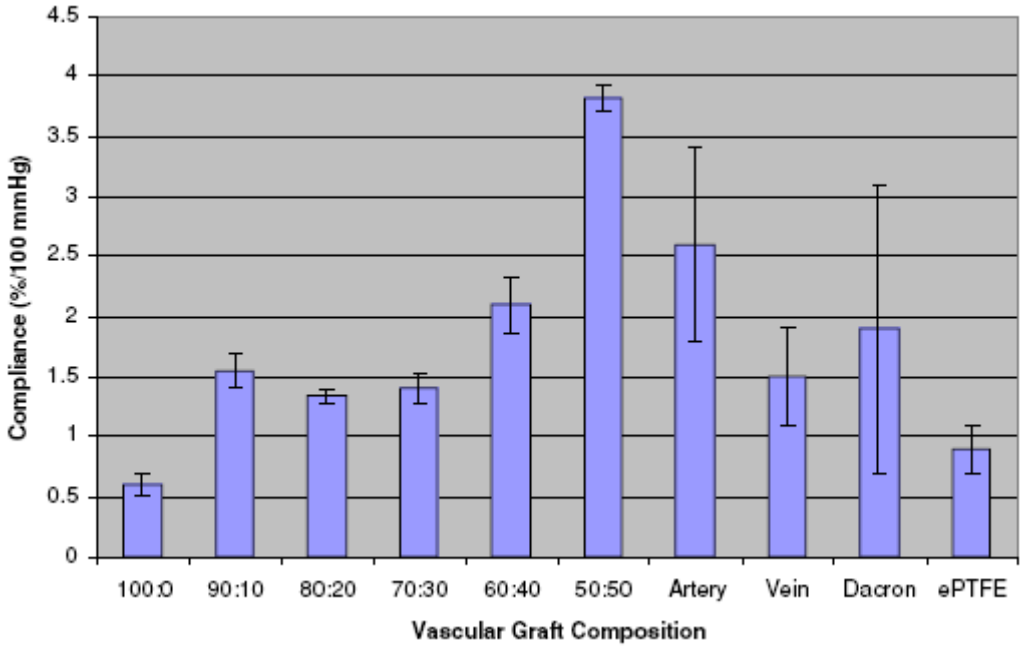

Figure 3.7. Compliance determined for a 120/80 mmHg cyclic internal pressure change (93.33 mmHg Mean Arterial Pressure (MAP)) for various vascular graft compositions. Reprinted from [20].

Immunogenicity of the materials must also be taken into consideration so as to decrease polymer degradation and protein encapsulation. A commonly used commercial suture, PDS, with good immunological properties was electrospun by Boland et al. [48] and mechanically tested at different concentrations. Others, however, have examined scaffold interaction on cell morphology with FBs, SMCs, or ECs. [142]

Biodegradable nanofiber mesh polymers were developed in one instance to maintain the phenotype and functions of hCAECs. The study found that ECs seeded onto electrospun poly(L-lactic acid)-co-poly(epsilon-caprolactone) (P(LLA-CL)) grew in the direction of the fiber itself, indicating a potential material for effective endothelialization. [247] PCL and polyurethane (PU) fibers were electrospun on a mandrel and tested for

EC attachment; ECs formed monolayers and expressed PECAM-1, a cellular adhesion molecule. [248] However, excessive cellular proliferation can also cause occlusion and graft failure. Mitigation of this aspect was studied by Luong-Van et al. where they used PCL fiber mats for controlled delivery of heparin. It has been suggested that a controlled release of heparin to the local adventitial surface of a graft could reduce the severity of intimal hyperplasia. [249] Surface properties of biomaterials, such as surface roughness, affect cell behavior and may induce thrombotic clots in some cases. Researchers have found that rough and smooth surfaces will encourage different types of cell adhesion. [250] Xu et al. electrospun PLLA and compared its surface roughness characteristics to a solvent cast PLLA scaffold. The results demonstrated that electrospun PLLA had a higher surface roughness than the solvent cast and cell number and attachment was greater on solvent cast PLLA than on electrospun PLLA. [250] This demonstrates that through electrospinning and the creation of non-woven fibers, surface roughness and cellular adhesion can be significantly altered.

In addition to using biodegradable and synthetic polymers, vascular graft development has incorporated the addition of natural polymers such as collagen (types I and III) and elastin, the major components of the native vascular ECM. Matthews et al. successfully electrospun collagen types I, II, and III out of HFP and demonstrated that cells seeded onto the scaffolds were viable. [19, 219] Others have taken this technology a step further, combining all ECM components of a blood vessel to create a graft material. Both Boland et al. [59] and Buttafoco et al. [120] electrospun soluble collagen and soluble elastin together to form a fibrous vascular graft material Buttafoco et al.

demonstrated that the combination of soluble collagen type I and elastin with a high molecular weight polymer such as PEO could allow native polymers to be electrospun from non-organic solvents. Boland et al. investigated soluble collagen types I and III and elastin and the effects of the electrospun structure on cellular culture in a rotary bioreactor. Both studies examined cross-linking methods: GLUT vapor, which can sometimes be problematic because of its cytotoxicity [59] and EDC in the presence of NHS, which is known to be non-cytotoxic. [120]

The chemical composition, construction parameters and biomechanics of a vascular graft influence its interaction with its host. The differences of graft materials, porosity, compliance, electrical charge, and surface texture all contribute to the magnitude and characteristics of the body's inevitable "foreign body" reaction. [251] The site of anastomosis between relatively compliant arteries and noncompliant grafts represents sites of flow disruption and complications with graft construction. New theories on ways to alleviate the problems are being tested, but so far nothing has arisen as an efficient replacement.

Urological Tissue. The need for urinary tract reconstruction can result from a large variety of urologic disorders such as stricture disease, cancer, trauma and congenial anomalies that may affect the ureters, bladder or urethra. Complications from inserting autologous tissue, such as enteric segments, into the urinary tract are well known and often manifest as metabolic and histopathologic abnormalities. These sequelae have motivated investigators to search for tissue-engineered alternatives.

The first use of electrospun scaffolds in urologic tissue engineering was reported in 2004 using a blend of elastin and PLA. [11] This feasibility study demonstrated that electrospun elastin:PLA scaffolds would support the growth of seeded neonatal rat BSMs. BSMs formed single to multiple cell layers with some areas of penetration through the scaffold surface. Histological evaluation also demonstrated intense staining concentrated beneath the cell-scaffold interface suggesting cellular production of ECM.

After the initial description of electrospinning fibrinogen [21], preliminary cell culture work was done with neonatal rat cardiac FBs (CFB) [78]. In comparison to the elastin culture, the CFB migrated into the fibrinogen scaffold more readily. More complete feasibility studies confirmed these preliminary results and demonstrated that neonatal rat BSMs (unpublished data) and cardiac FBs rapidly migrated into and remodeled electrospun fibrinogen scaffolds with deposition of native collagen fibrils. Follow-up studies demonstrated similar results when electrospun fibrinogen scaffolds were seeded with human BSMs (unpublished data). The caveat to these studies was that aprotinin, a protease inhibitor, was required to inhibit scaffold degradation during cell culture. [77]

In an effort to develop a scaffold for direct implantation and tissue regeneration, rather than *in vitro* cell culture, composite fibrinogen-PDO electrospun scaffolds were investigated (unpublished data). Blending natural and synthetic polymers has been used previously to add structural integrity to electrospun natural polymer scaffolds. This study was able to demonstrate that an electrospun fibrinogen-PDO composite scaffold could retain the superior cellular interaction of fibrinogen while producing a product with

functional strength for direct implantation. Uniaxial mechanical testing further demonstrated that stress-strain properties could be controlled in a predictable fashion by adjusting the polymer concentration ratio. Animal implantation studies are planned, but results are not yet available.

An acellular urinary bladder matrix has also been described utilizing electrospun cellulose. [252] Electrospinning conditions (solution flow rate and electric field strength) were varied to create multilayered scaffolds in a single-step production technique. Evaluation by SEM demonstrated a multi-layered scaffold that closely resembled porcine bladder ECM (figure 3.8).

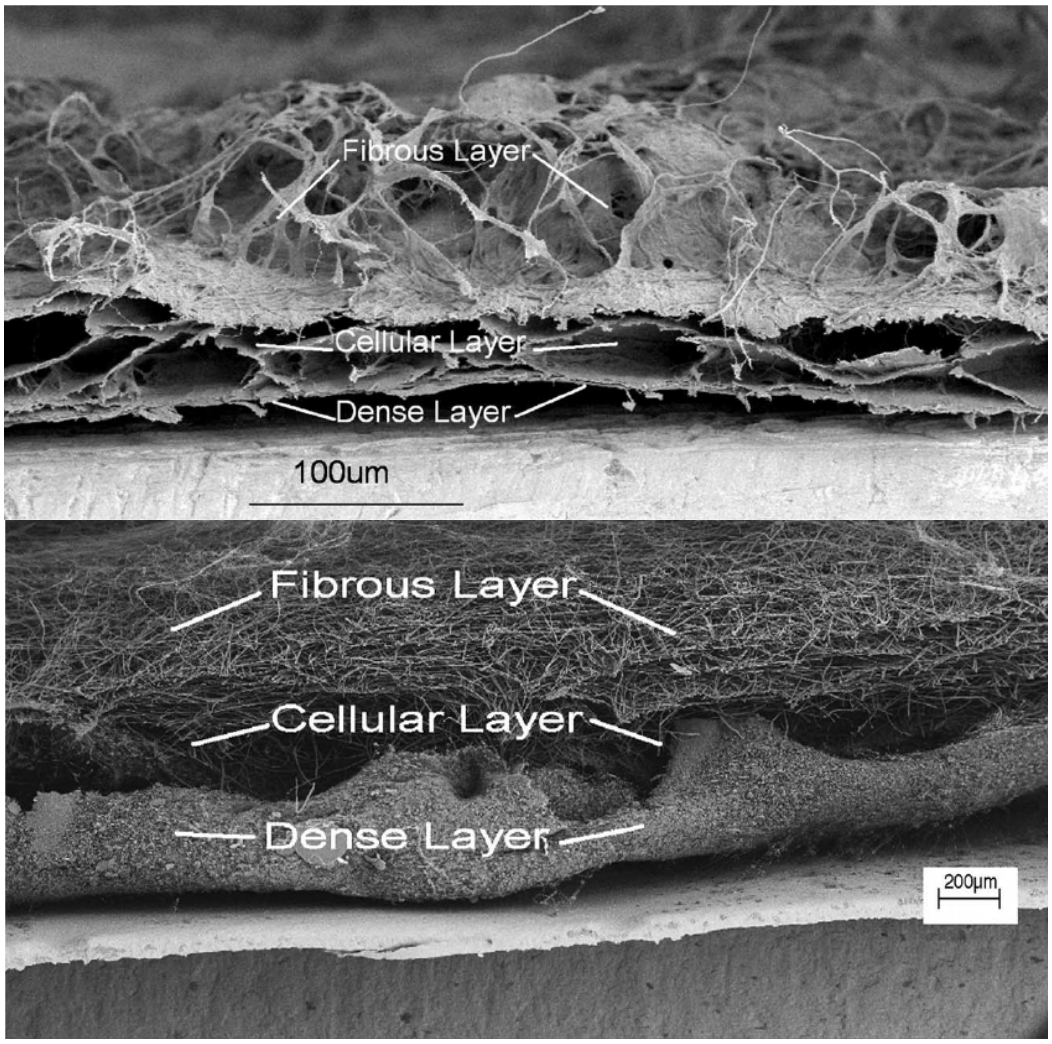

Figure 3.8. Cross sectional views of a porcine urinary bladder matrix (top) and an electrospun urinary bladder matrix mimicking scaffold composed of cellulose acetate (bottom). Reprinted from [252].

Electrospun polystyrene scaffolds have also been evaluated utilizing BSMs. [253] These scaffolds were not specifically studied for urologic tissue engineering purposes, but they were shown to support BSM growth, and argon plasma treatment resulted in a significant improvement in cell attachment after seeding.

There is only one report of electrospinning scaffolds for renal tissue engineering. [254] Polyamide was electrospun onto glass coverslips and seeded with normal rat kidney (NRK) cells. NRK cells grown on the electrospun polyamide demonstrated increased actin and vinculin fiber formation compared to NRK cells grown on a glass coverslip alone. The NRK cells grown on electrospun polyamide also produced long, slender aggregates of beta-1 integrin compared to the classical punctuate, focal adhesions seen when cultured on two-dimensional substrates.

Nerve. The tissue engineering of nerve represents a significant challenge to the field of tissue engineering. Research into understanding and controlling nerve regeneration is one of the most urgently needed areas of modern medicine. The solution may lie in the ability of the peripheral nerve to regenerate, or why olfactory neurons are the only type of neuron to undergo neogenesis every few weeks. Either way, perhaps one day there will be some breakthrough, and those with nerve injury (including such central nervous system injuries as spinal cord) will have some hope at restoring normal function.

Among the main components of peripheral nerve tissue are unmyelinated or myelinated axons, Schwann cells, capillary wall ECs, and connective tissue made up of collagen fibers. [255] It has been suggested that there are four essential components to the effective regeneration of peripheral nerve: the use of growth permissive scaffolds, stimulatory ECM proteins, the incorporation of growth factors (such as nerve growth factor, NGF) and the presence of Schwann cells or glial cells. [256] Of these, the major focus recently has been on scaffold development.

A vast majority of the focus in nerve regeneration has centered on the creation of nerve guidance conduits of various compositions. [257-261] The use of nerve guides to aid nerve regeneration extends back to the late 1800s, when arteries and veins were used in nerve repair applications, but these were met with little or no success. [262] Advances in the 1960s led to the use of silicone elastomer tubing, which was able to support regeneration in several mammalian species. Current investigations into the use of biodegradable polymers for guidance conduits may offer alternatives to current treatment options. Surprisingly, the application of electrospinning to this field is relatively new.

Yang, et al. [43] reported in 2005 on the potential of electrospun PLLA in neural tissue engineering applications. This work was expanded upon by Bini et al., [263] who reported the use of electrospun PLGA structures that encouraged nerve stem cell attachment and differentiation. They compared cell adhesion and differentiation between electrospun, microbraided, and polymer film scaffolds, and they found that cells appeared to adhere to the electrospun scaffolds better than the film. Furthermore, they found that micron-sized scaffolds (microbraided, not electrospun) that demonstrated a high degree of alignment encouraged the stem cells to grow in the direction of the fiber alignment, whereas on the electrospun nano-scale fibers, a more random orientation was noted. In a separate manuscript, Bini et al. [264] reported on the use of electrospun PLGA guidance conduits in a rat sciatic nerve model. However, results were not highly encouraging, with successful regeneration occurring in less than 50% of the animals.

The most effective efforts in nerve tissue engineering may be due to the mimicking of the ECM through the use of natural materials and electrospinning.

Recently, Schnell et al. reported on the ability of electrospun PCL and Collagen-PCL fibers to promote peripheral nerve regeneration. [265] They demonstrated that, while both groups promoted neurite outgrowth and glial migration, the blended collagen-PCL constructs improved Schwann cell migration and neurite orientation, providing further evidence that bioactivity improves cell-matrix interaction.

Finally, another consideration is the potential use of electrospun fibers for sustained release of NGF, which may offer additional help to the regenerating peripheral nerve. [198, 266] Perhaps the combination of electrospinning natural and synthetic polymer blends with the controlled addition of growth factors would be a well-advised change in focus for this area of tissue engineering.

Ligament. Native human ligament, due to its extremely limited repair capacity, and high occurrence of injury, has a large need for a tissue-engineered solution. It is estimated that more than 100,000 anterior cruciate ligament (ACL) reconstruction surgeries are performed each year in the United States, with the current options being cadaver allografts, autografts (patellar tendon, hamstring tendon), and synthetic grafts (Gore-Tex, Stryker-Dacron, etc.). However, none of these are ideal, and each has its own set of limitations: allografts are limited in number, and have the potential for infectious disease transfer, autografts are limited by donor site morbidity, and synthetic grafts exhibit poor long-term outcomes due to mechanical mismatch, poor abrasion resistance, and limited natural tissue integration. [267-271]

From a compositional standpoint, ligament is essentially a grouping of cross-linked collagen fibrils (70-80% type I by dry weight) bundled together with an orientation parallel to the direction of loading. It also contains some elastin, proteoglycans, and FBs. [268, 271-273] These components come together to form an extremely durable, anisotropic tissue essential for joint stabilization and the limitation of abnormal motion of the joint. Ideal tissue engineered grafts would have the ability to match the mechanical durability of native ACL, which on average will undergo a cyclic load of 300 N, nearly 1.5 million times a year. [268] In addition to mechanical durability, the graft would need to be porous to allow for cellular penetration and native tissue integration, critical to *in situ* repair and maintenance. It would also need to be bioresorbable at a rate which prevents stress shielding of surrounding tissues, eventually giving way to complete load bearing by native ligamentous tissue. [267, 269, 272]

There have been several preliminary attempts at creating fibrous tissue engineered ACL grafts utilizing electrospinning due to its high surface area to volume ratio, which is preferable for cellular infiltration. Bashur et al. [274] used electrospun PLGA fibers of various diameters and orientations to investigate the regulation of cell morphology. They determined that cells aligned themselves along the direction of fiber orientation. Additionally, cell spreading increased with increased fiber orientation. These findings show that electrospinning can effectively create an organized matrix for cellular infiltration, and bodes well for ligament engineering as poor mechanical properties of repaired ligament tissue are often associated with a disorganized ECM. Lee et al. [275] electrospun PU nanofibers and demonstrated that the morphology of human ligament

fibroblasts (hLF) has a direct impact on the amount of ECM they produce, with spindle shaped, oriented cells producing more collagen than randomly oriented cells. In an attempt to recreate their *in vivo* environment they also cyclically strained the hLF seeded scaffolds in the direction of their alignment, revealing that strained scaffolds produced 150% more collagen than unstrained scaffolds. Sahoo et al. [276] electrospun PLGA nanofibers onto a microfibrous knit PLGA scaffold, acting as a mechanical backbone, in order to create a strong structure with the potential for rapid cellular infiltration. Using bone marrow stromal cells they were able to demonstrate that the nanofibrous coating promoted cell attachment and proliferation. The cells on these nano-microfibrous scaffolds produced more collagen than an equivalent number of cells cultured on a knitted microfibrous scaffold without an electrospun coating.

CONCLUSION

While there is still much work to be done in electrospinning tissue scaffolds, preliminary results have been promising, especially from the standpoint of cell morphology and ECM production. There are still questions about the ability of electrospinning to produce scaffolds that can withstand the mechanical rigors inherent to tissue grafts, however the process's compatibility with a wide array of polymers and the potential to create nano-microfibrous constructs allows for a large number of different mechanically viable possibilities. The potential of electrospinning as a means to create

effective ECM analogue scaffolds is not limited to the select tissues listed here, and there are numerous other possibilities, including cardiac, corneal, and esophageal tissues.

CHAPTER 4 Electrospinning PDO and Elastin Blends

Preface: The following manuscript appeared in Biomedical Materials, 2006, volume 1, pages 72-80 [20]. The work included demonstrates the potential of combining PDO and elastin to produce a structure that could be used as a vascular grafting material. Scaffolds were created by mixing solutions of PDO and elastin prior to electrospinning in a number of different v/v ratios. Electrospun tubular scaffolds were then evaluated using a number of different vascular specific mechanical tests, exhibiting tailorable mechanical properties similar to those of native vessel.

Electrospun Polydioxanone-Elastin Blends: Potential for Bioresorbable Vascular Grafts

Scott A Sell[1], Michael J McClure[1], Catherine P Barnes[1], Danielle C Knapp[1], Beat H Walpoth[2], David G Simpson[1] and Gary L Bowlin[1]

[1]Department of Surgery, Division of Urology
Virginia Commonwealth University
Richmond, VA 23298

[2]University Hospital
Geneva, Switzerland

ABSTRACT

An electrospun cardiovascular graft composed of polydioxanone (PDO) and elastin has been designed and fabricated with mechanical properties to more closely match those of native arterial tissue, while remaining conducive to tissue regeneration. PDO was chosen to provide mechanical integrity to the prosthetic, while elastin provides elasticity and bioactivity (to promote regeneration *in vitro/in situ*). It is the elastic nature of elastin that dominates the low-strain mechanical response of the vessel to blood flow and prevents pulsatile energy from being dissipated as heat. Uniaxial tensile and suture retention tests were performed on the electrospun grafts to demonstrate the similarities of the mechanical properties between the grafts and native vessel. Dynamic compliance measurements produced values that ranged from 1.2 to 5.6 %/100 mmHg for a set of three different MAPs. Results showed the 50:50 ratio to closely mimic the compliance of native femoral artery, while grafts that contained less elastin exceeded the suture retention strength of native vessel. Preliminary cell culture studies showed the elastin-containing grafts to be bioactive as cells migrated through their full thickness within seven days, but failed to migrate into pure PDO scaffolds. The electrospinning of the PDO and elastin blended composite into a conduit for use as a small diameter vascular graft has extreme potential and warrants further investigation as it thus far compares favorably to native vessel.

INTRODUCTION

CVD, specifically coronary artery disease resulting from arteriosclerosis, remains one of the leading causes of death in the United States. Arteriosclerosis is a vascular disease that is characterized by thickening of the arterial wall and the subsequent decrease in the arterial lumen leading to eventual decrease or loss of circulation distal to the disease site. Once blood flow is compromised, vascular bypass is an option to restore blood flow to tissues distal to the restriction or blockage. In 2000 there were an estimated 519,000 coronary bypass surgeries performed [59], which typically involve the replacement of a coronary artery with an autologous saphenous vein or internal mammary artery. While these autologous alternatives perform at an acceptable patency level, they are not always a viable option as the vessels may themselves be diseased if the patient suffers from peripheral vascular disease, which in its own right affects upwards of 12 million Americans with significant associated mortality, or a previous bypass operation may have already required their use [106]. Synthetic vessels made of expanded e-PTFE and woven or knitted PET fibers (Dacron®) have been utilized as bypass grafts for peripheral arteries for quite some time. These graft materials function adequately as medium (6-10 mm internal diameter, ID) and large (> 10 mm ID) prosthetics in areas where there is high flow and low resistance. The functionality of these synthetic polymers as small diameter vessels (< 6 mm ID), such as the popliteal arteries, leaves much to be desired. In these low flow situations, synthetics have proven to be much more prone to thrombus formation and intimal hyperplasia [59, 106-110].

A synthetic vascular prosthetic would need to meet several performance criteria requisite to being considered ideal. These include ease of handling, suture retention, ease of suture placement, flexibility with kink resistance, biocompatibility, non-thrombogenicity, maintained durability post implantation and incorporation into surrounding tissue, compliance matching that of native artery, and resistance to aneurysm formation. From a production standpoint, the prosthetic must be easy to manufacture in a variety of different lengths and diameters, and must not require any complex storage protocol. This must all be accomplished while keeping the prosthetic economical and affordable [59, 107, 277].

The authors believe that electrospinning is a viable option for the fabrication of tissue engineered vascular grafts. Through electrospinning, our lab has successfully created seamless, non-woven fibrous structures of various geometries and sizes from an assortment of natural and synthetic polymers. The process used in this study has been previously described in detail in prior publications [19, 42, 48, 59, 77, 142, 219, 278]. Briefly, electrospinning requires a large electric potential to be applied to a polymer solution. An oppositely charged target is placed a set distance (air gap) from the charged polymer solution to create a static electric field. When the electric potential reaches a critical level, and the electrostatic forces within the solution overcome the surface tension of the solution, a fine jet of entangled polymer chains is drawn from the solution. As this jet travels through the air gap towards the target, solvent evaporation occurs, leaving a dry fiber. This fiber is then collected by the target, the translation/rotation of which controls the structural characteristics of the scaffold.

Native artery is an extremely complex tissue with unique biomechanical characteristics. In order to withstand the high flow rate, high pressure, and pulsatile nature of blood flow, artery is comprised of three distinct layers with three distinct compositions. The innermost layer, immediately surrounding the lumen, is known as the intima and is made of a single layer of ECs on a basement membrane composed of collagen type IV and elastin. This layer contacts the bloodstream and therefore provides a critical barrier to platelet activation. The thick middle layer, the media, is composed of several layers of MCs in a matrix of collagen types I and III, elastin, and proteoglycans. The outermost adventitial layer is made of FBs and randomly arranged collagen type I [59, 118]. Throughout the artery, SMC's maintain vascular tone, while the collagens provide tensile support and prevent vessel rupture, and elastin fibers confer elasticity to the vessel and provide the ability to recover from pulsatile deformations [120, 121]. It is the elastic nature of elastin that dominates the low-strain mechanical response of the vessel to blood flow and prevents pulsatile energy from being dissipated as heat [122].

With mechanical integrity being paramount to vascular graft success, it is obvious that an electrospun tissue engineered prosthesis would need to include a component capable of withstanding the rigors of circulation. While collagen fills this role in native vessel, its electrospun form lacks the strength and durability required [19, 219]. For this reason, PDO was chosen to be the major mechanical backbone of our tissue engineered vessel. PDO (Ethicon, Inc.) is a colorless, crystalline, bioabsorbable polymer that is currently in use as a commercially available wound closure suture. As a suture, PDO is highly flexible with excellent strength retention and shape memory, and a lower

inflammatory response and slower absorption rates than sutures composed of PGA and PGLA. Successful electrospinning of PDO has been performed in our lab previously, with promising mechanical results [48]. Elastin was incorporated into the graft to provide elasticity and bioactivity (i.e. to promote regeneration *in vitro/in situ*).

While mechanical integrity is of utmost importance, particularly in high pressure vessels to maintain suture placement and prevent aneurysm, compliance is of equal or greater importance in small diameter vessels, where diminished pulsatile flow can lead to flow stagnation and graft thrombosis. The compliant nature of native vessel actually assists in pushing blood through the circulation. In addition, the occurrence of intimal hyperplasia has been closely tied to the mismatch of graft and adjacent arterial compliance [107-109, 279]. This mismatch creates abnormal cyclical strains which trap activated platelets through anastomotic flow disturbance. These activated platelets release mitogens that stimulate perianastomotic SMCs, leading to a thickening of the arterial wall at the anastomosis (typically at the distal end) and a narrowing of the lumen [279].

This study created a non-woven scaffold for potential use as a vascular graft composed of electrospun blended nanofibrous PDO and elastin. A number of mechanical tests were performed to demonstrate the material to have sufficient mechanical integrity to resist aneurysm and compliance matching that of native artery. *In vitro* cell culture studies were performed to evaluate cell affinity towards the elastin containing scaffolds, and the potential for *in vivo* tissue regeneration.

MATERIALS AND METHODS

Electrospinning. Concentrations of 100 mg/mL of PDO (Ethicon, Inc.) and 200 mg/mL of elastin from bovine neck ligament (Elastin Products Co., Inc.) were dissolved in HFP (Sigma Aldrich Co.) and blended in ratios of 100:0, 90:10, 80:20, 70:30, 60:40, and 50:50 (PDO:Elastin). These solutions were then loaded into a Becton Dickinson syringe (either 3.0 or 5.0 mL) with an 18 gauge blunt tip needle and placed in a KD Scientific syringe pump to be dispensed at a rate between 4 and 8 mL/h, depending on the amount of elastin included in the solution (higher elastin equates to lower rate). Solutions were then electrospun onto a rotating flat mandrel (2.5 cm wide x 10.2 cm long x 0.3 cm thick) to produce a flat sheet with a random fiber orientation for scaffold characterization, uniaxial tensile testing, and preliminary cell culture. The same solutions were also electrospun on a rotating tubular mandrel to produce a seamless vascular graft with an internal diameter of 6 mm and a wall thickness of approximately 350 microns for suture retention testing and compliance measurement. All electrospinning was performed with an applied voltage of 22 kV, while the mandrel was rotated at a rate of 500 revolutions per minute (RPM) and placed 12 cm away from the needle tip.

Scaffold Characterization. Scaffold characterization was performed using SEM on small pieces cut from the electrospun mats (SEM, JEOL JSM-820 JE Electron Microscope). SEM images were digitized with a Hewlett-Packard Scanjet 5550c flatbed scanner and analyzed with ImageTool 3.0 software (Shareware provided by UTHSCSA).

Characterization included determining the average fiber diameter for the electrospun structure by taking the average of 60 measurements chosen randomly from across the image. In addition, the average pore area, which at this point is still a rather subjective measurement, was taken by measuring the circumference of 60 different pores from across the image. For all of the measurements made from the SEM images, calibration of the ImageTool software was done with the scale bar on each image.

Uniaxial Tensile Testing. Uniaxial tensile testing was performed to failure on dry samples, to determine handling characteristics, and hydrated samples (soaked in PBS for 24 hours at 37°C), to mimic physiological conditions. "Dog-bone" shaped samples were cut from the electrospun mat (2.75mm wide at their narrowest point with a gage length of 7.5 mm) and tested on a MTS Bionix 200 testing system with a 50 N load cell (MTS Systems Corp.) and an extension rate of 10.0 mm/min. Elastic modulus, peak stress, and strain at failure were calculated by the MTS software TestWorks 4.0 and recorded.

Preliminary Cell Culture. To evaluate preliminary cell interaction, three circular discs (5.9 mm in diameter) were punched from scaffolds of four different electrospun ratios (100:0, 90:10, 70:30, and 50:50), disinfected (by soaking in ethanol for 10 minutes followed by repeated rinses in PBS), and placed in a 96-well plate. Each disc was then seeded with human dermal FBs at a concentration of 50,000 cells/mL. Dulbecco's Modified Eagle Medium with Nutrient Mixture F-12 (Invitrogen Corp.)

supplemented with 10% fetal bovine serum (FBS) and 1% penicillin-streptomyocin (10,000 Units/ml each, Gibco BRL Life Technologies) was added in the center of each scaffold (100 μL of cells in media incubated for 45 minutes and followed by 100 μL of media). The scaffolds were then statically cultured under standard culture conditions (37°C and 5% CO_2) in an incubator. One disc of each ratio was removed after 24 hours for SEM analysis, while the others were left in culture for seven days, fixed in 10% formalin, and processed for histology (Hematoxylin and Eosin staining, H&E).

Suture Retention Testing. Suture retention testing was performed on 6 mm inner diameter tubular specimens, both dry and soaked in PBS for 24 hours at 37°C, on a MTS Bionix 200 testing system with a 50 N load cell (MTS Systems Corp.) and an extension rate of 150.0 mm/min in accordance with the straight across procedure described in section 8.8 of the American National Standards Institute (ANSI)/Association for the Advancement of Medical Instrumentation (AAMI) ANSI/AAMI VP20:1994 entitled "Cardiovascular Implants – Vascular Graft Prostheses" [280]. 5.0 commercial PDS™ II violet monofilament suture (Ethicon, Inc.) was placed 2 mm from the end of the sample and extended until the suture had pulled through the graft

Compliance Measurement. Dynamic compliance was determined for 6 mm inner diameter tubular grafts under simulated physiological conditions in accordance with section 8.10 of ANSI/AAMI VP20:1994 [280]. The specimens were tested in an Intelligent Tissue Engineering via Mechanical Stimulation (ITEMS™) Bioreactor

developed by Tissue Growth Technologies (Minnetonka, MN) filled with PBS at 37°C. The bioreactor provided a cyclic (1 Hz, representing 60 beats per minute) pressure change to the inside of the graft; three different pressure levels (90/50, 120/80, and 150/110 mmHg) were investigated to produce a range of MAPs. MAP is defined as

$$MAP = P_D + \frac{1}{3}(P_S - P_D) \tag{4.1}$$

where P_D is the diastolic pressure and P_S is the systolic pressure [281]. The MAPs tested in this experiment ranged from 63.33 mmHg to 123.33 mmHg (in accordance with section 8.10 of ANSI/AAMI VP20:1994 [280]), while physiological values for MAP are typically between 50 and 150 mmHg [282].

Grafts were also subjected to a pressure change of 80-120 mmHg for two hours to observe any change in compliance over that time. Internal pressure was measured with a pressure transducer capable of measuring dynamic pressure up to 200 ± 2 mmHg, while the external diameter was recorded with a laser micrometer system with an accuracy of ± 0.001 mm. Prior to insertion into the bioreactor, the grafts were soaked in PBS at 37°C for 24 hours, after which time their average wall thickness was measured. From this the internal radii of the graft was determined and used in the following equation to calculate compliance for each specimen:

$$\%\ Compliance = \frac{(R_{P2} - R_{P1})/R_{P1}}{(P_2 - P_1)} \times 10^4 \tag{4.2}$$

Where R is the internal radius, P_1 is the lower internal pressure, and P_2 is the higher internal pressure [280]. It was found that the pure PDO graft leaked through the pores under pressure, resulting in an inaccurate negative compliance. To counteract

phenomenon, the graft was lined with a latex balloon far more compliant than the graft itself, as recommended in section 8.10.2 of ANSI/AAMI VP20:1994 [280] Under pressure the balloon expanded and mated tightly to the internal surface of the graft to prevent leakage.

Statistical Analysis. Unless otherwise stated, all statistical analysis was based on a Kruskal-Wallis one way analysis of variance (ANOVA) on ranks and a Tukey-Kramer pair-wise multiple comparison procedure (α=0.05) performed with the JMP®IN 4.0.3 statistical software package (SAS Institute, Inc).

RESULTS AND DISCUSSION

Scaffold Characterization. Analysis via SEM revealed that all ratios of PDO to elastin were successfully electrospun into thin scaffolds composed of small diameter fibers (figure 4.1). It should be noted that the elastin forms ribbon-like (flat and thin) fibers while the PDO forms more typical round fibers. This is most evident in the 50:50 ratio, where a large number of ribbon-like fibers are clearly seen. This unique electrospun elastin characteristic may have led to some skewing of the measured average fiber diameter values (figure 4.2) depending on the orientation of the fiber. As the graph shows, fiber diameter decreases a statistically significant amount from the maximum at the 100:0 ratio to a minimum value for the 80:20 ratio. The diameter then increases an insignificant amount over the 100:0 ratio for the 70:30, and 60:40 ratios, with a

statistically significant increase for the 50:50 ratio over the previous ratios. This may be caused by a decrease in the amount of large, round PDO fibers and a transition to more flat, wide elastin fibers. As was expected, the pure PDO scaffold having the largest fiber diameter had the largest mean pore area, with the other ratios all having significantly smaller pores.

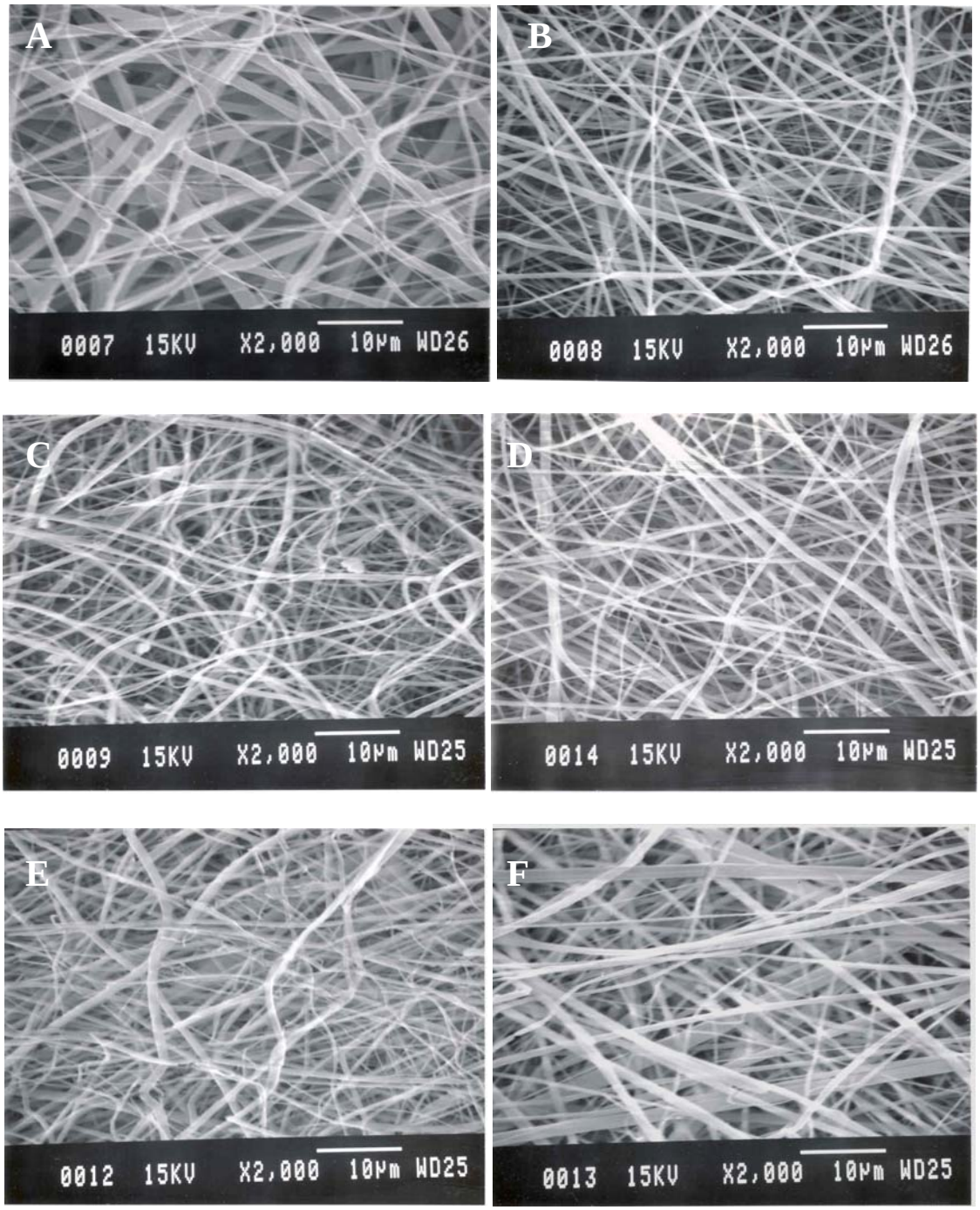

Figure 4.1. Scanning electron micrographs of electrospun PDO and elastin with ratios of 100:0 (A), 90:10 (B), 80:20 (C), 70:30 (D), 60:40 (E), and 50:50 (F). All micrographs were taken at x2000 magnification, and the scale bar is equivalent to 10 microns**.**

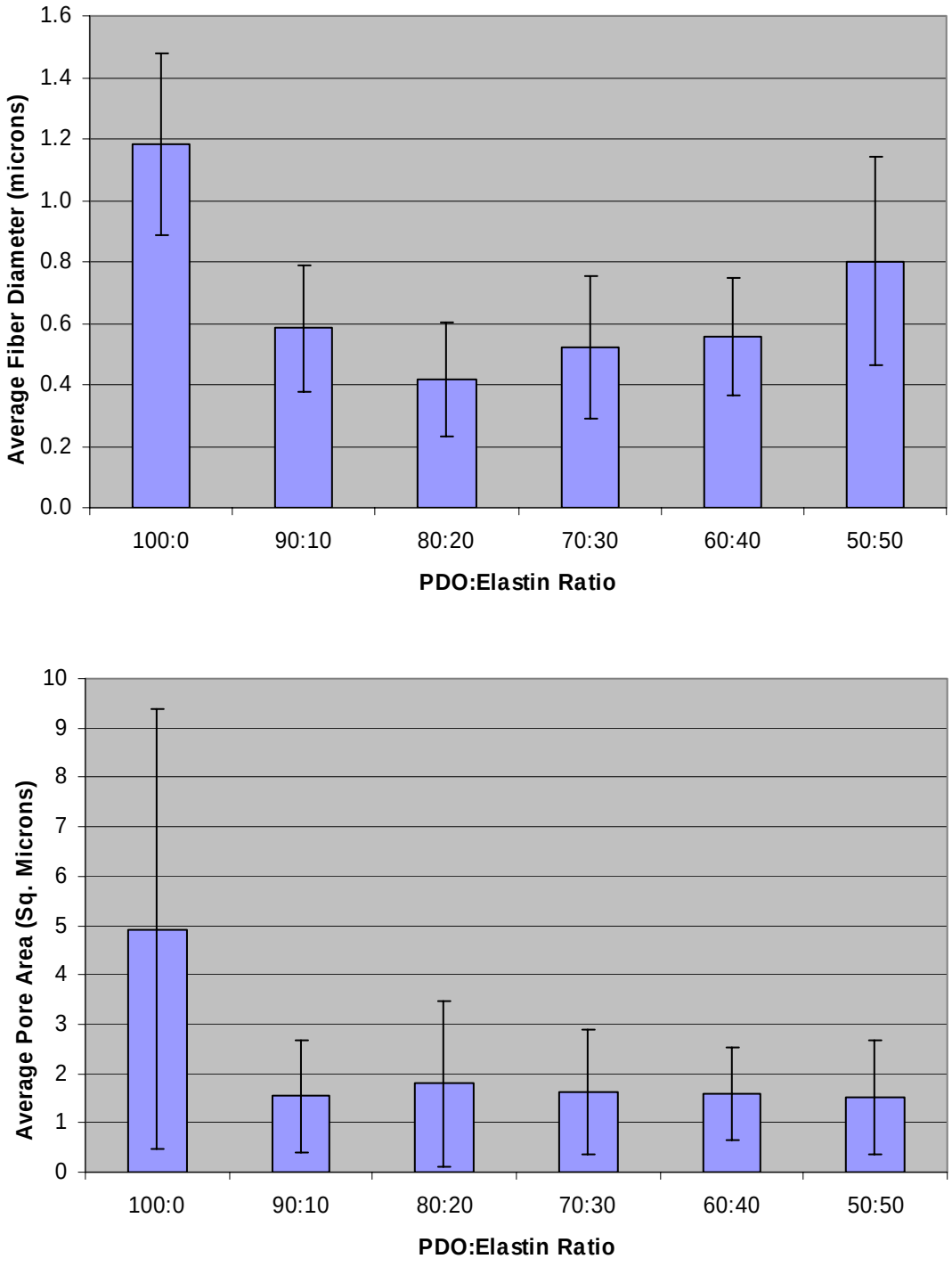

Figure 4.2. Graphs depicting the average fiber diameter (top) and pore area (bottom) for electrospun PDO:Elastin scaffolds.

Uniaxial Tensile Testing. The results of the mechanical testing of the electrospun PDO:elastin specimens can be seen in figure 4.3. Statistical analysis showed that the only significant difference between dry and hydrated peak stresses within a single ratio was with the 80:20 ratio, as all other ratios experienced insignificant differences going from the dry state to a hydrated one. The hydrated pure PDO scaffold experienced significantly higher peak stress than the three ratios with the lowest amounts of PDO, and the 60:40 and 50:50 ratios were significantly lower than the other four scaffolds. The 70:30 ratio stood alone, and was significantly different from all others. As the amount of PDO within a scaffold decreased the overall strength of the scaffold decreased. This result was expected because of the excellent strength of PDO and its inclusion as the mechanical backbone of the scaffold.

The trend seen in the dry moduli was rather surprising as there was a sudden significant decrease in modulus with the inclusion of elastin into the scaffold, followed by a steady significant increase of modulus as the amount of elastin was increased to the 60:40 ratio. The dry 50:50 ratio was not significantly different from the pure electrospun PDO scaffold. It is hypothesized that the initial decrease in modulus may have been caused by the inclusion of elastin fibers that were too few in number to contribute to the scaffold's overall elasticity and actually decreased the elastic integrity of the scaffold. The gradual increase represents some sort of transition from the highly elastic, strong PDO fibers to the highly elastic, but overall weaker elastin fibers dominating the mechanical characteristics of the scaffold. This will need to be investigated further in

future work. Soaking of the scaffolds had a significant negative effect on the modulus of the hydrated samples as, unlike the peak stress values, there were significant differences in the modulus of elasticity for all ratios between dry and hydrated specimens, with the dry specimens exhibiting a much higher modulus than their hydrated counterparts. The hydrated pure PDO scaffold exhibited a significantly reduced modulus compared to the dry scaffold; however it remained significantly larger than all of the hydrated elastin-containing specimens. The trend seen in the dry specimens was upheld in the hydrated specimens albeit with reduced values, as the modulus of the 50:50 ratio was significantly greater than those of the other scaffolds where elastin was present. However, unlike the dry specimens, the hydrated 50:50 ratio was significantly different from the pure PDO. The strain at break trends were consistent with previous uniaxial testing performed on PDO scaffolds [48]. Pure PDO scaffolds had the highest mean strain at break values for both the dry and hydrated specimens. This value then decreased with decreasing amounts of PDO contained in the scaffold. Strain at break values of the hydrated samples of the 90:10, 80:20, and 70:30 ratios were significantly higher than the corresponding dry samples, and there was an overall trend of hydrated values being larger than those of dry scaffolds that contained elastin.

While the peak stress and strain at break of the pure PDO scaffolds were significantly reduced with the addition of elastin, this reduction may actually enhance the attractiveness of PDO:Elastin blends for use in vascular applications. Table 4.1 shows the mechanical properties of hydrated PDO:Elastin scaffolds of various ratios compared to the mechanical properties of native femoral artery. Note that the pure electrospun

PDO scaffold had larger values than the femoral artery for all parameters investigated (modulus, ultimate stress, and strain at failure). It is also of interest that the more elastin present in the scaffold, the closer the values come to that of native artery. The mechanical properties of the 50:50 ratio fell within the range of the femoral artery values in nearly every instance, the only exception being that the electrospun scaffold exhibited higher ultimate stresses than the native vessel. This matching of mechanical properties may aid in reducing compliance mismatch between an electrospun graft and the native vasculature.

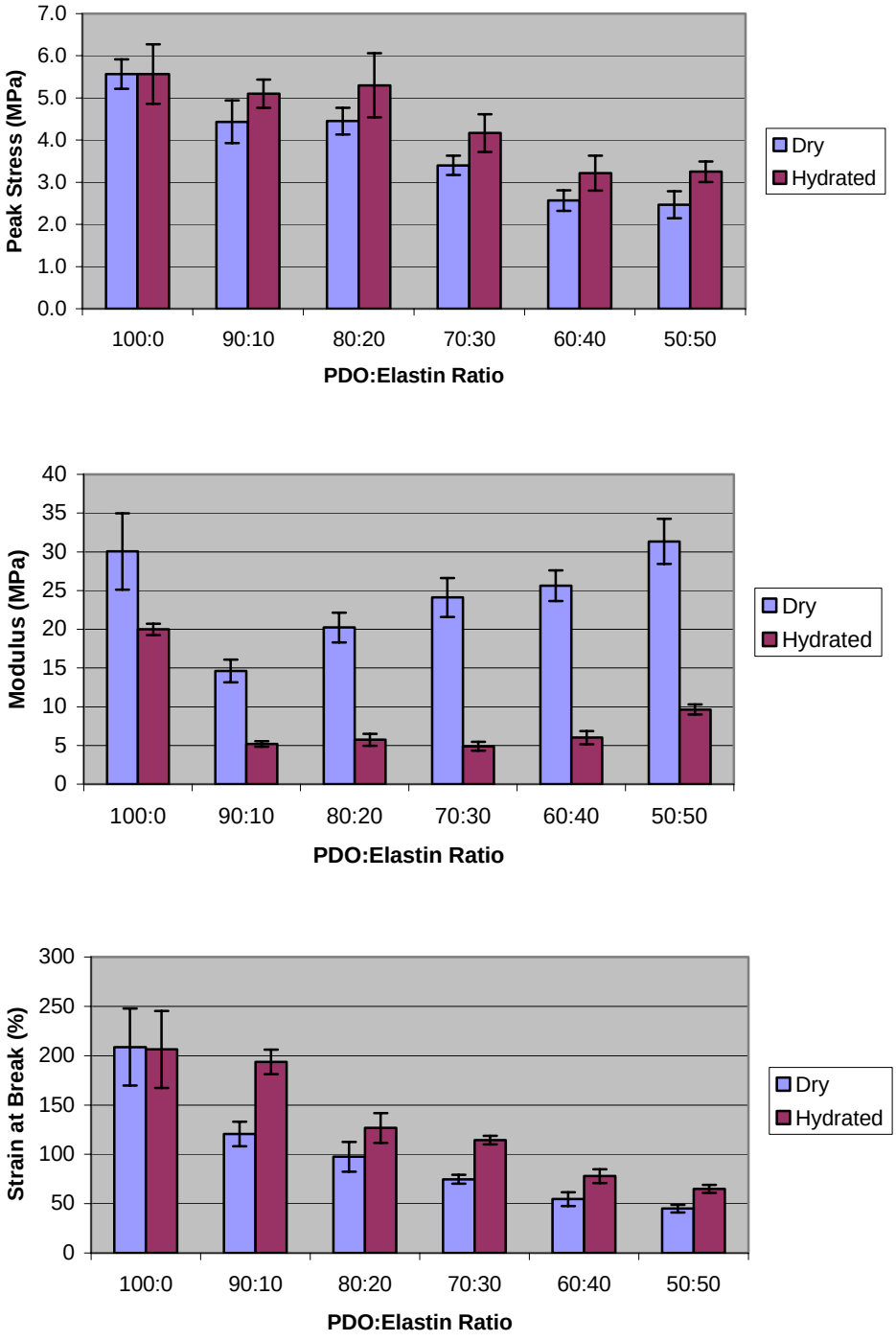

Figure 4.3. Mechanical properties for dry and hydrated samples of electrospun PDO:Elastin scaffolds of various ratios.

Table 4.1. Mechanical properties of hydrated electrospun scaffolds of various PDO:Elastin ratios compared to native femoral artery [283, 284] and e-PTFE [285].

Graft Material	Elastic Modulus (MPa)	Ultimate Stress (MPa)	Strain at Failure (%)
Femoral Artery	9 – 12	1 - 2	63 – 76
e-PTFE (30 micron internodal distance)	42 – 60	6 - 15	20 - 30
PDO (100:0)	19.98 ± 0.74	5.57 ± 0.7	206.33 ± 38.96
90:10	5.2 ± 0.35	5.1 ± 0.34	193.75 ± 12.48
80:20	5.73 ± 0.77	5.3 ± 0.76	126.7 ± 15.05
70:30	4.89 ± 0.59	4.17 ± 0.45	114.45 ± 4.37
60:40	6.0 ± 0.87	3.22 ± 0.42	77.95 ± 7.01
50:50	9.64 ± 0.66	3.25 ± 0.24	64.93 ± 3.97

Preliminary Cell Culture. Micrographs of scaffolds that had been cultured for 24 hours (figure 4.4) revealed that cells migrated into the fibrous networks of the 90:10, 70:30, and 50:50 ratios, while the human dermal FBs remained on the surface of the pure PDO scaffold after 24 hours. Histology performed at seven days in culture (figure 4.4) showed that the cells penetrated the full thickness of the elastin containing scaffolds, with no penetration of the pure PDO scaffold. This finding suggests that the inclusion of elastin into the electrospun scaffolds does in fact improve the in vitro bioactivity of the matrix through either chemical (cells recognizing elastin as a native ECM material) or mechanical (cells sense desirable, native-like mechanical properties of fibrous ECM)

signaling, or a combination of the two. This will have to be investigated further in future studies. At this point it does appear that elastin serves as a stimulus for the transduction of cellular signals to enhance the migration of the cells.

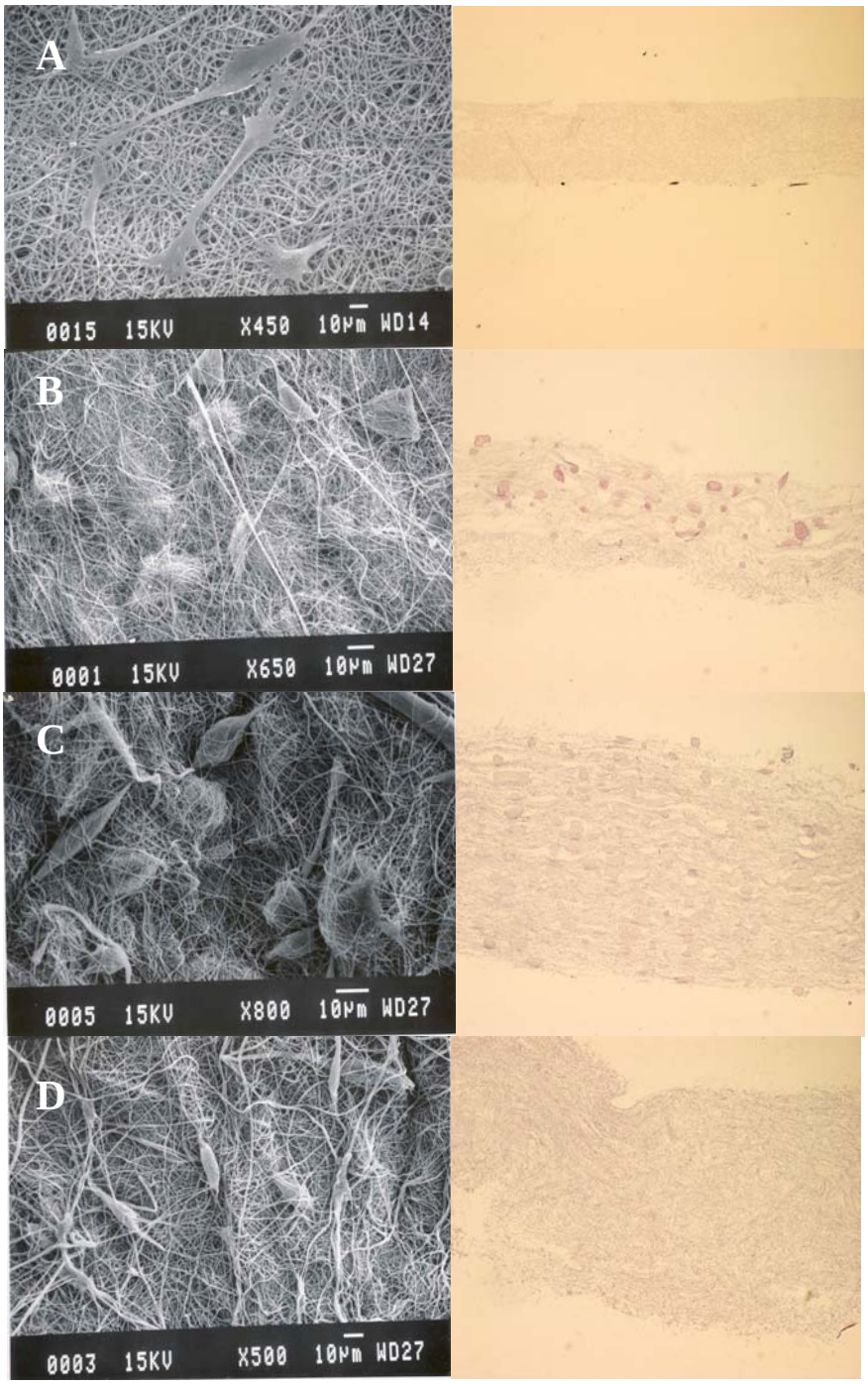

Figure 4.4. (Left) Scanning electron micrographs of electrospun scaffolds after one day in culture of pure PDO (A), 90:10 ratio of PDO to elastin (B), 70:30 ratio (C), and 50:50 ratio (D). (Right) Histology performed after seven days in culture for corresponding ratios (20x).

Suture Retention Testing. Suture retention testing on both dry and hydrated specimens resulted in retention strengths between those of saphenous vein [286] and e-PTFE, two of the most common vascular grafting materials in clinical use today (figure 4.5). For all ratios except the 50:50, the retention strengths of the hydrated samples were significantly less than the retention strengths of the dry samples. This was somewhat surprising as the differences in peak stress between dry and hydrated samples were, for the most part, insignificant during uniaxial tensile tests. While there was no significant difference between the hydrated and dry 50:50 ratio, this particular ratio experienced suture retention strengths that were overall significantly less than the other ratios, as well as that of the saphenous vein. Overall, three of the ratios (100:0, 90:10, and 80:20) tested in a hydrated state surpassed the requisite 375 gram force needed for suture pullout of native arterial structures utilizing 5-0 suture [287], i.e. native tissue at the anastomosis would fail before the electrospun graft at these ratios.

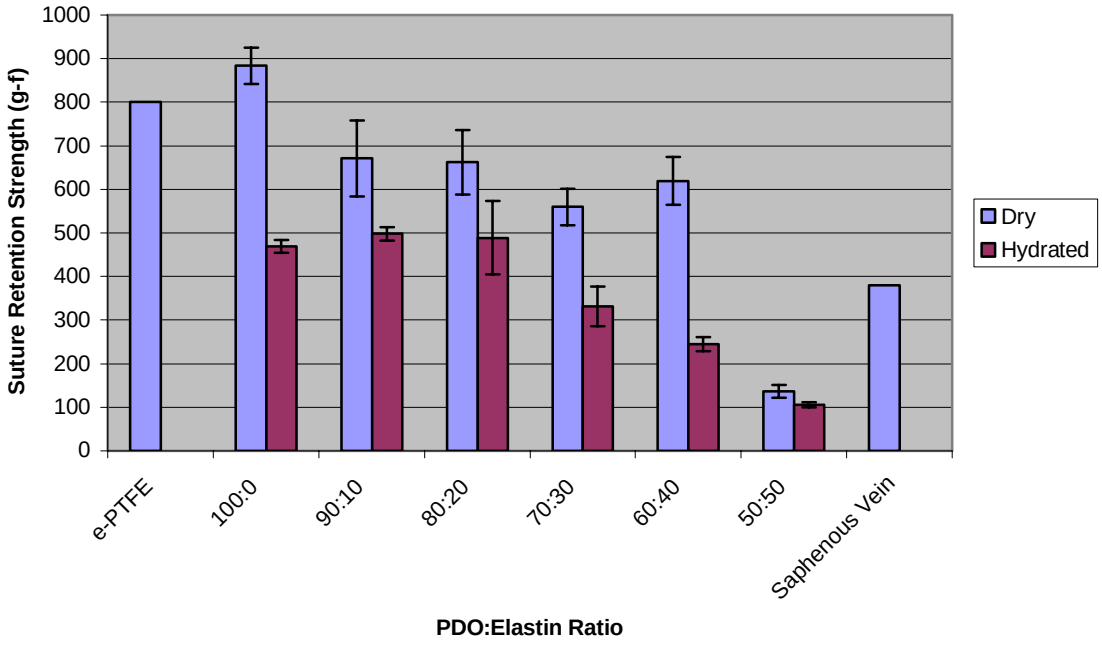

Figure 4.5. Suture retention strengths for electrospun PDO:Elastin ratios, e-PTFE vascular graft, and native saphenous vein. Saphenous vein data from [286].

Compliance Measurement. Testing graft compliance at three different pressure levels produced the data found in figure 4.6. As stated previously, this data was recorded after the graft had been subjected to each pressure level for 30 minutes to allow for equilibrium to be achieved. As expected, pure PDO grafts had the lowest compliance, while those grafts that contained elastin exhibited significantly greater compliance, with the 50:50 ratio being the most compliant. Interestingly, as the MAP was increased the compliance of the elastin containing grafts decreased. However, this trend is concurrent with the behavior of native arteries, particularly the large elastic arteries, where compliance decreases with increasing blood pressure [288].

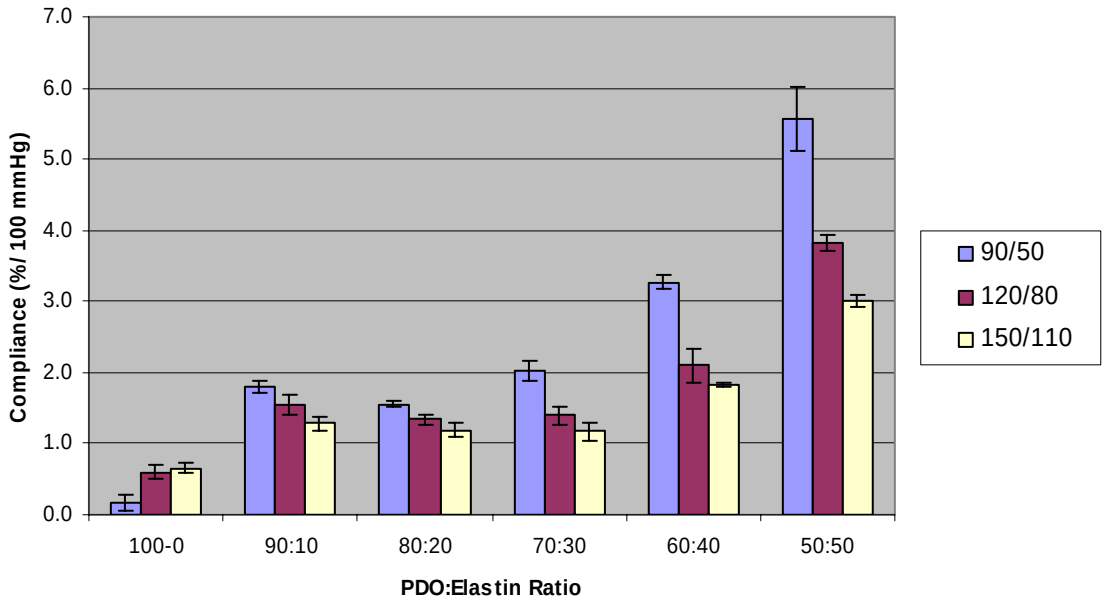

Figure 4.6. Compliance determined from internal radii at three different MAPs (90/50, 120/80, and 150/110 mmHg). All measurements were taken after the graft had been subjected to the target pressure for 30 minutes to allow for stabilization.

Compliance of the electrospun grafts was also determined for the 120/80 mmHg (93.33 mmHg MAP) pressure level at a time of 0 hours, 1 hour, and 2 hours (figure 4.7). Again, the pure PDO grafts had the lowest compliance, with the elastin containing ratios being significantly greater. There was a general trend of compliance increasing as the amount of elastin contained in the graft increased. The exception to this was the 60:40 ratio, where compliance values do not follow the same trend. This is unexplainable at this time, but may have simply been an aberration. There was also a trend of compliance falling off a significant amount after the initial measurement was taken at time zero for the elastin containing grafts. The 60:40, 70:30, and 90:10 all experienced a significant

decrease in compliance between the 0 hour and 1 hour measurements. This may be due to some amount of stiffening of the elastin fibers as they adjusted to being subjected to a sustained cyclic load. Of note is the behavior of the pure PDO graft, which actually became more compliant as time progressed. This may be due to the polymer fibers plasticizing under loading.

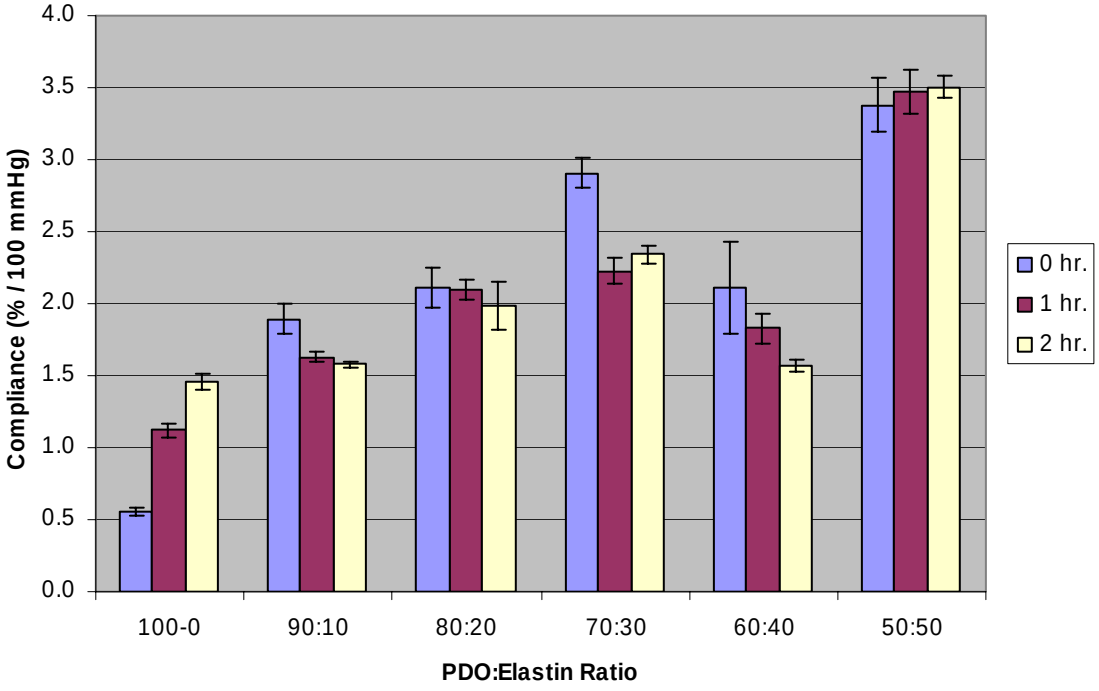

Figure 4.7. Compliance calculated from the graft's internal radius at internal pressures of 120/80 mmHg at times of 0, 1, and 2 hours.

Figure 4.8 compares the compliance values determined for the electrospun PDO:Elastin grafts to the compliance values of native artery and vein, as well as the common vascular graft materials Dacron® and e-PTFE. The range of compliances

achieved for the elastin containing grafts included the values for both artery and vein, with the 50:50 ratio significantly exceeding that of native artery.

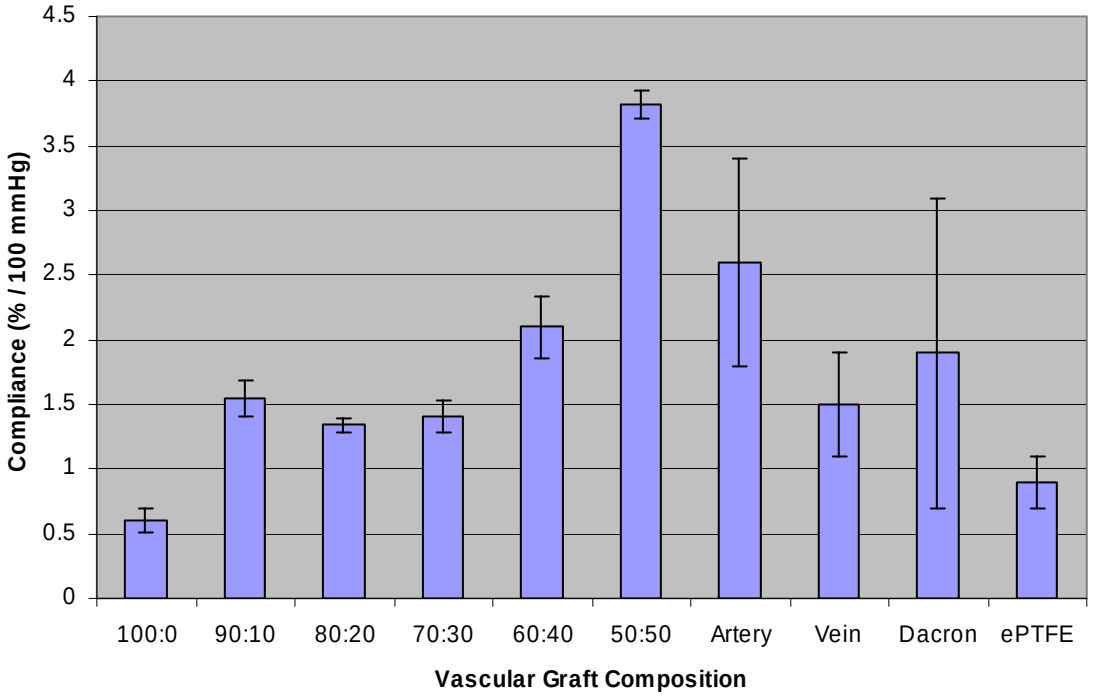

Figure 4.8. Compliance determined for 120/80 mmHg pressure level (93.33 mmHg MAP) for various vascular graft compositions. Values for artery, vein, Dacron®, and e-PTFE were obtained from [279].

CONCLUSION

In conclusion, an electrospun cardiovascular graft composed of non-woven, sub-micron scale PDO and elastin fibers was successfully designed and fabricated with a range of mechanical properties that included those of native arterial tissue. These

properties proved to be easily tailorable by varying the amount of elastin. These scaffolds hold the potential to be conducive to tissue regeneration based on the results of the *in vitro* cell culture study. While many researchers have published promising *in vitro* results on numerous vascular graft materials, what sets this study apart is the incorporation of the native-like elastin nanofibers. This study has shown that the presence of elastin not only vastly improves cellular response to the graft, but also positively contributes to the mechanical behavior of the graft through the same mechanisms as in native vessel. We believe that the promising results obtained herein will have successfully laid the groundwork for future *in vivo* testing of these grafts.

CHAPTER 5 Electrospinning PDO and Fibrinogen Blends

Preface: The following manuscript appeared in the Journal of Engineered Fibers and Fabrics, 2008, volume 3, pages 12-21 [180]. The work included demonstrates the efficacy of combining natural (fibrinogen) and synthetic (PDO) polymers together in the same scaffold to produce a structure with both tailorable mechanical properties and bioactivity. Scaffolds were created through the use of a 2-1 nozzle rather than mixing solutions together in the same syringe prior to electrospinning. The author's role in this work included the design of the nozzle and the fabrication and mechanical evaluation of the scaffolds.

Electrospun Fibrinogen-Polydioxanone Composite Matrix: Potential for In Situ Urologic Tissue Engineering

Michael C. McManus[1], Scott A. Sell[2], Whitney C. Bowen[2], Harry P. Koo[1], and Gary L. Bowlin[2]

[1]Department of Surgery, Division of Urology
Virginia Commonwealth University
Richmond, VA 23298

[2]Department of Biomedical Engineering
Virginia Commonwealth University
Richmond, VA 23284

ABSTRACT

Our objective is to demonstrate an electrospun fibrinogen-PDO composite scaffold will retain the superior cellular interaction of fibrinogen while producing a product with the functional strength needed for direct implantation. Fibrinogen-PDO composite scaffolds were electrospun with PDO ratios of 0% (pure fibrinogen), 10%, 20%, 30%, 40%, 50% and 100% (pure PDO) and disinfected using standard methods. Scaffolds were seeded with human BSM per scaffold and incubated with twice weekly media changes. Samples were removed at 7, 14 and 21 days for evaluation by collagen assay, SEM and histology. Cell seeding and culture demonstrated human BSM readily migrate throughout and remodel electrospun fibrinogen-PDO composite scaffolds with deposition of native collagen. Cell migration and collagen deposition increased with increasing fibrinogen concentration while scaffold integrity increased with increasing PDO concentration. Electrospun fibrinogen-PDO composite structures promote rapid cellular in-growth by human BSM while maintaining structural integrity. The fibrinogen to PDO ratio can be adjusted to achieve the desired properties required for a specific tissue engineering application. Our ultimate objective is to utilize this innovative biomaterial technology to produce an acellular, bioresorbable product that enables *in situ* tissue regeneration. While there is still much work to be done, these initial findings indicate fibrinogen-PDO composite scaffolds deserve further investigation.

INTRODUCTION

The need for urinary tract reconstruction can result from a large variety of urologic disorders such as congenital hypospadias, stricture disease, cancer and trauma. These disorders may affect the ureters, bladder or urethra, decreasing the availability of adequate autologous tissue. Moreover, complications from inserting autologous tissue, such as enteric segments, into the urinary tract are well known and often manifests metabolic and histopathologic abnormalities. These sequelae have motivated investigators to search for tissue-engineered alternatives.

Ideally, a tissue-engineered scaffold should mimic the structural and functional profile of the native ECM. To achieve this objective, the "ideal" scaffold has been described as having the following characteristics: 1) a three-dimensional structure with a surface chemistry that promotes cell attachment, proliferation and differentiation [289], 2) that does not induce adverse immune responses from the surrounding tissues [289], 3) mechanical properties to withstand organ-specific *in vivo* forces while being completely resorbable [290], and 4) a feasible production process that allows for various shapes and sizes [291]. Despite many recent advances, none of the scaffolds in use today meet all of the above mentioned criteria completely.

Fibrinogen is a naturally occurring soluble blood protein that functions as a major structural element in the coagulation cascade, clot formation and wound healing [292, 293]. The reaction of fibrinogen with thrombin produces fibrin. This exposes regions of opposite charge leading to the assembly of fibrous clots and/or other fibrous structures.

These fibrous structures function as nature's provisional matrix, on which tissues rebuild and repair themselves, making this type of structure an attractive scaffold for tissue engineering and regeneration [294-296].

Fibrin and fibrinogen have a well established track record in tissue engineering, due to their innate ability to induce cellular interaction and subsequent scaffold remodeling. Fibrinogen based scaffolds have previously been developed in the form of fibrin gels [295-302] and wet extrusion fibronectin-fibrinogen cables [303-305]. These studies demonstrated fibrinogen based scaffolds were easily degradable, nonimunogenic [297] and promoted increased cell migration [303, 305].

Electrospinning is a technology with the potential to fulfill the requirements of an ideal scaffold. Briefly, electrospinning is accomplished by inducing a large electric potential (15 to 30 kilovolts DC) in a polymer solution and separating that polymer from an oppositely charged target. This charge separation creates a static electric field. As the field strength grows, the charge separation overcomes the surface tension of the solution and a thin jet of entangled polymer chains is ejected from the polymer reservoir. As this jet travels toward the target, instabilities within the charged jet define its orientation in space (condition previously described as whipping). By the time the jet reaches the target, the solvent has evaporated and a dry fiber is collected in the form of a non-woven scaffold (figure 5.1).

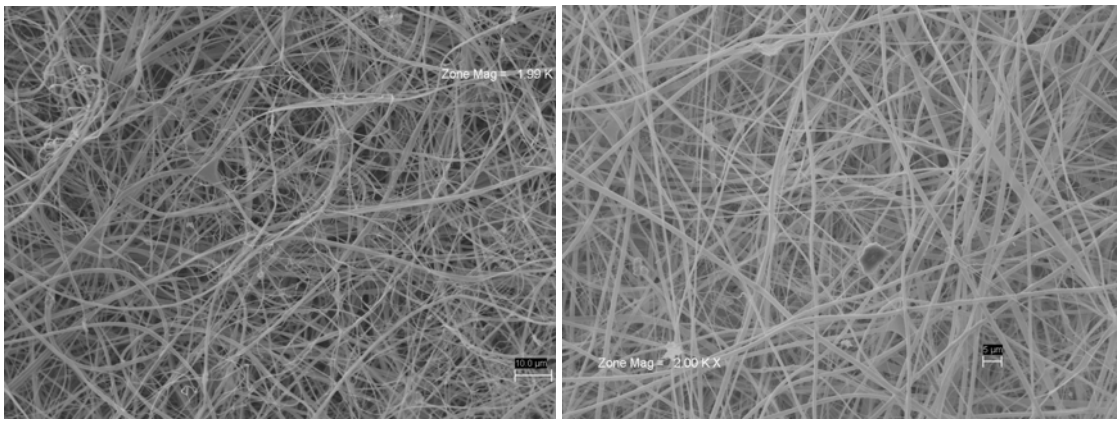

Figure 5.1. Scanning electron micrographs of electrospun fibrinogen-PDO composite scaffolds at 2000x magnification. 10% PDO composite (top) has a scale bar of 10 μm, while 40% PDO composite (bottom) has a scale bar of 5 μm.

METHODS

Electrospinning. For this study, fibrinogen (Bovine soluble fraction 1, Sigma Aldrich Chemical Co.) was dissolved in 9 parts HFP (Sigma Aldrich Chemical Co.) and 1 part 10X minimal essential medium (MEM) at a concentration of 110 mg/mL. PDO (Ethicon) was dissolved in HFP at a concentration of 100 mg/mL. These ratios were chosen based on previous work conducted by the authors that demonstrated the best mechanical and cellular interaction characteristics for further investigation. The solutions were then loaded into separate Becton Dickinson 5.0-mL syringes and placed in a KD Scientific syringe pump. The fibrinogen solution was dispensed at a rate of 1.8 mL/hr. The dispensing rate of the PDO solution was varied to produce scaffolds with PDO ratios of 0%, 10%, 20%, 30%, 40%, 50% and 100% by volume. The positive output lead of a high voltage power supply (Spellman CZE1000R; Spellman High Voltage Electronics Corp.), set to 22 kV, was attached to a custom designed 2 input - 1 output nozzle as

depicted in figure 5.2. This nozzle had an estimated component mixing length of 15 mm prior to exiting the nozzle. A grounded target (2.5 cm Wide × 10 cm Long × 0.3 cm Thick; 303 stainless steel) was placed 10 cm from the nozzle tip and rotated at 500 RPM to evenly coat the mandrel, but not impart a large degree of alignment to the deposited fibers.

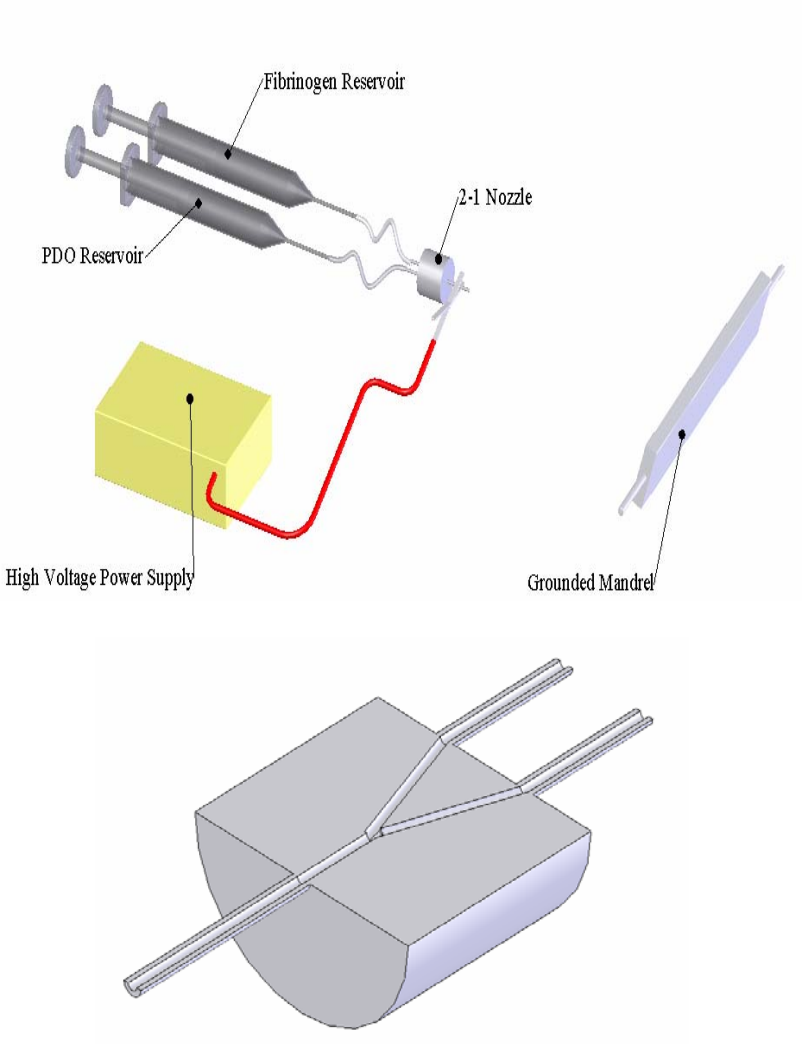

Figure 5.2. Diagrammatic representation of the custom designed nozzle in a typical electrospinning setup, attached to syringes with 18 gauge Tygon® tubing (top) and section view of the 2 input - 1 output nozzle (bottom).

Mechanical Evaluation. For determining the bulk mechanical properties, samples were incubated at 37ºC for 24 hours in complete culture media containing DMEM:F12 supplemented with 5% FBS and 1.2% penicillin-streptomycin antibiotic (10,000 I.U. penicillin/mL, 10,000 µg/mL streptomycin, Mediatech, Inc.). Uniaxial tensile testing was performed on a MTS Bionix 200 (MTS Systems Corp.) mechanical testing system incorporating a 50 N load cell with an extension rate of 10 mm/min to failure. A total of six test specimens (n=6) were tested for each study group. Specimens were punched from the scaffolds using a "dog-bone" shaped template to assure uniformity and isolate the failure point away from the grips. The specimens had a width of 2.67 mm and a gauge length of 11.25 mm. Specimen thickness was measured on a Mitutoyo IP54 digital micrometer (Mitutoyo American Corp.) and ranged from 0.03 to 0.20 mm. Tangent modulus (tangential method automatically selected by the MTS TestWorks 4.0 software), peak stress (engineering stress based on the initial cross-sectional area), and strain to failure (also calculated automatically by the software) were determined.

Cell Culture. Experiments were designed to evaluate cell proliferation and cell migration into the scaffolds at varying fibrinogen and PDO concentrations. Scaffolds were electrospun with PDO as previously described. Seventy-five 15 mm diameter die-cut scaffold specimens, five scaffolds at each concentration at each time point, were placed in separate wells of 24 well culture plates. All scaffolds were sanitized in 100%

ethanol for ten minutes then rinsed four times with sterile PBS for three minutes per rinse. Human BSM (Cambrex) were expanded utilizing standard cell culture protocol in complete culture media containing DMEM:F12 supplemented with the Cambrex BulletKit (hEGF, hFGF-B, insulin, gentamicin, amphotericin-B, 5% FBS). Scaffolds were seeded with $2x10^4$ cells per scaffold. Culture media was aspirated from the scaffold containing test wells and 500 µl of fresh media was added to each culture well and changed twice per week. Cultures were incubated at 37ºC in 5% CO_2 and removed for testing at 7, 14 and 21 days.

Collagen Assay. Collagen deposition by cultured cells was measured using the Sircol Collagen Assay (Biocolor). This is a colorimetric assay for the quantification of acid-soluble and pepsin-soluble collagens (Types I to IV) extracted from mammalian tissues. The Sircol dye reagent contains Sirius Red, which is an anionic dye with sulphonic acid side chain groups that react with the side chain groups of the basic amino acids present in collagen. The specific affinity of the dye for collagen, under the assay conditions, is due to the elongated dye molecules becoming aligned parallel to the long, rigid structure of native collagens that have intact triple helix organization. Increased collagen content leads to an increase in the amount of Sircol dye bound, which is measured with a spectrophotometer.

After the 7 and 14 day incubation periods, scaffolds were removed from the culture wells and placed in separate 1.5 mL centrifuge tubes. One milliliter of 0.5 M acetic acid solution containing 1 mg of pepsin was added to each centrifuge tube and

samples were placed on an orbital mixer overnight. The tubes were gently mixed and 100 μL of solution from each tube was transferred to a new centrifuge tube. To develop a standard curve, four control solutions were prepared by combining 5, 10, 25 and 50 μL (1μg/μL) of reference collagen standard with distilled water to total 100 μL. Four tubes were filled with 100 μL of distilled water to serve as background controls. One milliliter of Sircol dye was added to all tubes, mixed by inversion and then placed on an orbital mixer for thirty minutes. Tubes were then centrifuged at 10,000 times gravity for 10 minutes, the supernatant drained and 1.0 mL alkali reagent added. After mixing, 200 μL of solution from each tube was transferred into wells on a new 96 well microtiter plate where the absorbance of the samples was measured, against the background control, on a microtiter plate reader (SpectraMax Plus, Molecular Devices Corporation) at a wavelength of 540 nm.

Microscopy Evaluations. Scaffolds were fixed in 10% formalin solution for evaluation by SEM and histology. Samples to be evaluated by SEM were dehydrated; a representative sample from each scaffold was sputter coated in gold (Electron Microscope Sciences model 550) for SEM (JEOL JSM-820 JE Electron Microscope) and evaluated at 350 to 1500 times magnification. Samples for histologic evaluation were cross-sectioned for slide mounting and H&E staining (Harris Histology Relief Services). H&E slides were evaluated by optical light microscopy (Eclipse TE300, Nikon).

Statistics. All statistical analyses were performed utilizing Sigma Stat (Version 2.03; SPSS, Inc). For the data collected, normality and equal variance tests were set to reject for $P \leq 0.01$. All samples passed normality and equal variance tests and were evaluated using a one-way ANOVA and then subjected to a pair-wise multiple comparison procedure (Tukey Test). The a priori alpha value was set at 0.05.

RESULTS

Mechanical Evaluation of Electrospun Scaffolds. Results of mechanical testing of the various electrospun fibrinogen-PDO composite structures are presented in figures 5.3-5.5. Properties of pure fibrinogen scaffolds (no PDO) were similar to those previously reported [77]. In general, values for modulus and peak stress increased as PDO concentration increased (figure 5.3). Values for strain at failure varied from 84% to 130%, but differences were not statistically significant (figure 5.4).

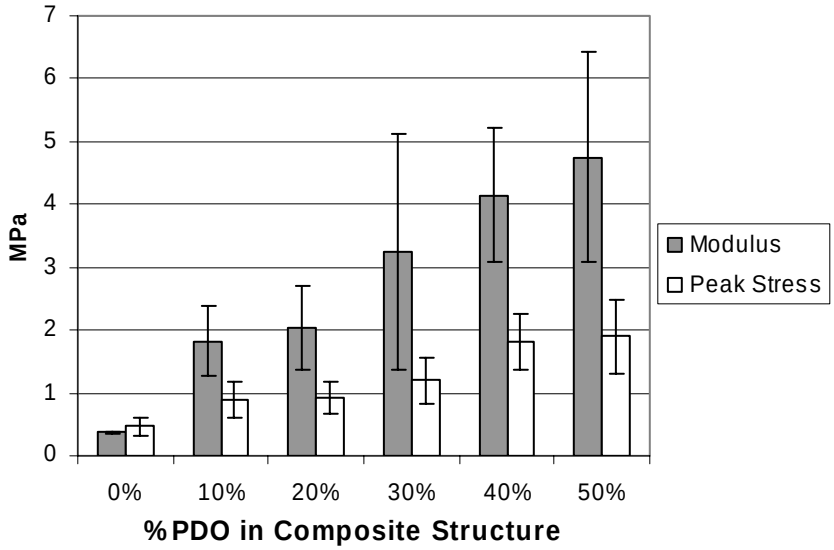

Figure 5.3. Results of mechanical testing of electrospun fibrinogen-PDO composite structures are illustrated in terms of modulus of elasticity (dark bars) and peak stress (white bars) verses the PDO concentrations in the solution from which structures were electrospun.

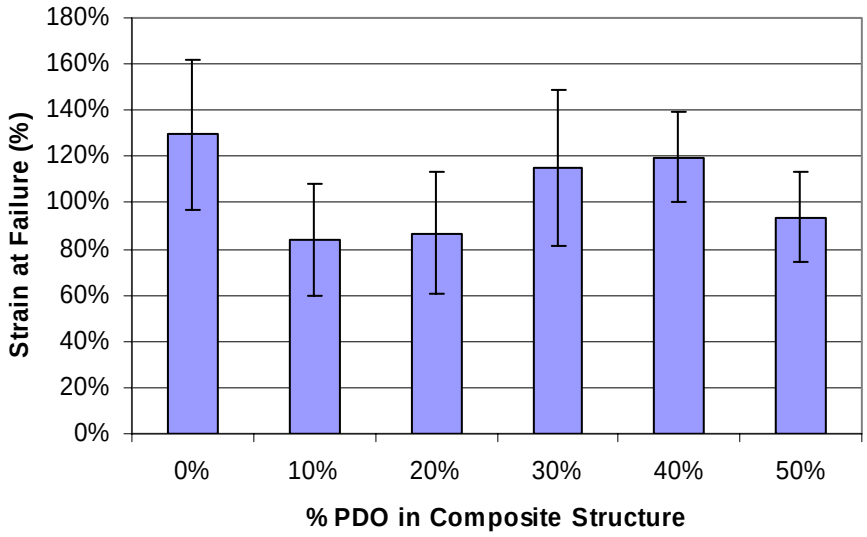

Figure 5.4. Results of mechanical testing of electrospun fibrinogen-PDO composite structures are illustrated in terms of percent strain at failure verses the PDO concentrations in the solution from which structures were electrospun.

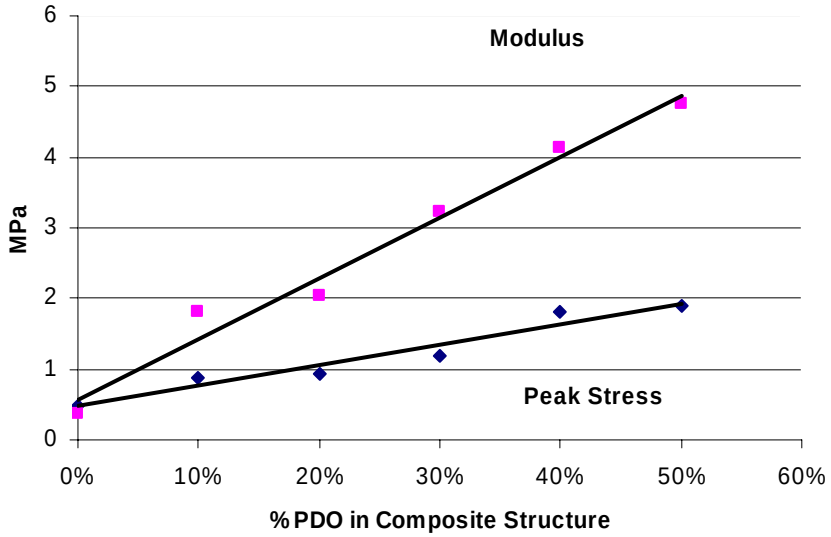

Figure 5.5. Modulus of elasticity and peak stress data demonstrate the linearity of these values from 0-50% PDO concentration. The R^2 value for the linear fit of the curve was 0.977 for modulus and 0.945 for peak stress.

Analysis of modulus of elasticity and peak stress data demonstrate the linearity of these values from 0-50% PDO concentration (figure 5.5) indicating a predictable increase in modulus of elasticity and peak stress as PDO concentration increases. The R^2 value for the linear fit of the curve was 0.977 for modulus and 0.945 for peak stress. An increase in PDO concentration of 20% and 30% was required to achieve a statistically significant increase in peak stress and modulus, respectively.

Collagen Assay. The controls in figure 5.6 demonstrate the linearity of the assay results from 5 µg to 50 µg. The R^2 value for the linear fit of the standard curve was 0.926 at 7 days and 0.991 at 14 days. Collagen content (figure 5.7) was calculated from the standard curve in figure 5.6. Comparison of collagen content at different PDO

concentrations demonstrated statistically significant differences at 7 and 14 days. Comparison between individual groups at day 7 only demonstrated statistical significance between the 0% PDO group and the 10% and 100% PDO groups. At 14 days, statistical significance was demonstrated between all individual groups except between the 10% and 100% PDO groups. Comparison of mean collagen content revealed two trends. First, there was a decrease in collagen content as PDO concentration increased up to 40% PDO, with an increase in collagen content in the 100% PDO group. Second, there was a higher collagen content at 7 days than at 14 days. These trends did not hold true for the 0% PDO concentration at 7 days which had a lower than expected collagen content.

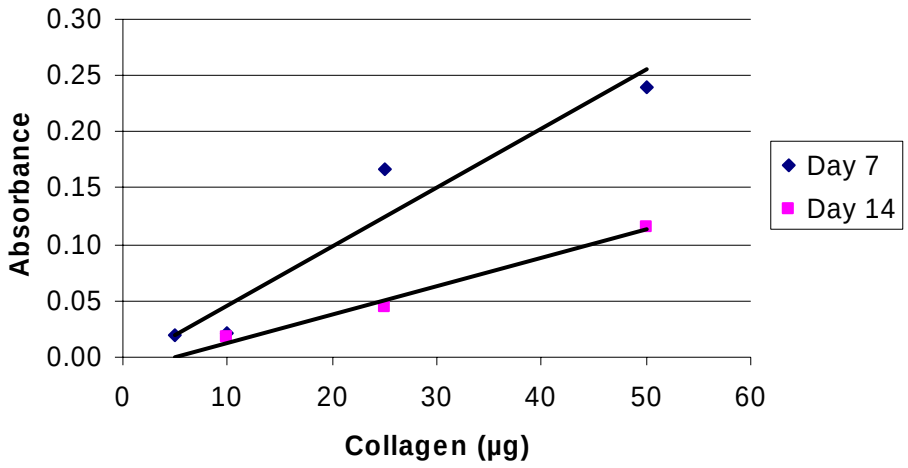

Figure 5.6. Collagen assay controls demonstrating the linearity of the assay results from 5 µg to 50 µg. The R^2 value for the linear fit of the standard curve was 0.926 at 7 days and 0.991 at 14 days.

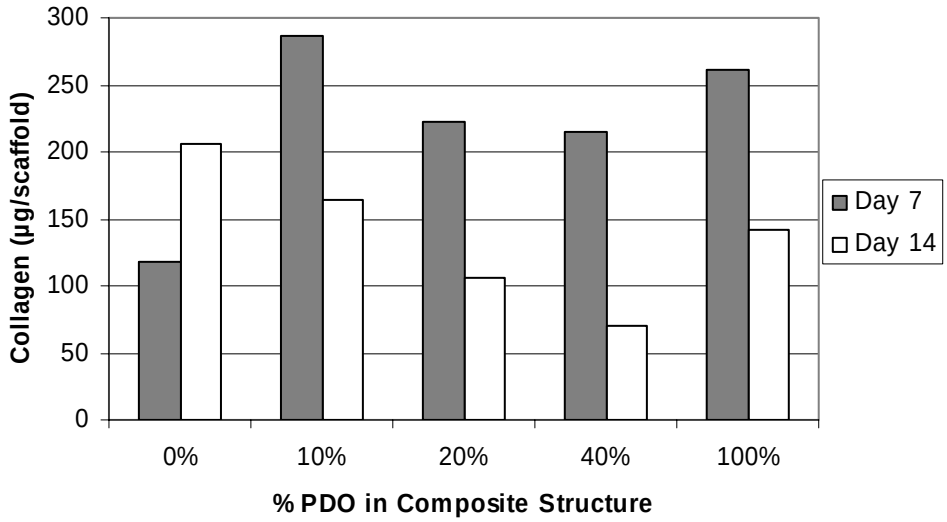

Figure 5.7. Bar graph depicting the collagen assay in terms of collagen content (based on the standard curve) for each scaffold condition.

Microscopy Evaluations. SEM analysis of post-cell culture electrospun scaffolds demonstrated evidence of cellular activity. This evidence is seen as areas of partial scaffold degradation and individual fibers having been pulled out of their expected orientation. Cells were not visible on the surface of the scaffolds.

Samples from the H&E stained histological sections are presented in figure 5.8. Histological evaluations of internal domains of the scaffolds revealed BSM cells had migrated into, and appear to be evenly distributed throughout, the scaffold thickness in fibrinogen containing groups at 7 days, indicating a substantial degree of cell migration transpired early in the study period. Further comparison of histologic samples revealed two trends. First, there was an increase in the structural integrity of scaffolds as PDO concentrations increased. Second, there was an increase in cell layering and cell spreading as PDO concentrations increased. These trends did not hold true for the 100%

PDO samples where no cells were identified on histological examination at any time point.

All PDO containing scaffolds remained structurally intact at 7 days, but areas of broken fibers were observed in the 0% PDO group demonstrating some early loss of structural integrity. Varying degrees of scaffold fragmentation and fusing of fibers with loss of the fibrous architecture were seen in the 0%, 10% and 20% PDO groups at 14 and 21 days. All samples in these groups were significantly fragmented by 21 days. The 40% PDO group maintained its structural integrity and fibrous structure throughout the study period.

Cell layering is an indicator of the extent to which a scaffold is directing cell growth and migration. Some degree of cell layering can be seen in all groups at 7 days, but it is most pronounced in the 40% PDO group. In the 0%, 10% and 20% PDO groups, cell layering is substantially decreased at 14 days and almost nonexistent at 21 days. Cell layering remains consistent throughout the study period in the 40% PDO group.

Cell spreading is an indicator of the degree to which a scaffold supports BSM cells assuming their natural morphology. At 7 days, there is an increase in cell spreading in the PDO containing groups compared to the 0% PDO group. This spreading is most pronounced in the 40% PDO group. There is a significant decrease in the amount of cell spreading in all groups, except the 40% PDO group, at 14 days and 21 days.

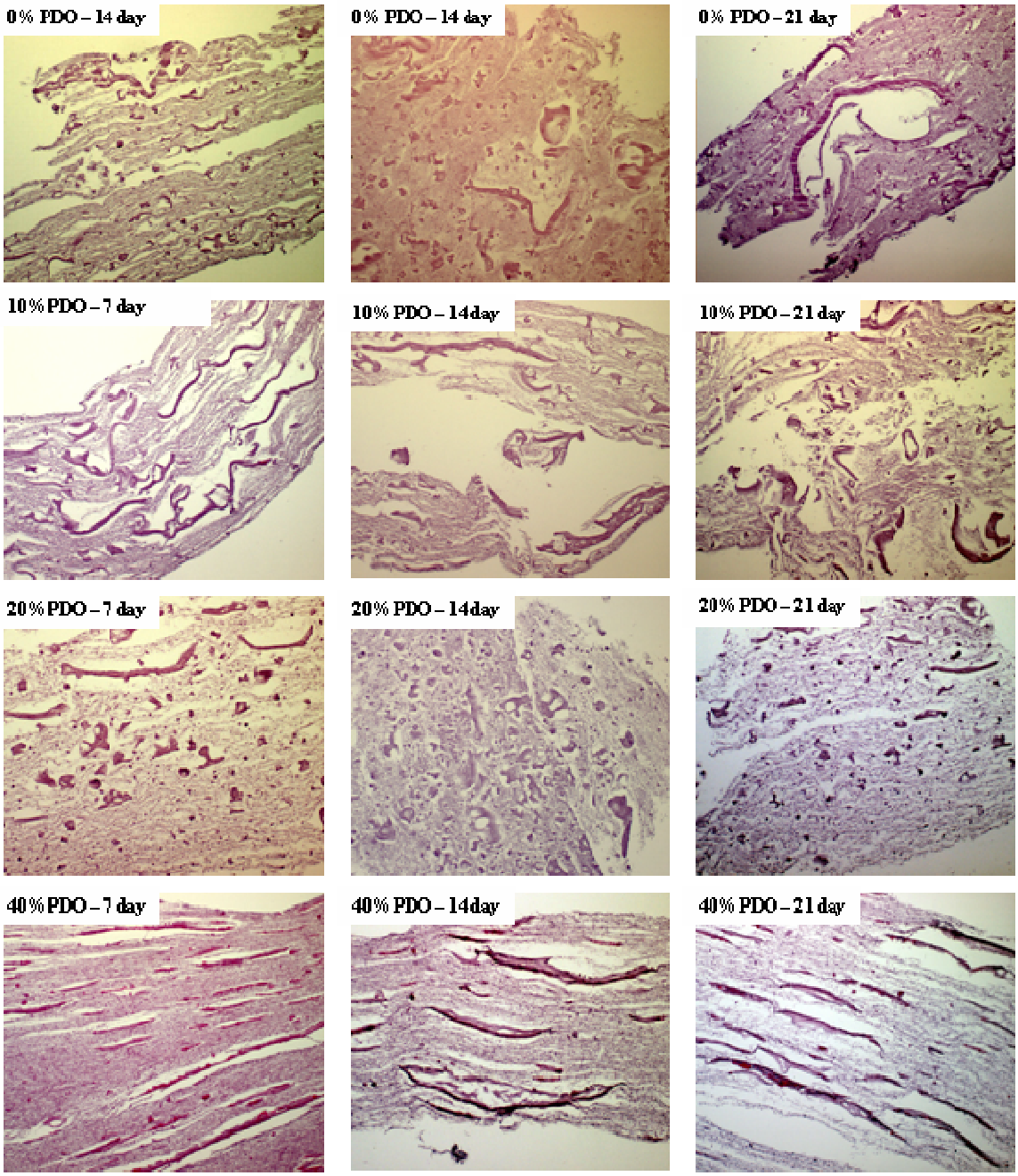

Figure 5.8. Optical micrographs of H&E stained electrospun fibrinogen-PDO composite scaffolds at 20 times magnification. BSM cells migrated through the full thickness of the scaffolds by day 7 (left column). Structural integrity of the scaffolds increased as PDO concentration increased (top to bottom). Cell layering and cell spreading also increased as PDO concentration increased.

DISCUSSION

The use of fibrinogen in tissue engineering applications is not new. Fibrinogen hydrogels have received much attention because they possess the benefits of homogeneous cell distribution and collagen deposition [297, 304, 306]. The use of hydrogels for tissue engineering requires mixing cells into the fibrinogen solution prior to forming the hydrogel. Electrospun fibrinogen scaffolds promote rapid cell migration into the scaffolds [78] allowing for cell seeding after scaffold production. However, these structures do not possess the structural integrity needed for direct implantation. Electrospun PDO structures have greater initial structural integrity and take longer to be degraded. The objective of this study was to demonstrate that an electrospun fibrinogen-PDO composite scaffold would retain the superior cellular interaction of fibrinogen while producing a product with functional strength for direct implantation.

In this study, mechanical testing data demonstrated that increasing the PDO concentration in electrospun fibrinogen-PDO composite scaffolds increased strength (peak stress) and stiffness (modulus) in a predictable fashion. All composite scaffolds maintained similar elasticity profiles, indicating composite scaffolds could be tailored to meet specific tissue engineering mechanical requirements.

The cell culture data demonstrated several trends related to scaffold composition. First, collagen deposition decreased as PDO concentration increased, with the exception of the 100% PDO group. Collagen deposition is an indication of the extent to which cells are remodeling a scaffold [78]. Second, there was increased cell spreading and cell

layering at higher PDO concentrations. Cell spreading demonstrates the scaffold supports cells assuming their natural morphology while cell layering within a scaffold demonstrates the scaffold is directing cell growth and migration. Third, higher PDO concentrations produced scaffolds with greater structural integrity and stability. In general, the higher PDO concentrations produced more stable scaffolds that allowed for slower scaffold remodeling and stimulated cells to assume a morphology closer to their native state.

One of the most attractive aspects of the electrospinning process is that scaffolds of various shapes and sizes can be constructed while at the same time precisely controlling fiber orientation, composition (blended fibers), and dimensions. Complex constructs can be fabricated to closely replicate the structural and chemical composition of the native structures. For example, flat sheets for on-lay grafts, seamless tubes, or any three dimensional shape in which a mandrel can be fabricated could be produced. Also, the ability to co-spin polymers with various additives (e.g. growth factors) offers the possibility of tailoring the scaffold to a specific site and application. Thus, with electrospinning, it may be possible to create ideal scaffolding for a wide array of tissue engineering applications.

Previous tissue engineered products for urinary tract reconstruction have been described utilizing decellularized submucosa, natural polymer hydrogels and synthetic polymer scaffolds created from a variety of production techniques [307-309]. Recent work by Atala et al. [310] has even demonstrated the feasibility of bladder augmentation with tissue engineered products using *in vitro* cell culture. This process is labor and

resource intensive with multiple procedures required to harvest cells for *in vitro* cell culture followed by later implantation. Electrospun scaffolds produced from other polymers have also been described for non-urologic applications [38, 59], but have failed to promote the rapid cellular in-growth demonstrated in this study.

While an electrospun PDO-elastin composite scaffold has been described [20], this is the first report of an electrospun fibrinogen-PDO scaffold and the first report utilizing an electrospun synthetic and natural polymer composite structure for urologic tissue engineering.

CONCLUSION

This study demonstrates human BSM cells rapidly migrate into and remodel an electrospun fibrinogen-PDO composite scaffold with deposition of native collagen. While there is still much work to be done, these initial findings indicate there is tremendous potential for electrospun fibrinogen-PDO composite structures as urologic tissue engineering scaffolds with the ultimate goal of producing an implantable acellular product that would promote cellular in-growth and *in situ* tissue regeneration.

CHAPTER 6 Cross-linking Electrospun Fibrinogen to Tailor Scaffold Properties

Preface: The following manuscript appeared in Biomedical Materials, 2008, volume 3, EPUB [181]. The work included demonstrates how the treatment of electrospun fibrinogen structures with two different cross-linkers, EDC and genipin, can affect the tensile strength, degradation rate, and bioactivity of the scaffold. Treatment with EDC and genipin enhanced scaffold mechanical properties and degradation time, making the normally insufficient fibrinogen structures mechanically stable as useful tissue engineering scaffolds.

Cross-linking Methods of Electrospun Fibrinogen Scaffolds for Tissue Engineering

Scott A. Sell[1], Michael Francis[2], Koyal Garg[1], Michael J. McClure[1], Catherine P. Barnes[1], David G. Simpson[3], and Gary L. Bowlin[1]

[1]Department of Biomedical Engineering
Virginia Commonwealth University
Richmond, VA 23284

[2]Department of Pathology
Virginia Commonwealth University
Richmond, VA 23298

[3] Department of Anatomy and Neurobiology
Virginia Commonwealth University
Richmond, VA 23298

ABSTRACT

The purpose of this study was to enhance the mechanical properties and slow the degradation of an electrospun fibrinogen scaffold, while maintaining the scaffolds high level of bioactivity. Three different cross-linkers were used to achieve this goal: GLUT vapor, EDC in ethanol, and genipin in ethanol. Scaffolds with a fibrinogen concentration of 120 mg/mL were electrospun and cross-linked with one of the aforementioned cross-linkers. Mechanical properties were determined through uniaxial tensile testing performed on scaffolds incubated under standard culture conditions for 24 hours, 7 days and 14 days. Cross-linked scaffolds were seeded with human foreskin FBs (BJ-GFP-hTERT) and cultured for 7, 14, and 21 days, with histology and SEM performed upon completion of the time course. Mechanical testing revealed significantly increased peak stress and modulus values for the EDC and genipin cross-linked scaffolds, with significantly slowed degradation. However, cross-linking with EDC and genipin was shown to have some negative affect on the bioactivity of the scaffolds as cell migration throughout the thickness of the scaffold was slowed.

INTRODUCTION

The interdisciplinary field of tissue engineering has blossomed in the brief two decades since the term was coined [2, 5]. While extensive research has been done in many areas that would fall under the umbrella name of tissue engineering, of particular

interest to this study is the research done on the creation of tissue engineering scaffolds that mimic the native ECM. A countless number of materials, both natural and synthetic in origin, and processing techniques have been used to engineer these ECM analogues, with varying degrees of success. While scaffolds may be designed and created to fit a specific application, ultimately all scaffolds regardless of application must meet a number of basic criteria to be successful. At its most fundamental, the scaffold should not elicit an immune response while remaining a viable framework for cellular infiltration/proliferation, ultimately mimicking both the fibrillar form and the complex function of the native ECM [11, 17-19, 27-29]. This requires the scaffold to have an idealized combination of mechanical properties, geometry, and surface chemistry [18, 25, 26].

Fibrinogen is a 340 kDa glycoprotein, synthesized by the liver and found freely circulating in the bloodstream, composed of three pairs of polypeptide chains: Aα, Bβ, and γ. During the coagulation cascade, more specifically the common pathway, fibrinopeptides A and B are cleaved from fibrinogen by thrombin to cause spontaneous polymerization of fibrin monomers. Fibrin then forms lateral protofibril associations, which result in the formation of a loosely assembled clot, subsequently stabilized by covalent cross-links created by plasma transglutaminase (factor XIIIa). This stable clot not only plays a haemostatic role, but also acts as an initial scaffold for tissue regeneration, serving as a platform for cell migration and proliferation [79, 173-175].

The effectiveness of fibrinogen in wound healing extends beyond its role in clotting; it is a protein with the capacity to bind a wide array of molecules that could be

beneficial from a tissue engineering standpoint. Fibrinogen contains two RGD integrin binding sites, located on the Aα chain, which commonly bind FBs and ECs. Additionally, fibrinogen has demonstrated the ability to bind with high affinity to functional VEGF and FGF. Fibrinogen also binds plasma fibronectin to its Aα chain, as well as insulin-like growth factor-binding protein-3 (IGFBP-3), which in turn binds insulin-like growth factor (IGF-1) [79, 176-178].

Our lab has previously reported on the electrospinning of fibrinogen scaffolds composed of nano-scale fibres for use as tissue engineering ECM analogues [21, 77, 78, 179, 180, 311]. Electrospinning is a simple process requiring little specialized equipment in order to create sub-micron scale, fibrous ECM analogues from a wide array of polymers. In brief, a polymer is placed in solution and drawn into a syringe fitted with a blunt tip needle. The surface tension of the polymer solution at the tip of the needle is overcome through the application of a large electric potential. A grounded target is placed a set distance from the charged polymer solution to create a static electric field. When the electric potential reaches a critical level, the electrostatic forces overcome the surface tension at the needle tip, and a fine jet of entangled polymer chains are drawn out. This jet whips through the air toward the grounded target, creating a dry fibre through the evaporation of the polymers solvent [11, 25, 48, 133, 134]. The electrospinning of fibrinogen produces scaffolds composed of fibres between 80 and 700 nm in diameter, dependant upon the starting concentration of the fibrinogen solution [21].

Fibrinogen has proven to be an intriguing polymer for use as a tissue engineering scaffold as it has consistently demonstrated excellent bioactivity, albeit with limited

mechanical integrity after several days in culture [77, 78, 179, 180]. As fibrinogen is readily broken down by thrombin and other serum proteases, it was determined that electrospun fibrinogen scaffolds needed to be successfully cross-linked in order to increase their lifespan both *in vivo* and *in vitro*. An ideal cross-linking agent would slow the rate of fibrinogen degradation, while having no negative impact on the bioactivity of the scaffold itself. Fibrin clots are cross-linked naturally through the inclusion of activated factor XIII (transglutaminase), which forms covalent bonds between glutamyl and lysyl residues of adjacent fibrin molecules [312-314]. However transglutaminase is expensive, and there are other cross-linking agents available that may prove to be more efficient and cost effective.

GLUT is the most common cross-linking agent in clinical use today for fixing collagenous tissues [315, 316]. GLUT is fairly inexpensive and has the ability to cross-link quickly over large distances with a wide array of amino groups [317]. However, GLUT has also been associated with increased cytotoxicity and material calcification [315, 316]. Heterobifunctional carbodiimides, more specifically EDC, have been gaining in popularity as tissue engineering cross-linkers and have recently been used in our laboratory to successfully cross-link both electrospun collagen [140] and elastin [71]. EDC is a zero-length cross-linker, as it does not become incorporated into the macromolecule, thereby decreasing the potential for cytotoxic effects [315, 316]. Genipin is a naturally occurring cross-linking agent that is derived from the fruits of *Geinpa Americana* and *Gardenia jasminoides Ellis*. It has been used mainly in herbal medicine, as well as in the creation of heat, pH, and light resistant food dyes as its

reaction with primary amines results in dark blue pigmentation [318]. There have been several publications reporting on the use of genipin to cross-link collagenous tissues, [316, 319, 320] polyethylene glycol hydrogels, [321] gelatin, [322] and chitosan [318]. Genipin has proven to be an effective cross-linker that increases a materials ultimate tensile strength and toughness, yet exhibits significantly less cytotoxicity than GLUT [323].

The purpose of this study was to determine an effective cross-linker for electrospun fibrinogen scaffolds; one that would ideally increase their mechanical properties and slow their degradation, while maintaining a high level of bioactivity. Uniaxial tensile testing over a two week period, *in vitro* cell culture, and scaffold porosity calculation results were compared to the results of uncross-linked scaffolds to determine the efficacy of the cross-linkers.

MATERIALS AND METHODS

Electrospinning. Solutions of 120 mg/mL of fibrinogen (Fraction 1, Type 1-S from bovine plasma, Sigma Aldrich, Co.) were made with a 90% by volume solution of HFP (TCI America Inc.) and 10% by volume 10x MEM (Sigma Aldrich, Co.). Solutions were left overnight on a shaker plate to ensure that all fibrinogen had dissolved and formed a homogenous solution. 5 mL of polymer solution were then drawn into a plastic Beckton Dickinson syringe and placed in a KD Scientific syringe pump (Model 100) to be dispensed at a rate of 3.5 ml/h. A high voltage power supply (Spellman CZE1000R;

Spellman High Voltage Electronics Corporation) was used to apply a voltage of 25 kV to a blunt tip 18 gauge needle fixed to the solution containing syringe. Solutions were electrospun onto a flat, stainless steel, grounded mandrel (2.5 cm wide × 10.2 cm long × 0.3 cm thick) placed 12 cm from the needle tip and rotating at a rate of ~500 rpm to produce a scaffold of randomly oriented fibers. Immediately after electrospinning, scaffolds were cut from the mandrel and placed in a fume hood for 30 minutes for degassing and removal of any residual HFP.

Glutaraldehyde Cross-linking. Scaffolds to be cross-linked with GLUT (Fisher Scientific Inc.) were placed in a 50% GLUT vapor chamber at room temperature for 1 hour. To construct the vapor chamber, 2 mL of GLUT were placed in a small (35 mm diameter) uncapped Petri dish, which was then placed inside of a large (100 mm diameter) Petri dish. The fibrinogen scaffold was also placed within the large Petri dish; the large dish was then covered and sealed with parafilm. After the 1 hour time period, the cover was removed and the scaffold was allowed to degas for 1 hour.

EDC Cross-linking. The EDC (Sigma-Aldrich Chemical Co.) cross-linking protocol used in this study was modified from a similar protocol used to cross-link electrospun type II collagen [140]. Based on the molecular weight of fibrinogen (340 kDa), the molarity of the electrospun fibrinogen solution was determined to be 0.35 mM. From this, an EDC solution at a 50 fold molar excess (17.6 mM) was created by dissolving the cross-linker in pure ethanol (Fisher Scientific Inc.). Electrospun scaffolds

were placed in 50 mL of cross-linking solution for 18 hours at room temperature, followed by a 2 hour rinse in 0.1 M sodium phosphate to hydrolyze any unreacted O-isoacylurea intermediates.

Genipin Cross-linking. The genipin cross-linking protocol used was similar to that of the EDC cross-linking protocol and was modified from a published protocol to cross-link porcine pericardia [320]. Genipin powder (Wako Pure Chemical Industries, Ltd.) was dissolved in pure ethanol to a molarity of 30 mM (determined by unpublished lab results). Fibrinogen scaffolds were placed in 50 mL of cross-linking solution for 72 hours at room temperature. It has been reported [321] that when the genipin cross-linking process is complete the cross-linked material will become dark blue in color. As such, it was noted that the electrospun fibrinogen scaffolds gradually changed color over the 3 day period, eventually reaching a dark blue near the end of day 3. Scaffolds were removed from the cross-linker solution at the completion of the time course.

Controls. As both the EDC and genipin cross-linkers were dissolved in ethanol, it was decided that a pure ethanol solution should be used as a control to ensure that the cross-linking effects were a result of the cross-linkers rather than the ethanol. Electrospun scaffolds were placed in an ethanol solution for 72 hours to mimic the 72 hour exposure time of the genipin cross-linked scaffolds.

Scaffold Porosity Measurement. Previous research has shown that electrospun fibrinogen scaffolds densify and contract when placed in an aqueous solution [311]. To determine what, if any, effect cross-linking had on scaffold densification, porosity was determined for uncross-linked, GLUT cross-linked, ethanol soaked, EDC cross-linked, and genipin cross-linked samples. Disks 21 mm in diameter were punched from dry, uncross-linked electrospun fibrinogen scaffolds. Each disk's dry mass and thickness was recorded, and the dry void fraction (porosity) of each disk was determined using the following equation:

$$Void\ Fraction = 1 - \left[\frac{Calculated\ Scaffold\ Density}{Known\ Material\ Density} x100 \right] \tag{6.1}$$

The calculated scaffold density was determined by dividing the mass of the disk by the total volume of the disk, while the dry density of fibrinogen was known to be 1.38 g/cm^3 [77].

Disks were then cross-linked according to protocols described previously. Once cross-linking had been completed, samples were rinsed 3 times in PBS to remove any residual cross-linker. Samples were then soaked for 24 hours in PBS at room temperature. The diameter and thickness of the samples were measured to determine their wet total volume after both the ethanol rinses and the PBS soak. Hydrated void fraction was calculated using equation (6.1) in the same way as the dry void fraction. The hydrated calculated scaffold density was determined by dividing the previously measured dry mass of the disks by the altered total volume of the hydrated disks, which was then divided by the dry density of fibrinogen. The dry mass and density were used

because it was assumed that the only difference in mass would be due to the presence of ethanol/water molecules in void spaces and not the actual electrospun fibers gaining or losing mass.

Uniaxial Tensile Testing. For uniaxial tensile testing, "dog-bone" shaped samples (2.75mm wide at their narrowest point with a gage length of 7.5 mm) were punched from each of the electrospun mats following cross-linking. These samples were then soaked in ethanol for 10 minutes, followed by 3 rinses in sterile PBS for disinfecting. These samples were soaked in DMEM-F12 (Invitrogen Corp.) supplemented with 10% FBS and 2% penicillin-streptomyocin (10,000 Units/mL each, Gibco BRL Life Technologies) under standard culture conditions (37°C and 5% CO_2) in an incubator for 1, 7, and 14 days. At the end of each time course, samples were tested to failure on a MTS Bionix 200 testing system with a 50 N load cell (MTS Systems Corp.) at an extension rate of 10.0 mm/min. Elastic modulus, peak stress, and strain at break were calculated by the MTS software TestWorks 4.0 and recorded.

In Vitro Cell Culture. To evaluate the effect of cross-linking on cell-scaffold interaction, circular disks (10 mm in diameter) were punched from each of the cross-linked scaffolds, disinfected (by soaking in ethanol for 10 minutes followed by 3 rinses in PBS), and placed in a 48-well plate. Each disk was then seeded in its center with immortalized human foreskin FBs (BJ-GFP-hTERT), containing a retroviral transduced human telomerase reverse transcriptase (hTERT) element and green fluorescent protein

(GFP), at a concentration of 16,500 cells / 100 μL. DMEM-F12 supplemented with 10% FBS and 1% penicillin-streptomyocin was added to each scaffold (100 μL of cells in media incubated for 45 minutes, followed by 200 μL of media). The scaffolds were then statically cultured under standard culture conditions (37°C and 5% CO_2) in an incubator. One disk of each sample was removed after 7, 14, and 21 days. Removed disks were fixed in 10% formalin and processed for SEM and histology. Samples for SEM were dehydrated and sputter coated in gold (Electron Microscope Sciences model 550). Micrographs were taken on a Zeiss EVO 50 XVP scanning electron microscope and evaluated between 500 and 5000 times magnification. Samples for histologic evaluation (H&E and Masons Trichrome) were cross-sectioned for slide mounting and stained by Harris Histology Relief Services. Slides were then evaluated by optical light microscopy (Eclipse TE300, Nikon).

Statistical Analysis. Statistical analysis was performed on mean scaffold porosities (n=6), as well as mean uniaxial tensile testing values (n=6). All statistical analysis was based on a Kruskal–Wallis one-way ANOVA on ranks and a Tukey–Kramer pairwise multiple comparison procedure ($\alpha = 0.05$) performed with the JMP®IN 4.0.3 statistical software package (SAS Institute, Inc.). Graphical depictions of mean data were constructed with Microsoft Excel 2000, with error bars representing standard deviations.

RESULTS

Electrospinning. Electrospinning of 120 mg/ml fibrinogen solutions from HFP resulted in formation of non-woven fibrous scaffolds. Fibrinogen fibers were randomly oriented and had a mean fiber diameter of 710 ± 220 nm (figure 6.1). The scaffolds appeared to be highly porous, with a large amount of void space.

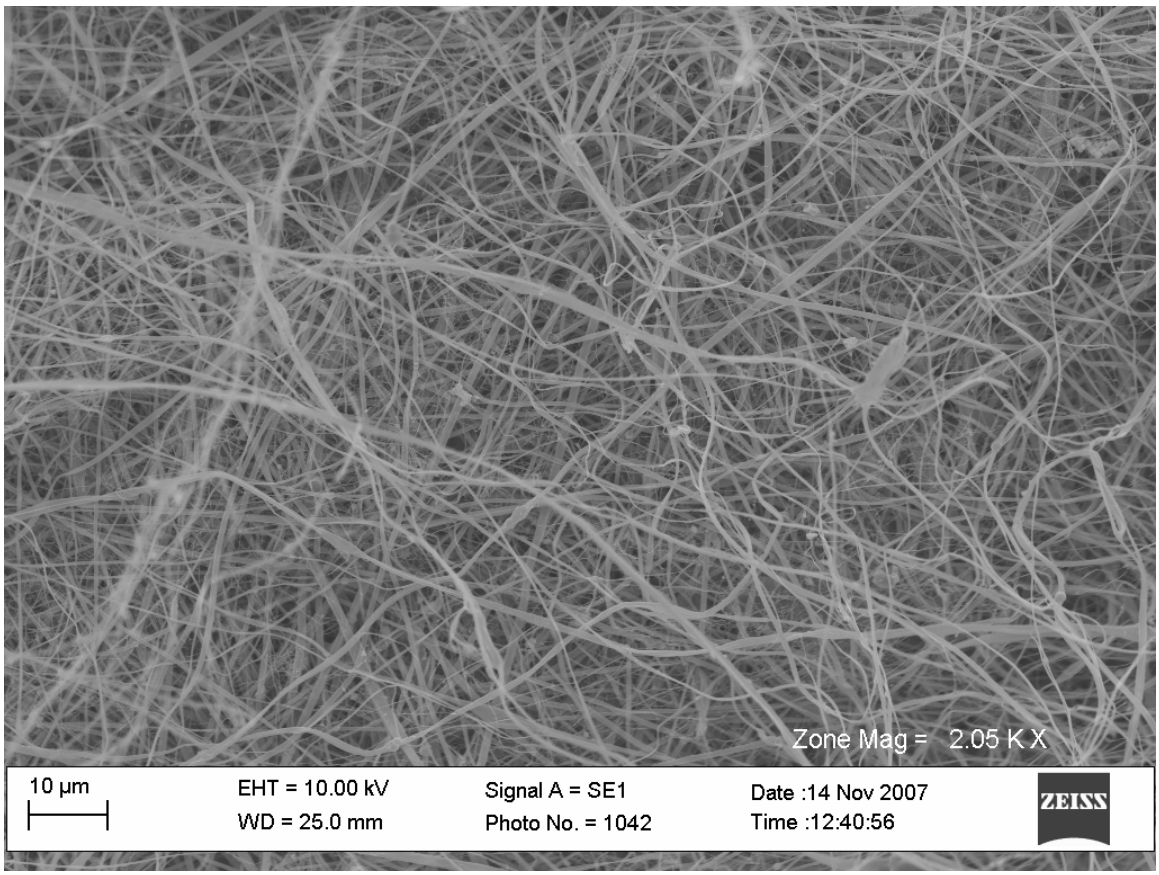

Figure 6.1. Scanning electron micrograph of electrospun fibrinogen at 2050x.

Cross-linking. Scanning electron micrographs of electrospun fibrinogen scaffolds taken before and after the various cross-linking methods were taken to provide insight into the fibers morphology (figure 6.2). Scaffolds were dipped in ethanol and dehydrated prior to sputter coating and SEM.

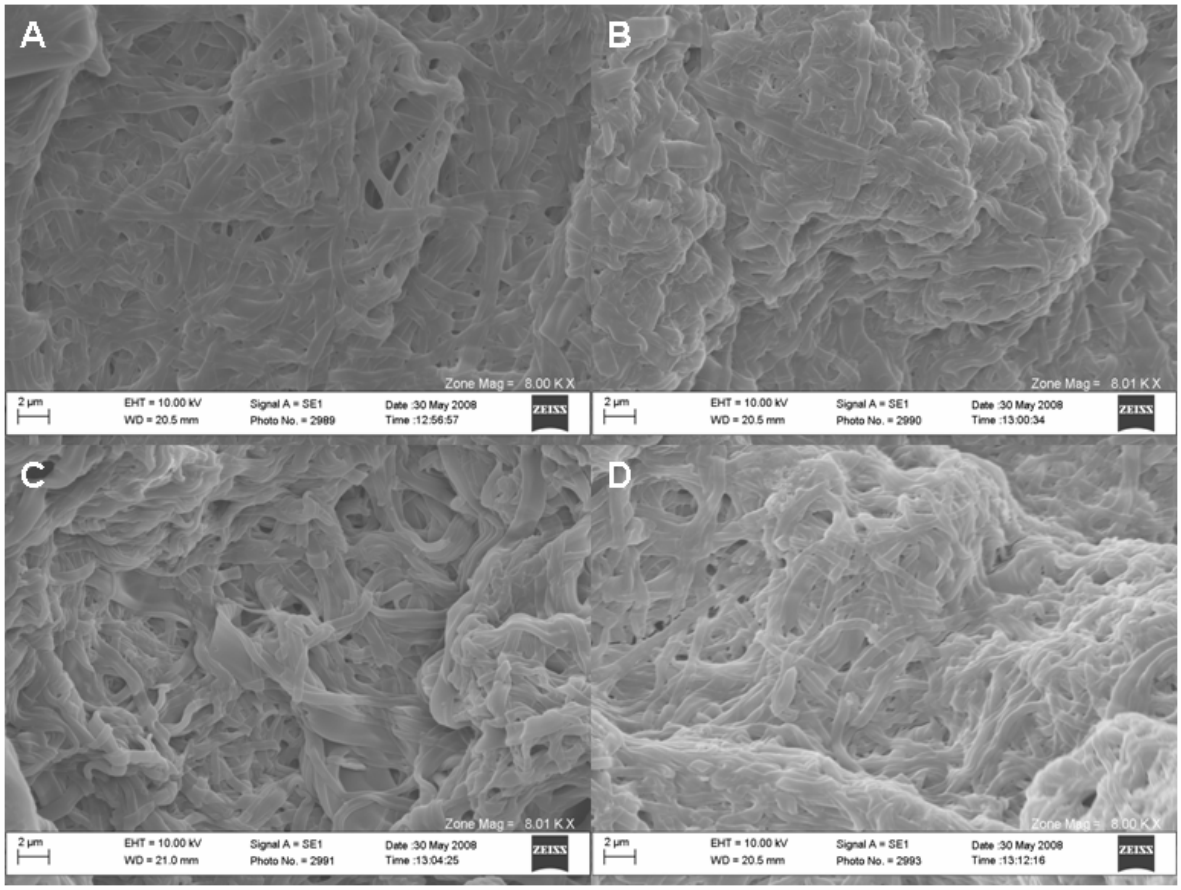

Figure 6.2. Scanning electron micrograph of electrospun fibrinogen scaffolds after treatment with GLUT (A), ethanol (B), EDC (C), and genipin (D). All images were taken at 8000x.

Scaffold Porosity Measurement. Mean scaffold porosity measurements are shown in figure 6.3. While all scaffolds tested maintained a high percentage of void space, significant decreases in porosity occurred in a number of samples after they were placed in PBS. The control scaffolds (no fixation and ethanol soaked) exhibited the largest amount of densification, while the GLUT cross-linked specimens also exhibited a significant decrease in mean scaffold porosity. EDC cross-linked specimens did not experience significant densification, while genipin cross-linked scaffolds exhibited a small significant difference between the dry and PBS soaked samples. There was no significant difference between PBS soaked samples cross-linked with EDC and genipin, which may indicate that a larger sample size would have reduced the standard deviation and eliminated the difference seen in the genipin specimens.

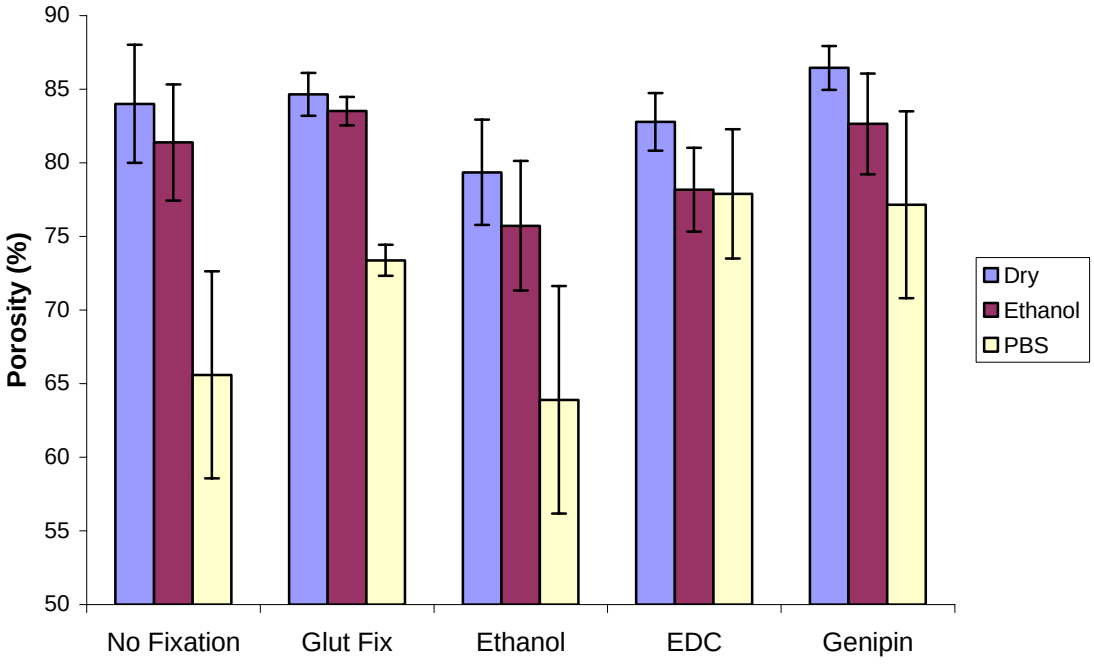

Figure 6.3. Mean scaffold porosities for different cross-linking groups.

Uniaxial Tensile Testing. The results of the uniaxial tensile testing 2 week degradation study are presented in figure 6.4. After 1 day in solution under standard culture conditions, peak stress values were significantly higher for the EDC and genipin cross-linked scaffolds when compared to the uncross-linked, GLUT, and ethanol soaked samples. Modulus values mirrored these results, while strain at break values were significantly reduced for the EDC and genipin cross-linked scaffolds. This reduced straining of cross-linked samples is consistent with prior results, and is believed to be due to the stiffening of the scaffold fibers through the cross-linking procedure.

By day 7 the uncross-linked and GLUT cross-linked scaffolds lacked the mechanical integrity needed to undergo mechanical testing. While these scaffolds maintained their "dog-bone" shape and were able to be placed in the grips of the MTS, their extension resulted in an extremely noisy stress-strain curve of low value that did not allow for the extraction of results. Surprisingly, the ethanol soaked samples were still mechanically viable, albeit with significantly reduced mechanical properties. The EDC and genipin cross-linked scaffolds maintained their original mechanical properties with no significant differences.

By day 14 the only surviving samples were those that had been cross-linked with EDC and genipin. For these scaffolds, there was no significant difference between the mechanical properties achieved on day 14 when compared to day 1. The other scaffolds, while appearing to maintain their "dog-bone" shape, immediately fell apart when they were removed from solution, making mechanical evaluation impossible.

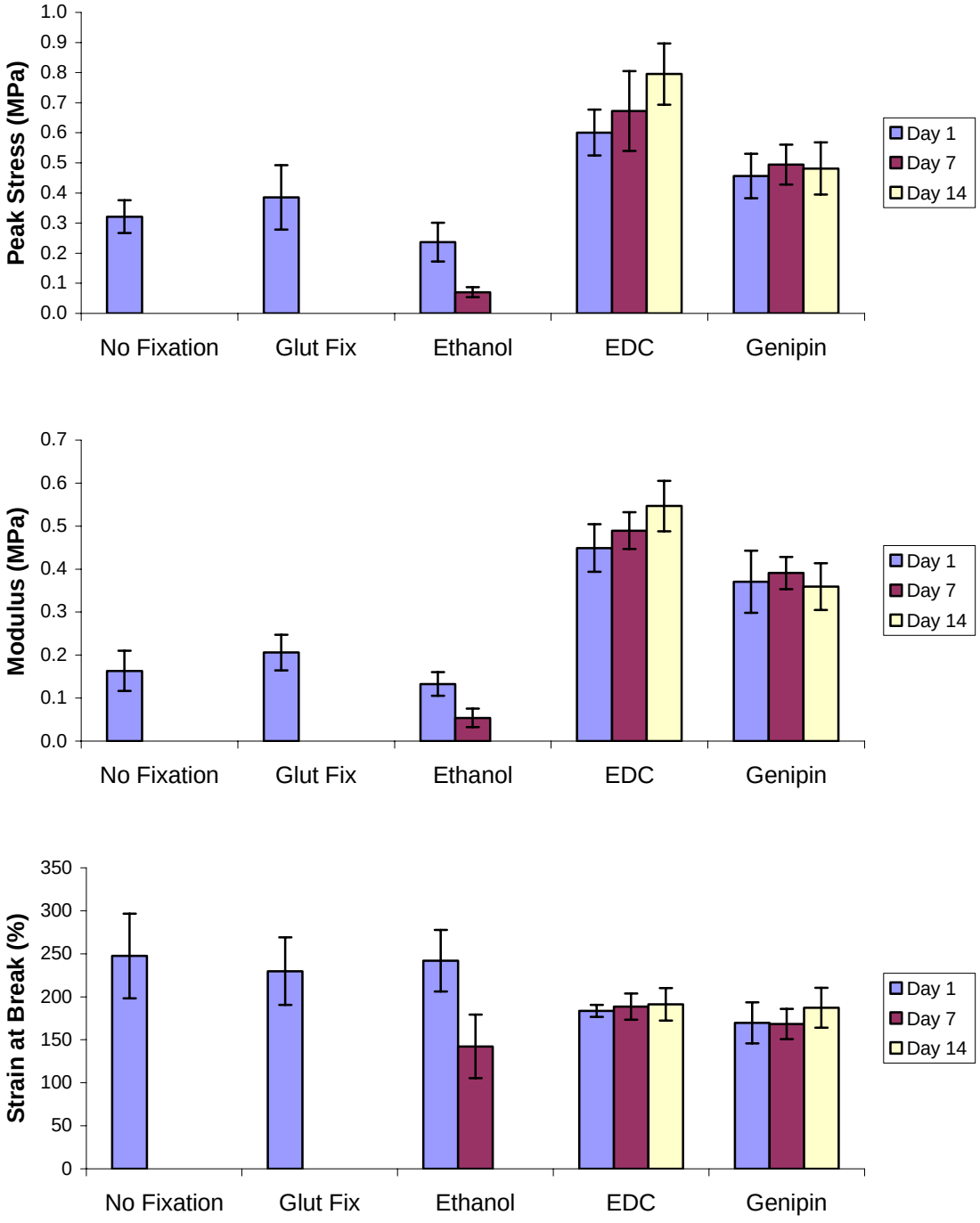

Figure 6.4. Peak stress (top), modulus (middle), and strain at break (bottom) values for cross-linked scaffolds achieved through uniaxial tensile testing over a 2 week degradation period.

In Vitro Cell Culture. Results of the SEM analysis and histological evaluation are shown in figures 6.5, 6.6, and 6.7. The SEM analysis provided qualitative information on cell proliferation as well as cell migration across the scaffolds' surface, while histology provided an indication of cellular migration into the scaffold as well as the degree to which collagen was produced and the scaffold was remodeled. Cell proliferation was evident in each of the scaffolds seeded with FBs as there is a definite increase in the number of cells seen on the surface of the scaffolds at the end of the time course. Surface migration of cells was also apparent for all scaffolds regardless of cross-linking as FBs were seen on almost all areas of the scaffolds surface by day 21, as opposed to cells being present in only localized areas for day 7. However, cross-linking appeared to play a major role in the ability for cells to migrate into the thickness of the scaffold. As evidenced clearly by the trichrome stained samples taken at day 21, the uncross-linked and ethanol soaked fibrinogen scaffolds (red) were almost entirely replaced by newly produced collagen (blue). The GLUT cross-linked scaffold showed a gradual transition from electrospun fibrinogen to newly produced collagen, while both the EDC and genipin cross-linked scaffolds exhibited very little remodeling

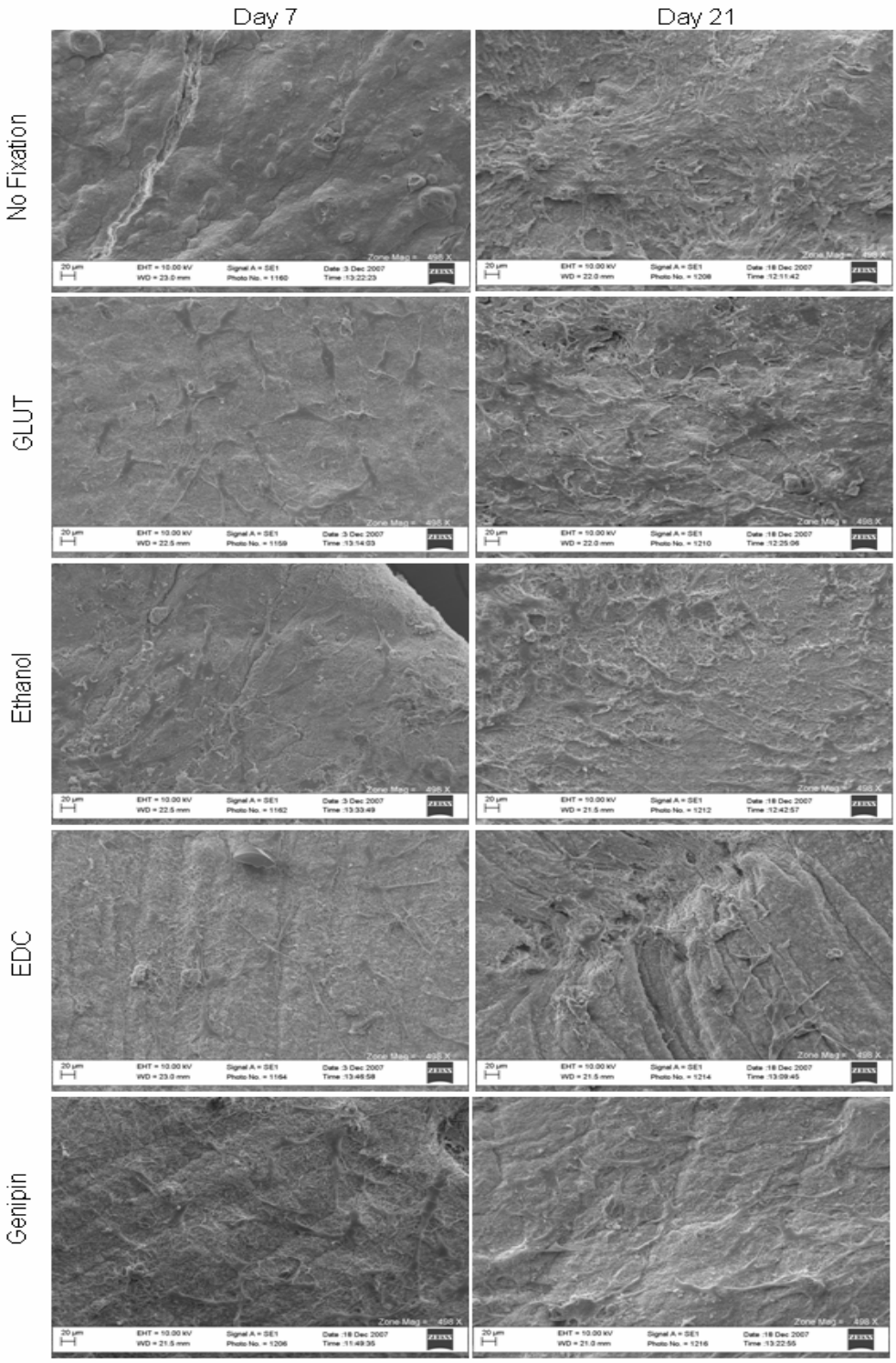

Figure 6.5. SEM analysis of electrospun scaffolds seeded with FBs. All micrographs were taken at 498x.

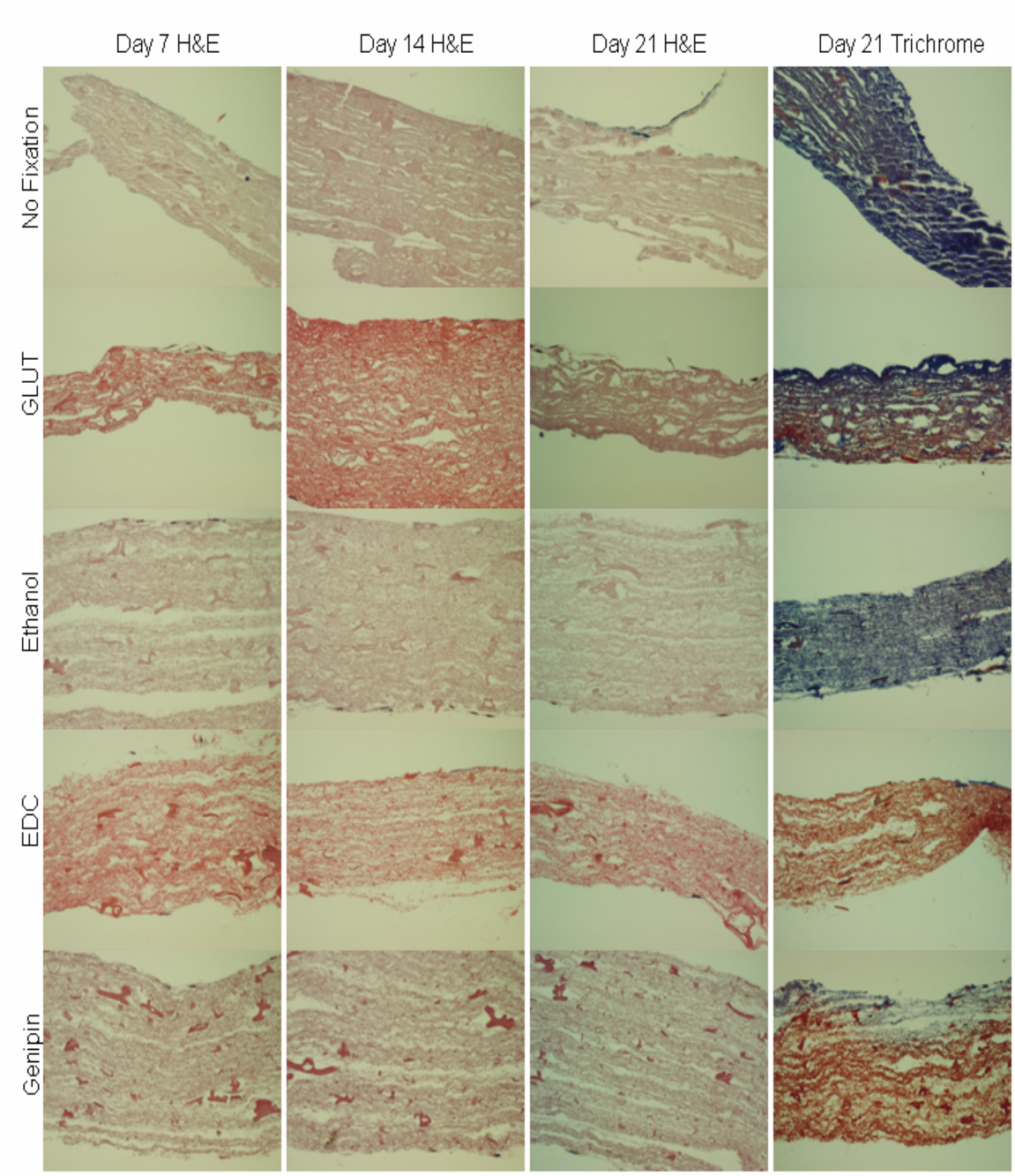

Figure 6.6. Histological evaluation of cross-linked scaffolds observed under an optical light microscope at 40x magnification. For trichrome stained samples fibrinogen appears red while collagen is blue.

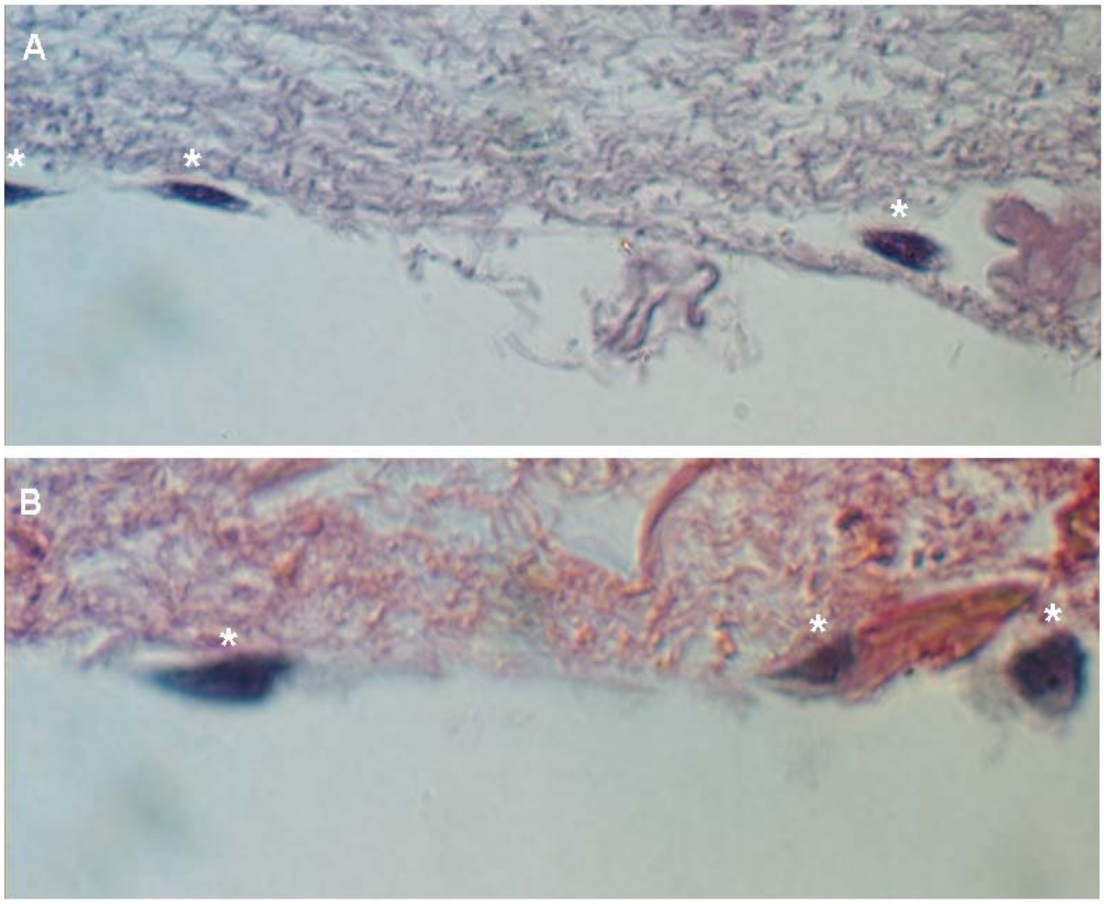

Figure 6.7. High magnification (100x) images of H&E stained cells (*) on electrospun fibrinogen scaffolds treated with ethanol (A) and EDC (B) after 21 days in culture.

DISCUSSION

Scaffold Porosity Measurement. The scaffold porosity measurement results demonstrated that fibrinogen scaffolds electrospun from HFP were highly porous. However, this porosity changes when the scaffolds become hydrated in an aqueous environment. This densification may be due in part to some short term ultra-hydrophobicity caused by residual solvent left within the scaffold. The sub-micron scale

roughness of the scaffolds may also contribute, however further investigation is necessary before any concrete explanation can be provided. Regardless of the reason for the densification, it was shown that cross-linking of the fibrinogen scaffolds could significantly reduce the degree to which the scaffold contracted. GLUT cross-linking resulted in a significant increase in hydrated scaffold porosity (74%) over uncross-linked scaffold porosity (66%), while EDC and genipin cross-linking resulted in even larger sustained porosities (roughly 78% for both). Interestingly, soaking the scaffolds in ethanol as a control had no effect on hydrated scaffold porosity. This would indicate that the ethanol itself played no role in altering the scaffolds hydrophobicity, rather it was the cross-linkers themselves which enhanced the mechanical properties of the scaffold, which in turn hindered densification. The sustainability of a highly porous scaffold would be of great benefit in a tissue engineering application as this high porosity would in turn enhance scaffold permeability, making cell migration and nutrient/waste transport more feasible over longer distances.

Uniaxial Tensile Testing. The uniaxial tensile testing results achieved over the 14 day time course of this study provided data that definitively shows fibrinogen scaffold mechanical enhancement through the use of EDC and genipin cross-linkers. Electrospun fibrinogen, while highly bioactive, lacked the mechanical integrity needed to become a reliable tissue engineering scaffold. Clearly, the total loss of mechanical properties after one week in solution demonstrates the purely short term possibilities of a tissue engineering scaffold made of uncross-linked fibrinogen for use in vivo. While the

uncross-linked scaffolds retained their shape at one week, they lacked any significant mechanical properties and would surely have failed in the more rigorous in vivo setting. By the second week of the test, breakdown of the uncross-linked scaffolds was visually evident, as the original "dog bone" shaped specimens had begun to break apart.

GLUT cross-linking failed to produce any significant improvement. This was somewhat surprising as GLUT is one of the most commonly used fixatives available. The poor performance of the GLUT in this study may have been improved by utilizing an alternate form of GLUT cross-linking. The gas vapor method was used here, rather than an immersion technique, to prevent large quantities of residual GLUT from becoming trapped within the scaffold, as GLUT has been proven to be highly cytotoxic. Increasing the contact between GLUT and the fibrinogen scaffolds may have enhanced the amount of cross-linking that occurred, but would have also run the risk of making the scaffold uninhabitable and prone to calcification.

The use of both the EDC and genipin cross-linkers in ethanol proved to be highly effective in enhancing the mechanical properties of the electrospun scaffolds, opening the door for fibrinogen to be used as a scaffolding material in more tissue engineering applications where mechanical stability is paramount (haemostatic patches, skin grafts, tubes and conduits, etc). Peak stress and modulus values for the EDC and genipin cross-linked scaffolds were significantly improved over the remaining groups, while strain at break values were significantly reduced. Yet, there was little difference between the samples cross-linked with EDC and the samples cross-linked with genipin. This was somewhat surprising as, at least in collagenous structures, the two cross-linkers act

through different mechanisms [316]. Further testing is necessary to quantify the amount of cross-linking that each cross-linker produces, using a ninhydrin assay [324] to measure free amine groups.

Not only did the EDC and genipin cross-linking improve the mechanical properties of the electrospun scaffolds, but it was also effective in slowing the rate of fibrinogen degradation. Scaffolds cross-linked with EDC and genipin retained their shape and remained mechanically viable during the 14 day course of the study with no significant decrease in mechanical properties. More long term studies are required to determine just how long the cross-linked scaffolds remain viable in solution; the ultimate test being implantation in vivo. However, from these preliminary results it certainly seems feasible to tailor the rate of scaffold degradation, at least to some extent, by altering the amount of cross-linking that takes place. By reducing the concentration of the cross-linkers in ethanol, or reducing the exposure time of the scaffolds to the cross-linking solutions, one could alter the amount of cross-linking that occurs. A reduction in the degree to which the fibers are cross-linked would lead to a reduction in their degradation time. As a nano-fibrous bioactive scaffold, with a controllable rate of degradation, electrospun fibrinogen could have potential as a slow release drug delivery vehicle.

In Vitro Cell Culture. The results of the SEM and histological evaluation demonstrated that while cross-linking with EDC and genipin positively enhanced electrospun fibrinogens' mechanical properties, it also played a role in altering the

scaffolds previously excellent bioactivity. Uncross-linked and ethanol soaked scaffolds showed nearly complete scaffold remodeling by 21 days, while the scaffolds cross-linked with EDC and genipin resulted in very little collagen deposition. Samples cross-linked with the cytotoxic GLUT exhibited a gradual top down remodeling of the scaffold. This was quite surprising as the EDC and genipin cross-linked scaffolds maintained the highest porosity, as shown previously. However it was the scaffolds that experienced the most densification and had the lowest porosities that had the best cell migration. This may be due to the fact that cells have shown the ability to move electrospun fibers to create pores as large or small as they require for migration [28], and require the transduction of certain chemical or mechanical signaling to occur between cells and matrix for subsurface migration to occur. As shown previously, the modulus of the scaffolds was significantly increased when cross-linked with EDC and genipin. These altered fibers may have then been too stiff to allow for subsurface cell migration to occur. Additionally, the cross-linking process may have masked the integrin binding sites that are normally exposed on fibrinogen, causing the cells to no longer recognize the matrix as an ECM analogue. Further testing will need to be done to determine exactly what caused the reduction in scaffold bioactivity.

CONCLUSION

This preliminary investigation into the cross-linking of electrospun fibrinogen scaffolds for tissue engineering applications yielded mixed results. Of the cross-linking

methods tested, EDC and genipin in ethanol proved to be highly effective in enhancing scaffold mechanical properties, with significant increases seen over uncross-linked samples. Moreover, these cross-linkers were successful in retarding the rate of scaffold degradation in culture media under standard culture conditions over a period of 14 days. While these cross-linkers strengthened the electrospun scaffolds, they also had a negative impact on the ability for FBs to migrate below the surface of the scaffold and remodel it with collagen. Further investigation is needed to determine what mechanisms were affected by cross-linking to reduce scaffold bioactivity; whether it was plasticizing of the fibrinogen fibers which ultimately led to loss of inherent cell binding sites, or alteration of individual fiber mechanical properties. It will also be necessary to perform a more in-depth analysis of the degree to which cross-linking is controllable by altering the exposure time and concentration of the EDC and genipin cross-linkers. Regardless, the enhanced mechanical properties and degradation time were seen as positive results that may outweigh the reduced subsurface migration when placed *in vivo*. The use of these cross-linkers could open doors for further use of electrospun fibrinogen ECM analogue scaffolds to be used in more applications that require tailorable degradation rates and long term mechanical stability, such as a steady state drug release vehicle.

CHAPTER 7 Creation of Aligned Silk Scaffolds for Tissue Engineering

Preface: The following manuscript has been submitted for review to Biomedical Materials at the time this document was prepared. The included work investigates differences in anisotropy of electrospun silk-based scaffolds for potential use as both ligament and vascular grafts. A number of different silk-based structures were created with varying degrees of fiber alignment, and were subsequently evaluated through mechanical testing and FFT. The author's role in this work was silk fibroin extraction and the creation, imaging, and mechanical testing of structures intended for use as ligament analogues.

Electrospinning Aligned and Random Polydioxanone- and Polycaprolactone- Silk Fibroin Blended Scaffolds: Geometry for Two Matrices

Michael J. McClure[1], Scott A. Sell[1], Chantal E. Ayres[2], David G. Simpson[2], and Gary L. Bowlin[1]

[1]Department of Biomedical Engineering
Virginia Commonwealth University
Richmond, VA 23284

[2]Department of Anatomy and Neurobiology
Virginia Commonwealth University
Richmond, VA 23298

ABSTRACT

Extracellular matrices are arranged with a specific geometry based on tissue type and mechanical stimulus. For ligaments and blood vessels in the body, preferential alignment of fibers is in the direction of repetitive force. Electrospinning is a controllable process which can result in fiber alignment and randomization depending on the parameters utilized. In this study, both ACL and arterial scaffolds were studied to determine if fibers could be controllably aligned in the circumferential direction of a large 80 mm diameter mandrel for ACL and a small 4 mm diameter mandrel for blood vessel applications. Results revealed that large and small diameter mandrels produced different degrees of fiber alignment based on the analysis of SEM images. Uniaxial tensile testing further demonstrated scaffold anisotropy through changes in peak stress, modulus, and strain at break at mandrel rotational speeds of 500 and 8000 RPM. Additional mechanical testing was performed on vascular grafts using dynamic compliance, burst strength, and longitudinal strength displaying that grafts electrospun at higher rotational rates produced stiffer conduits which had lower compliance and higher burst strength compared to the lower mandrel rotational rate. Scaffold properties were found to depend on several parameters in the electrospinning process: mandrel rotational rate, polymer type, and

mandrel size. The electrospinning of PCL, PDO, and silk together in different polymer blends demonstrates promise for both ACL and artery and warrants further investigation into parameter optimization.

INTRODUCTION

Anterior Cruciate Ligament. Ligament injury, particularly injury to the ACL, is becoming extremely common in our society due to our desire to perform physical activities. These injuries to ligaments residing inside the knee capsule (cruciate ligaments) lack the ability to heal spontaneously and must be repaired surgically [271]. In 2002, more than 5 billion dollars were spent to reconstruct 200,000 ligaments in the United States [268]. In the short term, ligament damage can result in severe pain and discomfort as well as limitations in mobility and the ability to participate in athletics and exercise [80]. Prolonged joint use without the benefit of the ACL will lead to joint instability, altered load bearing, articular cartilage damage, and ultimately OA [325]. Currently there is no clinical graft material to replace a damaged ligament that would be considered ideal.

There have been many different approaches taken to tissue engineering ligament replacements. Most involve the use of bioresorbable synthetic polymers such as PLA [268, 269, 273, 326, 327], PLGA [267, 269, 276, 328, 329], PCL [80, 268], and PDO [22, 80, 83-85, 268, 270, 273, 330]. Natural biopolymers such as silk, and collagen [61, 268, 270, 273, 326] have also been used extensively. These materials have been used almost

exclusively as braided, knitted, or extruded micron scale fibers, with no evidence of a ligament analogue composed entirely of electrospun nanofibers in the literature.

The creation of an ideal tissue engineered ligament replacement requires a structural scaffold (ECM analogue) that can support cell activity, host reparative cells with the ability to produce ECM, and have an overall structure conducive to the repair process with appropriate nutrient supply. The engineered ECM analogue should ideally have mechanical properties similar to those of native ACL; for a complex load bearing structure, this is no small feat and as such there are several major hurdles. Foremost, the initial mechanical properties of the structure (i.e. ultimate stress, modulus, and strain at break) need to replicate those of ACL. To prevent catastrophic failure, the mechanical properties of the implanted structure need to remain high *in vivo* as the material degrades and cells infiltrate and remodel the scaffold.

Artery. CVD, specifically CHD resulting from arteriosclerosis, remains the leading cause of death in the United States and has been so virtually every year since 1900 [105]. Arteriosclerosis is a vascular disease characterized by thickening of the arterial wall and a subsequent decrease in the arterial lumen leading to an eventual decrease or loss of circulation distal to the disease site. Once blood flow is compromised, vascular bypass is an option to restore blood flow to tissues distal to the restriction or blockage [59]. In 2005 there were 469,000 bypass procedures performed due to CHD [105], which typically involve the replacement of a coronary artery with a patients own saphenous vein, the gold standard. Synthetic alternatives include e-PTFE and woven or

knitted PET fibers (Dacron®). However, at the small diameter level, in low flow environments, these grafts are prone to thrombus formation and intimal hyperplasia.

Developments of vascular graft materials have undergone several pathways. Bioresorbable scaffolds such as PLA [331-333], PGA [334, 335], PDO [48, 154], PCL [145, 248, 336, 337], in addition to natural polymers such as collagen [19, 59, 87, 120, 338] and elastin [20, 71], have been at the top the list. Electrospinning has provided a possible key to unlocking the synthetic graft bypass mystery, where synthetic polymers and biopolymers can be blended together with tunable mechanical properties. However, tuning these mechanical properties can be a difficult task when attempting to mimic the arterial wall.

The arterial wall is composed of three separate layers: the intima, media, and adventitia, each imparting its own biomechanical function, while being subjected to both axial, circumferential, and torsional forces. The most intricately arranged layer of the three is the media, whereby elastic fenestrae, specific smooth muscle orientation, and ECM proteins such as elastin and collagen provide a network that is both highly elastic and strong. Several studies have found the medial layer in both elastic arteries (i.e. aorta) and muscular arteries (facial, brachial, femoral) to be arranged with specific pitch geometry, composed of SMCs and their matrix [339].

The natural geometry of native human ECM provides a mechanical advantage for tissues which undergo constant deformation and stress. In particular, both ACL and arteries are continuously loaded and unloaded. Ligaments, like the ACL, are composed of closely packed collagen fiber bundles oriented in a parallel fashion to provide for

stability of joints in the musculoskeletal system, creating a structure that is best suited for the longitudinal direction. Arteries are composed of a combination of mainly collagen and elastin, where collagen fibers are positioned specifically to provide maximum resistance to the three dimensional stress variables while elastin generates elastic recoil and minimizes energy loss.

Synthetics such as PDO and PCL have displayed strong mechanical properties while remaining flexible, properties that are conducive to both ligament and arterial tissue engineering. Silk, as a suture, has been used for centuries, however, it is relatively new to the field of tissue engineering and has demonstrated promise in several ligament and vascular studies [80, 84, 86, 183, 340-342]. This study focuses on the generation of either aligned or random electrospun fiber matrices using combinations of PDO, PCL, and silk. These polymer blends were analyzed for fiber alignment on small, 4 mm diameter, and large, 80 mm diameter, mandrels using fast Fourier transform (FFT) and mechanical characterization.

MATERIALS AND METHODS

Silk Fibroin Extraction. SF was extracted from the cocoons of *Bombyx mori* silkworms (The Yarn Tree) through an established protocol [88]. Briefly, silk cocoons were cut into pieces and boiled in a 0.02 M Na_2CO_3 (Sigma Aldrich) solution for 30 minutes to remove the sericin gum, followed by thorough rinsing in de-ionized water (DI), and drying in a fume hood. The SF is then dissolved in a LiBr (Fisher Scientific)

solution at 60°C for 4 hours. This solution is then dialyzed against DI water for 3 days using 3500 MWCO dialysis tubing (Fisher Scientific). The SF solution is then frozen and lyophilized to provide a pure SF powder for electrospinning.

Scaffold Preparation. PCL:Silk and PDO:Silk scaffolds were prepared in ratios of 100:0 and 50:50 (v:v) by volume dissolved in HFP (TCI America). PCL (MW 65,000 kDa Sigma) and PDO (Ethicon, Inc.) were dissolved at a concentration of 100 mg/ml. SF was dissolved at a concentration of 70 mg/ml. These solutions were then inserted into a plastic 5 ml Becton Dickinson syringe with a blunt tip 18 gauge Becton Dickinson PrecisionGlide® needle. The syringe and needle were placed in a KD Scientific syringe pump to be dispensed at rates of 6 ml/hr for 100:0 PDO:Silk and PCL:Silk and at 4 ml/hr for 50:50 PDO:Silk and PCL:Silk. For vascular applications, the solutions were electrospun onto a cylindrical rotating mandrel with a 4 mm diameter with a 12 cm length at both 500 RPM and 8000 RPM with a translational speed of 6 cm/s over a distance of 12 cm to produce a cylindrical tube with either random or aligned fiber orientation, respectively. For ACL applications, the solutions were electrospun onto a cylindrical rotating mandrel with an 80 mm diameter at both 1000 RPM and 8000 RPM and a translational speed of 0 cm/s to determine degree of alignment between the two groups, and the solutions were electrospun onto a rectangular mandrel (2.5 cm wide x 10.2 cm long x 0.3 cm thick) at 500 RPM with a translational speed of 6 cm/s over a distance of 12 cm to produce random fiber orientation. PDO:Silk and PCL:Silk 100:0 blends were electrospun with an applied voltage of 22 kV to the needle tip and -8 kV on a round, 15

cm diameter aluminum target placed behind the mandrel, while PDO:Silk and PCL:Silk 50:50 blends had an applied voltage of 25 kV and a grounded, round, 15 cm diameter aluminum target placed behind the mandrel. After electrospinning was complete, the scaffolds were dipped in methanol for 30 minutes to force β-sheet formation in silk fibers [22].

Scanning Electron Microscopy. Scaffold characterization was performed using SEM of the electrospun mats (Zeiss EV050). SEM micrographs were analyzed with ImageTool 3.0 software (Shareware provided by UTHSCSA). Characterization included determining the average fiber diameter for the electrospun structure by taking the average of 60 measurements chosen randomly from across the image. Calibration of the ImageTool software was done with the scale bar on each image.

Fast Fourier Transform. As described in [343], an FFT method was used to evaluate relative fiber alignment in electrospun scaffolds. The FFT function converts information present in an optical data image from a ‘‘real’’ domain into a mathematically defined ‘‘frequency’’ domain. The resulting FFT output image contains grayscale pixels that are distributed in a pattern that reflects the degree of fiber alignment present in the original data image. A graphical depiction of the FFT frequency distribution is generated by placing an oval projection on the FFT output image and conducting a radial summation of the pixel intensities for each angle between 0 and 360^{o}, in 1^{o} increments. The pixel intensities are summed along each radius and then plotted as a function of the

angle of acquisition (position of the radial projection on the oval profile), usually between 0 and 180^{o} (FFT data are symmetric so a pixel summation to 360^{o} is unnecessary). The degree of alignment present in the original data image is reflected by the height and overall shape of the peak present in this plot. The position of the peak on the plot reports the principal axis of alignment. For analysis, grayscale, 8-bit .TIF SEM micrograph images were cropped to 2048 x 2048 pixels. FFT analysis was conducted using ImageJ software (NIH,http://rsb.info.nih.gov/ij) supported by an oval profile plug-in (created by William O'Connnell). The FFT data was normalized to a baseline value of 0 and plotted in arbitrary units ranging from 0 to 0.3.

Uniaxial Tensile Testing. Uniaxial tensile testing was performed on samples previously hydrated for 24 hours. "Dog-bone" shaped samples were punched from the electrospun tubes and electrospun mats (2.75 mm wide at their narrowest point with a gage length of 7.5 mm) and tested on a MTS Bionix 200 testing system with a 100 N load cell (MTS Systems Corp.) and an extension rate of 10.0 mm/min. Punches from electrospun tubes were taken in the circumferential direction (the direction of mandrel rotation), and punches from electrospun mats were taken in both the *X* direction (direction of mandrel rotation) and the *Y* direction (the direction perpendicular to mandrel rotation). Peak stress, modulus, and strain at break were calculated using TestWorks version 4. The sample size for each specimen was n = 6.

Vascular Dynamic Compliance. Dynamic compliance was determined for 4 mm inner diameter tubular grafts under simulated physiological conditions in accordance with section 8.10 of ANSI/AAMI VP20:1994 [280]. The specimens were tested in an ITEMS™ Bioreactor developed by Tissue Growth Technologies (Minnetonka, MN) filled with PBS at 37°C and lined with a thin latex balloon (Party Like Crazy, Target Corporation) to prevent graft leakage. The bioreactor provided a cyclic (1 Hz, representing 60 beats per minute) pressure change to the inside of the graft; three different pressure levels (90/50, 120/80, and 150/110 mmHg) were investigated.

Internal pressure was measured with a pressure transducer capable of measuring dynamic pressure up to 200 ± 2 mmHg, while the external diameter was recorded with a laser micrometer system with an accuracy of ± 0.001 mm. Prior to insertion into the bioreactor, the grafts were soaked in PBS at 37°C for 24 hours, after which time their average wall thickness was measured. From this the internal radii of the graft was determined and used in the following equation to calculate compliance for each specimen:

$$\%\ Compliance = \frac{(R_{P2} - R_{P1})/R_{P1}}{(P_2 - P_1)} \times 10^4 \qquad (7.1)$$

Where R is the internal radius, P_1 is the lower internal pressure, and P_2 is the higher internal pressure [280]. Grafts were then fixed onto distal and proximal nozzles in the ITEMS with 2-0 Silk suture. 37°C PBS was pumped through the inner lumen, brought to a static pressure of 80 mmHg, and allowed to stress relax for a period of 15 minutes. At

each pressure level (systolic/diastolic), the graft was allowed 500 cycles of stress relaxation prior to compliance measurement.

Vascular Burst Strength. Burst strength testing (n = 6) was completed using a device designed in accordance with section 8.3.3.3 of ANSI/AAMI VP20:1994 [280]. Tubes, 2–3 cm in length, were hydrated in PBS, fitted over 3.0 mm diameter nipples attached to the device, and secured with 2-0 silk suture. Air was introduced into the system, increasing the pressure at a rate of 5–10 mmHg/s until the tubes burst. Results are reported as the pressure in mmHg at which tubes ruptured.

Vascular Longitudinal Strength. Longitudinal strength was performed on hydrated, whole graft samples (n = 6) in accordance with section 8.3.2.4 ANSI/AAMI VP20:1994 [280]. 4 mm inner diameter grafts were cut to a length of 3.5 cm and tested on a MTS Bionix 200 testing system with a 100 N load cell (MTS Systems Corp.), a gage length of 2 cm, and an extension rate of 50.0 mm/min. Peak load and strain at break were calculated using TestWorks version 4.

Statistical Analysis. Unless otherwise stated, all statistical analysis was based on a Kruskal-Wallis one way ANOVA on ranks and a Tukey-Kramer pair-wise multiple comparison procedure (α=0.05) performed with the JMP®IN 4.0.3 statistical software package (SAS Institute, Inc).

RESULTS

Fiber Characterization. SEM images (figure 7.1 and 7.2) were analyzed using fiber diameter measurements to determine average fiber size and FFT to determine fiber alignment [343, 344]. Previous studies determined that mandrel rotational speed at 6000 RPM did not adversely affect fiber diameter. However, in those studies a rectangular mandrel was used, which could alter the electrospinning parameters. Therefore, it was thought that a change in fiber diameter could be possible at a higher rotational rate of 8000 RPM and a cylindrical mandrel, where the electric field would stretch and strain the fibers as they approached the mandrel. Furthermore, as fibers adhered to the surface of the spinning mandrel and were whipped due to high angular momentum they would be stretched and strained to an even higher degree.

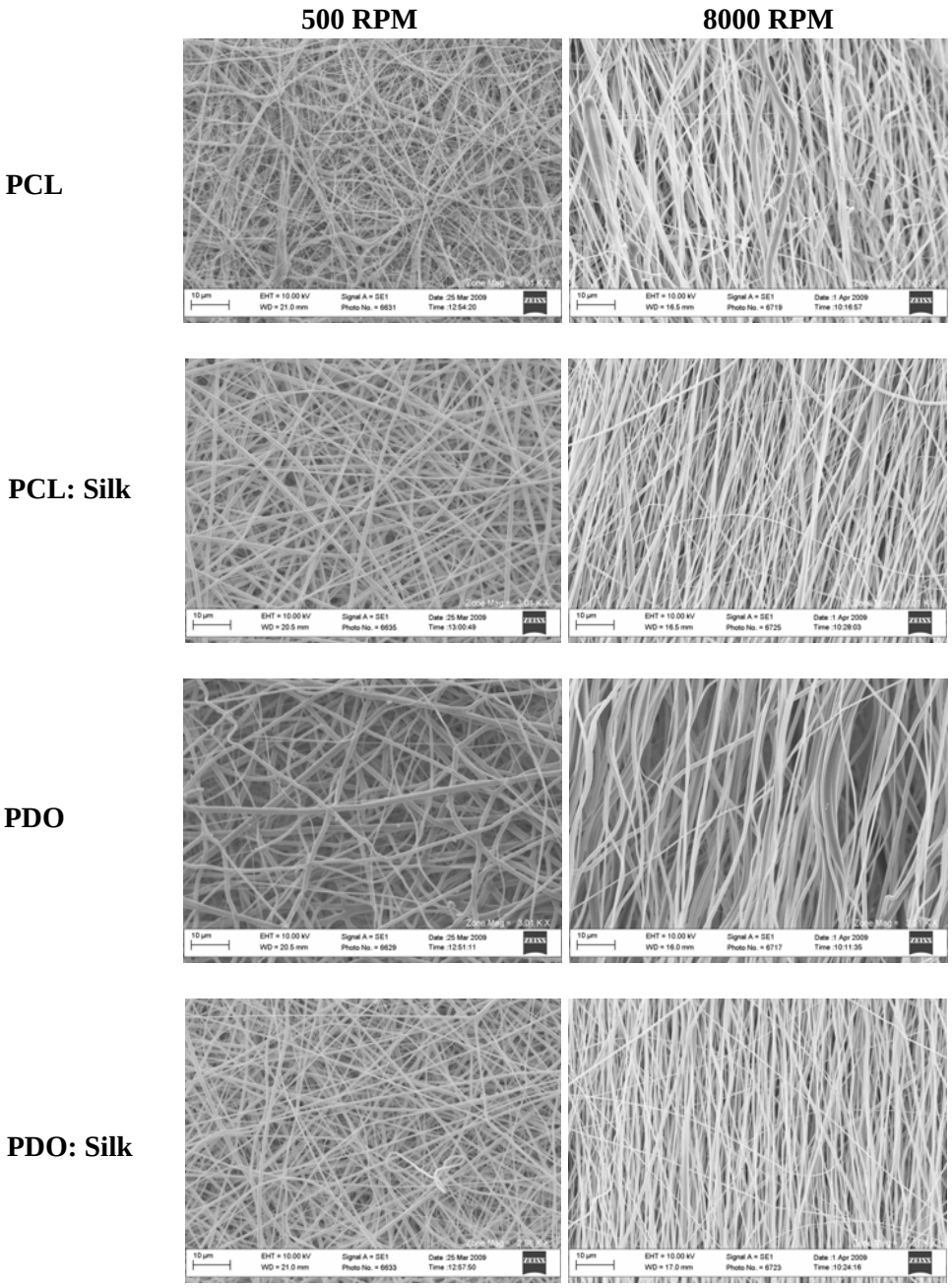

Figure 7.1. Scanning electron micrographs for PCL, PCL:Silk, PDO, and PDO:Silk blends high rotational rates of 500 RPM (left) and low rotational rates of 8000 RPM (right) on an 80 mm diameter mandrel. All micrographs are taken at 3000x.

According to the SEM images displayed in figure 7.1, there are clear fiber alignment differences between the scaffolds as the rotational rate is increased from 500

RPM to 8000 RPM. The degree of alignment in a data image is reported by the height and shape of the peak generated by the FFT plot. The higher the peak, the more precisely aligned the fibers are along a single axis of orientation. There were no significant differences between fibers at different rotational rates according to fiber diameter measurements, agreeing with previous experiments. FFT analysis (figure 7.3) of the images from figure 7.1 proves that alignment increases with increasing rotational rates, demonstrating a clear trend in higher peak values as the rotational rate is increased. PDO increased incrementally with normalized values of 0.04, 0.19, and 0.30, PCL increased with values of 0.03, 0.21, and 0.28, and PCL:Silk increased with values of 0.07, 0.10, and 0.23 for 500, 1000, and 8000 RPM, respectively. PDO:Silk was an exception decreasing from 0.07 to 0.02 for 500 and 1000 RPM, respectively, but increasing to a value of 0.22 for 8000 RPM. The highest peak values came from pure synthetics, producing alignment values of 0.30 and 0.28 for PDO and PCL scaffolds, respectively. When silk was added to the polymer blend, values tended to decrease.

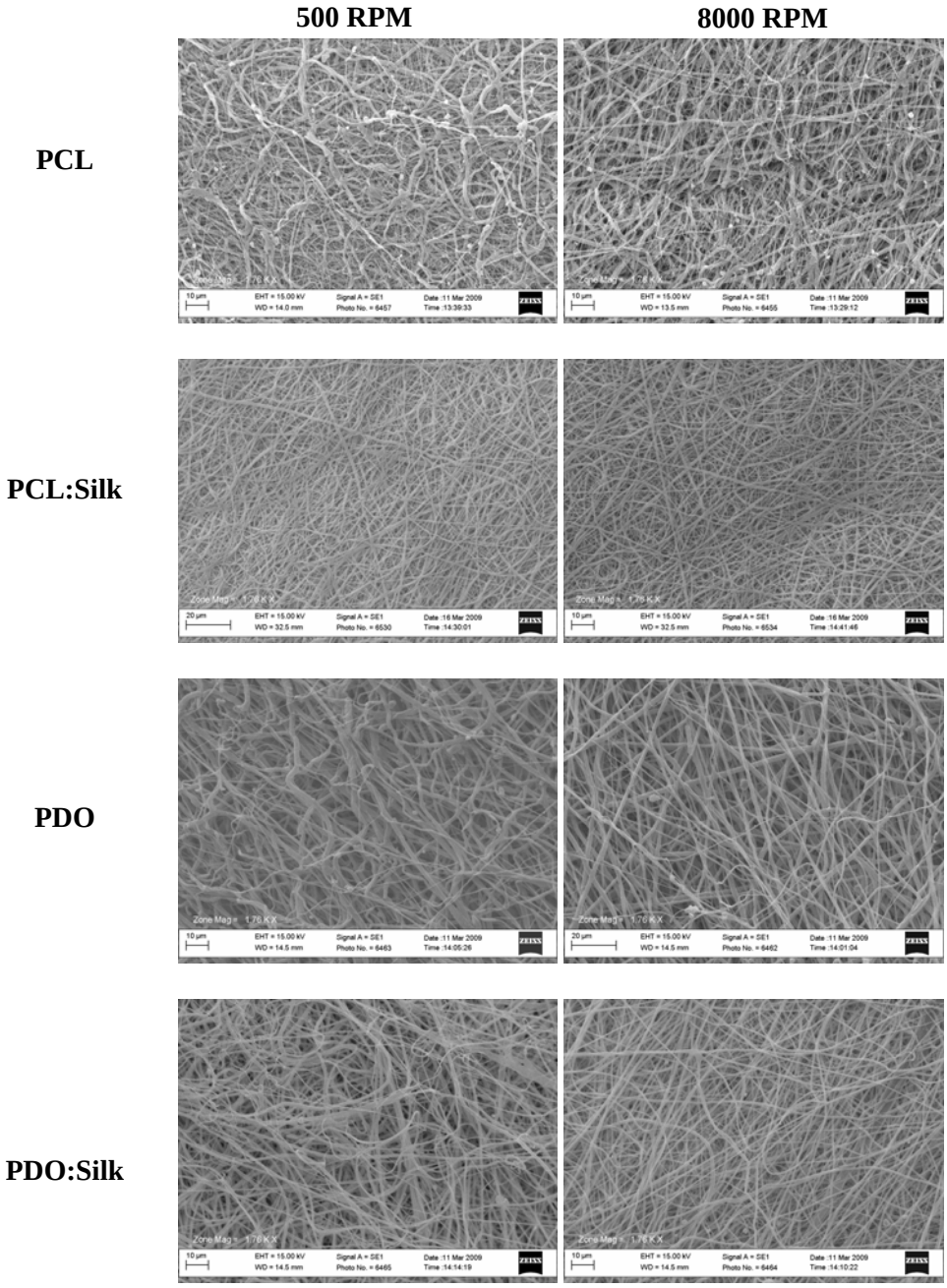

Figure 7.2. Scanning electron micrographs for PCL, PCL:Silk, PDO, and PDO:Silk blends high rotational rates of 500 RPM (left) and low rotational rates of 8000 RPM (right) on a 4 mm diameter mandrel. All micrographs are taken at 1760x.

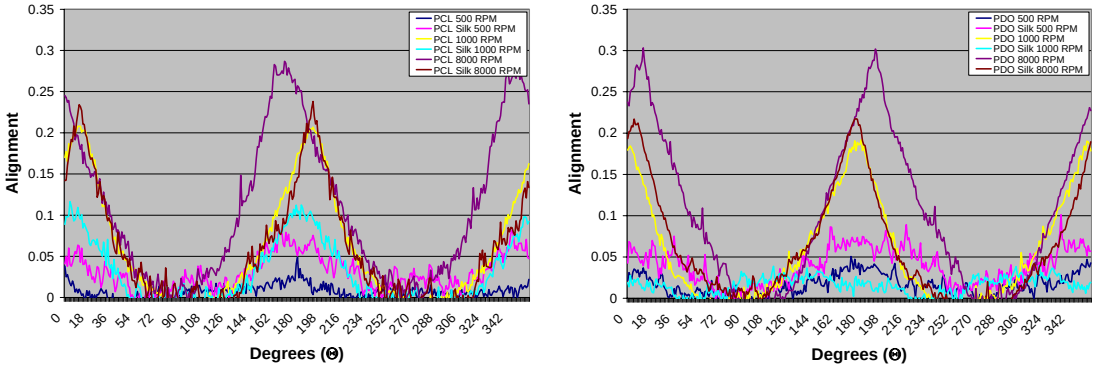

Figure 7.3. FFT alignment analysis of SEM pictures for ACL grafts containing PCL, PCL:Silk (left), PDO, and PDO:Silk (right) scaffold structure as a function of mandrel RPM with an 80 mm diameter mandrel.

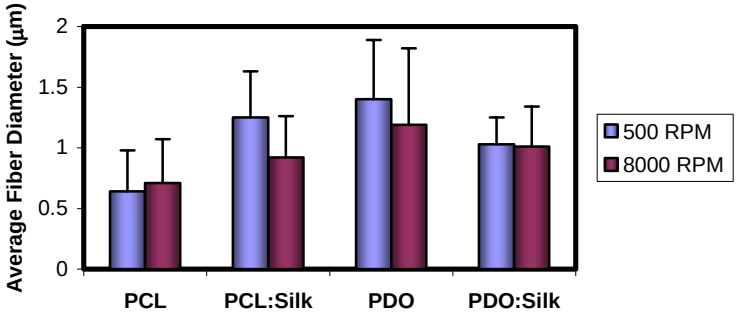

Figure 7.4. Average fiber diameter of PCL, PCL:Silk, PDO, and PDO:Silk blends at high rotational rates of 8000 RPM and low rotational rates of 500 RPM on a 4 mm diameter mandrel.

Success in creating fiber alignment for ACL graft structures thereby led to a confident approach for vascular applications, using a smaller mandrel. Fiber diameter results (figure 7.4) revealed that for mandrel rotations of 500 RPM and 8000 RPM, PCL had an average of 0.6 ± 0.4 and 0.7 ± 0.3 µm, PCL:Silk had an average of 1.3 ± 0.3 µm and 0.9 ± 0.4 µm, PDO had an average of 1.4 ± 0.6 and 1.2 ± 0.5 µm, and PDO:Silk had

an average of 1.0 ± 0.3 and 1.0 ± 0.2 μm, respectively. Statistically significant differences between rotational rates of 500 and 8000 RPM existed only for the PCL:Silk blend. Again, it was determined that mandrel rotational rate did not have an impact on fiber diameter even with small mandrel diameters. However, examining the SEM micrographs closely, fiber packing density is high for higher mandrel rotational rates, resulting in a more compact matrix. These findings are consistent with previous testing [343].

Additional FFT analysis was performed on SEM images in figure 7.3 to characterize fiber alignment properties. Images of both the inside and outside of each electrospun graft were taken and analyzed. Results of FFT analysis are displayed in table 7.1 and figure 7.5.

Table 7.1. FFT alignment analysis of SEM micrographs

RPM (graft side)	**PCL**	**PCL:Silk**	**PDO**	**PDO:Silk**
8000 (Inside)	0.07	0.10	0.09	0.10
8000 (Outside)	0.13	0.06	0.10	0.08
500 (Inside)	0.03	0.10	0.08	0.05
500 (Outside)	0.05	0.10	0.10	0.12

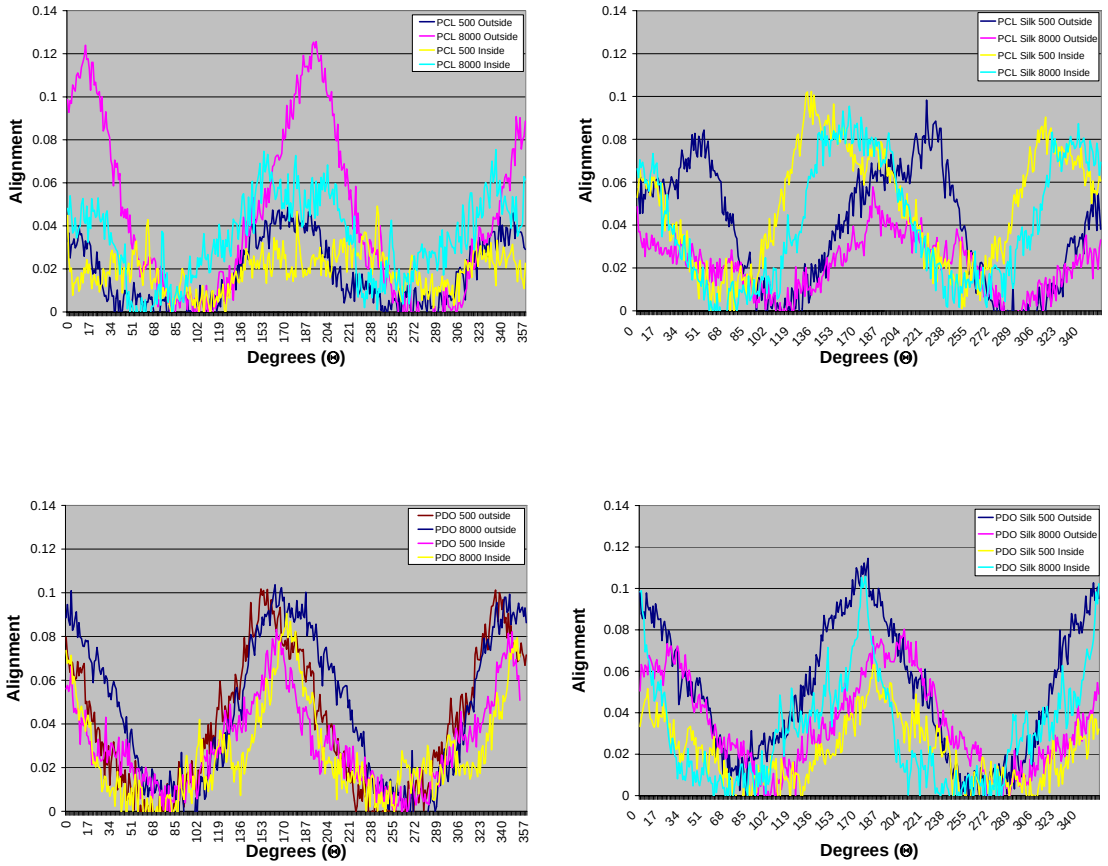

Figure 7.5. FFT alignment analysis of inside and outside graft SEM pictures containing PCL (top left), PCL:Silk (top right), PDO (bottom left), and PDO:Silk (bottom right) scaffold structure as a function of mandrel RPM with a 4 mm diameter.

Uniaxial Tensile Testing for Ligament. Initially looking at the FFT results from table 7.1 there is a clear distinction between the X and Y directions for both 1000 and 8000 RPM, indicating that fibers are preferentially aligned in the X direction. This distinction is more prevalent in synthetic polymers (PCL and PDO) than their blended counterparts (PCL:Silk and PDO:Silk), which demonstrates that the addition of Silk, in this case, provides for a less preferential direction when electrospun under these conditions. Significant differences for the X direction demonstrated that as mandrel

RPM increased from 500 to 8000 RPM peak stress and modulus increased in an incremental fashion, indicating step-wise increases in alignment. This can be shown with PCL where there was a 128 % increase between 500 and 1000 RPM and a 125 % increase between 1000 and 8000 RPM. Additionally, significant differences existed between the X and Y directions for peak stress and modulus when scaffolds were electrospun at a rotational rate greater than 1000 RPM. This further proves changes in scaffold alignment as there were incremental decreases in peak stress and modulus in the Y direction. Additionally, the highest values for strain at break existed in the Y direction verifying fiber alignment in the X direction. This can be shown with PDO where strain values increase from 3.0 to 5.7 mm/mm between 1000 and 8000 RPM.

Table 7.2. Uniaxial tensile test results for the 80 mm diameter drum

	Peak Stress (MPa)		Modulus (MPa)		Strain at Break (mm/mm)	
	X	**Y**	**X**	**Y**	**X**	**Y**
PCL						
500 RPM	3.9 ± 0.3	2.6 ± 0.6	9.4 ± 0.4	7.3 ± 0.7	0.9 ± 0.1	1.3 ± 0.2
1000 RPM	8.9 ± 1.5	1.2 ± 1.2	18.0 ± 1.8	1.0 ± 0.1	1.0 ± 0.1	4.3 ± 0.4
8000 RPM	20.0 ± 2.3	1.4 ± 0.2	42.7 ± 6.4	0.6 ± 0.2	1.0 ± 0.1	6.0 ± 0.6
PCL:Silk						
500 RPM	1.4 ± 0.2	1.4 ± 0.1	13.4 ± 2.1	15.6 ± 0.9	0.5 ± 0.1	0.5 ± 0.2
1000 RPM	2.1 ± 0.1	0.9 ± 0.1	11.1 ± 1.1	4.2 ± 1.0	0.5 ± 0.1	0.7 ± 0.1
8000 RPM	4.8 ± 0.4	0.7 ± 0.2	16.2 ± 1.3	0.8 ± 0.2	0.5 ± 0.1	2.7 ± 0.7
PDO						
500 RPM	4.6 ± 0.4	5.1 ± 0.5	12.3 ± 0.9	9.9 ± 1.2	2.4 ± 0.3	3.3 ± 0.5
1000 RPM	8.1 ± 0.1	1.3 ± 0.5	23.1 ± 0.8	1.1 ± 0.3	0.7 ± 0.7	3.0 ± 0.7
8000 RPM	12.5 ± 0.5	0.7 ± 0.1	35.7 ± 2.8	0.2 ± 0.1	0.7 ± 0.1	5.7 ± 0.6
PDO:Silk						
500 RPM	2.3 ± 0.2	2.7 ± 0.6	1.7 ± 0.1	2.2 ± 0.3	1.5 ± 0.1	1.4 ± 0.3
1000 RPM	3.9 ± 0.3	1.4 ± 0.3	3.7 ± 0.3	1.1 ± 0.1	1.3 ± 0.1	1.5 ± 0.2
8000 RPM	7.6 ± 0.4	0.7 ± 0.1	20.5 ± 0.7	0.5 ± 0.1	0.6 ± 0.1	2.7 ± 0.1

Uniaxial Tensile Testing for Vascular Graft. Uniaxial tensile testing reported peak stress, tangential modulus, and strain to break for all samples tested. Vascular grafts were splayed open and punched into "dog bone" shapes for materials testing. It should be recognized that the event of punching "dog bones" from the grafts provides an initial

stress and compression to the inner lumen and outer portion of the graft, respectively. In order to allow for consistency amongst the graft samples, all punches were clamped between the grips with slack and the slack was then carefully taken out to a force of 0.1 N. Figure 7.6 displays the results from the test.

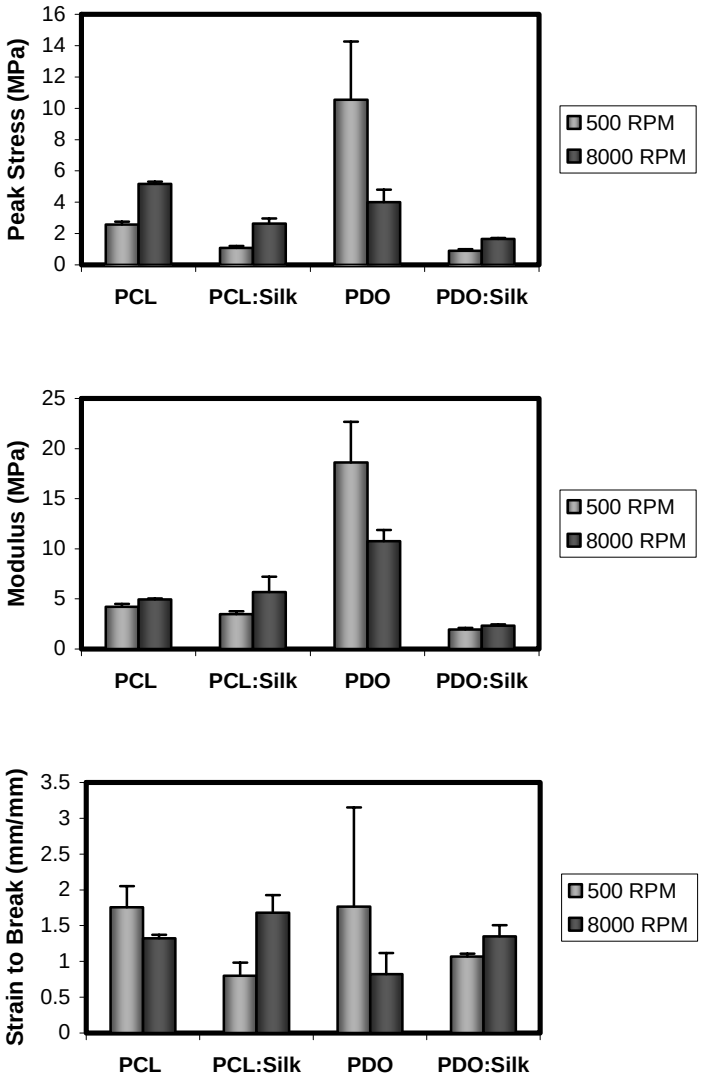

Figure 7.6. Uniaxial tensile test values for peak stress, tangential modulus, and strain to break for PCL, PCL:Silk, PDO, and PDO:Silk spun at both 500 RPM and 8000 RPM on a 4 mm diameter mandrel.

The results revealed two similar trends between peak stress and modulus, where electrospun fibers at high rotational rates demonstrate a higher modulus and peak stress. For peak stress, PCL, PCL:Silk, and PDO:Silk had values of 2.6, 1.1, and 0.9 MPa for 500 RPM, while 8000 RPM had values of 5.2, 2.6, and 1.7 MPa, respectively. Modulus displayed values for PCL, PCL:Silk, and PDO:Silk at 4.2, 3.5, and 1.9 MPa for 500 RPM, and 8000 RPM had values of 5.0, 5.7, and 2.3 MPa, respectively. PDO, however, displayed opposite characteristics with a higher peak stress and modulus for 500 RPM compared to 8000 RPM. Amongst these grafts, pair wise differences were examined between the two rotational rates to determine significance. Significant differences existed for PCL and PDO scaffolds for peak stress and only PDO scaffolds for modulus. No differences existed for strain to break.

Examination of the data displays an encouraging trend whereby higher rotational rates induce a larger average peak stress and average modulus in all samples except for PDO. If fiber alignment is present through the entire scaffold, then fibers aligned in the circumferential direction would contribute to an increase in peak stress and modulus.

Longitudinal Strength Testing. Whole grafts were cut to a length of 3.5 cm and clamped between two grips with a 100 N load cell for strength testing. If fiber alignment were to occur throughout the entire wall of the graft sample, then a marked difference between the aligned scaffolds and random scaffolds should be present under uniaxial loading conditions perpendicular to the axis of alignment. Peak force for PCL, PCL:Silk, PDO, and PDO:Silk displayed values of 20.9, 8.6, 16.5, and 16.4 N for 500 RPM

rotational rates, while 8000 RPM displayed values of 15.1, 8.8, 6.5, and 10.1 N, respectively. According to figure 7.7 statistically significant differences for peak load exist between 500 and 8000 RPM for the synthetic scaffolds, PDO and PCL. However, when silk was blended with the synthetics no differences were present. Strain to break for longitudinal graft testing displayed a significant difference only between the high and low rotational rates of PCL, a trend that was opposite from the rest of the data set.

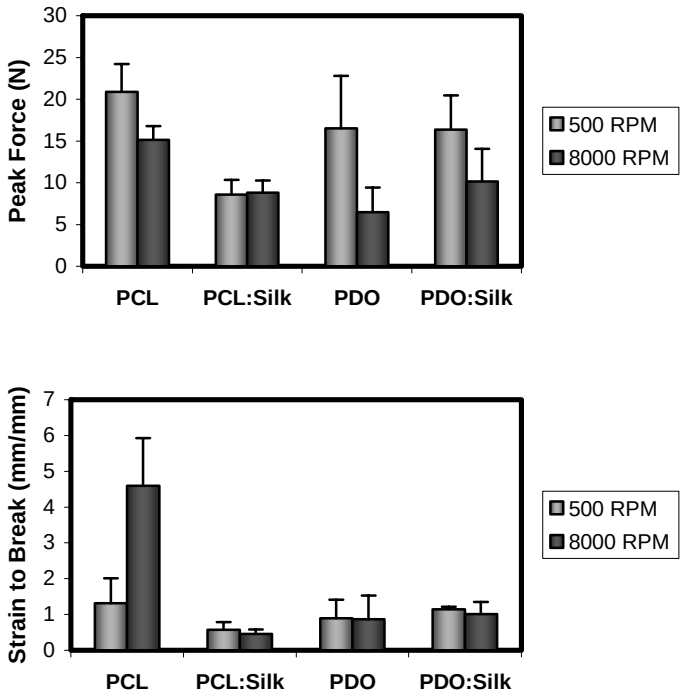

Figure 7.7. Longitudinal strength values for peak force and strain to break on 3.5 cm whole graft samples of PCL, PCL:Silk, PDO, and PDO:Silk spun at 500 RPM and 8000 RPM on a 4 mm diameter mandrel.

Burst Strength. As the "gold standard" of vascular grafts, human saphenous vein (hSV) burst strength is commonly used as a comparison tool for the burst strength of other manufactured grafts. HSV has been reported to reach an average burst pressure of 1599 mmHg [345]. Vascular grafts were tested to determine if their values were comparable to HSV. Overall, aligned fibers in the circumferential direction would require higher burst pressure strength in comparison to a more randomized matrix. This was confirmed with the test results in figure 7.8, where mean comparisons between 500 and 8000 RPM for PCL, PCL:Silk, PDO, and PDO:Silk were significantly different from each other. The grafts spun at 8000 RPM were superior in burst strength quality with values of 3095, 2009, 3336, and 1256 mmHg compared to grafts spun at 500 RPM which had values of 2202, 1237, 1152, and 834 mmHg for PCL, PCL:Silk, PDO, and PDO:Silk. Lastly, the majority of high rotational rate grafts exceeded the HSV average, while the majority of low rotational rates were lesser than the HSV average.

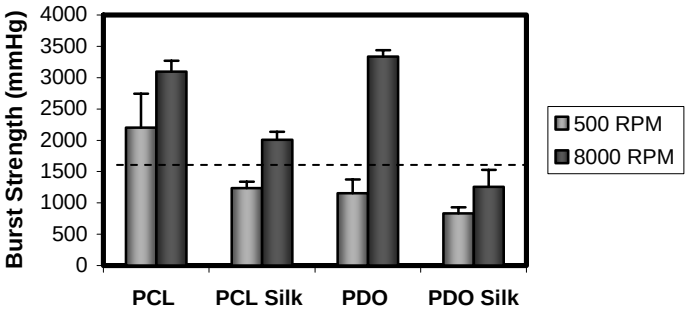

Figure 7.8. Burst strength pressure (mmHg) values for PCL, PCL:Silk, PDO, and PDO:Silk at rotational speeds of 8000 and 500 RPM on a 4 mm diameter mandrel. Dashed line represents HSV average burst strength.

Dynamic Compliance Testing. Compliance measurements were determined using three different pressure intervals of 90/50, 120/80, and 150/110 mmHg (systolic/diastolic). The results are displayed in figure 7.9.

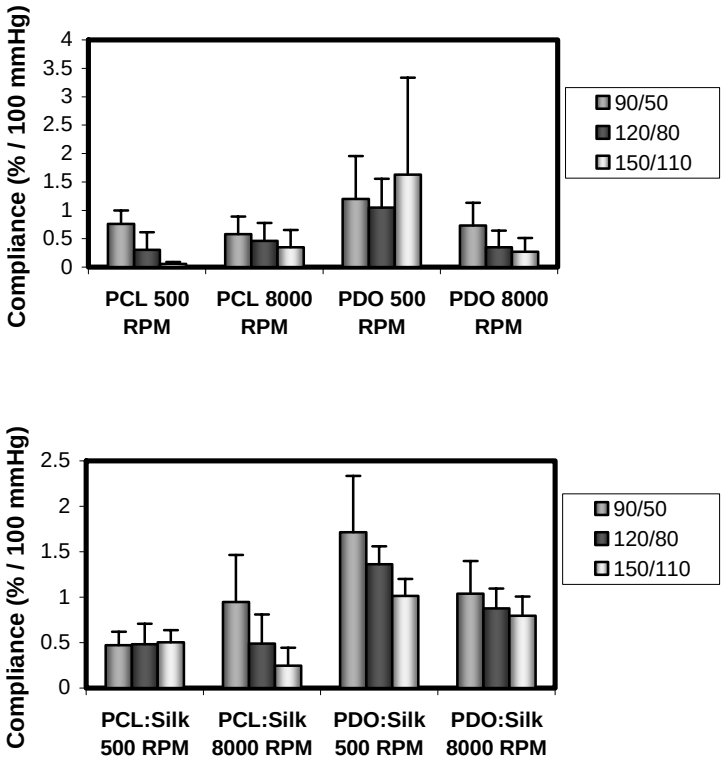

Figure 7.9. Compliance determined from internal radii at three different arterial pressures (90/50, 120/80, and 150/110 mmHg).

PCL displayed an increase in compliance for pressures of 120/80 and 150/110 mmHg when mandrel rotational rate is increased from 500 to 8000 RPM. When silk was added to make a 50-50 blend with PCL, an increase in compliance was only seen for a pressure of 90/50 mmHg. Thereafter, decreases were observed in both 120/80 and

150/110 mmHg as mandrel rotation was increased from 500 to 8000 RPM. Consistent decreases in compliance were seen for PDO and PDO:Silk at all three pressure levels as mandrel speed was increased from 500 to 8000 RPM. Significant differences amongst the three pressure intervals occur in both PCL spun at 500 RPM and PDO:Silk spun at 500 RPM. Differences between pressures at 90/50 and 150/110 mmHg were present for all grafts spun at 8000 RPM. Significant differences were absent in both PCL:Silk and PDO grafts spun at 500 RPM. In addition to these highlighted significant differences, the majority of the graft compliance values decrease with each interval. This is consistent with previous findings for synthetics, synthetic and natural polymer blends, and native artery [20].

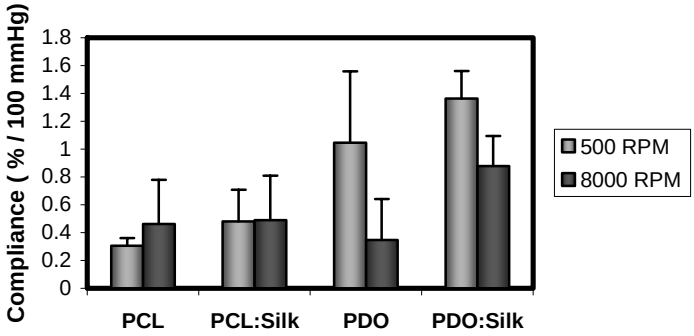

Figure 7.10. Compliance determined from internal radii at 120/80 mmHg for PCL, PCL:Silk, PDO, and PDO:Silk at rotational speeds of 500 RPM and 8000 RPM on a 4 mm diameter mandrel.

In figure 7.10, 120/80 mmHg arterial pressures were determined to have significant differences between 500 RPM and 8000 RPM scaffolds manufactured with PDO and PDO:Silk. PDO had values decreasing from 1.1 to 0.3 % / 100 mmHg, and

PDO:Silk had values decreasing from 1.4 to 0.9 % / 100 mmHg as mandrel rotation was increased from 500 to 8000 RPM, respectively. This translated to a 68 % and 35 % change for PDO and PDO:Silk, respectively. Both PCL and PCL:Silk scaffolds did not have significant differences. Instead, an average compliance increase was seen in PCL while PCL:Silk stayed even between the two mandrel speeds.

DISCUSSION

Fiber Characterization. Fiber size and orientation can contribute to changes in anisotropy which can then lead to changes in material properties and scaffold functionality. For the purpose of this study, scaffolds to mimic ACL and arterial geometry were being investigated to determine both fiber orientation and its impact on mechanical characterization as a function of mandrel rotational speed and mandrel size. Previous alignment studies have shown that both mandrel rotational speed and mandrel size play a large role in fiber alignment [346, 347]. Therefore, in order to develop highly aligned fibers for the purpose of ACL replacement, a mandrel with a diameter of 8 cm was used. Small caliber arteries require a significantly smaller mandrel < 6 mm in diameter. Therefore, a 4 mm diameter mandrel was used for arterial testing.

SEM characterization produced fiber diameter and degree of fiber alignment results for both ACL and arterial applications. As mandrel speed increased, fiber diameter did not change for either mandrel size, indicating that fiber diameter is not influenced by mandrel rotational speed. This is important in terms of mechanical

analysis, whereby a larger or smaller diameter can increase or decrease modulus. However, if nothing changes between the two groups, then it is then assumed that fiber orientation, in regards to this study, is the primary contributor to any mechanical changes observed.

FFT analysis for fiber alignment of both vascular and ACL grafts demonstrated visible differences between 500 RPM and 8000 RPM. Vascular scaffolds tended to have a more compact matrix that was aligned to some degree while ACL grafts had equally compact matrices with highly aligned fibers. The characteristics of both scaffold types can be directly attributable to the manufacturing process, displaying a clear difference between small diameter mandrels and large diameter mandrels. Alignment at the small diameter level revealed that certain pure synthetics, such as PCL, could be manipulated through mandrel rotational rates. However, certain pure synthetics, such as PDO, were nearly the same at both mandrel speeds. This indicates that surface speed, molecular structure, fiber diameter, and its associated electrohydrodyamics play a role in fiber alignment, where fibers repel and attract one another in a particular fashion prior to landing on the mandrel. Yang et al. [348] has studied electrohydrodynamics and demonstrated how electrospinning parameters can affect jet whipping. In our case, this directly impacts fiber alignment, and, based on certain polymer blends, may require a threshold surface speed in order to result in higher degrees of alignment. This can be seen with the large diameter mandrel, producing decreases in FFT alignment for silk blended polymers compared to pure synthetics.

Uniaxial Tensile Testing. Tensile testing results present further defense for fiber alignment in both cases. PCL and PDO displayed significant differences for peak stress and modulus between 500 and 8000 RPM for vascular and ACL scaffolds in the circumferential and *X* directions, respectively. Interestingly, PDO vascular scaffolds demonstrated a significantly higher modulus and peak stress at 500 RPM than at 8000 RPM. This could be due to PDO's specific electrical properties during the electrospinning process, where if the graft is spun at too high a speed then it will produce a more random matrix through inconsistent polymer deposition onto the mandrel surface. In addition to synthetics, biopolymers, such as gelatin, have been shown to exhibit similar behavior. This was observed when spinning gelatin at 130 mg/ml transitioning from 6000 to 7000 RPM, resulting in a decrease in peak stress from 2.7 to 1.7 MPa [343]. In our case, PDO could be creating a more random matrix at 8000 RPM, which could help to explain similar FFT results.

When silk was blended with PCL and PDO in ACL scaffolds, significant differences were present in both blends for peak stress and modulus, however, vascular scaffolds were not different. This again portrays the differences in electrospinning when another polymer is introduced, changing the electrodynamics and decreasing fiber alignment.

Y direction tensile testing was also performed on ACL scaffolds to compare to the *X* direction and show fiber preference (longitudinal tensile testing for vascular scaffolds is discussed in the next section). Again fiber alignment was proven to be in the *X* direction where peak stress and modulus were higher when compared to the *Y* direction.

Additionally, strain to break was highest overall in the *Y* direction. This data shows that when fibers are parallel to one another the force to break them increases because of fiber recruitment. Instead, if fibers are perpendicular to the axis of force, then there is nothing to resist that force and the fibers pull apart.

Vascular Longitudinal Strength Testing. If fibers are aligned in the circumferential direction, then a whole scaffold sample tested in the longitudinal direction should exhibit a lower peak stress for higher rotational rates in comparison to lower rotational rates. According to the data, both PCL and PDO showed pairwise differences between 500 and 8000 RPM, indicating that fibers were preferentially aligned in the circumferential direction. Again, the addition of silk changed the electrospun scaffolds and produced no significant differences between 500 and 8000 RPM. The overall results pointed towards a higher preferential alignment when scaffolds were electrospun at 8000 RPM.

Vascular Burst Strength Testing. Utilization of burst strength testing incorporates biaxial loading to failure, which provides an additional picture of scaffold anisotropy. From the previous two tests, we were able to show that fibers preferentially align themselves in the circumferential direction. If this is true, then burst strength in addition to the other tests would be higher for 8000 RPM then for 500 RPM. Figure 7.8 demonstrates a higher average burst pressure for all scaffolds spun at 8000 RPM. Inclusion of all fibers in the electrospun scaffold in the testing scenario demonstrated the

contribution of each individual fiber to the group of fibers surrounding it, thereby providing further strength for the whole scaffold instead of observing a small section of the scaffold which could exhibit slight differences introduced during the manufacturing process.

Vascular Dynamic Compliance Testing. Another whole scaffold test is dynamic compliance. Much like the burst strength test preformed in the previous section, fiber behavior can be inferred at the macroscopic level under physiological pressures. The results of the test showed that both PDO and PDO:Silk had significantly higher compliance values at 500 RPM than at 8000 RPM, demonstrating fiber anisotropy in the circumferential direction at higher speeds. Compliance results emulate results from burst strength testing and show that a stiffer, less compliant scaffold is present at 8000 RPM.

Trends in figure 7.10 show that when silk is blended with the synthetic, a higher average compliance value is reached. These trends coupled with the encouraging cellular results from Soffer et al. [183] reveal the potential importance of silk in arterial tissue engineering. Although further testing and optimization must be performed with silk blended scaffolds, results from this study and previous studies point towards a promising future.

Vascular applications demonstrated that fibers preferentially aligned themselves in the circumferential direction compared to the longitudinal direction. However, electrohydrodynamics and polymer type share an important role in regulating and optimizing electrospinning parameters. Mostly, scaffolds spun at 8000 RPM were very

compact and stiff to the touch, characteristics which would decrease cellular infiltration and cause mechanical mismatch between the scaffold and artery which could then result in intimal hyperplasia. Therefore, if the biological geometry of an artery were to be considered in vascular replacements, a good approach could be using a flat sheet of aligned fibers and rolling them onto a cylindrical mandrel at different angles.

CONCLUSION

Silk has been explored as a replacement tool for ligaments, and its elastic nature creates a scenario that is primed for cyclic loading environments, providing low energy dissipation. As an arterial replacement subject to repetitive pulsatile forces, silk is also beneficial and has been proven already to exhibit similar material properties in comparison to native artery [183]. Results from this preliminary study using PDO and PCL with and without silk, indicated that fiber alignment could be successfully achieved using a large diameter mandrel. Additionally, varying the rotational speed on this mandrel allows the user to control the degree of alignment and its subsequent mechanical properties. The small diameter mandrel, 4 mm, displayed mechanical characteristics indicating preferential fiber alignment, yet, as a vascular scaffold, its ability to distend with aligned, compact fibers provides far less compliance than that of random fibers which still seem to produce signs of alignment. An alternative would be to roll a flat sheet of aligned fibers from the ligament set up. As a natural protein, SF has shown to be a beneficial polymer for tissue engineering of both ligament and artery. Further

optimization of the parameters associated with electrospinning will have laid the groundwork for future *in vitro* and *in vivo* experimentation.

CHAPTER 8 Creating Cellularized Ligament Analogues

INTRODUCTION

Ligament Structure. Ligaments are dense connective tissues which attach bone to bone and act principally in tension to guide and restrict joint movements [349]. In the human knee there are four primary ligaments: the medial collateral ligament (MCL), lateral collateral ligament (LCL), posterior cruciate ligament (PCL), and ACL. These four ligaments work both individually and in concert to resist unwanted motion in the knee. Of the four knee ligaments, the ACL is the main stabilizer of the knee for athletic pivotal activities and has attachment sites on the tibia and femur [350]. As such, ACL resists the anterior displacement of the tibia with respect to the tibia, as well as assisting in the resistance of hyperextension and playing a role in the rotational stability of the extended knee for internal and external tibial rotation [351].

Gross dissection of the knee reveals the ACL to be an anisotropic collagenous structure wrapped in a thin synovial membrane. The ACL is heterogeneous, with two distinct bundles playing two distinct roles: the anteromedial bundle (AM), taught in flexion, and the posterolateral bundle (PM), taught in extension. ACL also has two bony insertion sites (one each on the tibia and femur), with each insertion site comprised to four distinct zones. Zone 1 comprises the majority of the ligament and is composed

entirely of ligamentous tissue, zone 2 is a transition to fibrocartilage, zone 3 is stiffer mineralized fibrocartilage, and zone 4 is bone [268, 271, 352-354].

For this study the focus was on engineering zone1, the ligamentous tissue. The ECM of zone 1 is composed almost entirely of type I collagen and water. Type I collagen makes up 70-80% of a ligament's dry weight, while water constitutes 60% of the wet weight. Other ECM molecules present in ligamentous tissue include type III collagen (8% dry weight), type V collagen (12% dry weight), elastin (<5% dry weight), and proteoglycans (<1% dry weight) [271, 353]. Structurally, ligament has a hierarchical organization (figure 8.1) whose basic unit is parallel fibrils of collagen 30-100 nm in diameter which combine to form collagen fibers 1-20 μm in diameter. The parallel collagen fibers then merge together to form a subfasicular unit between 100 and 250 μm in diameter. Subfasicular units are surrounded by connective tissue known as the endotenon. Endotenon wrapped subfasicular units then aggregate into collagen fascicules wrapped with epitenon connective tissue. These fascicules are wrapped by a paratenon, followed by a synovial sheath which supplies blood flow to the ligament [268, 354]. The collagen fascicles experience a crimping pattern with an amplitude of <5 μm and period of 45-60 μm. This crimp provides shock absorbing capabilities to the ligament and allows for 7-16% creep to occur prior to permanent deformation [268, 349, 355].

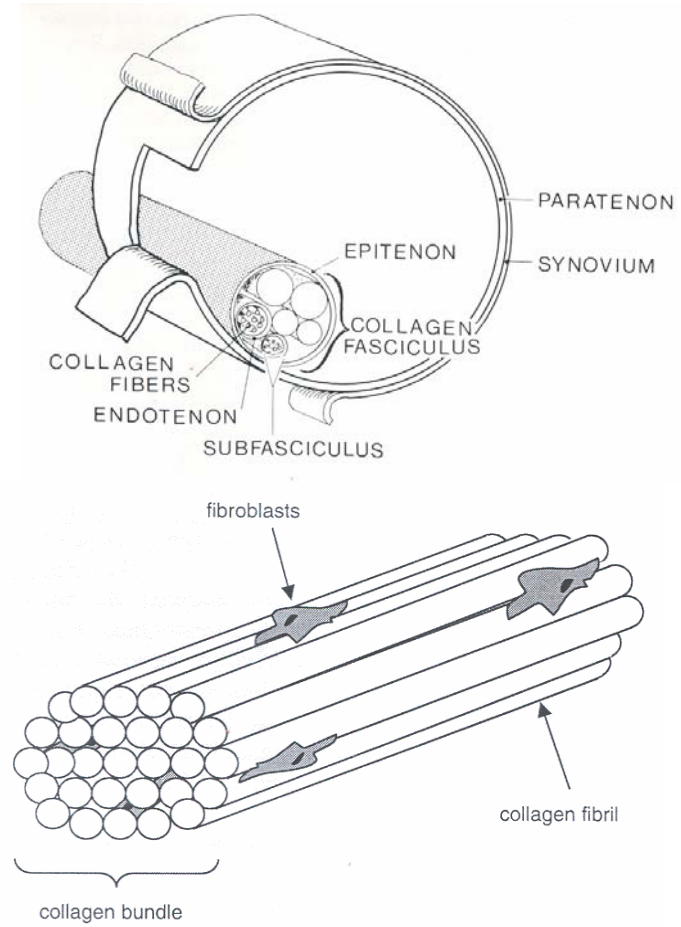

Figure 8.1. A diagram of the cruciate ligament structure shown down to the individual collagen fiber level (top) [354], and the interaction between collagen fibrils and ligament FBs (bottom) [349].

The primary cellular component of ligamentous tissue is the FB. These cells tend to be sparsely distributed throughout the ligament, and make up only a small volume of the total tissue. Typically, FBs will take a fusiform shape (figure 8.1) and align themselves parallel to the collagen fibers [349]. FBs have also been seen to take on an ovoid shape, lacking extensive cytoplasmic processes, and arrange in columns between collagen fibers. Regardless of their shape, these cells function to secrete and maintain the ECM of the ligament. Due to low cell densities matrix turnover is often very slow,

partially explaining the poor reparative capacity of ACL. Ligament also contains a limited number of vascular and neural cells [353, 356].

Ligament Mechanics. The *in situ* loading of the ACL is extremely complex and not easily modeled as the knee joint is a 6 degree of freedom joint. As such, native ligament and ligament grafts are generally first tested to failure in tension as a bone-ligament-bone complex. The uniaxial tensile properties of ligament owe much to the tissues hierarchical collagenous structure. When testing a ligament in tension, there are typically four main regions seen on the load-elongation curve (figure 8.2). The initial 'toe' region is a period of high elongation at low load due to the crimped nature of the structure. ACL tends to have a larger 'toe' region than other collagenous structures (i.e. tendon) due to its anisotropic nature. The presence of the two distinct bundles, the AM and PM, and their different physiologic roles, ensures that not all the collagen fibers will be tensed at the same time leading to an extended period of crimp removal. Following the 'toe' region, when the collagen crimp has been exhausted, the ligament will experience a linear elastic region followed by a region where plastic deformation occurs, and eventually catastrophic failure [352]. In a study by Chandrashekar et al., in which human ACL was isolated and tested in tension to failure at 100% strain per second, ACL was found to exhibit a modulus of elasticity of 113 $\pm$ 45 MPa, a failure stress of 24.36 $\pm$ 9.38 MPa, and a strain at failure of 0.28 $\pm$ 0.07 mm/mm [357].

As with most biological materials ligament exhibits viscoelastic behavior, and is both time and history dependant. It has been shown that preconditioning of ligament to low levels of strain results in rapid decreases in hysteresis and increases in both resting

length and stiffness. This causes the ligament to act more like a spring and become more energy efficient. Testing has also revealed ligament to be highly rate sensitive, with increases in loading rate leading to increases in failure load, extension to failure, energy to failure, and stiffness [352, 358]. The presence of elastin in ligamentous tissue assists in the elastic recoverability of the structure due to its spring-like nature and ability to recoil from tensile loading [353]. The presence of negatively charged proteoglycans provides the matrix with viscous properties. The glycosaminoglycan chains which constitute proteoglycans attract water, resulting in proteoglycan swelling and entrapment among collagen fibrils. This adds compressive strength to the ligament and causes the proteoglycans to act like hydraulic dampers [349].

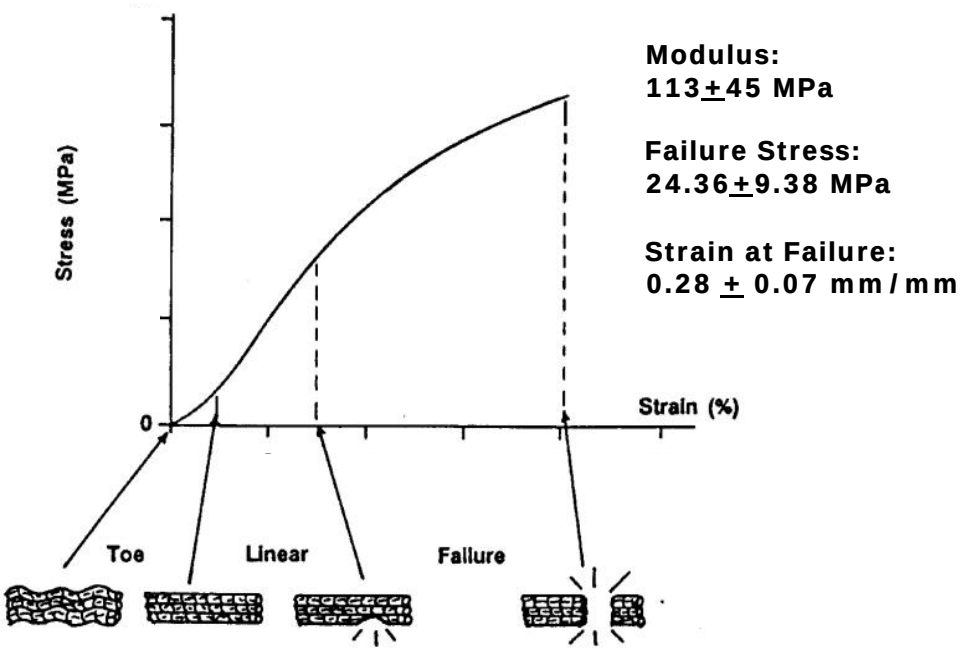

Figure 8.2. Diagram of typical stress-strain curve for human ACL [359].

Ligament Repair and Healing. It has been well documented that the MCL, a ligament residing outside the articular capsule of the knee, has the ability to spontaneously repair itself. Adult MCL repair is a 3 phase process that begins with hemostasis and inflammation, followed by cell proliferation and matrix deposition, and finally long-term remodeling. Within the first 72 hours after injury, a hematoma will develop in the soft tissue adjacent to the wound, and inflammatory cells will invade the site. These inflammatory cells (monocytes, leukocytes, and macrophages) release cytokines and growth factors to begin clean-up of the wound site and initiate repair. FBs then enter the area and begin to produce ECM proteins, primarily collagen type III and type I, in a relatively disorganized manner, which then forms a vascular scar. During the remodeling stage this scar is transformed into tissue more similar in structure to that of native MCL due to the production of greater quantities of type I collagen arranged parallel to the injured ligament [270, 271, 360, 361].

The ACL, an intra-articular ligament, exhibits an extremely poor reparative capacity. In fact, rapid degeneration of the ACL has been observed following acute injury. Blood flow to the ACL is provided by the thin synovial sheath surrounding the ligament. When the ACL is injured, this sheath is damaged and blood flow and nutrient delivery is disrupted. The dissipation of blood prevents the formation of a localized hematoma and ultimately results in retarded healing due to a lack of cytokines and growth factors [270]. Additionally, the damaged synovial membrane exposes the collagenous ligament tissue to a potentially hostile hemarthrotic fluid environment inside the articular capsule of the knee. This combination of blood and synovial fluid has been

shown to contain degradatory enzymes such as collagenase, as well as have an adverse effect on FB proliferation. The lack of mechanical stimulation within a ruptured ACL may also contribute to a lack of new ECM produced by hLFs [362].

Tissue Engineering of Ligament. The creation of an ideal tissue engineered ligament replacement requires a structural scaffold that can support cell activity, host reparative cells with the ability to produce ECM, and have an overall structure conducive to the repair process with appropriate nutrient supply [270]. The engineered ECM analogue should ideally have mechanical properties similar to those of native ACL; for a complex load bearing structure, this is no small feat and as such there are several major hurdles. Foremost, the initial mechanical properties of the structure (i.e. ultimate stress, modulus, and strain at break) need to replicate those of ACL. To prevent catastrophic failure, the mechanical properties of the implanted structure need to remain high *in vivo* as the material degrades and cells infiltrate and remodel the scaffold. The ability to withstand multidirectional stresses and creep are also essential to ACL graft success [268].

There have been many different approaches taken to engineering ligament replacements. Most involve the use of bioresorbable synthetic polymers such as PLA [268, 269, 273, 326, 327], PLGA [267, 269, 276, 328, 329], PCL [268, 270], and PDO [273, 363]. Natural biopolymers such as silk [22, 80, 83-85, 268, 270, 273, 330], and collagen [61, 268, 270, 273, 326] have also been used extensively. These materials have been used almost exclusively as braided, knitted, or extruded micron scale fibers, with no

evidence of a ligament analogue composed entirely of electrospun nanofibers in the literature.

Electrospinning Ligament Analogue Structures. Electrospinning allows for the easy creation of scaffolds made of highly aligned fibers. The degree of fiber alignment contained within an electrospun scaffold can be quantified through the use of FFT algorithm [343, 344]. Aside from obvious anisotropic mechanical advantages in the direction of fiber alignment (increased peak stress and modulus) [343, 344, 364], aligned fibers have been shown to effect cell behavior as well. When FBs were cultured on highly aligned nanofibrous scaffolds, they exhibited a morphology similar to that seen *in vivo* and produced more ECM than FBs seeded on randomly aligned scaffolds [274, 275]. MSCs have been shown to align themselves along the long axis of fibers with actin organization determined by the fiber orientation when seeded on aligned scaffolds [364].

There are several ways to create electrospun scaffolds of highly aligned nanofibers, most easily by altering the shape and rotational speed of the collection target. Solid and wire frame rotating drums have been shown to create aligned fibers at different rotational speeds for different polymers. The use of a rotating knife edged disk has also proven successful. Manipulation of the electric field, such as the use of a patterned array of conducting and insulating strips, can also create aligned scaffolds [132]. It is also possible to create 3-dimensional structures, as opposed to flat sheets, of aligned fibers by employing air-gap electrospinning (figure 8.3.). Air-gap electrospinning requires the charged needle of the polymer solution to be placed equidistant between a pair of conductive parallel collectors. The profile of the electric field created causes the

electrospinning jet to stretch itself across the gap between the two collectors and deposit aligned fibers between them. The charge of the individual fibers creates a mutual repulsion which enhances their ability to align and be distributed evenly [132, 365].

The purpose of this study was to create aligned electrospun structures of SF, PDO, and PCL for ligament engineering fabricated through traditional electrospinning as well as air-gap electrospinning. These scaffolds were characterized through SEM and FFT, had their structural and mechanical properties evaluated, as well as their levels of celllar affinity to determine which material and fabrication process were best suited for use as a ligament analogue structure.

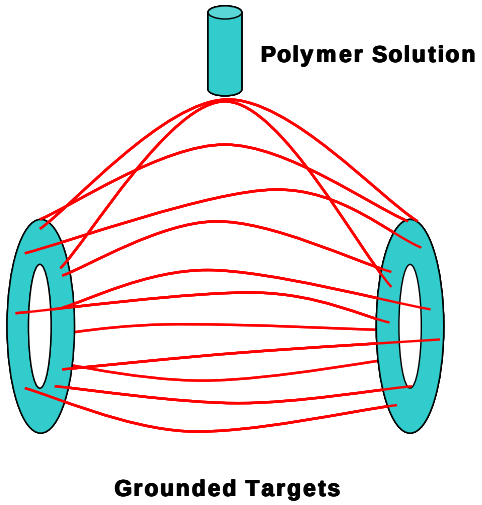

Figure 8.3. Schematic of air-gap electrospinning

MATERIALS AND METHODS

SF Extraction. SF was extracted from the cocoons of *Bombyx mori* silkworms (The Yarn Tree) through an established protocol [88]. Briefly, silk cocoons were cut into

pieces and boiled in a 0.02 M Na_2CO_3 (Sigma Aldrich) solution for 30 minutes to remove sericin gum, followed by thorough rinsing in DI water, and drying in a fume hood. The SF was then dissolved in a LiBr (Fisher Scientific) solution at 60°C for 4 hours. This solution was then dialyzed against DI water for 3 days using 3500 MWCO dialysis tubing (Fisher Scientific). The SF solution was then frozen and lyophilized to provide a pure SF powder for electrospinning.

Scaffold Fabrication. For the creation of randomly aligned scaffolds, a rectangular mandrel (2.5 cm wide x 10.2 cm long x 0.3 cm thick) rotating at 400 RPM and translating at 6 cm/s over a distance of 12 cm was used as the collecting target. Based upon preliminary electrospinning results (Appendix A), SF solution was dissolved in HFP at a concentration of 70 mg/ml or 100 mg/ml and was loaded into a Becton Dickinson syringe fitted with a blunt tip 18 gauge needle and dispensed at a rate of 4 ml/hr with a KD Scientific syringe pump. A charging voltage of +25 kv was applied to the needle tip, with an air-gap distance of 20 cm between the needle tip and the grounded mandrel. Random PDO (Ethicon, Inc.) and PCL (MW 65,000 kDa, Sigma) scaffolds were electrospun at a concentration of 100 mg/ml from HFP with a flow rate of 6 ml/hr, charging voltage of +25 kv, and an air-gap of 20 cm. Randomly oriented 50:50 blends by volume of SF:PDO (SPDO) and SF:PCL (SPCL) were electrospun using parameters identical to those of pure SF scaffolds. These blends utilized solutions of 70 mg/ml SF and 100 mg/ml synthetic polymers.

Aligned scaffolds of the aforementioned materials and blends were created using identical electrospinning parameters to those of the randomly oriented structures, but

rather than a slowly rotating rectangular mandrel, aligned scaffolds were electrospun onto an 8 cm diameter drum rotating at 8000 RPM and translating at 0 cm/s. Following electrospinning, all samples were soaked in ethanol for 30 minutes to force β-sheet formation in the SF fibers [22].

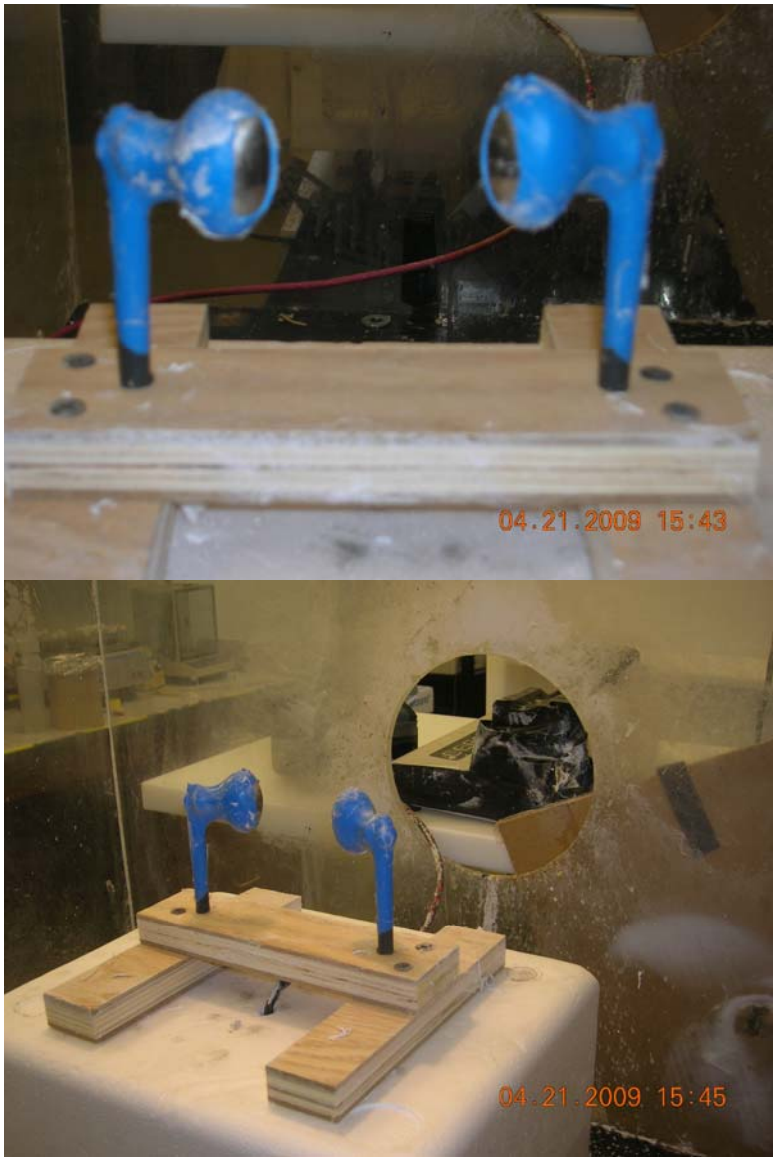

Figure 8.4. Photographs of preliminary air-gap electrospinning setup made from 1 ml syringe, cabinet door knobs, and insulating plastic coating.

Air-gap electrospun constructs were fabricated using the system shown in figure 8.4. The preliminary air-gap electrospinning setup consisted of two conductive towers, with each constructed from a cabinet door knob (1 ¼" Satin Nickel Egg Knob, Gatehouse) attached to a plastic 1 ml Becton Dickinson syringe through which a heavy gauge wire had been run. The entire system was then coated with an insulating plastic dip (Plasti Dip®, Plasti Dip International), and a small area (1 cm wide x 2 cm high) on the face of each door knob was scraped clean to provide a conductive surface. The conductive towers were then mounted in a piece of wood with 5 cm between their faces. 70 mg/ml SF solution was air-gap electrospun using a charging voltage of +25 kv on the needle tip, -5 kv applied to the conductive towers, a flowrate of 10 ml/hr, and a distance of 25 cm between the needle tip and the towers. Pure PDO and PCL constructs, with concentrations and ratios identical to those used in standard electrospinning, were electrospun with a charging voltage of +22 kv on the needle tip, -5 kv applied to the towers, a flowrate of 16 ml/hr, and a distance of 25 cm between the needle tip and conductive tower. SPDO and SPCL constructs were created with parameters identical to those of pure SF.

Scaffold Characterization. Each of the electrospun scaffolds was characterized through SEM (Zeiss EV050). Average fiber diameters were calculated by taking 60 random fiber measurements from across the SEM image using ImageTool 3.0 software (Shareware provided by UTHSCSA). Additionally, an FFT was used to quantify relative fiber alignment in each of the scanning electron micrographs using a method that has been previously described [343]. The FFT was performed on SEM micrographs taken at

500x (not shown) to provide a more complete representation of the entire scaffolds alignment than is visible in the 3000x images shown in figure 8.5.

Porosity / Permeability Measurement. Using a previously published method [311] the porosity of random, aligned, and air-gap electrospun scaffolds was determined. Briefly, 10 mm disks of each scaffold (n=3) were punched from the electrospun constructs, massed, and had their thicknesses recorded. Porosity was then calculated using the following equation:

$$Porosity = \left(1 - \frac{Calculated\ Scaffold\ Density}{Known\ Material\ Density}\right) \times 100 \qquad (8.1)$$

The calculated scaffold density was determined by dividing the mass of the scaffold by the total volume of the scaffold, while the material densities of SF (1.25 g/cm^3), PDO (1.3 g/cm^3), and PCL (1.14 g/cm^3) are known.

Scaffold permeability was measured using a previously described method [311]. Briefly, 10 mm samples of each scaffold (n=3) were punched from the electrospun constructs and allowed to soak in DI water for 1 hr prior to testing. Sample thickness was recorded, and the samples were then placed in a permeability flowmeter with an applied pressure head of 120 mmHg. The time for 10 ml of DI water to flow through a known volume of sample was recorded and the scaffold's permeability was calculated as flow of fluid volume over 1 cm^3 scaffold volume and time.

Uniaxial Tensile Testing. Dog-bone shaped samples (n=5) were punched from random (400 RPM), aligned (8000 RPM) and air-gap electrospun structures of SF (70 mg/ml), PDO, SPDO, PCL, and SPCL. These specimens were punched in two different

directions: parallel to the direction of mandrel rotation or (preferred fiber direction), or perpendicular to the direction of mandrel rotation (non-preferred fiber direction). Testing samples taken from both directions would confirm fiber alignment and would serve as a better indicator of scaffold anisotropy than the strictly superficial SEM based FFT. All specimens were then soaked in ethanol for 30 minutes for force β-sheet formation in the SF, followed by a 2 hour soak in DI water. Samples were then uniaxially tested to failure at a rate of 10 mm/min using an MTS Bionix 200 testing system with a 100 N load cell (MTS Systems Corp.) Peak stress, modulus, and strain at break were calculated using TestWorks version 4.

Cellular Migration / Penetration. Human dermal FBs (Cascade Biologics) were seeded onto SF (70 mg/ml), PDO, SPDO, PCL, and SPCL constructs fabricated through 400 RPM, 8000 RPM, and air-gap electrospinning. Two disks 6 mm in diameter were punched from each of the aforementioned material / fabrication combinations, disinfected (30 minute soak in ethanol followed by three 10 minute rinses in PBS), and placed in a 96-well plate. Each disk was then seeded with 50,000 FBs / well suspended in 50 µl Medium 106 (Cascade Biologics) supplemented with 1% penicillin-streptomyocin (10,000 Units/mL each, Gibco BRL Life Technologies) and 2% low serum growth supplement (Cascade Biologics). Well plates were then placed in an incubator under standard culture conditions for 1 hour prior to the addition of an additional 150 µl Medium 106 and returned to incubation. Culture media was completely changed every third day, and specimens were removed from culture on days 7 and 21 for Live/Dead® Cell Viability Assay (Molecular Probes) and histological evaluation (H&E staining).

Live/Dead® images were captured using a Nikon Eclipse TE300 under fluorescence at 10x, while histology was imaged with the same microscope under normal light at 10x.

Mechanical Degradation / Collagen Matrix Production. To determine the rates of electrospun construct degradation and eventual replacement by native ECM, human dermal FBs (Cascade Biologics) were seeded onto SF (100 mg/m), SPDO, and SPCL electrospun scaffolds. These scaffolds were all created with the 8 cm drum mandrel rotating at 8000 RPM using the parameters specified previously. Dog-bone specimens (n=3) were punched from the electrospun mats, disinfected using the previously described method, and prepared for seeding and culture both statically and in a Rotary Wall Vessel Bioreactor (RWVB, Synthecon, Inc.).

Static culture was done in 6-well plates. Each well was filled with 400 µl of 12 mg/ml polyhema in ethanol, which was then allowed to evaporate, to ensure cells would not adhere to the bottom of the well plate. Three dog-bone specimens were then laid flat on the well plate and seeded with FBs at a concentration 150,000 cells/well (50,000 cells/ml total volume in well) suspended in 1 ml of media (same as previous). Plates were placed in an incubator under standard culture conditions for 1 hour to ensure cell attachment to the scaffolds had taken place prior to the addition of 2 more ml of media. Media was completely changed every third day and samples were removed at days 7, 14, 21, and 28. Control samples (no cells) were treated identically and were collected on days 7 and 28.

Dynamic culture was done in 110 ml RWVBs. Each bioreactor was sterilized by autoclaving, allowed to cool to room temperature, and filled with 60 ml of media (same

as previous). Twelve disinfected dog-bone shaped specimens of the same material were added to each RWVB and allowed to sit for 30 minutes to soak up media and sink to the bottom of the bioreactor. $5.5x10^6$ FBs suspended in 50 ml of media (50,000 cells / ml total volume in bioreactor) were added to each bioreactor. The bioreactors were sealed and placed in an incubator under standard culture conditions. The bioreactors were set to rotate at a constant 7 RPM, a speed that kept specimens from being pushed to the outer wall of the bioreactor while also preventing them from floating to the top of the bioreactor. 50 ml of media was changed once every 7 days, and samples were removed on days 7, 14, 21, and 28. Control samples (no cells) were treated identically and were collected on days 7 and 28.

At the end of each 7 day period samples were removed from culture and placed in PBS. Samples were then uniaxially tested to failure on an MTS Bionix 200 in a method previously described. Tested samples were then collected and stored for use with the Sircol™ Collagen Detection Assay via a slightly modified protocol. Briefly, individual samples were placed in 2 ml microcentrifuge tubes to which 1 ml of HFP was added to dissolve the electrospun construct. This HFP was then allowed to evaporate and 1 ml of 0.5 M acetic acid containing 2.5 mg/ml pepsin was added to the tube to solubilize any collagen contained within. This solution was then centrifuged at 10,000 g for 10 min to remove any residual scaffold polymer, and the collagen containing supernatant was collected and tested using the standard Sircol protocol.

Preliminary Microintegration of Air-gap Constructs. While traditional cell culture requires several weeeks for cells seeded on the surface of an electrospun scaffold

to migrate and proliferate enough to create a cellularized structure, microintegration of simultaneously electrospun polymers and electrosprayed cells creates a cellularized structure during the electrospinning process [366]. To determine the effectiveness of the microintegration process, air-gap electrospun constructs of SF (70 mg/ml), PDO, SPDO, PCL, and SPCL were created using parameters identical to those listed previously. These scaffolds were either electrospun simultaneously with cells, or were surface seeded after fabrication.

For microintegration, a setup similar to that of figure 8.5 was used. With polymer solution ready to be electrospun, $3x10^6$ human dermal FBs (Cascade Biologics) were suspended in 1 ml of cell culture media (same as previous) and loaded into a 1 ml Becton Dickinson syringe fitted with a blunt tipped 18 gauge needle. This cell solution was charged to +10 kv and dispensed by a KD Scientific syringe pump at such a rate that the cell loaded syringe would finish dispensing at the same time as the polymer loaded syringe (~4 ml/hr). Upon completion, cellularized scaffolds were placed in a 6-well plate with 3 ml of culture media and incubated under standard culture conditions. Media was completely changed after the first 8 hours and then again every third day. Non-cellularized constructs were placed in polyhema coated 6-well plates, and $3x10^6$ FBs suspended in 1 ml of media were seeded on top of them. Scaffolds were incubated for 1 hour to allow for cell adhesion prior to the addition of 2 ml of media. Media was completely changed on the same schedule as microintegrated constructs. Samples were removed from culture after 28 days and fixed in paraformaldehyde (30 mg/ml in PBS for

10 min) prior to preparation for histological evaluation (H&E) and confocal imaging with DAPI staining (Zeiss LSM META NLO multiphoton laser scanning microscope).

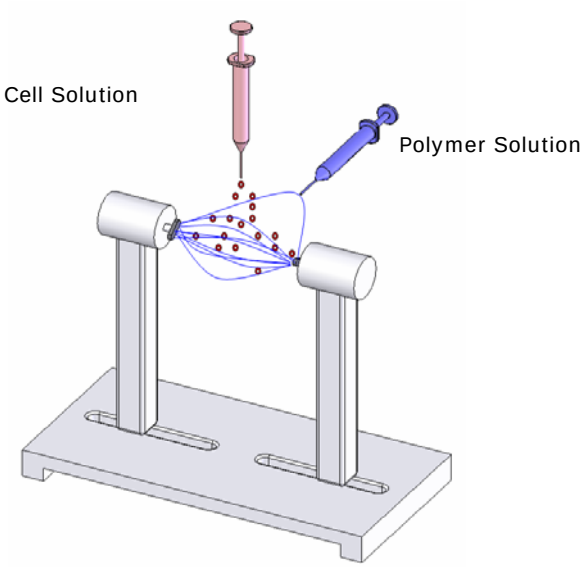

Figure 8.5. Schematic representation of a cellularized air-gap electrospun scaffold created through the microintegration of electrosprayed cell solution and electrospun polymer solution.

Statistical Analysis. All statistical analysis was based on a Kruskal–Wallis one-way ANOVA on ranks and a Tukey–Kramer pairwise multiple comparison procedure ($\alpha = 0.05$) performed with the JMP®IN 7.0 statistical software package (SAS Institute, Inc.). Graphical depictions of mean data were constructed with Microsoft Excel 2000, with error bars representing standard deviations.

RESULTS AND DISCUSSION

Scaffold Characterization. Scanning electron micrographs of random, aligned and air-gap electrospun structures are shown in figure 8.6. Using the ImageTool software

program it was determined that the average fiber diameter was around 1 micron for each of the polymers regardless of the electrospinning process used in their fabrication (figure 8.7). However, the average fiber diameters ranged from 0.7 microns for air-gap electrospun PCL to 1.42 microns for aligned SF structures electrospun onto a drum mandrel rotating at 8000 RPM. Statistical analysis revealed few significant differences between the fabrication methods for each polymer. The synthetic polymers, PDO and PCL, had significantly smaller fibers created through air-gap electrospinning than through either the traditional random or aligned electrospinning process. Air-gap electrospun scaffolds containing SF failed to be different from the other two fabrication methods. This result was somewhat surprising as it was anticipated that there would be large differences in the fibers created through the air-gap electrospinning process and those fibers created through standard electrospinning simply due to the differences between the electrospinning parameters of the two. The air-gap electrospinning process uses flowrates that were more than double those of the standard electrospinning process; historically increased flowrates lead to larger diameter fibers. The significantly smaller diameter synthetic polymer fibers may potentially be attributable to the differences in the electric fields of the two methods, with standard electrospinning providing a simple grounded target while air-gap electrospinning provides a pair of charged targets that may actually draw and stretch the polymer fibers between them. It should be noted that the air-gap electrospun PCL had a vastly different feel than the other air-gap electrospun materials, being much thiner and more fragile. It may be necessary to alter the electrospinning concentration of PCL in future air-gap electrospinning studies.

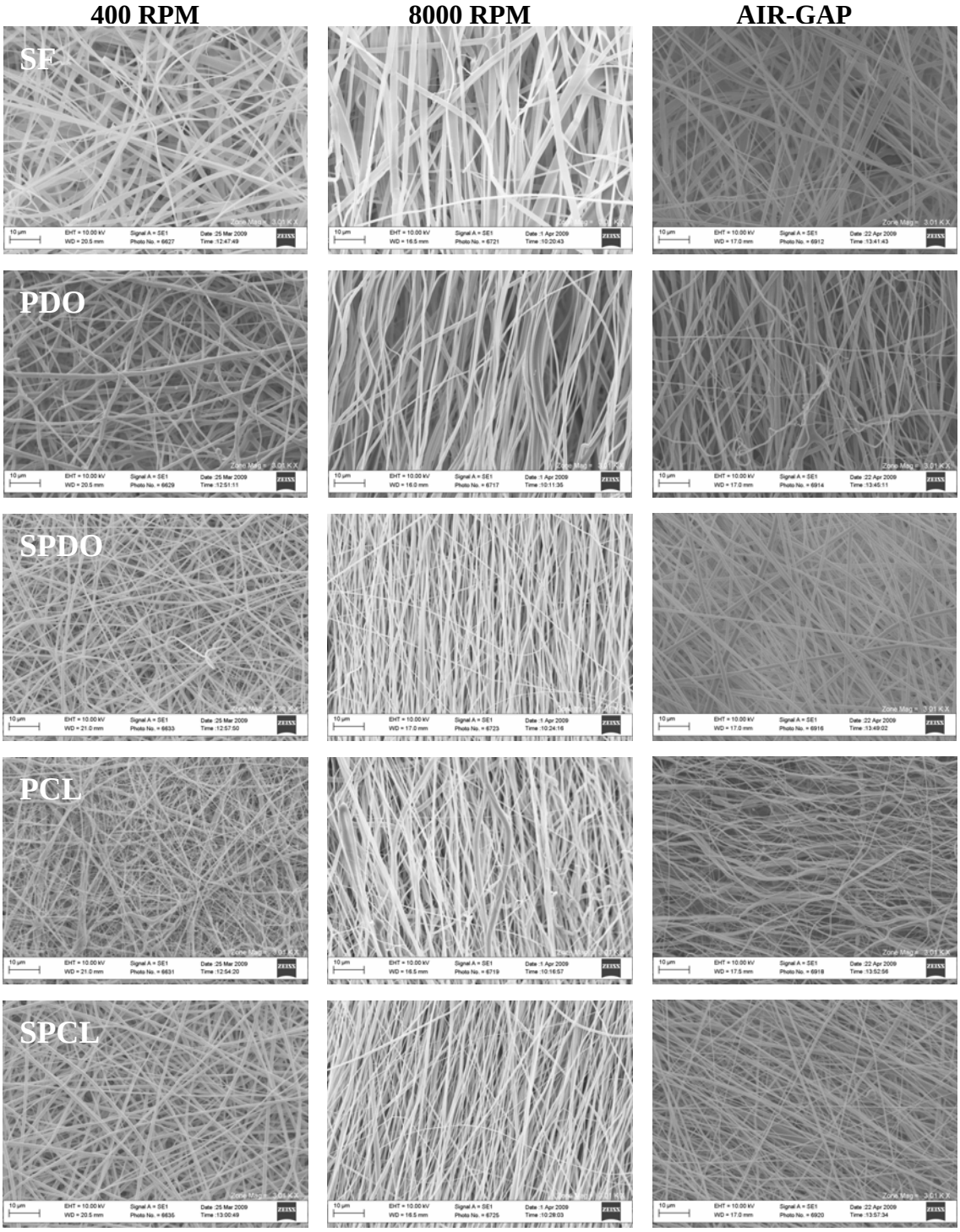

Figure 8.6. Scanning electron micrographs of SF, PDO, SPDO, PCL, and SPCL electrospun at 400 RPM, 8000 RPM and through the use of an air-gap electrospinner. All images taken at 3000x.

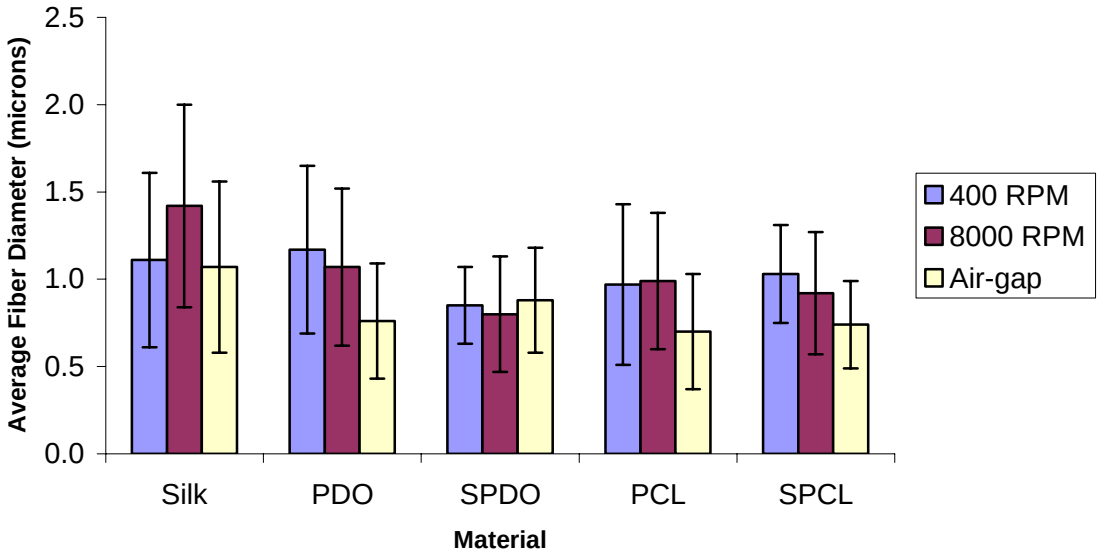

Figure 8.7. Average fiber diameters of random (400 RPM), aligned (8000 RPM), and air-gap electrospun scaffolds.

FFT analysis of the electrospun structures revealed there to be distinct differences in the degree to which the structures were aligned. As expected, the 400 RPM scaffolds exhibited no fiber alignment. The 8000 RPM scaffolds exhibited fiber alignment in the direction of mandrel rotation, with the pure PDO scaffold being the most aligned and the pure SF scaffold being the least aligned. The difficulty in aligning SF is evident throughout table 8.1, as the addition of SF to the synthetic polymers resulted in a drop in their degree of alignment. Surprisingly, structures created through the air-gap electrospinning process exhibited less alignment than those created at 8000 RPM. This may be attributable to the overall thickness of the structures and the lack of rotation of the collecting targets. As such, while the polymer fibers are visibly highly aligned during the initial minutes of air-gap electrospinning, subsequent fiber collection occurs only on the

front surface of the already formed construct. As the structure becomes increasingly thick the fibers may become increasingly random, resulting in a surface that appears to be fairly random under SEM. To more accurately assess the alignment of the air-gap structures, it may be necessary to create thinner air-gap electrospun constructs and use a light microscope image to obtain more accurate FFT results. The creation of an air-gap electrospinning system that has the ability to rotate the collecting targets to obtain an evenly distributed electrospun matrix may provide a way to create more uniformly aligned structures.

Table 8.1. Table of FFT peak intensity values achieved for scaffolds electrospun onto a mandrel rotating at 400 and 8000 RPM, as well as through the air-gap electrospinning method.

Polymer	Air-gap	400 RPM	8000 RPM
Silk	0.037	0.044	0.144
PDO	0.110	0.051	0.302
SPDO	0.104	0.074	0.217
PCL	0.145	0.051	0.284
SPCL	0.156	0.076	0.238

Porosity / Permeability Measurement. Scaffold porosity measurements are shown in figure 8.8. As anticipated, most materials (except PCL) exhibited significantly higher porosities at 400 RPM than 8000 RPM. Additionally, each polymer or polymer

blend of the aligned air-gap electrospun structures were significantly more porous than the aligned structures created at 8000 RPM, and at least equal to if not more porous than the randomly aligned 400 RPM structures. This confirms what one can visually infer from the SEM micrographs of figure 8.6, where the structures created at 8000 RPM appear to be very compact with little void space. This demonstrates that the air-gap electrospinning method, while perhaps not creating scaffolds as aligned as those at 8000 RPM (on the surface at least), does create a structure that is considerably more porous and thereby more conducive to cellular infiltration.

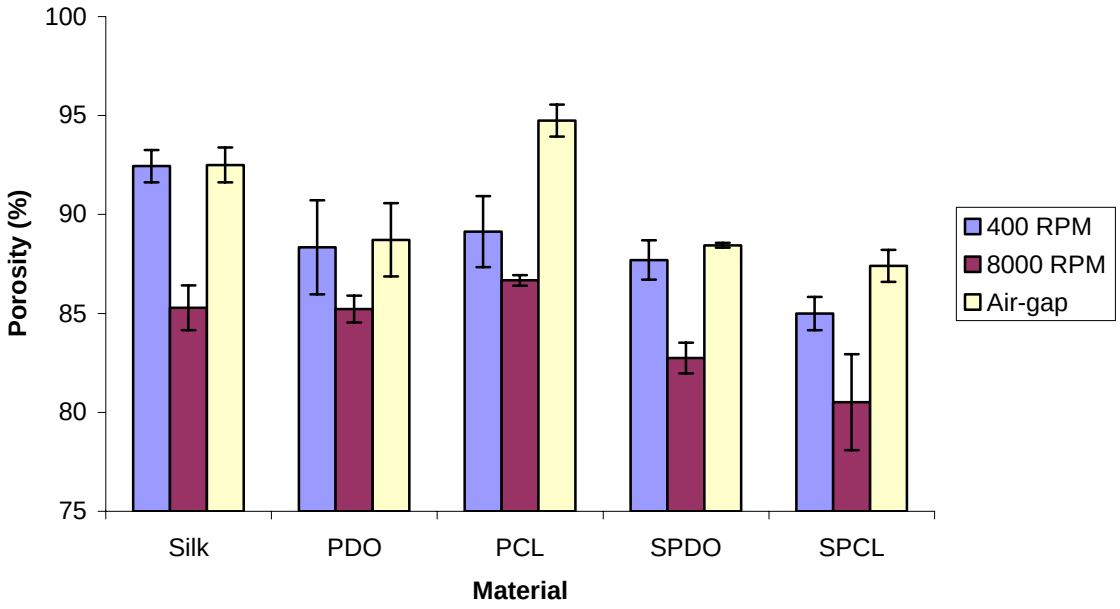

Figure 8.8. Average porosity values for random (400 RPM), aligned (8000 RPM), and air-gap electrospun structures.

Surprisingly, permeability results (figure 8.9) revealed something completely contradictory to the results of the porosity testing. It was anticipated that the more porous

air-gap electrospun structures would also be more permeable than their 8000 RPM counterparts, which would be less permeable than the 400 RPM structures due to their high fiber packing density. However, this was not the case with the majority of the materials tested (SF, PDO, SPDO) exhibiting no significant differences between fabrication methods. PCL containing scaffolds actually exhibited significantly higher permeabilities for the 8000 RPM scaffolds than both the air-gap and the 400 RPM structures. While porosity and permeability are related, with more porous structures typically exhibiting a higher permeability, a change in one does not necessarily correspond to a change in the other. Scaffold porosity, pore size and distribution, pore interconnectivity, and pore orientation and scaffold tortuosity all play roles in the hydraulic permeability of an ECM analogue scaffold [30, 31]. This is especially true with an electrospun structure, where the fiber organization is dynamic and can move freely in response to changes around it. It may be possible that the application of the 120 mmHg pressure head compressed the highly porous scaffolds and resulted in a structure with collapsed pores. The highly aligned 8000 RPM scaffolds, being less porous, may have experienced less fiber shifting resulting in a less tortuous path for fluid flow.

Regardless, the author maintains that the high scaffold porosities are more telling of the behavior of the structures than the permeability results. *In vivo* these structures, intended for use as a ligament analogue, will not be subjected to high pressures that would force pore collapse like they would if they were to be used in a vascular grafting application. *In vitro* cell culture will provide further insight into the ability for cells to migrate into the thickness of the structures

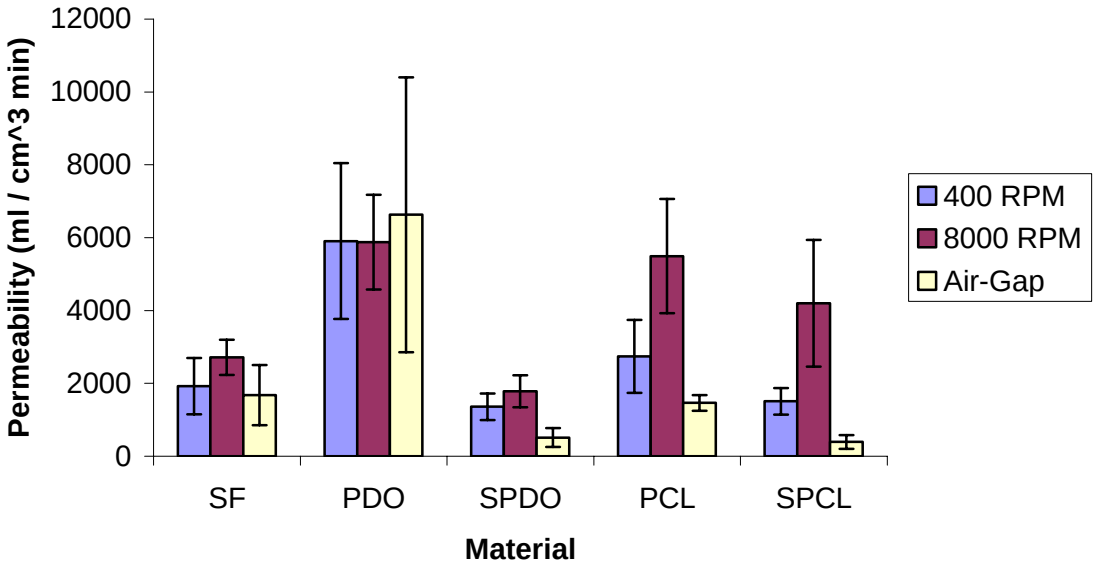

Figure 8.9. Average permeability values for random (400 RPM), aligned (8000 RPM), and air-gap electrospun structures.

Uniaxial Tensile Testing. The results of the uniaxial tensile testing of the random (400 RPM), aligned (8000 RPM), and air-gap electrospun structures, tested in two directions are shown in figure 8.10. As expected, there were no significant differences between mechanical properties of the parallel and perpendicular directions of the randomly oriented 400 RPM structures, indicating the structures were isotropic due to their random nature. Additionally, there were significant differences between the mechanical properties of the parallel and perpendicular directions of the 8000 RPM structures for all materials (except SF), confirming the anisotropy seen through SEM and FFT analysis. Air-gap electrospun structures demonstrated some significant anisotropy, with PDO and SPDO having higher peak stresses and moduli in the parallel direction and

higher strain at break in the perpendicular direction. Air-gap electrospun PCL and SPCL exhibited significantly higher peak stress and moduli in the parallel direction, with no significant differences in strain at break, while SF structures had no significant differences in mechanical properties with respect to testing direction.

There were also significant differences in the peak stress and moduli of the synthetic containing polymer structures created through air-gap electrospinning and those created through standard electrospinnig at 8000 RPM, with the air-gap structures being significantly weaker in the perpendicular direction. These differences may simply be indicative of differences in the degree of fiber alignment between the two. FFT results showed air-gap electrospun structures to be less aligned than 8000 RPM structures and mechanical testing would seem to confirm this. The decrease in mechanical properties seen in the air-gap constructs may also be dependant upon their increased porosity, with the highly porous structures containing less fiber volume per dog-bone specimen to resist loading than the less porous 8000 RPM structures.

Surprisingly, regardless of fabrication method the pure SF structures exhibited no significant anisotropy. Superficially this would seem to indicate that the SF structures were simply not aligned. However, FFT results showed more surface alignment in the 8000 RPM SF structures than in the air-gap PDO and SPDO structures, which both exhibited anisotropic mechanical properties. The lack of demonstrable anisotropy of the SF structures is currently unexplainable and will need further investigation, but may be due to changes in the SF fibers when they become hydrated.

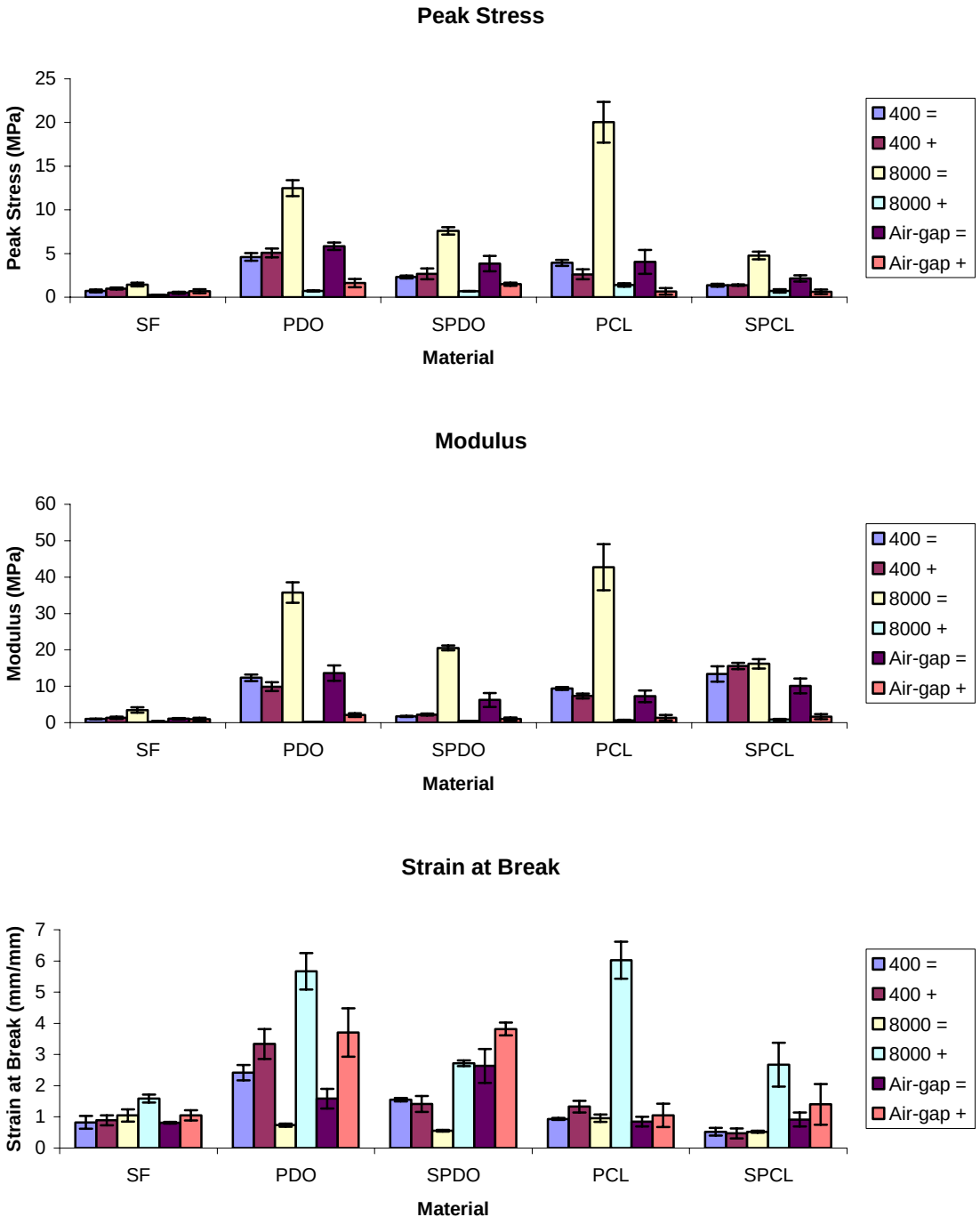

Figure 8.10. Uniaxial tensile testing results of SF, PDO, SPDO, PCL, and SPCL at 400 RPM, 8000 RPM, and air-gap electrospun. Specimens were tested parallel to the direction of fiber orientation (=) and perpendicular to the direction of fiber orientation (+).

Cell Migration / Penetration. The Live/Dead® Cell Viability Assay was used not only to show viable FBs but to also provide insight into cell proliferation and migration of cells across the surface of the scaffolds, and show orientation of cells with respect to fiber alignment. Live stained images taken at day 7 (figure 8.11) showed almost ompletely viable cell populations for all materials and fabrication techniques, with few dead cells (not shown) randomly scattered across the surface of the scaffolds. Scaffolds electrospun at 400 RPM, particularly those scaffolds containing SF, showed FBs that were spread out and exhibited no preferential direction of alignment. Those scaffolds that were created at 8000 RPM contained FBs that had begun to align themselves along the direction of fiber alignment, while still maintaining spaces between the cells indicating that the orientation of the FBs was due to alignment with fibers as opposed to a forced orientation due to contact with neighboring cells. Air-gap electrospun contstucts in general exhibited some degree of FB alginment, though less than seen in 8000 RPM scaffolds. Air-gap electrospun constructs containing SF also had a large number of cells that were out of focus, similar to that of the 400 RPM scaffolds, possibly indicating some penetration of the cells into the scaffolds. By day 21 (figure 8.12) nearly all the scaffolds, with the exception of the pure SF, demonstrated a preferential direction of cellular alignment. It is hypothesized that this cellular orientation was brought about by contact with neighboring cells as the FBs proliferated and free space on the scaffolds decreased. This forced orientation left little distinction between fabrication techniques. While nearly all of the scaffolds contained confluent sheets of FBs on their surfaces by day 21, the pure SF scaffolds did not. These scaffolds

still contained cells that were out of focus, indicating that cells were not limited to simply attaching to the surface of the structure but had the opportunity to penetrate its thickness. This cellular penetration is critical to successful tissue engineering to allow for an acellular scaffold to become cellularized and eventually degraded and replaced by native ECM.

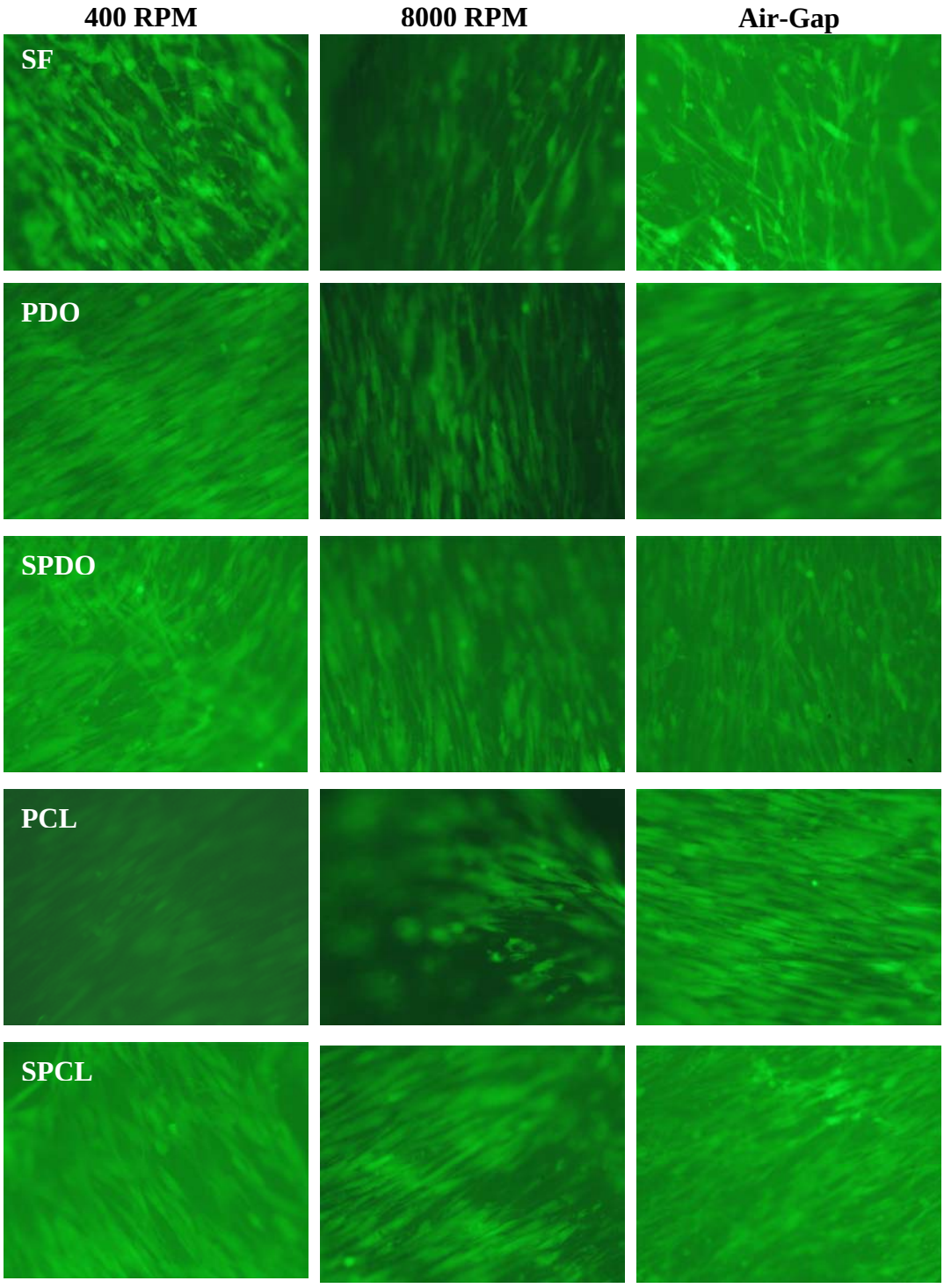

Figure 8.11. Live stained images of FBs seeded on SF, PDO, SPDO, PCL, and SPCL scaffolds taken after 7 days in culture. All images taken at 10x.

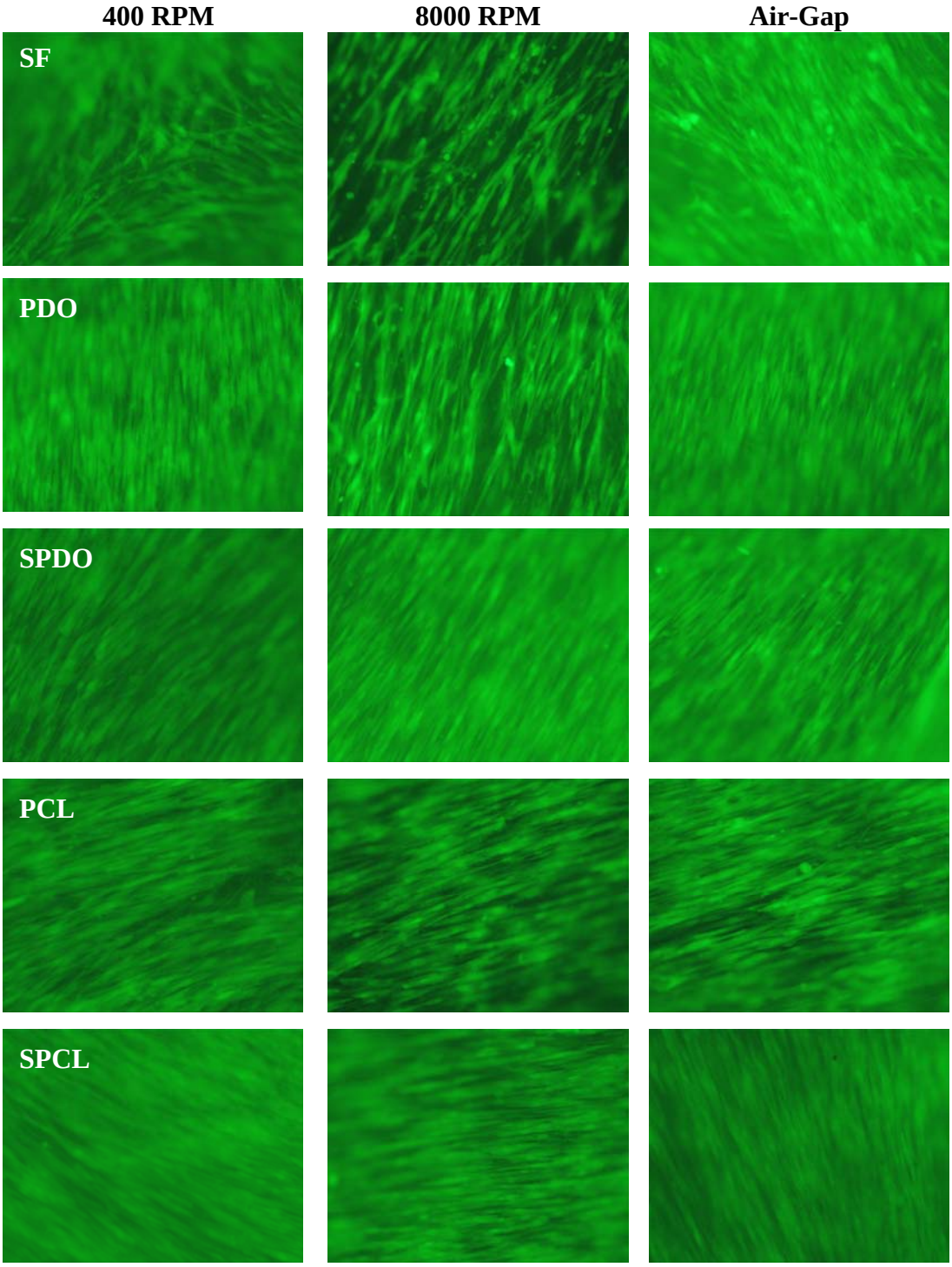

Figure 8.12. Live stained images of FBs seeded on SF, PDO, SPDO, PCL, and SPCL scaffolds taken after 21 days in culture. All images taken at 10x.

H&E staining of FB seeded constructs removed from culture on day 21 is shown in figure 8.13. These images provide more conclusive evidence of cellular penetration into the thickness of the electrospun structures than the surface images of the Live/Dead® assay. By day 21 FBs were seen to have migrated into all of the air-gap electrospun structures, with significant penetration seen in the pure SF structure. As expected, the relatively low porosity 8000 RPM structures had little cellular presence below the surface due to their highly packed fiber organization. Not surprisingly, histology of the high porosity 400 RPM structures looked very similar to that of the air-gap electrospun structures. This may lead one to believe that scaffold porosity is responsible for successful cellular penetration. However, looking at the air-gap electrospun PCL which exhibited the highest porosity (94%) and the similarly porous air-gap electrospun SF (92%) one sees that their histology is very different. The SF structure was more conducive to cell penetration than the pure PCL structure. This would indicate that scaffold porosity, while certainly a contributing factor to cell penetration, is not solely responsible for it. It may be that fiber stiffness and surface chemistry play a large part in the ability, or desire, for cells to penetrate an electrospun scaffold.

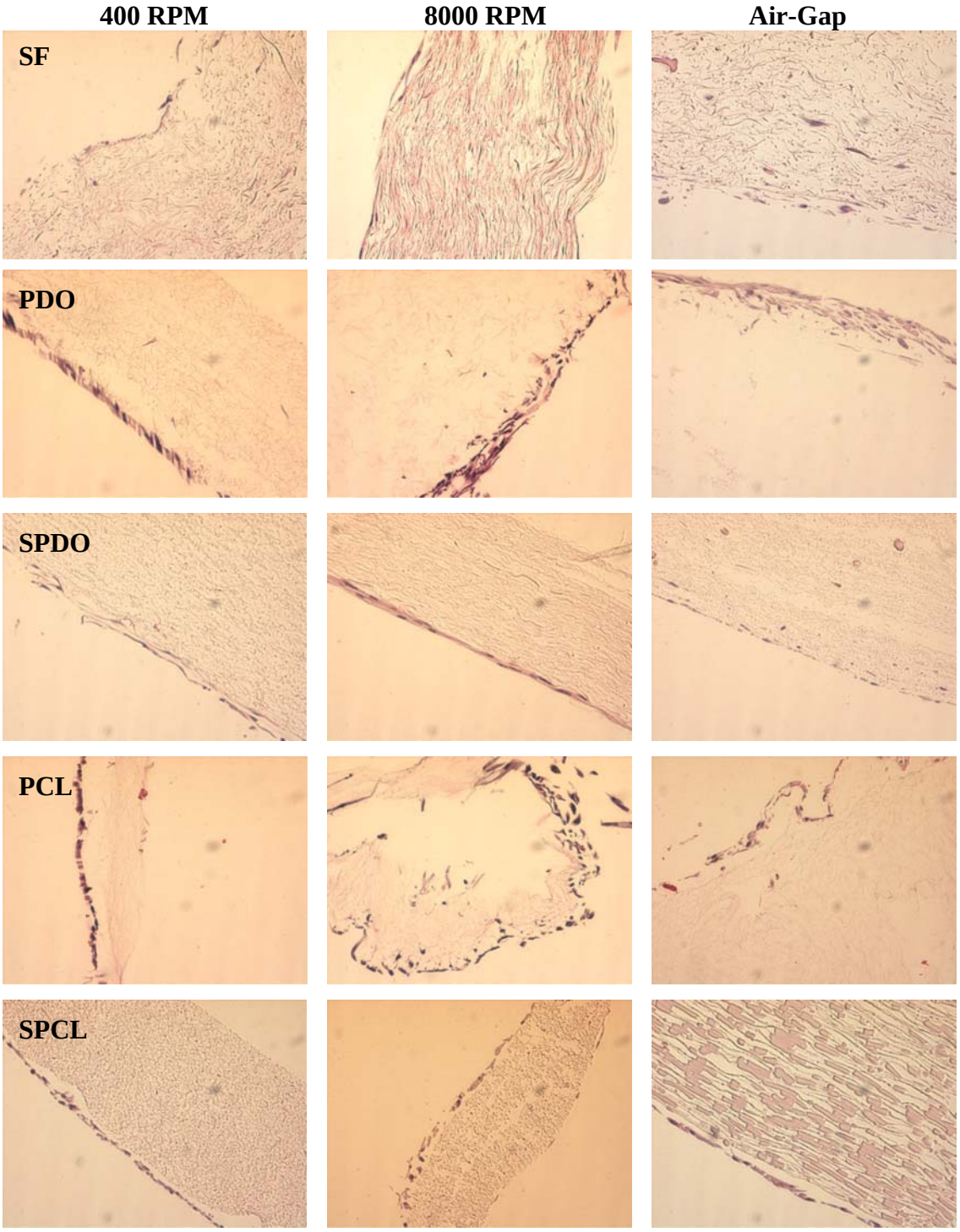

Figure 8.13. H&E staining of FB seeded SF, PDO, SPDO, PCL, and SPCL electrospun constructs taken after 21 days in culture. All images taken at 10x.

Mechanical Degradation / Collagen Matrix Production. Results of uniaxial tensile testing for both static and dynamic culture of dog-bone specimens seeded with FBs after 28 days are shown in figures 8.14 and 8.15, respectively. Surprisingly, this data shows little difference between the two culture methods and virtually no change in mechanical properties after the 28 day time course. Scaffolds of all three materials exhibited no significant differences between static culture and dynamic culture in peak stress, modulus, or strain at break. Additionally, there was no statistically significant change in the mechanical properties of the materials taken at each of the four durations tested. The implications of this result are two-fold. First, this demonstrates that the polymers chosen for this study have not begun to break down after four weeks of culture *in vitro*. This is a positive for a tissue such as the ACL, where cellular infiltration and matrix turnover are very slow, meaning that the electrospun ECM analogue will not degrade at a rapid pace and be resorbed to a point where it can no longer support load prior to the creation of substantial native ECM. Second, this would indicate that if native collagen matrix had been produced by the cells attached to the scaffolds, this collagen was either not in sufficient quantities or of sufficient strength to significantly alter the mechanical properties of the electrospun structures. This is undoubtedly a negative result, at it was anticipated that by the 28th day of culture, there would have been significant amounts of matrix produced which would have altered scaffold mechanical properties.

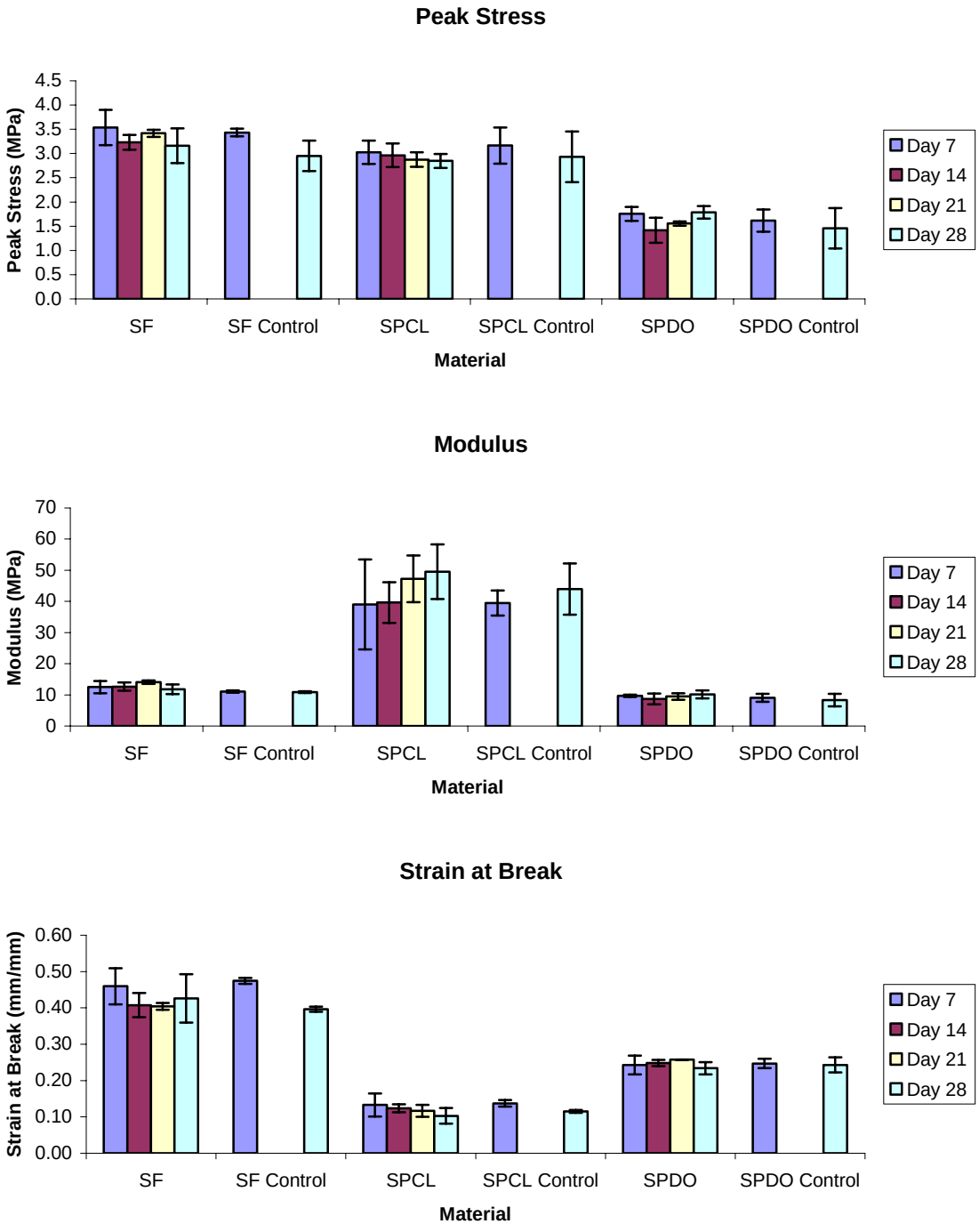

Figure 8.14. Mechanical properties of electrospun materials after 28 days in static culture in a 6-well plate.

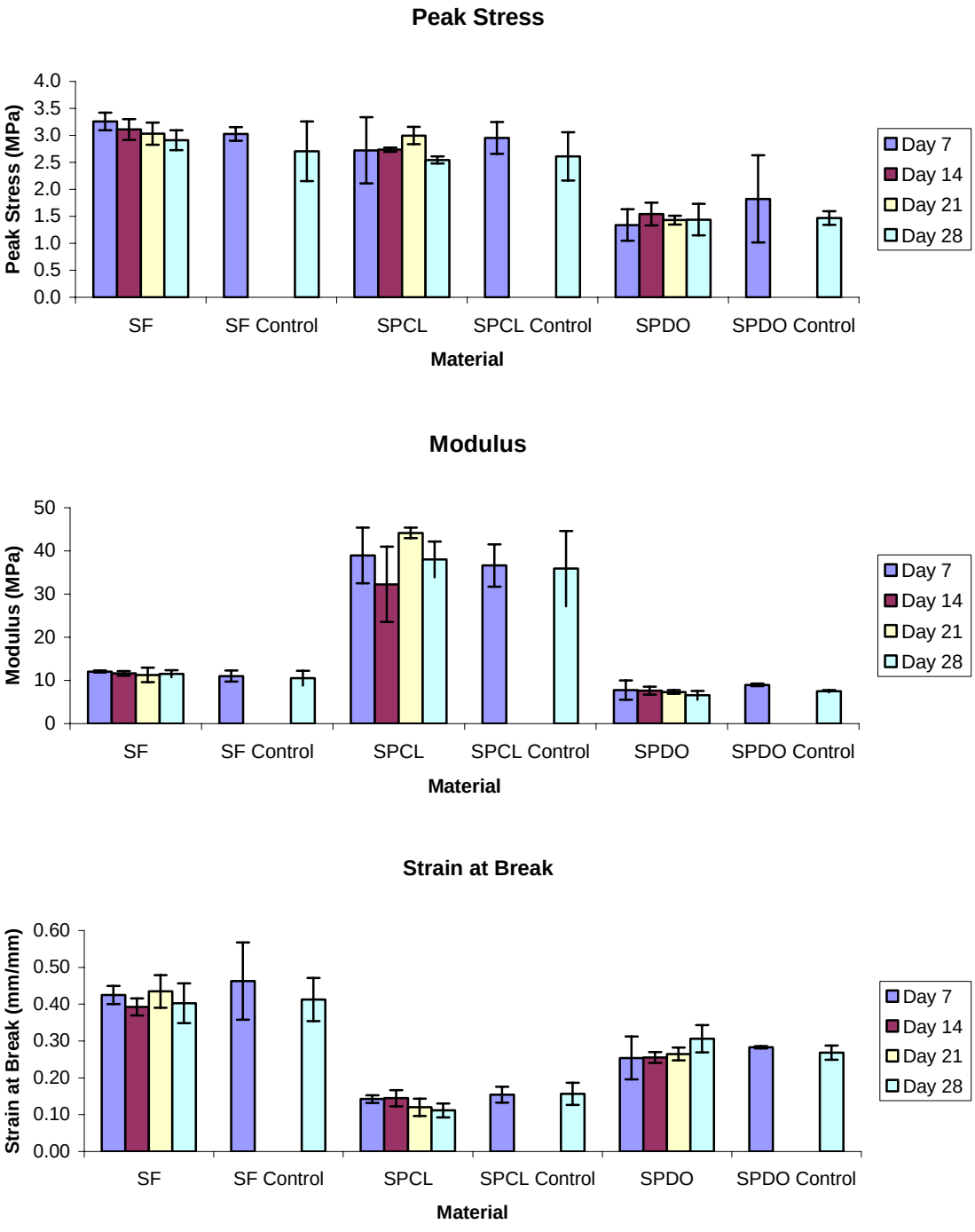

Figure 8.15. Mechanical properties of electrospun materials after 28 days in dynamic culture in RWVB.

Results of the Sircol collagen quantification assay are shown in figure 8.16. These results showed there to be some significant differences between those dog-bones that were cultured statically and those that were cultured dynamically in the RWVB, while the majority of samples were not different from one another. SPCL demonstrated a significant increase in collagen produced on day 21 in dynamic culture compared to other time points, while SPDO scaffolds exhibited no significant differences between time points or culture methods. Pure SF scaffolds also exhibited an increased amount of collagen production at day 21 in dynamic culture, with days 14 and 28 of dynamic culture also being significantly higher than those of static culture. In all, SF at day 21 of dynamic culture had by far the highest amount of collagen production.

It is apparent from this data that the dynamic culture of FB seeded dog-bones aids in their production of ECM. However, it should be noted that the standard deviations of the dynamic samples were much larger than those of the statically cultured samples. This would seem to indicate that cell-scaffold interactions were less uniform in the RWVBs than in static culture. In future work it may be beneficial to statically seed the specimens for a period of time prior to placing them in the bioreactor to ensure adequate interaction and adhesion of the cells to the scaffold, rather than allowing cells and specimens to interact haphazardly. Yet, this random interaction demonstrated the affinity of FBs for the pure SF scaffolds as opposed to those containing synthetic materials. From this result, coupled with the H&E staining of figure 8.13, one could assume that FBs successfully migrated into the pure SF scaffold and began to produce their own ECM while the FBs were less likely to attach to and penetrate the SPDO and SPCL scaffolds,

eventually forming confluent sheets on the surface. Any matrix these surface dwelling cells produced was likely lost during media changes in culture or through handling of the specimens during mechanical testing, as opposed to matrix produced within the electrospun structure which would be somewhat protected.

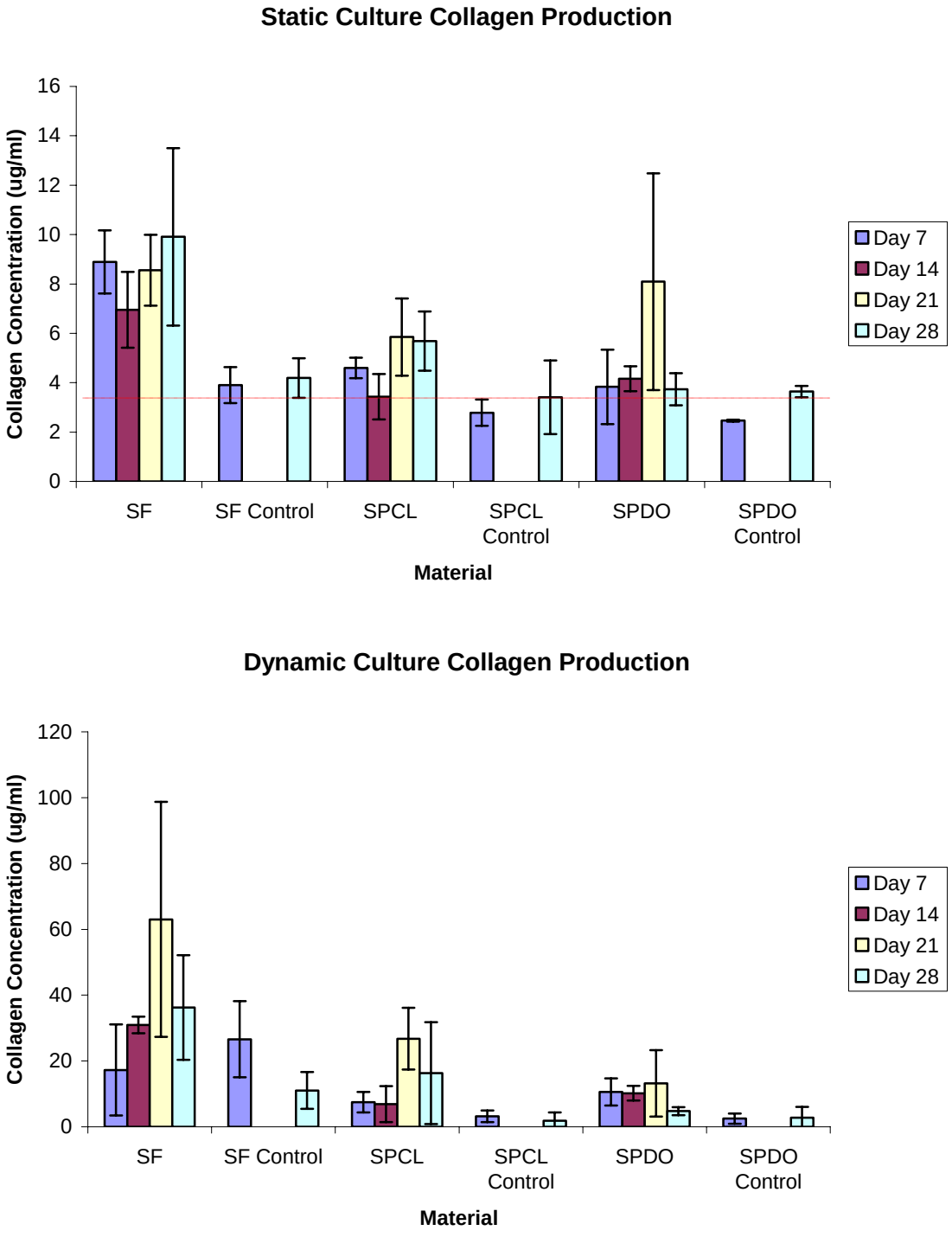

Figure 8.16. Results of Sircol collagen quantification assay for scaffolds cultured under both static (top) and dynamic (bottom) conditions. Dashed line indicates minimum level of detection.

Preliminary Microintegration of Air-gap Constructs. Microintegration of FBs into electrospun scaffolds by simultaneously electrospraying cells and electrospinning polymer was seen as a promising method to create a fully cellularized electrospun structure. As such, air-gap electrospun constructs were created both with and without simultaneous electrospraying of cells. Structures created without cells were surface seeded after fabrication for comparison to those structures that had been microintegrated. H&E stained histology of the surface seeded structures and the microintegrated structures after 28 days in culture are shown in figures 8.17 and 8.18, respectively, while DAPI stained confocal images are shown in figures 8.19 and 8.20.

It was intended that microintegrated scaffolds of SF, PDO, SPDO, PCL, and SPCL would be created through air-gap electrospinning using previously estabilished parameters, however this was determined not to be possible for SF, PCL, and SPCL. Syringes of SF and FBs were setup in a fashion similar to figure 8.5, with the two syringed separated by 180°. The SF formed fibers initially, however once the electrosprayed cell/media droplets made contact with the structure it dissolved. While HFP has been shown to force β-sheet formation during electrospinning, it may not have had time to fully evaporate and dehydrate the fibers to make them non-soluble. As such, it may not be possible to electrospin SF from HFP and create a microintegrated structure without the electrospun fibers dissolving. Additonally, PCL, which was previously noted as being extremely fine and fragile, and SPCL experienced the formation of large holes in their fibrous structure where cell/media droplets made contact and were unable to be

removed from the electrospinniner. Surprisingly, both the PDO and SPDO structures were electrospun and microintegrated without a problem and formed thick constructs nearly identical in size to those of the air-gap electrospun structures that had not been microintegrated.

H&E staining showed significant cellular penetration into the air-gap electrospun scaffolds after 28 days in culture. As expected from previous work, SF had cells migrate well into its thickness. PDO, SPDO, and SPCL all demonstrated cellular penetration, while most surprisingly the pure PCL structure was almost completely cellularized after 28 days. The penetration was more significant than that shown in figure 8.13, and may be due to the increased number of cells seeded on the structures and the additional week of culture time.

Results of the microintegrated structures were not nearly as encouraging. After 28 days in culture, it was noted that the microintegrated pure PDO constructs had lost all mechanical stability and fell apart upon removal from culture. As such the pure PDO structure was difficult to image, and consisted mostly of pieces of fibers held loosely together by FBs. It has been hypothesized that the incorporation of a large number of cells into the PDO structure exacerbated the breakdown of the polymer and led to its premature loss of mechanical properties. However, the SPDO microintegrated structure was completely intact after 28 days and appeared to have lost none of its mechanical stability, likely due to the presence of the slowly degrading SF. Histology of the SPDO microintegrated structures showed there to be a large number of cells scattered

throughout the thickness of the structure, demonstrating some preliminary success in the microintegration of FBs and electrospun polymers.

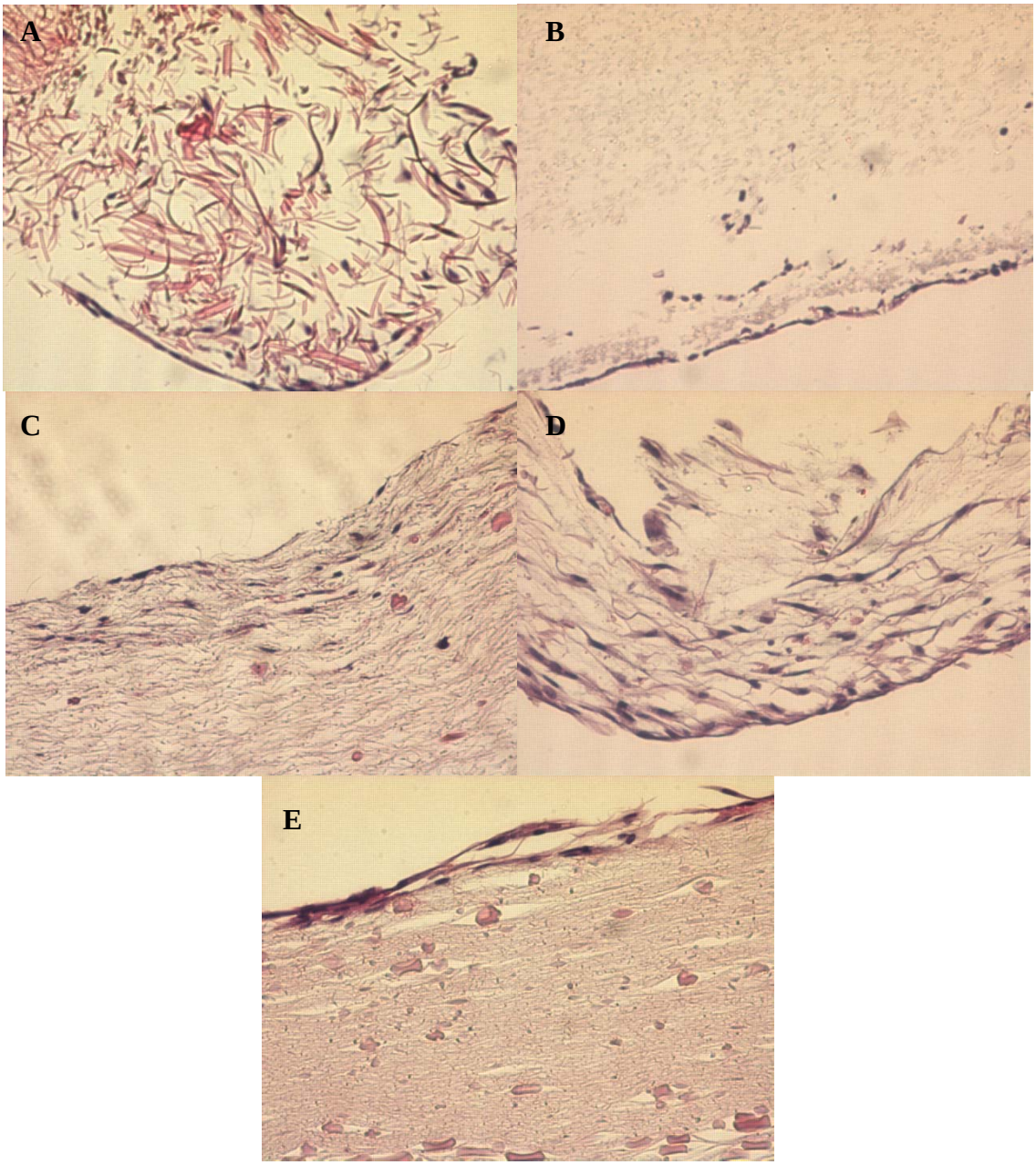

Figure 8.17. Histological evaluation of surface seeded air-gap electrospun SF (A), PDO (B), SPDO (C), PCL (D), and SPCL (E) after 28 days in static culture. All images were taken at 10x.

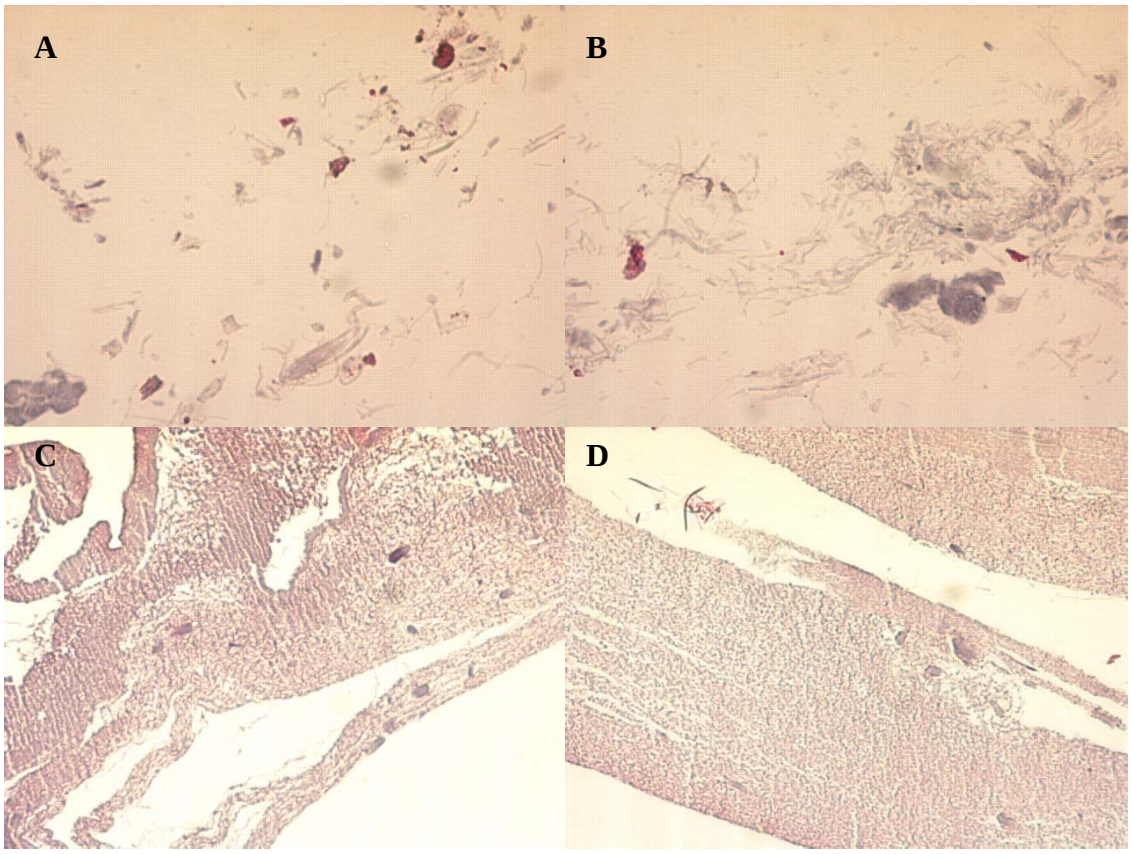

Figure 8.18. Histological evaluation of microintegrated air-gap electrospun PDO (A and B) and SPDO (C and D) after 28 days in static culture. All images were taken at 10x.

Confocal images further confirmed what was seen in the histology shown above. Surface seeded scaffolds exhibited a nearly confluent layer of FBs on the surface and a number of out of focus cells that appeared to have penetrated the surface of the structure. Both the seeded surface and the un-seeded surface were imaged to demonstrate that the electrospun fibers in fact autofluoresced, but appeared to be virtually non-existent in the images of the seeded side due to the nearly confluent layer of cells. While difficult to discern definitively with only DAPI staining, it appears that many of the imaged nuclei (figure 8.19 A, C, E, and G) are of an ellipsoid shape in a uniform direction and may be

indicative of FBs that have oriented themselves along the preferred direction of fiber alignment.

The microintegrated structures were also imaged on both sides, and again confirm what was seen previously in histology. The PDO samples were nothing more than clumps of fragmented fibers with a small number of sporadically interspersed FBs, providing little information about the success of the microintegration technique with PDO. Meanwhile, the SPDO samples revealed a number of cell nuclei visible on both imaged surfaces and a number of out of focus nuclei that appeared to reside below the surface. Interestingly, the nuclei residing on the surface of the microintegrated SPDO did not have the same shape as those that were seen on the surface seeded structures. Rather than being ellipsoid in a uniform direction, the nuclei on the microintegrated structure were very random in shape, possibly signifying a lack of orientation of their respective cells.

In all, while the microintegration process was capable of creating a cellarized SPDO structure, it failed to create a structure with FBs oriented along the direction of fiber alignment. Additionally, the process of microintegrating cells is quite difficult and poses a number of technical problems that make it exponentially more complicated than simple surface seeding. While microintegration may present itself as a viable method for creating cellularized constructs in the future, currently the end product does not appear to be advantageous over traditional surface seeding.

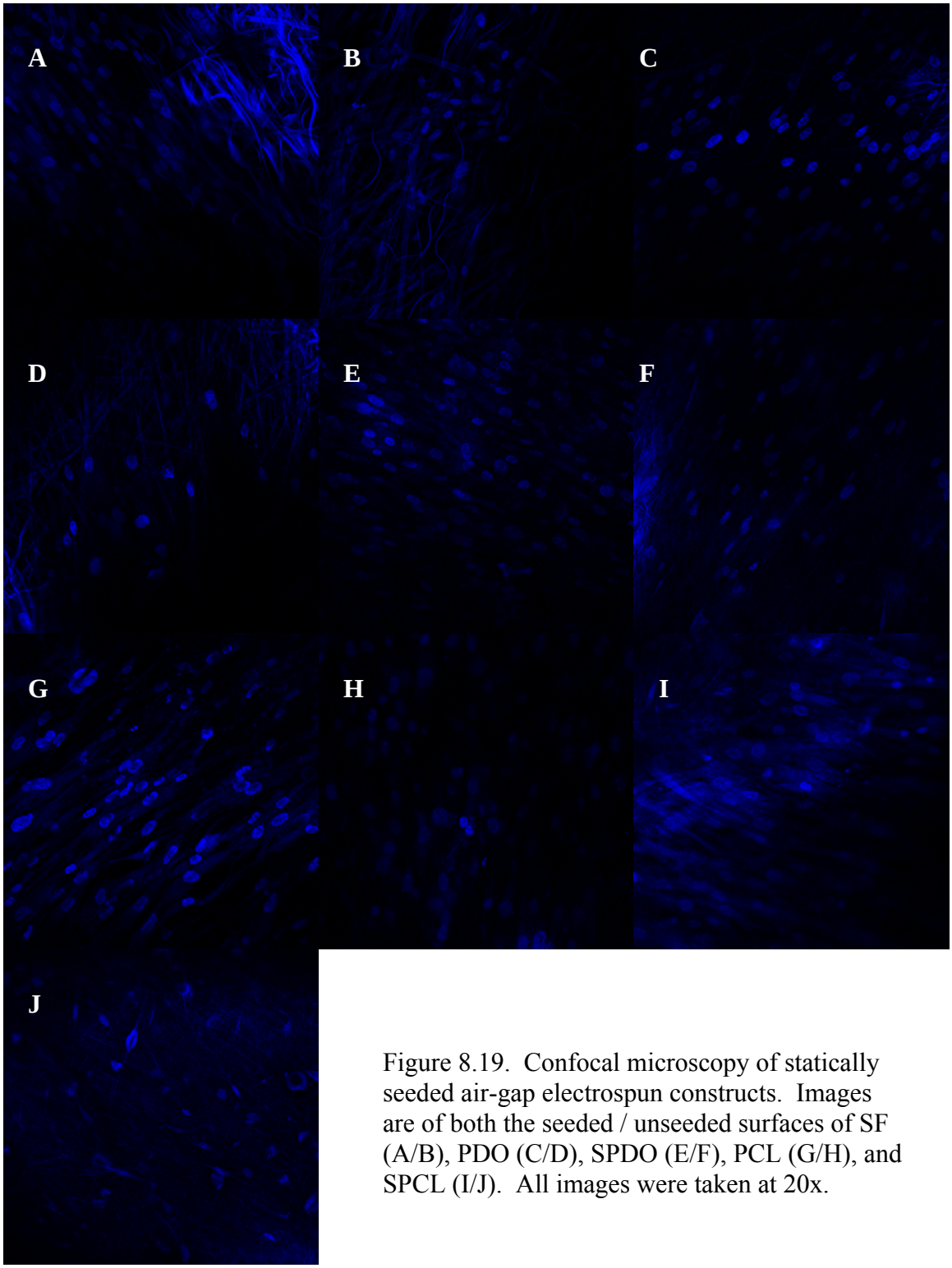

Figure 8.19. Confocal microscopy of statically seeded air-gap electrospun constructs. Images are of both the seeded / unseeded surfaces of SF (A/B), PDO (C/D), SPDO (E/F), PCL (G/H), and SPCL (I/J). All images were taken at 20x.

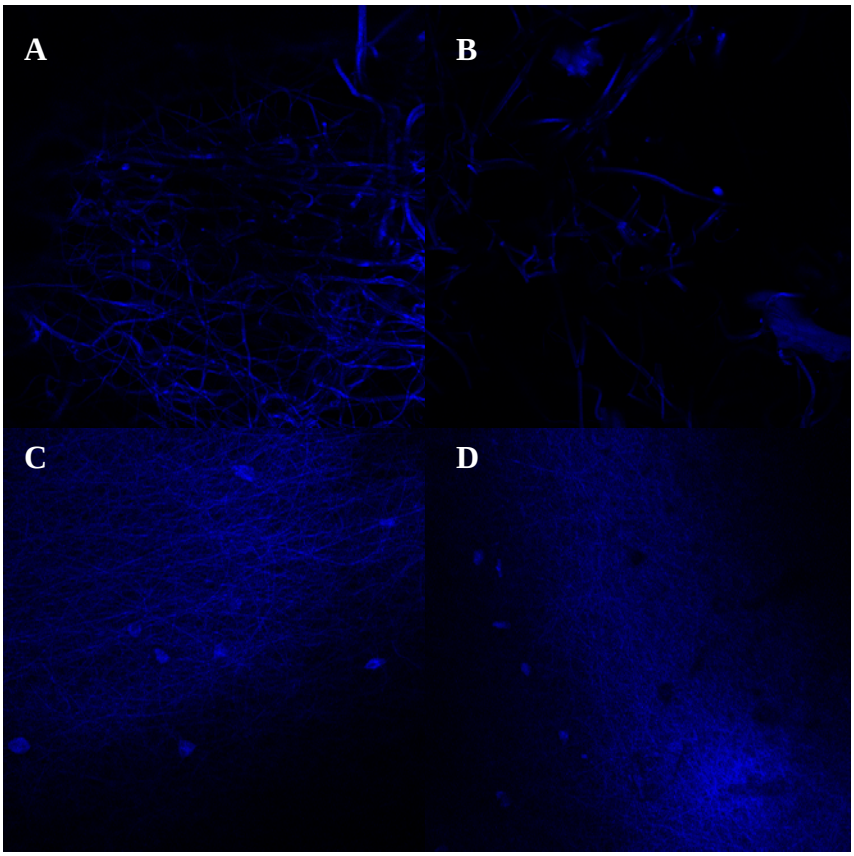

Figure 8.20. Confocal microscopy of air-gap electrospun PDO (A) and SPDO (B) microintegrated with FBs during the electrospinning process. Images show both the top surface (C) and the bottom surface (D) of the scaffold after 28 days in culture. All images were taken at 20x.

CONCLUSIONS

In conclusion, the methods presented here for the creation of cellularized ligament analogue structures, air-gap electrospinning and the microintegration of cells into an electrospun structure, provided mixed results. Air-gap electrospinning was capable of providing structures with enhanced porosity that played a major role in the penetration of

cells into the scaffold; however, these air-gap structures did not possess the same degree of fiber alignment or mechanical properties as highly aligned structures created through standard electrospinning methods. Meanwhile, the simultaneous electrospraying of FBs and electrospinning of polymers was successful in creating cellularized structures but was usable with only a select few polymers. These structures contained a distribution of cells throughout their thickness, but did not exhibit the same physiologic organization as native ligament which could be more closely achieved through standard surface seeding. The author believes that both fabrication techniques have a place in tissue engineering, but work needs to be done modifying the procedures to yield better results.

CHAPTER 9 Conclusions and Future Research

The creation of an ideal ECM analogue scaffold is a goal that tissue engineers have strived for since the inception of the field, and will have to work many years yet to achieve. While superficially the ECM would seem like a simple thing to successfully replicate, a simple fibrous structure intended to support cell growth; the diversity and multifuncionality of the ECM in the human body make such a task daunting. To replicate such a simple yet varied structure, one needs a fabrication technique that is equally as simple and widely adaptable. Electrospinning has come to the forefront in ECM analogue scaffold fabrication because of its ability to be performed simply while allowing engineers to fabricate structures from an array of different materials. In this study, a number of different fabrication and post-fabrication techniques were investigated to demonstrate the seemingly innumerable iterations available to tissue engineers employing electrospinning towards the creation of tissue specific ECM. Through the blending of polymers, cross-linking of scaffolds, modification of fiber alignment, and alteration of the electrospinning setup, one can tailor a tissue engineering scaffold to fit nearly any tissue of the body.

The first approach to scaffold modification was done simply through the blending of synthetic and natural polymers for use as vascular and urologic grafts. PDO was blended with elastin in solution prior to electrospinning, and blended with fibrinogen at the needle tip through the use of a specially designed nozzle. In both cases, the presence

of PDO enhanced the mechanical properties of the structure above that of the natural polymer alone, and enhanced the bioactivity of the scaffold above that of PDO alone. PDO:elastin proved promising as a vascular conduit, undergoing uniaxial tensile testing, dynamic compliance testing, suture retention testing, and *in vitro* cell culture. Mechanical properties similar to those seen in native vessel were achievable through the blending of the two polymers, while the presence of elastin also provided cells with a recognizable fibrous structure. Fibrinogen, which is quickly broken down by cells *in vitro* was also enhanced by the blending with PDO. Again, the blending of the polymers resulted in a mechanically viable structure that still exhibited levels of bioactivity well above those of purely synthetic scaffolds.

Following the blending of natural and synthetic polymers, post-fabrication cross-linking was investigated as a means to modify scaffold mechanical properties and rates of degradation. Again using fibrinogen, because of its rapid rate of degradation and low mechanical stability, a number of different cross-linking agents were used (GLUT, EDC, and genipin) to varying effect. It was found that both EDC and genipin were successful in enhancing scaffold mechanical integrity and retarding its rate of degradation. While the use of these cross-linkers had a negative impact on scaffold bioactivity, it has been hypothesized that decreasing the degree of cross-linking would inversely affect the ability of cells to remodel the structure.

Modifying the alignment of fibers in electrospun structures was also shown to be a way of altering the mechanical properties of an ECM analogue. SF based structures were electrospun at a number of different mandrel rotational speeds and sizes to produce

scaffolds with varying degrees of fiber alignment. When these structures were tested in tissue specific mechanical evaluations for ligament and vascular engineering, it was shown that, as in nature, different ECM replacement structures require different degrees of fiber alignment. Structures composed of fibers aligned in the direction of rotation around a mandrel rotating at high RPMs, while effective as a ligament analogue, failed to produce vascular grafts with the compliance necessary to be successful.

Finally, this study utilized air-gap electrospinning and the microintegration of cells to produce scaffolds for ligament engineering. Rather than use a drum mandrel rotating at high RPMs to produce thin sheets of aligned fibers, air-gap electrospinning was used to create substantial structures with varying degrees of fiber alignment as revealed by FFT analysis. Uniaxial tensile testing confirmed this alignment by demonstrating the anisotropy of the structures mechanical properties. Air-gap electrospinning was also shown to produce highly porous structures that proved to be conducive to cellular penetration. Microintegration was capable of producing cellularized scaffolds; however these cellularized structures did not contain FBs oriented along the direction of fiber alignment that is seen in native ligament.

Overall, the results of this study highlight some of the ways that electrospinning can be used to tailor the properties of a scaffold to the requirements of a tissue both during and post-fabrication. Through simple modifications like the blending of various polymers, cross-linking of scaffolds, and orientation of fibers, nearly every physical property of the scaffold (mechanical properties, rates of degradation, levels of bioactivity, porosity, permeabitliy, etc.) can be altered. Additionally, dramatic changes to the way

that polymers are electrospun, through the mandrel-less air-gap electrospinning process and the microintegration of polymer and cells, further increases the options available to the tissue engineer attempting to create ideal tissue specific scaffolds.

FUTURE RESEARCH

Future work in this study will focus further on the creation of cellularized ligament analogue structures. While the preliminary microintegration work presented here demonstrated that the process could be used to incorporate cells into electrospun structures, the author was not completely satisfied with the end result. The creation of a cellularized structure straight off the electrospinner was intriguing, but a higher density of organized cells oriented with the direction of fiber alignment would be necessary to mimic the physiologic structure, and therefore function, of ligament. Further work with the microintegration of cells and scaffolds would be interesting, as well as other methods of creating cellularized ligament analogues. One such method may be to air-gap electrospin a relatively thin, highly porous structure and surface seed the structure with FBs. Once the FBs have become confluent, the structure could be folded upon itself and sealed with fibrin glue, followed by dynamic culture in a RWVB.

Additionally, more in depth mechanical evaluation would be needed on both acellular and cellularized structures. This current study focused solely on uniaxial tensile testing to failure of electrospun structures, while future work should also include dynamic mechanical analysis. Dynamic mechanical analysis provides insight into the mechanical

properties of a structure in its usable range, as opposed to uniaxial tensile testing which provides information into the ultimate properties of a material. Dynamic mechanical analysis would also provide much needed information on the viscoelastic nature of the materials used, something that was not addressed in this study but is critical to success of a load bearing ligament replacement.

Finally, the incorporation and investigation of a number of different chemokines into the electrospun scaffolds would be of interest. A wide range of chemokines are at work in the body during the wound healing process and could be beneficial if incorporated into a ligament graft. These chemokines could serve to attract FBs or even macrophages, which could then in turn release their own chemokines. Chemokines could also be used to promote cellular proliferation or enhance matrix production. In addition to an array of different chemokines, the incorporation and *in vivo* assessment of small wound resolution molecules known as resolvins would also be interesting.

Literature Cited

Literature Cited

1. Barnes, C.P., et al., *Nanofiber technology: Designing the next generation of tissue engineering scaffolds.* Advanced Drug Delivery Reviews, 2007. **59**: p. 1413-1433.

2. Heineken, F.G. and R. Skalak, *Tissue engineering: A brief overview.* J Biomech Eng, 1991. **113**: p. 111.

3. Langer, R., *Editorial: Tissue engineering: Perspectives, challenges, and future directions.* Tissue Engineering, 2007. **13**(1): p. 1.

4. Langer, R. and J.P. Vacanti, *Tissue engineering.* Science, 1993. **260**(5110): p. 920-926.

5. Palsson, B.O., Bhatia SN, *Tissue Engineering*. 2004, Upper Sadle River, New Jersey: Pearson Prentice Hall.

6. Weigel, T., G. Schinkel, and A. Lendlein, *Design and preparation of polymeric scaffolds for tissue engineering.* Expert Reviews in Medical Devices, 2006. **3**(6): p. 835-851.

7. Farach-Carson, M.C., R.C. Wagner, and K.L. Kiick, *Extracellular matrix: Structure, function, and applications to tissue engineering*, in *Tissue Engineering*, J.P. Fisher, A.G. Mikos, and J.D. Bronzino, Editors. 2007, CRC Press: Boca Raton, FL. p. 3-1 - 3-22.

8. Vacanti, J.P. and C.A. Vacanti, *The challenge of tissue engineering*, in *Principles of Tissue Engineering*, R. Lanza, R. Langer, and W. Chick, Editors. 1997, Academic Press: San Diego. p. 1-5.

9. Simpson, D.G. and G.L. Bowlin, *Tissue-engineering scaffolds: can we re-engineer mother nature?* Expert Rev Med Devices, 2006. **3**(1): p. 9-15.

10. Yoon, D.M. and J.P. Fisher, *Polymeric scaffolds for tissue engineering applications*, in *Tissue Engineering*, J.P. Fisher, A.G. Mikos, and J.D. Bronzino, Editors. 2007, CRC Press: Boca Raton, FL. p. 8-1 - 8-18.

11. Boland, E.D., P.G. Espy, and G.L. Bowlin, *Tissue engineering scaffolds*, in *Encyclopedia of Biomaterials and Biomedical Engineering*, G. Wnek, Bowlin G, Editor. 2004, Marcel Dekker, Inc.: New York. p. 1-9.

12. Huang, J.I., J.U. Yoo, and V.M. Goldberg, *Orthopedic applications of stem cells*, in *Essentials of Stem Cell Biology*, R. Lanza, et al., Editors. 2006, Elsevier Academic Press: Burlington, MA. p. 449-456.

13. Chamberlain, G., et al., *Concise Review: Mesenchymal stem cells: Their phenotype, differentiation capacity, immunological features, and potential for homing.* Stem Cells, 2007. **25**: p. 2739-2749.

14. Bell, E., *Tissue engineering: a perspective.* J Cell Biochem, 1991. **45**(3): p. 239-41.

15. Vacanti, J.P., et al., *Selective cell transplantation using bioabsorbable artificial polymers as matrices.* J Pediatr Surg, 1988. **23**(1 Pt 2): p. 3-9.

16. Martins-Green, M., *The dynamics of Cell-ECM interactions with implications for tissue engineering*, in *Principles of Tissue Engineering*, R. Lanza, Langer R, and Chick W, Editor. 1997, R. G. Landes Company. p. 23-46.

17. Agrawal, C.M. and R.B. Ray, *Biodegradable polymeric scaffolds for musculoskeletal tissue engineering.* Journal of Biomedical Materials Research, 2001. **55**(2): p. 141-150.

18. Zong, X., et al., *Electrospun fine-textured scaffolds for heart tissue constructs.* Biomaterials, 2005. **26**: p. 5330-5338.

19. Matthews, J.A., et al., *Electrospinning of collagen nanofibers.* Biomacromolecules, 2002. **3**(2): p. 232-238.

20. Sell, S.A., et al., *Electrospun polydioxanone-elastin blends: potential for bioresorbable vascular grafts.* Biomedical Materials, 2006. **1**(2): p. 72-80.

21. Wnek, G.E., et al., *Electrospinning of nanofiber fibrinogen structures.* Nano Letters, 2003. **3**(2): p. 213-216.

22. Altman, G.H., et al., *Silk-based biomaterials.* Biomaterials, 2003. **24**: p. 401-416.

23. Mooney, D.J. and R.S. Langer, *Engineering biomaterials for tissue engineering: The 10 - 100 micron size scale*, in *Tissue Engineering*, B. Palsson, et al., Editors. 2000, CRC Press: Boca Raton, FL.

24. Sell, S., et al., *Extracellular matrix regenerated: tissue engineering via electrospun biomimetic nanofibers.* Polymer International, 2007. **56**(11): p. 1349-1360.

25. Norman, J.J. and T.A. Desai, *Methods for fabrication of nanoscale topography for tissue engineering scaffolds.* Annals of Biomedical Engineering, 2006. **34**(1): p. 89-101.

26. Venugopal, J. and S. Ramakrishna, *Applications of polymer nanofibers in biomedicine and biotechnology.* Appl Biochem Biotechnol, 2005. **125**(3): p. 147-58.

27. Berry, C.C., et al., *The influence of microscale topography on fibroblast attachment and motility.* Biomaterials, 2004. **25**(26): p. 5781-8.

28. Telemeco, T.A., et al., *Regulation of cellular infiltration into tissue engineering scaffolds composed of submicron diameter fibrils produced by electrospinning.* Acta Biomater, 2005. **1**(4): p. 377-385.

29. Levesque, S.G., R.M. Lim, and M.S. Shoichet, *Macroporous interconnected dextran scaffolds of controlled porosity for tissue-engineering applications.* Biomaterials, 2005. **26**(35): p. 7436-46.

30. Karande, T.S., J.L. Ong, and C.M. Agrawal, *Diffusion in musculoskeletal tissue engineering scaffolds: design issues related to porosity, permeability, architecture, and nutrient mixing.* Ann Biomed Eng, 2004. **32**(12): p. 1728-43.

31. Li, S., et al., *Macroporous biphasic calcium phosphate scaffold with high permeability/porosity ratio.* Tissue Eng, 2003. **9**(3): p. 535-48.

32. Kannan, R.Y., et al., *The roles of tissue engineering and vascularisation in the development of micro-vascular networks: a review.* Biomaterials, 2005. **26**(14): p. 1857-75.

33. Griffith, C.K., et al., *Diffusion limits of an in vitro thick prevascularized tissue.* Tissue Eng, 2005. **11**(1-2): p. 257-66.

34. Sander, E.A. and E.A. Nauman, *Permeability of musculoskeletal tissues and scaffolding materials: experimental results and theoretical predictions.* Crit Rev Biomed Eng, 2003. **31**(1-2): p. 1-26.

35. Wong, W.H. and D.J. Mooney, *Synthesis and properties of biodegradable polymers used as synthetic matrices for tissue engineering*, in *Synthetic Biodegradable Polymer Scaffold*, A. Atala and D.J. Mooney, Editors. 1997, Birkhauser: Boston. p. 50-82.

36. Gunatillake, P.A. and R. Adhikari, *Biodegradable synthetic polymers for tissue engineering.* Eur Cell Mater, 2003. **5**: p. 1-16; discussion 16.

37. van Dijkhuizen-Radersma, R., et al., *Degradable polymers for tissue engineering*, in *Tissue Engineering*, C. van Blitterswijk, Editor. 2008, Elsevier Inc: San Diego. p. 193-221.

38. Boland, E.D., et al., *Utilizing acid pretreatment and electrospinning to improve biocompatibility of poly(glycolic acid) for tissue engineering.* Journal of Biomedical Materials Research Part B: Applied Biomaterials, 2004. **71B**: p. 144-152.

39. Freed, L.E., et al., *Biodegradable polymer scaffolds for tissue engineering.* Biotechnology (N Y), 1994. **12**(7): p. 689-93.

40. Middleton, J.C. and A.J. Tipton, *Synthetic biodegradable polymers as orthopedic devices.* Biomaterials, 2000. **21**(23): p. 2335-46.

41. Mikos, A.G. and J.S. Temenoff (2000) *Formation of highly porous biodegradable scaffolds for tissue engineering*. Electronic Journal of Biotechnology **Volume**, 114-119

42. Boland, E.D., et al., *Tailoring tissue engineering scaffolds using electrostatic processing techniques: A study of poly(glycolic acid) electrospinning.* Journal of Macromolecular Science. Part A: Pure and Applied Chemistry, 2001. **A38**(12): p. 1231-1243.

43. Yang, F., et al., *Electrospinning of nano/micro scale poly(L-lactic acid) aligned fibers and their potential in neural tissue engineering.* Biomaterials, 2005. **26**: p. 2603-2610.

44. Ishaug-Riley, S.L., et al., *Human articular chondrocyte adhesion and proliferation on synthetic biodegradable polymer films.* Biomaterials, 1999. **20**: p. 2245-2256.

45. Zong, X., et al., *Structure and morphology changes during in vitro degradation of electrospun poly(glycolide-co-lactide) nanofiber membrane.* Biomacromolecules, 2003. **4**(2): p. 416-23.

46. Kim, K., et al., *Control of degradation rate and hydrophilicity in electrospun non-woven poly(D,L-lactide) nanofiber scaffolds for biomedical applications.* Biomaterials, 2003. **24**(27): p. 4977-85.

47. Yoshimoto, H., et al., *A biodegradable nanofiber scaffold by electrospinning and its potential for bone tissue engineering.* Biomaterials, 2003. **24**(12): p. 2077-2082.

48. Boland, E.D., et al., *Electrospinning polydioxanone for biomedical applications.* Acta Biomaterialia, 2005. **1**: p. 115-123.

49. Fecek, C., et al., *Chondrogenic derivatives of embryonic stem cells seeded into 3D polycaprolactone scaffolds generated cartilage tissue in vivo.* Tissue Engineering Part A, 2008. **8**: p. 1403-1413.

50. Walpoth, B.H. and G.L. Bowlin, *The daunting quest for a small diameter vascular graft.* Expert Review of Medical Devices, 2005. **2**(6): p. 647-651.

51. Lee, K.Y. and D.J. Mooney, *Hydrogels for tissue engineering.* Chem Rev, 2001. **101**(7): p. 1869-79.

52. Ratner, B.D. and S.J. Bryant, *Biomaterials: where we have been and where we are going.* Annu Rev Biomed Eng, 2004. **6**: p. 41-75.

53. Zalipsky, S., *Functionalized poly(ethylene glycol) for preparation of biologically relevant conjugates.* Bioconjug Chem, 1995. **6**(2): p. 150-65.

54. Riley, S.L., et al., *Formulation of PEG-based hydrogels affects tissue-engineered cartilage construct charateristics.* Journal of Materials Science: Materials in Medicine, 2001. **12**: p. 983-990.

55. Gomes, M., et al., *Natural polymers in tissue engineering applications*, in *Tissue Engineering*, C. van Blitterswijk, Editor. 2008, Elsevier Inc: San Diego. p. 145-192.

56. Rosso, F., et al., *Smart materials as scaffolds for tissue engineering.* J Cell Physiol, 2005. **203**(3): p. 465-70.

57. Song, E., et al., *Collagen scaffolds derived from a marine source and their biocompatibility.* Biomaterials, 2006. **27**(15): p. 2951-2961.

58. Yang, C., et al., *The application of recombinant human collagen in tissue engineering.* BioDrugs, 2004. **18**(2): p. 103-119.

59. Boland, E.D., et al., *Electrospinning collagen and elastin: Preliminary vascular tissue engineering.* Frontiers In Bioscience, 2004. **9**: p. 1422-1432.

60. Gentleman, E., et al., *Mechanical characterization of collagen fibers and scaffolds for tissue engineering.* Biomaterials, 2003. **24**(21): p. 3805-3813.

61. Gentleman, E., et al., *Development of ligament-like structural organization and properties in cell-seeded collagen scaffolds in vitro.* Annals of Biomedical Engineering, 2006. **34**(5): p. 726-736.

62. Tang, S. and M. Spector, *Incorporation of hyaluronic acid into collagen scaffolds for the control of chondrocyte-mediated contraction and chondrogenesis.* Biomedical Materials, 2007. **2**(3): p. S135-S141.

63. Huss, F.R.M. and G. Kratz, *Mammary epithelial cell and adipocyte co-culture in a 3-D matrix: The first step towards tissue-engineered human breast tissue.* Cells Tissues Organs, 2001. **169**: p. 361-367.

64. Zhang, S., et al., *Gelatin nanofibrous membrane fabricated by electrospinning of aqueous gelatin solution for guided tissue regeneration.* Journal of Biomedical Materials Research, 2008. **Part A**: p. 1549-3296.

65. Zhang, Y., et al., *Electrospinning of gelatin fibers and gelatin/PCL composite fibrous scaffolds.* Journal of Biomedical Materials Research Part B: Applied Biomaterials, 2005. **72B**: p. 156-165.

66. Ghasemi-Mobarakeh, L., et al., *Electrospun poly(e-carpolactone)/gelatin nanofibrous scaffolds for nerve tissue engineering.* Biomaterials, 2008. **29**: p. 4532-4539.

67. Jiankang, H., et al., *Preparation of chitosan-gelatin hybrid scaffolds with well-organized microstructures for hepatic tissue engineering.* Acta Biomaterialia, 2008.

68. Tan, H., et al., *Gelatin/chitosan/hyaluronan scaffold integrated with PLGA microspheres for cartilage tissue engineering.* Acta Biomaterialia, 2008.

69. Debelle, L., et al., *The secondary structure and architecture of human elastin.* Eur J Biochem, 1998. **258**(2): p. 533-9.

70. Daamen, W.F., et al., *Tissue response of defined collagen-elastin scaffolds in young and adult rats with special attention to calcification.* Biomaterials, 2005. **26**: p. 81-92.

71. McClure, M.J., et al., *Cross-linking electrospun polydioxanone-soluble elastin blends: Material characterization.* Journal of Engineered Fibers and Fabrics, 2008. **3**(1): p. 1-10.

72. Rabaud, M., F. Lefebvre, and D. Ducassou, *In vitro association of type III collagen with elastin and with its solubilized peptides.* Biomaterials, 1991. **12**(3): p. 313-319.

73. Lim, D.W., et al., *In situ cross-linking of elastin-like polypeptide block copolymers for tissue repair.* Biomacromolecules, 2008. **9**(1): p. 222-230.

74. Daamen, W.F., et al., *A biomaterial composed of collagen and solubilized elastin enhances angiogenesis and elastic fiber formation without calcification.* Tissue Engineering, 2007. **In Press**.

75. Heydarkhan-Hagvall, S., et al., *Three-dimensional electrospun ECM-based hybrid scaffolds for cardiovascular tissue engineering.* Biomaterials, 2008. **29**(19): p. 2907-2914.

76. Simionescu, D.T., et al., *Biocompatibility and remodeling potential of pure arterial elastin and collagen scaffolds.* Biomaterials, 2006. **27**(5): p. 702-713.

77. McManus, M.C., et al., *Mechanical properties of electrospun fibrinogen structures.* Acta Biomater, 2006. **2**: p. 19-28.

78. McManus, M.C., et al., *Electrospun fibrinogen: Feasibility as a tissue engineering scaffold in a rat cell culture model.* J. Biomed. Mater. Res. A, 2007. **81**(2): p. 299-309.

79. Mosesson, M.W., K.R. Siebenlist, and D.A. Meh, *The structure and biological features of fibrinogen and fibrin.* Annals of the New York Academy of Sciences, 2001. **936**: p. 11-30.

80. Altman, G.H., et al., *Silk matrix for tissue engineered anterior cruciate ligaments.* Biomaterials, 2002. **23**: p. 4131-4141.

81. Wang, Y., et al., *Stem cell-based tissue engineering with silk biomaterials.* Biomaterials, 2006. **27**: p. 6064-6082.

82. Zhao, C. and T. Asakura, *Structure of silk studied with NMR.* Progress in Nuclear Magnetic Resonance Spectroscopy, 2001. **39**: p. 301-352.

83. Liu, H., et al., *The interaction between a combined knitted silk scaffold and microporous silk sponge with human mesenchymal stem cells for ligament tissue engineering.* Biomaterials, 2008. **29**: p. 662-674.

84. Seo, Y.-K., et al., *The biocompatibility of silk scaffold for tissue engineering ligaments.* Key Engineering Materials, 2007. **342-343**: p. 73-76.

85. Toh, S.L., et al., *Novel silk scaffolds for ligament tissue engineering applications.* Key Engineering Materials, 2006. **326-328**(1): p. 727-730.

86. Alessandrino, A., et al., *Electrospun silk fibroin mats for tissue engineering.* Engineering in Life Sciences, 2008. **8**(3): p. 219-225.

87. Jeong, S.I., et al., *Tissue-engineered vascular grafts composed of marine collagen and PLGA fibers using pulsatile perfusion bioreactors.* Biomaterials, 2007. **28**: p. 1115-1122.

88. Jin, H.J., et al., *Human bone marrow stromal cell responses on electrospun silk fibroin mats.* Biomaterials, 2004. **25**(6): p. 1039-47.

89. Jin, H.J., et al., *Electrospinning Bombyx mori silk with poly(ethylene oxide).* Biomacromolecules, 2002. **5**(3): p. 786-792.

90. Kawahara, Y., et al., *Structure for electro-spun silk fibroin nanofibers.* Journal of Applied Polymer Science, 2008. **107**: p. 3681-3684.

91. Min, B.-M., et al., *Electrospinning of silk fibroin nanofibers and its effect on the adhesion and spreading of normal human keratinocytes and fibroblasts in vitro.* Biomaterials, 2004. **25**: p. 1289-1297.

92. Sukigara, S., et al., *Regeneration of Bombyx mori silk by electrospinning - part 1: processing parameters and geometric properties.* Polymer, 2003. **44**: p. 5721-5727.

93. Wang, M., et al., *Mechanical properties of electrospun silk fibers.* Macromolecules, 2004. **37**: p. 6856-6864.

94. Zarkoob, S., et al., *Structure and morphology of electrospun silk nanofibers.* Polymer, 2004. **45**: p. 3973-3977.

95. Garcia-Fuentes, M., et al., *The effect of hyaluronic acid on silk fibroin conformation.* Biomaterials, 2008. **29**: p. 633-642.

96. Zuo, B., L. Liu, and Z. Wu, *Effect on Properties of Regenerated Silk Fibroin Fiber Coagulated with Aqueous Methanol/Ethanol.* Journal of Applied Polymer Science, 2007. **106**: p. 53-59.

97. Badylak, S., T. Gilbert, and J. Myers-Irvin, *The extracellular matrix as a biologic scaffold for tissue enigneering*, in *Tissue Engineering*, C. van Blitterswijk, et al., Editors. 2008, Academic Press: London. p. 121-143.

98. Badylak, S.F., *The extracellular matrix as a scaffold for tissue reconstruction.* Cell and Developmental Biology, 2002. **13**: p. 377-383.

99. Badylak, S.F., et al., *Small intestinal submucosa as a large diameter vascular graft in the dog.* Journal of Surgical Research, 1989. **47**(1): p. 74-80.

100. Cobb, M.A., et al., *Porcine small intestinal submucosa as a dural substitute.* Surg Neurol, 1999. **51**(1): p. 99-104.

101. Lantz, G.C., et al., *Small intestinal submucosa as a vascular graft: a review.* J Invest Surg, 1993. **6**(3): p. 297-310.

102. Suckow, M.A., et al., *Enhanced bone regeneration using porcine small intestinal submucosa.* J Invest Surg, 1999. **12**(5): p. 277-87.

103. Yoo, J.J., et al., *Bladder augmentation using allogenic bladder submucosa seeded with cells.* Urology, 1998. **51**: p. 221-225.

104. Sell, S.A., et al., *Electrospinning of collagen / biopolymers for regenerative medicine and cardiovascular tissue engineering.* Advanced Drug Delivery Reviews, 2009. **In Press**.

105. Rosamond, W., et al., *Heart disease and stroke statistics--2008 update: a report from the American Heart Association Statistics Committee and Stroke Statistics Subcommittee.* Circulation, 2008. **117**(4): p. e25-146.

106. Buijtenhuijs, P., et al., *Tissue engineering of blood vessels: characterization of smooth-muscle cells for culturing on collagen-and-elastin-based scaffolds.* Biotechnology and Applied Biochemistry, 2004. **39**: p. 141-149.

107. Greenwald, S.E. and C.L. Berry, *Improving vascular grafts: the importance of mechanical and haemodynamic properties.* The Journal Of Pathology, 2000. **190**(3): p. 292-299.

108. Kannan, R.Y., et al., *Current status of prosthetic bypass grafts: a review.* Journal Of Biomedical Materials Research. Part B, Applied Biomaterials, 2005. **74B**(1): p. 570-581.

109. Tiwari, A., et al., *Improving the patency of vascular bypass grafts: the role of suture materials and surgical techniques on reducing anastomotic compliance mismatch.* European Journal Of Vascular And Endovascular Surgery, 2003. **25**(4): p. 287-295.

110. Tiwari, A., et al., *New prostheses for use in bypass grafts with special emphasis on polyurethanes.* Cardiovascular Surgery, 2002. **10**(3): p. 191-197.

111. Sarkar, S., et al., *Achieveing the ideal properties for vascular bypass grafts using a tissue engineered approach: a review.* Med Bio Eng Comput, 2007. **45**: p. 327-336.

112. Vara, D.S., et al., *Cardiovascular tissue engineering: state of the art.* Pathologic Biologie, 2005. **53**: p. 599-612.

113. Thomas, A.C., G.R. Campbell, and J.H. Campbell, *Advances in vascular tissue engineering.* Cardiovascular Pathology, 2003. **12**: p. 271-276.

114. Wang, X., et al., *Development of small-diameter vascular grafts.* World Journal of Surgery, 2007. **31**: p. 682-689.

115. Xue, L. and H.P. Greisler, *Biomaterials in the development and future of vascular grafts.* Journal of Vascular Surgery, 2003. **37**(2): p. 472-480.

116. Mitchell, S.L. and L.E. Niklason, *Requirements for growing tissue-engineered vascular grafts.* Cardiovascular Pathology, 2003. **12**: p. 59-64.

117. Zarge, J.I., P. Huang, and H.P. Greisler, *Blood Vessels*, in *Principles of Tissue Engineering*, R. Lanza, R. Langer, and W. Chick, Editors. 1997, R.G. Landes Company: Austin, Texas. p. 349-364.

118. Niklason, L.E., *Replacement Arteries Made to Order.* Science, 1999. **286**(5444): p. 1493.

119. Rhodin, J.A.G., *Architecture of the vessel wall*, in *Handbook of Physiology*, S. Geiger, Editor. 1980, American Physiological Society: Bethesda, MD. p. 1-31.

120. Buttafoco, L., et al., *Electrospinning of collagen and elastin for tissue engineering applications.* Biomaterials, 2006. **27**(5): p. 724-734.

121. Berglund, J.D., R.M. Nerem, and A. Sambanis, *Incorporation of intact elastin scaffolds in tissue-engineered collagen-based vascular grafts.* Tissue Eng, 2004. **10**: p. 1526-1535.

122. Huang, L., et al., *Generation of synthetic elastin-mimetic small diameter fibers and fiber networks.* Macromolecules, 2000. **33**(8): p. 2989-2997.

123. Strandness, D.E. and D.S. Sumner, *Hemodynamics for Surgeons*. 1975, New York: Grune & Stratton, Inc. 698.

124. Wesolowski, S.A., et al., *The compound prosthetic vascular graft: A pathologic survey.* Surgery, 1963. **53**(1): p. 19-44.

125. Wesolowski, S.A., et al., *Arterial prosthetic materials.* Annals of The New York Academy Of Sciences, 1968. **146**(1): p. 325-344.

126. Bowald, S., C. Busch, and I. Eriksson, *Arterial regeneration following polyglactin 910 suture mesh grafting.* Surgery, 1979. **86**(5): p. 722-729.

127. Bowald, S., C. Busch, and I. Eriksson, *Absorbable material in vascular prostheses: A new device.* Acta Chir Scand, 1980. **146**: p. 391-395.

128. Greisler, H.P., *Arterial regeneration over absorbable prostheses.* Archives of Surgery, 1982. **117**: p. 1425-1431.

129. Greisler, H.P., et al., *Derivation of neointima in vascular grafts.* Circulation, 1988. **78**(3, Part 2): p. I6-12.

130. Greisler, H.P., et al., *Arterial regeneration over polydioxanone prostheses in the rabbit.* Archives Of Surgery, 1987. **122**(6): p. 715-721.

131. L'Heureux, N., et al., *A completely biological tissue-engineered human blood vessel.* The FASEB Journal, 1998. **12**(1): p. 47-56.

132. Ramakrishna, S., et al., *Introduction to Electrospinning and Nanofibers*. 2005: World Scientific Publishing Company, Incorporated.

133. Smith, L.A. and P.X. Ma, *Nano-fibrous scaffolds for tissue engineering.* Colloids and Surfaces. B: Biointerfaces, 2004. **39**: p. 125-131.

134. Wen, X., D. Shi, and N. Zhang, *Applications of Nanotechnology in Tissue Engineering*, in *Handbook of nanostructured biomaterials and their applications in nanobiotechnology*, H.S. Nalwa, Editor. 2005, American Scientific Publishers: Stevenson Ranch, CA. p. 1-23.

135. Barnes, C.P., et al., *Feasibility of electrospinning the globular protiens hemoglobin and myoglobin.* Journal of Engineered Fibers and Fabrics, 2006. **1**(2): p. 16-29.

136. Beckman, M.J., K.J. Shields, and R.F. Diegelmann, *Collagen*. Encyclopedia of Biomaterials and Biomedical Engineering. 2004, New York: Marcel Dekker.

137. Barnes, C.P., et al., *Preliminary investigation of electrospun collagen and polydioxanone for vascular tissue engineering applications.* International Journal of Electrospun Nanofibers and Applications, 2007. **1**: p. 73-87.

138. Zeugolis, D.I., et al., *Electro-spinning of pure collagen nano-fibres - Just an expensive way to make gelatin?* Biomaterials, 2008. **29**(15): p. 2293.

139. Dong, B., et al., *Electrospinning of collagen nanofiber scaffolds from benign solvents.* Macromol Rapid Commun, 2009. **30**: p. Early View.

140. Barnes, C.P., et al., *Cross-linking electrospun type II collagen tissue engineering scaffolds with carbodiimide in ethanol.* Tissue Engineering, 2007. **13**(7): p. 1593-1605.

141. He, W., et al., *Fabrication and endothelialization of collagen-blended biodegradable polymer nanofibers: potential vascular graft for blood vessel tissue engineering.* Tissue Eng, 2005. **11**(9-10): p. 1574-88.

142. Stitzel, J.D., et al., *Arterial smooth muscle cell proliferation on a novel biomimicking, biodegradable vascular graft scaffold.* J Biomater Appl, 2001. **16**(1): p. 22-33.

143. Kidoaki, S., I.K. Kwon, and T. Matsuda, *Mesoscopic spatial designs of nano- and microfiber meshes for tissue-engineering matrix and scaffold based on newly devised multilayering and mixing electrospinning techniques.* Biomaterials, 2005. **26**(1): p. 37-46.

144. Lee, S.J., et al., *Development of a composite vascular scaffolding system that withstands physiological vascular conditions.* Biomaterials, 2008. **29**(19): p. 2891-8.

145. Tillman, B.W., et al., *The in vivo stability of electrospun polycaprolactone-collagen scaffolds in vascular reconstruction.* Biomaterials, 2009. **30**(4): p. 583-8.

146. Venugopal, J., Y.Z. Zhang, and S. Ramakrishna, *Fabrication of modified and functionalized polycaprolactone nanofibre scaffolds for vascular tissue engineering.* Nanotechnology, 2005. **16**: p. 2138-2142.

147. Rodgers, U.R. and A.S. Weiss, *Cellular interactions with elastin.* Pathol Biol (Paris), 2005. **53**(7): p. 390-8.

148. Debelle, L. and A.M. Tamburro, *Elastin: molecular description and function.* Int J Biochem Cell Biol, 1999. **31**(2): p. 261-72.

149. Vrhovski, B. and A.S. Weiss, *Biochemistry of tropoelastin.* Eur J Biochem, 1998. **258**(1): p. 1-18.

150. Partridge, S.M. and H.F. Davis, *The chemistry of connective tissues. 3. composition of the soluble proteins derived from elastin.* Biochem. J., 1955. **61**: p. 21-30.

151. Duca, L., et al., *Elastin as a matrikine.* Crit Rev Oncol Hematol, 2004. **49**(3): p. 235-44.

152. Daamen, W.F., et al., *Elastin as a biomaterial for tissue engineering.* Biomaterials, 2007. **28**(30): p. 4378-98.

153. Li, M., et al., *Electrospun protein fibers as matrices for tissue engineering.* Biomaterials, 2005. **26**(30): p. 5999-6008.

154. Smith, M.J., et al., *Suture-reinforced electrospun polydioxanone-elastin small-diameter tubes for use in vascular tissue engineering: a feasibility study.* Acta Biomater, 2008. **4**(1): p. 58-66.

155. Thomas, V., et al., *Functionally graded electrospun scaffolds with tunable mechanical properties for vascular tissue regeneration.* Biomed Mater, 2007. **2**(4): p. 224-32.

156. El-Kurdi, M.S., et al., *Transient elastic support for vein grafts using a constricting microfibrillar polymer wrap.* Biomaterials, 2008. **29**(22): p. 3213-20.

157. Smith, M.J., et al., *In vitro evaluations of innate and acquired immune responses to electrospun polydioxanone-elastin blends.* Biomaterials, 2009. **30**(2): p. 149-59.

158. Stitzel, J., et al., *Controlled fabrication of a biological vascular substitute.* Biomaterials, 2006. **27**(7): p. 1088-94.

159. Lee, S.J., et al., *In vitro evaluation of electrospun nanofiber scaffolds for vascular graft application.* J Biomed Mater Res A, 2007. **83**(4): p. 999-1008.

160. Isenberg, B.C., C. Williams, and R.T. Tranquillo, *Small-diameter artificial arteries engineered in vitro.* Circ Res., 2005. **98**: p. 25-35.

161. Li, J., et al., *Gelatin and gelatin-hyaluronic acid nanofibrous membranes produced by electrospinning of their aqueous solutions.* Biomacromolecules, 2006. **7**: p. 2243-2247.

162. Song, J.-H., H.-E. Kim, and H.-W. Kim, *Production of electrospun gelatin nanofiber by water-based co-solvent approach.* Journal of Materials Science: Materials in Medicine, 2008. **19**(1): p. 95-102.

163. Songchotikunpan, P., J. Tattiyakul, and P. Supaphol, *Extraction and electrospinning of gelatin from fish skin.* International Journal of Biological Macromolecules, 2008. **42**: p. 247-255.

164. Chong, E.J., et al., *Evaluation of electrospun PCL/gelatin nanofibrous scaffold for wound healing and layered dermal reconstitution.* Acta Biomaterialia, 2007. **3**: p. 321-330.

165. Kim, H.-W., H.-S. Yu, and H.-H. Lee, *Nanofibrous matrices of poly(lactic acid) and gelatin polymeric blends for the improvement of cellular responses.* Journal of Biomedical Materials Research, 2008. **87A**: p. 25-32.

166. Powell, H.M. and S.T. Boyce, *Fiber density of electrospun gelatin scaffolds regulates morphogenesis of dermal-epidermal skin substitutes.* Journal of Biomedical Materials Research, 2008. **84A**: p. 1078-1086.

167. Bordenave, L., et al., *Experimental evaluation of a gelatin-coated polyester graft used as an arterial substitute.* Biomaterials, 1989. **10**(4): p. 235-242.

168. Ginalska, G., D. Kowalczuk, and M. Osinska, *A chemical method of gentamicin bonding to gelatine-sealed prosthetic vascular grafts.* International Journal of Pharmaceutics, 2005. **288**(1): p. 131-140.

169. Niu, S., et al., *Small diameter vascular prostheses with incorporated bioabsorbable matrices. A preliminary study.* American Society for Artificial Internal Organs, 1993. **39**(3): p. M750-753.

170. Zdrahala, R., *Small caliber vascular grafts. Part 1: state of the art.* Journal of Biomaterials Applications, 1996. **10**(4): p. 309-329.

171. Li, M., et al., *Electrospinning polyaniline-contained gelatin nanofibers for tissue engineering applications.* Biomaterials, 2006. **27**: p. 2705-2715.

172. Li, M., et al., *Co-electrospun poly(lactide-co-glycolide), gelatin, and elastin blends for tissue engineering scaffolds.* J Biomed Mater Res A, 2006. **79**(4): p. 963-73.

173. Clark, R.A.F., *Fibrin is a many splendored thing.* The Journal of Investigative Dermatology, 2003. **121**(5): p. xxi-xxii.

174. Fuss, C., J.C. Palmaz, and E.A. Sprague, *Fibrinogen: Structure, function, and surface interactions.* Journal of Vascular and Interventional Radiology, 2001. **12**(6): p. 677-682.

175. Hanson, S.R., *Blood Coagulation and Blood-Materials Interactions*, in *Biomaterials Science: An Introduction to Materials in Medicine*, B.D. Ratner, et al., Editors. 2004, Elsevier Academic Press: San Diego, CA. p. 332-338.

176. Drew, A.F., et al., *Wound-healing defects in mice lacking fibrinogen.* Blood, 2001. **97**(12): p. 3691-3698.

177. Rybarczyk, B.J., S.O. Lawrence, and P.J. Simpson-Haidaris, *Matrix-fibrinogen enhances wound closure by increasing both cell proliferation and migration.* Blood, 2003. **102**(12): p. 4035-4043.

178. Sahni, A. and C.W. Francis, *Vascular endothelial growth factor binds to fibrinogen and fibrin and stimulates endothelial cell proliferation.* Blood, 2000. **96**(12): p. 3772-3778.

179. McManus, M., et al., *Electrospun nanofibre fibrinogen for urinary tract tissue reconstruction.* Biomedical Materials, 2007. **2**(4): p. 257-262.

180. McManus, M.C., et al., *Electrospun fibrinogen-polydioxanone composite matrix: Potential for in situ urologic tissue engineering.* Journal of Engineered Fibers and Fabrics, 2008. **3**(2): p. 12-21.

181. Sell, S.A., et al., *Cross-linking methods of electrospun fibrinogen scaffolds for tissue engineering applications.* Biomedical Materials, 2008. **3**: p. Epub.

182. Zhang, X., C.B. Baughman, and D.L. Kaplan, *In vitro evaluation of silk fibroin scaffolds for vascular cell growth.* Biomaterials, 2008. **29**: p. 2217-2227.

183. Soffer, L., et al., *Silk-based electrospun tubular scaffolds for tissue-engineered vascular grafts.* J. Biomater. Sci. Polymer Edn., 2008. **19**(5): p. 653-664.

184. Lannutti, J., Reneker D, Ma, T, Tomasko D, and Farson D, *Electrospinning for tissue engineering scaffolds.* Mater. Sci. Eng. C Biomimetic Supramol. Syst., 2006. **In Press**.

185. Liao, S., et al., *Biomimetic electrospun nanofibers for tissue regeneration.* Biomed Mater, 2006. **1**: p. R45-R53.

186. Venugopal, J., Ramakrishna S, *Applications of Polymer Nanofibers in Biomedicine and Biotechnology.* Applied Biochemistry and Biotechnology, 2005. **125**: p. 147-157.

187. Sanders, J.E., et al., *Fibro-porous meshes made from polyurethane micro-fibers: effects of surface charge on tissue response.* Biomaterials, 2005. **26**: p. 813-818.

188. Burd, A., *Burn Dressing*, in *Encyclopedia of Biomaterials and Biomedical Engineering*. 2004.

189. Pareanteau, N.L., J. Harden-Young, and R.N. Ross, *Skin*, in *Principles of Tissue Engineering*, R. Lanza, Langer R, Vacanti J, Editor. 2000, Academic Press: San Diego. p. 879-890.

190. Simpson, D.G., *Dermal templates and the wound-healing paradigm: the promise of tissue regeneration.* Expert Review Of Medical Devices, 2006. **3**(4): p. 471-484.

191. van De Graaf, K., *Human Anatomy*. 6 ed. 2002: McGraw Hill. 108.

192. Diegelmann, R.F. and M.C. Evans, *Wound healing: An overview of acute, fibrotic and delayed healing.* Frontiers In Bioscience, 2004. **9**: p. 283-289.

193. Yannas, I.V. and J.F. Burke, *Design Of An Artificial Skin.1. Basic Design Principles.* Journal Of Biomedical Materials Research, 1980. **14**(1): p. 65-81.

194. Ramos-e-Silva, M. and M.C.R. De Castro, *New dressings, including tissue-engineered living skin.* Clinics In Dermatology, 2002. **20**(6): p. 715-723.

195. Pham, Q.P., U. Sharma, and A.G. Mikos, *Electrospinning of polymeric nanofibers for tissue engineering applications: A review.* Tissue Engineering, 2006. **12**(5): p. 1197-1211.

196. Sun, T., et al., *Self-organization of skin cells in three-dimensional electrospun polystyrene scaffolds.* Tissue Engineering, 2005. **11**(7-8): p. 1023-1033.

197. Venugopal, J.R., Y.Z. Zhang, and S. Ramakrishna, *In vitro culture of human dermal fibroblasts on electrospun polycaprolactone collagen nanofibrous membrane.* Artificial Organs, 2006. **30**(6): p. 440-446.

198. Kenawy, E., et al., *Release of tetracycline hydrochloride from electrospun poly(ethylene-co-vinylacetate), poly(lactic acid), and a blend.* J Control Release, 2002. **81**: p. 57-64.

199. Fung, Y.C., *Bone and cartilage*, in *Biomechanics: Mechanical Properties of Living Tissues*. 1993, Springer-Verlag: New York. p. 500-544.

200. Mow, V.C., D.C. Fithian, and M.A. Kelly, *Fundamentals of articular cartilage and meniscus biomechanics*, in *Articular Cartilage and Knee Joint Function: Basic Science and Arthroscopy*, J.W. Ewing, Editor. 1990, Raven Press: New York. p. 1-18.

201. Temenoff, J.S. and A.G. Mikos, *Review: tissue engineering for regeneration of articular cartilage.* Biomaterials, 2000. **21**(5): p. 431-440.

202. Randolph, M.A., K. Anseth, and M.J. Yaremchuk, *Tissue engineering of cartilage.* Clinics in Plastic Surgery, 2003. **30**(4): p. 519-537.

203. Mow, V.C., W. Zhu, and A. Ratcliffe, *Structure and function of articular cartilage and meniscus*, in *Basic Orthopaedic Biomechanics*, V.C. Mow and W.C. Hayes, Editors. 1991, Raven Press: New York. p. 143-198.

204. Buckwalter, J.A., L.C. Rosenberg, and E.B. Hunziker, *Articular cartilage: Composition, structure, response to injury, and methods of facilitating repair*, in

Articular Cartilage and Knee Joint Function: Basic Science and Arthroscopy, J.W. Ewing, Editor. 1990, Raven Press: New York. p. 19-56.

205. Buckwalter, J.A. and H.J. Mankin, *Instructional Course Lectures, The American Academy of Orthopaedic Surgeons - Articular cartilage. Part II: Degeneration and osteoarthrosis, repair, regeneration, and transplantation.* Journal of Bone and Joint Surgery Am., 1997. **79**(4): p. 612-632.

206. Frenkel, S.R. and P.E. Di Cesare, *Scaffolds for articular cartilage repair.* Annals of Biomedical Engineering, 2004. **32**(1): p. 26-34.

207. Vunjak-Novakovic, G., *The fundamentals of tissue engineering: scaffolds and bioreactors*, in *Tissue Engineering of Cartilage and Bone*, G. Bock and J. Goode, Editors. 2003, Wiley: Chichester, West Sussex. p. 34-51.

208. Nesic, D., et al., *Cartilage tissue engineering for degenerative joint disease.* Advanced Drug Delivery Reviews, 2006. **58**(2): p. 300-322.

209. Cancedda, R., et al., *Tissue engineering and cell therapy of cartilage and bone.* Matrix Biology, 2003. **22**(1): p. 81-91.

210. Hunziker, E.B., *Articular cartilage repair: basic science and clinical progress. A review of the current status and prospects.* Osteoarthritis And Cartilage, 2002. **10**(6): p. 432-463.

211. Lindahl, A., M. Brittberg, and L. Peterson, *Cartilage repair with chondrocytes: clinical and cellular aspects*, in *Tissue Engineering of Cartilage and Bone*, G. Bock and J. Goode, Editors. 2003, Wiley: Chichester, West Sussex. p. 175-189.

212. Beris, A.E., et al., *Advances in articular cartilage repair.* Injury, Int. J. Care Injured, 2005. **36**(Suppl 4): p. S14-23.

213. Kuo, C.K., et al., *Cartilage tissue engineering: its potential and uses.* Current Opinion In Rheumatology, 2006. **18**(1): p. 64-73.

214. Capito, R.M. and M. Spector, *Scaffold-based articular cartilage repair.* IEEE Eng Med Biol Mag., 2003. **22**(5): p. 42-50.

215. Huckle, J., et al., *Differentiated chondrocytes for cartilage tissue engineering*, in *Tissue Engineering of Cartilage and Bone*, G. Bock and J. Goode, Editors. 2003, Wiley: Chichester, West Sussex. p. 103-117.

216. Almarza, A.J. and K.A. Athanasiou, *Design characteristics for the tissue engineering of cartilaginous tissues.* Annals of Biomedical Engineering, 2004. **32**(1): p. 2-17.

217. Lee, J.H., J. Kisiday, and A.J. Grodzinsky, *Tissue-engineered versus native cartilage: linkage between cellular mechano-transduction and biomechanical properties*, in *Tissue Engineering of Cartilage and Bone*, G. Bock and J. Goode, Editors. 2003, Wiley: Chichester, West Sussex. p. 52-69.

218. Freed, L.E. and G. Vunjak-Novakovic, *Tissue engineering of cartilage*, in *The Biomedical Engineering Handbook*, J.D. Bronzino, Editor. 2000, CRC Press LLC: Boca Raton.

219. Matthews, J.A., et al., *Electrospinning of collagen type II: A feasibility study.* Journal of Bioactive and Compatible Polymers, 2003. **18**: p. 125-134.

220. Shields, K.J., et al., *Mechanical properties and cellular proliferation of electrospun collagen type II.* Tissue Engineering, 2004. **10**(9-10): p. 1510-1517.

221. Bhattarai, N., et al., *Alginate-based nanofibrous scaffolds: Structural, mechanical, and biological properties.* Advanced Materials, 2006. **18**(11): p. 1463-1467.

222. Li, W.J., et al., *Fabrication and characterization of six electrospun poly(alpha-hydroxy ester)-based fibrous scaffolds for tissue engineering applications.* Acta Biomaterialia, 2006. **2**(4): p. 377-385.

223. Shin, H.J., et al., *Electrospun PLGA nanofiber scaffolds for articular cartilage reconstruction: mechanical stability, degradation and cellular responses under mechanical stimulation in vitro.* Journal of Biomaterials Science-Polymer Edition, 2006. **17**(1-2): p. 103-119.

224. Subramanian, A., et al., *Preparation and evaluation of the electrospun chitosan/PEO fibers for potential applications in cartilage tissue engineering.* Journal of Biomaterials Science-Polymer Edition, 2005. **16**(7): p. 861-873.

225. Hollinger, J.O. and J.C. Kleinschmidt, *The critical size defect as an experimental model to test bone repair materials.* J Craniofac Surg, 1990. **1**(1): p. 60-8.

226. Lindsey, W.H., et al., *A nasal critical-size defect: an experimental model for the evaluation of facial osseous repair techniques.* Arch Otolaryngol Head Neck Surg, 1998. **124**(8): p. 912-5.

227. Weiner, S. and H.D. Wagner, *The material bone: Structure-mechanical function relations.* Annual Review of Materials Science, 1998. **28**: p. 271-298.

228. Laurencin, C., Y. Khan, and S.F. El-Amin, *Bone graft substitutes.* Expert Rev Med Devices, 2006. **3**(1): p. 49-57.

229. Yiquan, W., et al., *Preparation of hydroxyapatite fibers by electrospinning technique.* J. Am. Ceram. Soc., 2004. **87**(10): p. 1988-1991.

230. Kim, H.W., Kim HE, *Nanofiber generation of hydroxyapatite and fluor-hydroxyapatite bioceramics.* J Biomed Mater Res B Appl Biomater., 2005. **77**(2): p. 323-8.

231. Kim, H.W., J.H. Song, and H.E. Kim, *Bioactive glass nanofiber-collagen nanocomposite as a novel bone regeneration matrix.* J Biomed Mater Res A, 2006. **79**(3): p. 698-705.

232. Zhang, H.B. and M.J. Edirisinghe, *Electrospinning zirconia fiber from a suspension.* J. Am. Ceram. Soc., 2006. **89**(6): p. 1870-1875.

233. Wutticharoenmongkol, P., et al., *Novel bone scaffolds of electrospun polycaprolactone fibers filled with nanoparticles.* J Nanosci Nanotechnol, 2006. **6**(2): p. 514-22.

234. Laurencin, C.T. and L.S. Nair, *Polyphosphazene nanofibers for biomedical applications: preliminary studies.* Nanoengineered nanofibrous materials, NATO-ASI Proceedings., 2004: p. 281-300.

235. Bhattacharyya, S., et al., *Development of biodegradable polyphosphazene-nanohydroxyapatite composite nanofibers via electrospinning.* MRS Symposium Proceedings, 2005. **845**: p. 91-96.

236. Walker-Simmons, M. and C.A. Ryan, *Proteinase Inhibitor Synthesis in Tomato Leaves: Induction by Chitosan Oligomers and Chemically Modified Chitosan and Chitin.* Plant Physiol., 1984. **76**(3): p. 787-90.

237. Okamoto, Y., et al., *Effects of chitin/chitosan and their oligomers/monomers on migrations of fibroblasts and vascular endothelium.* Biomaterials., 2002. **23**(9): p. 1975-9.

238. Duan, B., Dong C, Yuan X, Yao K, *Electrospinning of chitosan solutions in acetic acid with poly(ethylene oxide).* J Biomater Sci Polym Ed, 2004. **15**(6): p. 797-811.

239. Geng, X., O.H. Kwon, and J. Jang, *Electrospinning of chitosan dissolved in concentrated acetic acid solution.* Biomaterials, 2005. **26**(27): p. 5427-32.

240. Bhattarai, N., et al., *Electrospun chitosan-based nanofibers and their cellular compatibility.* Biomaterials, 2005. **26**(31): p. 6176-84.

241. Li, C., et al., *Electrospun silk-BMP-2 scaffolds for bone tissue engineering.* Biomaterials, 2006. **27**(16): p. 3115-24.

242. Kannan, R.Y., et al., *Current status of prosthetic bypass grafts: a review.* J Biomed Mater Res B Appl Biomater, 2005. **74**(1): p. 570-81.

243. Conte, M.S., *The ideal small arterial substitute: a search for the Holy Grail?* Faseb J, 1998. **12**(1): p. 43-5.

244. Vaz, C.M., et al., *Design of scaffolds for blood vessel tissue engineering using a multi-layering electrospinning technique.* Acta Biomater, 2005. **1**(5): p. 575-82.

245. Matsuda, T., et al., *Mechano-active scaffold design of small-diameter artificial graft made of electrospun segmented polyurethane fabrics.* J Biomed Mater Res A, 2005. **73**(1): p. 125-31.

246. Lee, Y.H., et al., *Electrospun dual-porosity structure and biodegradation morphology of Montmorillonite reinforced PLLA nanocomposite scaffolds.* Biomaterials, 2005. **26**(16): p. 3165-72.

247. He, W., et al., *Biodegradable polymer nanofiber mesh to maintain functions of endothelial cells.* Tissue Eng, 2006. **12**(9): p. 2457-66.

248. Williamson, M.R., R. Black, and C. Kielty, *PCL-PU composite vascular scaffold production for vascular tissue engineering: attachment, proliferation and bioactivity of human vascular endothelial cells.* Biomaterials, 2006. **27**(19): p. 3608-16.

249. Luong-Van, E., et al., *Controlled release of heparin from poly(epsilon-caprolactone) electrospun fibers.* Biomaterials, 2006. **27**(9): p. 2042-50.

250. Xu, C., et al., *In vitro study of human vascular endothelial cell function on materials with various surface roughness.* J Biomed Mater Res A, 2004. **71**(1): p. 154-61.

251. Lanza, R., et al., *Principles of Tissue Engineering*. 1997, Boston: R.G. Landes Company.

252. Han, D., Gouma PI, *Electrospun bioscaffolds that mimic the topology of extracellular matrix.* Nanomed. Nanotechnol. Biol. Med., 2006. **2**: p. 37-41.

253. Baker, S.C., et al., *Characterization of electrospun polystyrene scaffolds for three-dimensional in vitro biological studies.* Biomaterials, 2006. **27**: p. 3136-3146.

254. Schindler, M., et al., *A synthetic nanofibrillar matrix promotes in vivo-like organization and morphogenesis for cells in culture.* Biomaterials, 2005. **26**: p. 5624-5631.

255. Fazan, V.P., H.C. Salgado, and A.A. Barreira, *A descriptive and quantitative light and electron microscopy study of the aortic depressor nerve in normotensive rats.* Hypertension, 1997. **30**: p. 693-698.

256. Bellamkonda, R.V., *Peripheral nerve regeneration: An opinion on channels, scaffolds and anisotropy.* Biomaterials, 2006.

257. Ao, Q., et al., *Manufacture of multimicrotubule chitosan nerve conduits with novel molds and characterization in vitro.* J Biomed Mater Res A, 2006. **77**(1): p. 11-8.

258. Bini, T.B., et al., *Development of fibrous biodegradable polymer conduits for guided nerve regeneration.* J Mater Sci Mater Med, 2005. **16**(4): p. 367-75.

259. Hurtado, A., et al., *Poly (D,L-lactic acid) macroporous guidance scaffolds seeded with Schwann cells genetically modified to secrete a bi-functional neurotrophin implanted in the completely transected adult rat thoracic spinal cord.* Biomaterials, 2006. **27**(3): p. 430-42.

260. Katayama, Y., et al., *Coil-reinforced hydrogel tubes promote nerve regeneration equivalent to that of nerve autografts.* Biomaterials, 2006. **27**(3): p. 505-18.

261. Zhang, M. and I.V. Yannas, *Peripheral nerve regeneration.* Adv Biochem Eng Biotechnol, 2005. **94**: p. 67-89.

262. Fine, E.G., R.F. Valentini, and P. Aebischer, *Nerve Regeneration*, in *Principles of Tissue Engineering*, R.P. Lanza, R. Langer, and J. Vacanti, Editors. 2000, Academic Press: San Diego, CA. p. 785-798.

263. Bini, T.B., et al., *Poly(L-lactide-co-glycolide) biodegradable microfibers and electrospun nanofibers for nerve tissue engineering: an in vitro study.* J Mater Sci, 2006. **41**: p. 6453-6459.

264. Bini, T.B., et al., *Electrospun poly(L-lactide-co-glycolide) biodegradable polymer nanofibre tubes for peripheral nerve regeneration.* Nanotechnology, 2004. **15**: p. 1459-1464.

265. Schnell, E., et al., *Guidance of glial cell migration and axonal growth on electrospun nanofibers of poly-e-caprolactone and a collagen/poly-e-caprolactone blend.* Biomaterials, 2007. **28**: p. 3012-3025.

266. Chew, S.Y., et al., *Sustained release of proteins from electrospun biodegradable fibers.* Biomacromolecules, 2005. **6**(4): p. 2017-2024.

267. Cooper, J.A., et al., *Fiber-based tissue-engineered scaffold for ligament replacement: design considerations and in vitro evaluation.* Biomaterials, 2005. **26**: p. 1523-1532.

268. Ge, Z., et al., *Biomaterials and scaffolds for ligament tissue engineering.* J Biomed Mater Res A, 2006. **77A**: p. 639-652.

269. Lu, H., et al., *Anterior cruciate ligament regeneration using braided biodegradable scaffolds: in vitro optimization studies.* Biomaterials, 2005. **26**: p. 4805-4816.

270. Petrigliano, F.A., D.R. McAllister, and B.M. Wu, *Tissue engineering for anterior cruciate ligament reconstruction: A review of current strategies.* Arthroscopy, 2006. **22**(4): p. 441-451.

271. Woo, S.L.Y., et al., *Biomechanics of knee ligaments: injury, healing, and repair.* J Biomech, 2004. **39**: p. 1-20.

272. Doroski, D., Brink KS, and Temenoff JS, *Techniques for biological characterization of tissue-engineered tendon and ligament.* Biomaterials, 2007. **28**: p. 187-202.

273. Laurencin, C.T. and J.W. Freeman, *Ligament tissue engineering: An evolutionary materials science approach.* Biomaterials, 2005. **26**: p. 7530-7536.

274. Bashur, C.A., L.A. Dahlgren, and A.S. Goldstein, *Effect of fiber diameter and orientation on fibroblast morphology and proliferation on electrospun poly(D,L-lactic-co-glycolic acid) meshes.* Biomaterials, 2006. **27**: p. 5681-5688.

275. Lee, C.H., et al., *Nanofiber alignment and direction of mechanical strain affect the ECM production of human ACL fibroblast.* Biomaterials, 2005. **26**: p. 1261-1270.

276. Sahoo, S., et al., *Characterization of a novel polymeric scaffold for potential application in tendon/ligament tissue engineering.* Tissue Eng, 2006. **12**(1): p. 91-99.

277. Conte, M.S., *The ideal small arterial substitute: a search for the Holy Grail?* The FASEB Journal, 1998. **12**(1): p. 43-45.

278. Bowlin, G.L., et al., *Electrospinning of polymer scaffolds for tissue engineering*, in *Tissue engineering and biodegradable equivalents: scientific and clinical*

applications, K. Lewandrowski, Editor. 2002, Marcel Dekker: New York. p. 165-178.

279. Tai, N.R., et al., *Compliance properties of conduits used in vascular reconstruction.* The British Journal Of Surgery, 2000. **87**(11): p. 1516-1524.

280. ANSI, *ANSI 2000 Cardiovascular implants - Vascular graft prostheses*, A.f.t.A.o.M. Instrumentation, Editor. 1994.

281. Humphrey, J.D., *Cardiovascular Solid Mechanics: Cells, Tissues, and Organs*. 2002, New York: Springer.

282. Goldman, L. and D. Ausiello, *Cecil Textbook of Medicine*. 22nd ed. 2004, Philadelphia: W.B. Saunders Company.

283. Fung, Y.C., *Biodynamics: circulation*. blood flow in arteries. 1984, New York: Springer-Verlag.

284. Hiroshi, Y., *Strength of biological materials*. 1970, New York: Robert E. Krieger Publishing Company.

285. Catanese, J., 3rd, et al., *Mechanical properties of medical grade expanded polytetrafluoroethylene: the effects of internodal distance, density, and displacement rate.* J Biomed Mater Res, 1999. **48**(2): p. 187-92.

286. Donovan, D.L., et al., *Material and structural characterization of human saphenous vein.* J Vasc Surg, 1990. **12**(5): p. 531-7.

287. Weinberg, S.L., G.B. Cipolletti, and R.J. Turner, *Human umbilical vein grafts: Physical evaluation criteria*, in *Biological and Synthetic Vascular Prostheses*, J.C. Stanley, Editor. 1982, Grune and Stratton: New York.

288. Li, J.K.-J., *The Arterial Circulation: Physical Principles and Clinical Applications*. 2000, Totowa, New Jersey: Humana Press.

289. Mooney, D.L., R, *Engineering biomaterials for tissue engineering: the 10 - 100 micron size scale*, in *The Biomedical Engineering Handbook*, J. Bronzino, Editor. 1995, CRC Press: Boca Raton. p. 1609-1618.

290. Greisler, H.P., et al., *Biointeractive polymers and tissue engineered blood vessels.* Biomaterials, 1996. **17**(3): p. 329-336.

291. Hutmacher, D.W., *Scaffold design and fabrication technologies for engineering tissues--state of the art and future perspectives.* Journal Of Biomaterials Science. Polymer Edition, 2001. **12**(1): p. 107-124.

292. Weigel, P.H., G.M. Fuller, and R.D. LeBoeuf, *A model for the role of hyaluronic acid and fibrin in the early events during the inflammatory response and wound healing.* Journal Of Theoretical Biology, 1986. **119**(2): p. 219-234.

293. Erban, J.K., *P-selectin and wound healing.* Behring Institute Mitteilungen, 1993(92): p. 248-257.

294. Clark, R.A., et al., *Fibronectin and fibrin provide a provisional matrix for epidermal cell migration during wound reepithelialization.* The Journal Of Investigative Dermatology, 1982. **79**(5): p. 264-269.

295. Passaretti, D., et al., *Cultured chondrocytes produce injectable tissue-engineered cartilage in hydrogel polymer.* Tissue Engineering, 2001. **7**(6): p. 805-815.

296. Peretti, G.M., et al., *A biomechanical analysis of an engineered cell-scaffold implant for cartilage repair.* Annals Of Plastic Surgery, 2001. **46**(5): p. 533-537.

297. Ye, Q., et al., *Fibrin gel as a three dimensional matrix in cardiovascular tissue engineering.* European Journal Of Cardio-Thoracic Surgery: Official Journal Of The European Association For Cardio-Thoracic Surgery, 2000. **17**(5): p. 587-591.

298. Mol, A., et al., *Fibrin as a cell carrier in cardiovascular tissue engineering applications.* Biomaterials, 2005. **26**(16): p. 3113-3121.

299. Karp, J.M., et al., *Fibrin-filled scaffolds for bone-tissue engineering: An in vivo study.* J Biomed Mater Res A, 2004. **71**(1): p. 162-171.

300. Cummings, C.L., et al., *Properties of engineered vascular constructs made from collagen, fibrin, and collagen-fibrin mixtures.* Biomaterials, 2004. **25**(17): p. 3699-3706.

301. Ross, J.J. and R.T. Tranquillo, *ECM gene expression correlates with in vitro tissue growth and development in fibrin gel remodeled by neonatal smooth muscle cells.* Matrix Biology: Journal Of The International Society For Matrix Biology, 2003. **22**(6): p. 477-490.

302. Shreiber, D.I., P.A. Enever, and R.T. Tranquillo, *Effects of pdgf-bb on rat dermal fibroblast behavior in mechanically stressed and unstressed collagen and fibrin gels.* Experimental Cell Research, 2001. **266**(1): p. 155-166.

303. Underwood, S., et al., *The physical properties of a fibrillar fibronectin-fibrinogen material with potential use in tissue engineering.* Bioprocess Engineering, 1999. **20**(3): p. 239-248.

304. Ahmed, Z., S. Underwood, and R.A. Brown, *Low concentrations of fibrinogen increase cell migration speed on fibronectin/fibrinogen composite cables.* Cell Motility And The Cytoskeleton, 2000. **46**(1): p. 6-16.

305. Underwood, S., et al., *Wet extrusion of fibronectin-fibrinogen cables for application in tissue engineering.* Biotechnology and Bioengineering, 2001. **73**(4): p. 295-305.

306. Jockenhoevel, S., et al., *Fibrin gel -- advantages of a new scaffold in cardiovascular tissue engineering.* European Journal Of Cardio-Thoracic Surgery: Official Journal Of The European Association For Cardio-Thoracic Surgery, 2001. **19**(4): p. 424-430.

307. Atala, A., *Tissue engineering for the replacement of organ function in the genitourinary system.* Am J Transplant, 2004. **4 Suppl 6**: p. 58-73.

308. De Filippo, R.E., J.J. Yoo, and A. Atala, *Urethral replacement using cell seeded tubularized collagen matrices.* J Urol, 2002. **168**(4 Pt 2): p. 1789-92; discussion 1792-3.

309. Pariente, J.L., B.S. Kim, and A. Atala, *In vitro biocompatibility evaluation of naturally derived and synthetic biomaterials using normal human bladder smooth muscle cells.* J Urol, 2002. **167**(4): p. 1867-71.

310. Atala, A., et al., *Tissue-engineered autologous bladders for patients needing cystoplasty.* The Lancet, 2006. **367**(9518): p. 1241-1246.

311. Sell, S., et al., *Scaffold permeability as a means to determine fiber diameter and pore size of electrospun fibrinogen.* J Biomed Mater Res A, 2007. **85A**(1): p. 115-126.

312. Achyuthan, K.E., A. Mary, and C.S. Greenberg, *The binding sites on fibrin(ogen) for guinea pig liver transglutaminase are similar to those of blood coagulation factor XIII.* The Journal of Biological Chemistry, 1988. **263**(28): p. 14296-14301.

313. Dickneite, G., et al., *The importance of factor XIII as a component of fibrin sealants.* Journal of Surgical Research, 2002. **107**: p. 186-195.

314. Mosesson, M.W. and K.R. Siebenlist, *The covalent structure of factor XIIIa crosslinked fibrinogen fibrils.* Journal of Structural Biology, 1995. **115**: p. 88-101.

315. Olde Damink, L.H.H., et al., *Cross-linking of dermal sheep collagen using a water-soluble carbodiimide.* Biomaterials, 1996. **17**: p. 765-773.

316. Sung, H.-W., et al., *Crosslinking of biological tissues using genipin and/or carbodiimide.* Journal of Biomedical Materials Research Part A, 2003. **64**: p. 427-438.

317. Jayakrishnan, A. and S.R. Jameela, *Glutaraldehyde as a fixative in bioprostheses and drug delivery matrices.* Biomaterials, 1996. **17**: p. 471.

318. Chiono, V., et al., *Genipin-crosslinked chitosan/gelatin blends for biomedical applications.* Journal of Materials Science, 2008. **19**(2): p. 889-898.

319. Huang, L.L.H., et al., *Biocompatibility study of a biological tissue fixed with a naturally occurring crosslinking reagent.* Journal of Biomedical Materials Research, 1998. **42**: p. 568-576.

320. Sung, H.-W., et al., *Feasibility study of a natural crosslinking reagent for biological tissue fixation.* J Biomed Mater Res, 1998. **42**: p. 560-567.

321. Ferretti, M., et al., *Controlled in vivo degradation of genipin crosslinked polyethylene glycol hydrogels within osteochondral defects.* Tissue Engineering, 2006. **12**(9): p. 2657-2663.

322. Chen, Y.-S., et al., *An in vivo evaluation of a biodegradable genipin-cross-linked gelatin peripheral nerve guide conduit material.* Biomaterials, 2005. **26**: p. 3911-3918.

323. Tsai, C.-C., et al., *In vitro evaluation of the genotoxicity of a naturally occurring crosslinking agent (genipin) for biologic tissue fixation.* Journal of Biomedical Materials Research, 2000. **52**: p. 58-65.

324. Zhang, G., et al., *A PEGylated fibrin patch for mesenchymal stem cell delivery.* Tissue Engineering, 2006. **12**(1): p. 9-19.

325. Jenner, J.M.G.T., et al., *Effect of transforming growth factor-beta and growth differentiation factor-5 on proliferation and matrix production by human bone marrow stromal cells cultured on braided poly lactic-co-glycolic acid scaffolds for ligament tissue engineering.* Tissue Engineering, 2007. **13**(7): p. 1573-1582.

326. Dunn, M.G., et al., *Preliminary development of a collagen-PLA composite for ACL reconstruction.* Journal of Applied Polymer Science, 1997. **63**: p. 1423-1428.

327. Kimura, Y., et al., *Regeneration of anterior cruciate ligament by biodegradable scaffold combined with local controlled release of basic fibroblast growth factor and collagen wrapping.* Tissue Engineering Part C, 2008. **14**(1): p. 47-57.

328. Bashur, C.A., S.A. Guelcher, and A.S. Goldstein. *Electrospun polymers for ligament tissue engineering*. in *Bioengineering Conference, Proceedings of the 32nd Annual Northeast*. 2006.

329. Sahoo, S., et al. *Towards an ideal polymer scaffold for tendon/ligament tissue engineering*. in *Third Intl Conf on Experimental Mechanics and Third Conf. of the Asian Committee on Experimental Mechanics*. 2005.

330. Liu, H., et al., *Modification of sericin-free silk fibers for ligament tissue engineering applications.* Journal of Biomedical Materials Research Part B, 2007. **82B**: p. 129-138.

331. Roh, J.D., et al., *Small-diameter biodegradable scaffolds for functional vascular tissue engineering in the mouse model.* Biomaterials, 2008. **29**(10): p. 1454-63.

332. Ryu, W., et al., *The construction of three-dimensional micro-fluidic scaffolds of biodegradable polymers by solvent vapor based bonding of micro-molded layers.* Biomaterials, 2007. **28**(6): p. 1174-84.

333. Yokota, T., et al., *In situ tissue regeneration using a novel tissue-engineered, small-caliber vascular graft without cell seeding.* J Thorac Cardiovasc Surg, 2008. **136**(4): p. 900-7.

334. Lim, S.H., et al., *Tissue-engineered blood vessels with endothelial nitric oxide synthase activity.* J Biomed Mater Res B Appl Biomater, 2008. **85**(2): p. 537-46.

335. Pullens, R.A., et al., *The influence of endothelial cells on the ECM composition of 3D engineered cardiovascular constructs.* J Tissue Eng Regen Med, 2009. **3**(1): p. 11-8.

336. Pektok, E., et al., *Degradation and healing characteristics of small-diameter poly(epsilon-caprolactone) vascular grafts in the rat systemic arterial circulation.* Circulation, 2008. **118**(24): p. 2563-70.

337. Venugopal, J., et al., *In vitro study of smooth muscle cells on polycaprolactone and collagen nanofibrous matrices.* Cell Biol Int, 2005. **29**(10): p. 861-7.

338. He, W., et al., *Fabrication of collagen-coated biodegradable polymer nanofiber mesh and its potential for endothelial cells growth.* Biomaterials, 2005. **26**(36): p. 7606-15.

339. Bohr, D.F., A.P. Somlyo, and H.V. Sparks, *The Cardiovascular System*, in *Handbook of Physiology*, S.R. Greiger, Editor. 1980, American Physiological Society: Bethesda. p. 1-31.

340. Fan, H., et al., *In vivo study of anterior cruciate ligament regeneration using mesenchymal stem cells and silk scaffold.* Biomaterials, 2008. **29**: p. 3324-3337.

341. Lovett, M.L., et al., *Gel spinning of silk tubes for tissue engineering.* Biomaterials, 2008. **29**(35): p. 4650-7.

342. Seo, Y.K., et al., *Increase in cell migration and angiogenesis in a composite silk scaffold for tissue-engineered ligaments.* J Orthop Res, 2008.

343. Ayres, C., et al., *Modulation of anisotropy in electrospun tissue-engineering scaffolds: Analysis of fiber alignment by the fast Fourier transform.* Biomaterials, 2006. **27**: p. 5524-5534.

344. Ayres, C.E., et al., *Incremental changes in anisotropy induce incremental changes in the material properties of electrospun scaffolds.* Acta Biomaterialia, 2007. **3**: p. 651-661.

345. Konig, G., et al., *Mechanical properties of completely autologous human tissue engineered blood vessels compared to human saphenous vein and mammary artery.* Biomaterials, 2009. **30**(8): p. 1542-50.

346. Thomas, V., et al., *Mechano-morphological studies of aligned nanofibrous scaffolds of polycaprolactone fabricated by electrospinning.* J Biomater Sci Polym Ed, 2006. **17**(9): p. 969-84.

347. Wang, H.B., et al., *Creation of highly aligned electrospun poly-L-lactic acid fibers for nerve regeneration applications.* J Neural Eng, 2009. **6**(1): p. 16001.

348. Yang, Y., et al., *Effect of electric field distribution uniformity on electrospinning.* Journal Of Applied Physics, 2008. **103**(10).

349. Doroski, D.M., K.S. Brink, and J.S. Temenoff, *Techniques for biological characterization of tissue-engineered tendon and ligament.* Biomaterials, 2007. **28**: p. 187-202.

350. Johnson, D., *The ACL Made Simple*. 2004, New York: Springer Verlag. 213.

351. O'Connor, J.J. and A. Zavatsky, *Anterior Cruciate Ligament Function in the Normal Knee*, in *The Anterior Cruciate Ligament: Current and Future Concepts*, D.W. Jackson, et al., Editors. 1993, Raven Press, Ltd.: New York. p. 39-52.

352. Amis, A.A., *Biomechanics of Bone, Tendon and Ligament*, in *Sciences Basic to Orthopaedics*, S.P.F. Hughes and I.D. McCarthy, Editors. 1998, W. B. Saunders Company, Ltd.: London. p. 222-239.

353. Arnoczky, S.P., et al., *Anatomy of the Anterior Cruciate Ligament*, in *The Anterior Cruciate Ligament: Current and Future Concepts*, D.W. Jackson, et al., Editors. 1993, raven Press, Ltd.: New York. p. 5-22.

354. Burks, R.T., *Gross Anatomy*, in *Knee Ligaments: Structure, Function, Injury, and Repair*, D.M. Daniel, W.H. Akeson, and J.J. O'Connor, Editors. 1990, Raven Press, Ltd.: New York. p. 59-76.

355. Amiel, D., E. Billings, Jr., and W.H. Akeson, *Ligament Structure, Chemistry, and Physiology*, in *Knee Ligaments: Structure, Function, Injury, and Repair*, D.M. Daniel, W.H. Akeson, and J.J. O'Connor, Editors. 1990, Raven Press, Ltd.: New York. p. 77-91.

356. Woo, S.L.-Y., K.J. Ohland, and P.J. McMahon, *Biology, healing, and repair of ligaments*, in *Biology and Biomechanics of the Traumatized Synovial Joint: The Knee as a Model*, G.A.M. Finerman and F.R. Noyes, Editors. 1992, American Academy of Orthopaedic Surgeons: Rosemont, IL. p. 241-273.

357. Chandrashekar, N., et al., *Sex-based differences in the tensile properties of the human anterior cruciate ligament.* Journal of Biomechanics, 2006. **39**: p. 2943-2950.

358. Lydon, C., et al., *Effect of elongation rate on the failure properties of the rabbit anterior cruciate ligament.* Clinical Biomechanics, 1995. **10**(8): p. 428-433.

359. Lee, M. and W. Hyman, *Modeling of failure mode in knee ligaments depending on the strain rate.* BMC Musculoskeletal Disorders, 2002. **3**(3): p. EPUB.

360. Murphy, P.G., C.B. Frank, and D.A. Hart, *The Cell Biology of Ligaments and Ligament Healing*, in *The Anterior Cruciate Ligament: Current and Future Concepts*, D.W. Jackson, et al., Editors. 1993, Raven Press, Ltd.: New York. p. 165-177.

361. Woo, S.L.-Y., et al., *The response of ligaments to injury: Healing of the collateral ligaments*, in *Knee Ligaments: Structure, Function, Injury, and Repair*, D.M. Daniel, W.H. Akeson, and J.J. O'Connor, Editors. 1990, Raven Press, Ltd.: New York. p. 351-364.

362. Amiel, D., S. Kuiper, and W.H. Akeson, *Cruciate Ligaments: Response to Injury*, in *Knee Ligaments: Structure, Function, Injury, and Repair*, D.M. Daniel, W.H. Akeson, and J.J. O'Connor, Editors. 1990, Raven Press, Ltd.: New York. p. 365-377.

363. Buma, P., et al., *Augmentation in anterior cruciate ligament reconstruction - a histological and biomechanical study on goats.* International Orthopaedics, 2004. **28**: p. 91-96.

364. Li, W.-J., et al., *Engineering controllable anistoropy in electrospun biodegradable nanofibrous scaffolds for musculoskeletal tissue engineering.* Journal of Biomechanics, 2007. **40**: p. 1686-1693.

365. Dalton, P.D., D. Klee, and M. Moller, *Electrospinning with dual collection rings.* Polymer, 2005. **46**: p. 611-614.

366. Stankus, J.J., et al., *Fabrication of cell microintegrated blood vessel constructs through electrohydrodynamic atomization.* Biomaterials, 2007. **28**: p. 2738-2746.

APPENDIX A: PRELIMINARY ELECTROSPINNING OF SF

MATERIALS AND METHODS

SF Extraction. SF was extracted from the cocoons of *Bombyx mori* silkworms (The Yarn Tree) through an established protocol [88]. Briefly, silk cocoons were cut into pieces and boiled in a 0.02 M Na_2CO_3 (Sigma Aldrich) solution for 30 minutes to remove the sericin gum, followed by thorough rinsing in DI water, and drying in a fume hood. The SF was then dissolved in a LiBr (Fisher Scientific) solution at 60°C for 4 hours. This solution was then dialyzed against DI water for 3 days using 3500 MWCO dialysis tubing (Fisher Scientific). The SF solution was then frozen and lyophilized to provide a pure SF powder for electrospinning.

Scaffold Fabrication. Initial electrospinning was performed using three different concentrations of SF in HFP (TCI America, Inc.): 70, 100, and 150 mg/ml. These three different concentrations constituted the spinnable range of the SF solution, and were used to provide insight into the fiber size and structural morphology of the electrospun scaffolds. Preliminary electrospinning of SF was done using a standard electrospinning setup with a rectangular mandrel (2.5 cm wide x 10.2 cm long x 0.3 cm thick) rotating at 400 RPM and translating at 6 cm/s over a distance of 12 cm to create randomly oriented

fibrous structures. SF solution was loaded into a Becton Dickinson syringe fitted with a blunt tip 18 gauge needle and dispensed at a rate of 4 ml/hr with a KD Scientific syringe pump. A charging voltage of +25 kv was applied to the needle tip, with an air-gap distance of 20 cm between the needle tip and the grounded mandrel.

Scaffold Characterization. Each of the electrospun scaffolds was characterized through SEM (Zeiss EV050). Average fiber diameters were calculated by taking 60 random fiber measurements from across the SEM image using ImageTool 3.0 software (Shareware provided by UTHSCSA).

Uniaxial Tensile Testing. Uniaxial tensile testing was performed on dog-bone shaped samples punched from the electrospun scaffolds (2.75 mm wide at their narrowest point with a gage length of 7.5 mm) and tested on a MTS Bionix 200 testing system with a 100 N load cell (MTS Systems Corp.) an extension rate of 10.0 mm/min. Samples (n=3) were tested both dry and after a 30 minute soak in ethanol followed by a 1 hour soak in DI water. The ethanol soak was performed to force β-sheet formation in the SF fibers [22].

RESULTS AND DISCUSSION

Scaffold Characterization. SEM revealed fibrous structures for all three concentrations of SF electrospun (figure A.1). SF electrospun at 70 mg/ml exhibited an average fiber diameter of 0.72 $\pm$ 0.3 microns, 100 mg/ml produced average fiber diameters of 1.64 $\pm$ 0.8 microns, and 150 mg/ml produced average fiber diameters of 3.68

± 1.5 microns (figure A.2). Interestingly, the fibers produced by the 150 mg/ml concentration SF solution appeared to be completely flat and ribbon-like as opposed to the round fibers produced by the 70 mg/ml SF concentration. The 100 mg/ml SF concentration resulted in a mixture of both large flat fibers and smaller round fibers. This transition to ribbon-like fibers is evident in the increasing standard deviations of figure A.2. As SF concentration increases, and ribbon-like fibers become more prevalent, the standard deviation of the fiber diameters also increase. This flattened fiber morphology, coupled with their large average diameter, makes the 150 mg/ml concentration SF scaffolds non-ideal for tissue engineering applications, as historically it has been shown that sub-micron scale diameter fibers produce less of an immune response than larger diameter fibers [187].

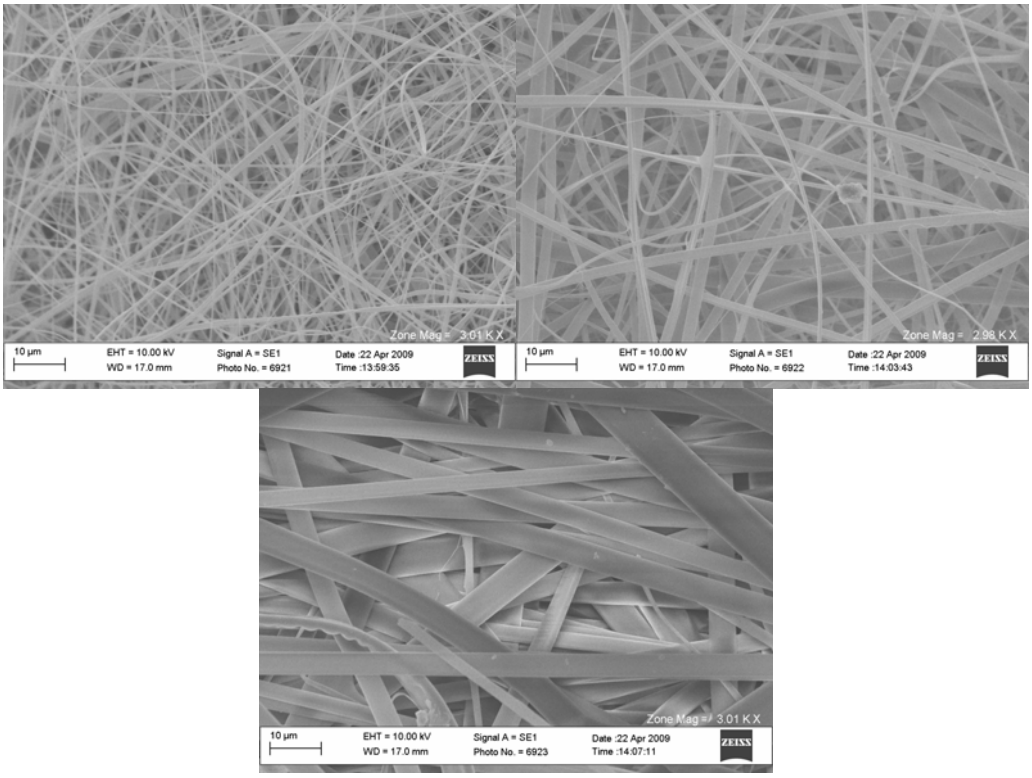

Figure A.1. Scanning electron micrographs of electrospun SF at 70 (top left), 100 (top right), and 150 mg/ml (bottom). All images were taken at 3000x.

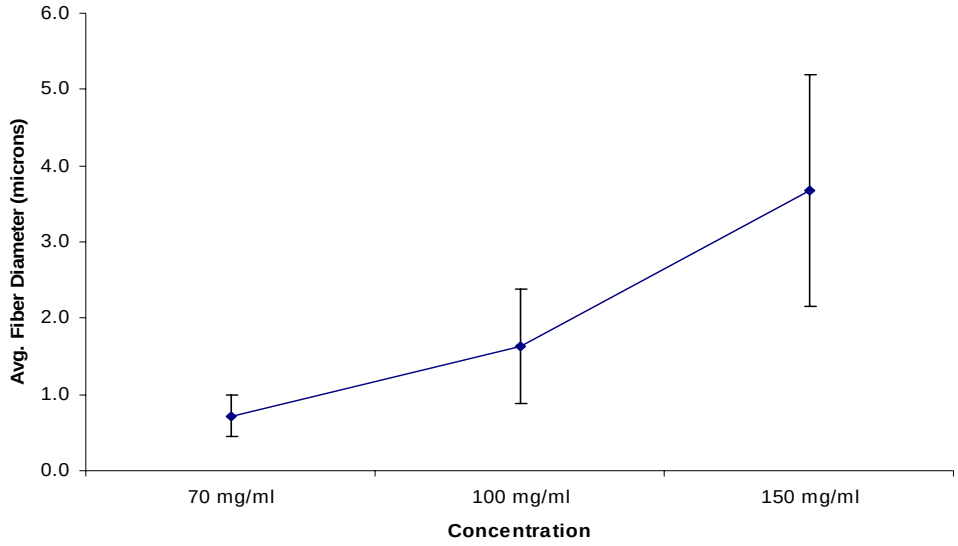

Figure A.2. Average fiber diameter of SF electrospun from three different concentrations.

Uniaxial Tensile Testing. The results of both dry and hydrated uniaxial tensile testing of preliminary SF scaffolds are shown in figure A.3. These results revealed significant differences between concentrations in the peak stress and modulus of the dry samples, yet no significant differences between concentrations in strain at break. Hydration resulted in significant changes in scaffold strength with hydrated moduli being nearly 20 times lower than dry moduli regardless of SF concentration. Surprisingly, there were few significant differences in the mechanical properties (70 mg/ml peak stress different than 150 mg/ml, and 150 mg/ml strain at break different from the other two concentrations) between concentrations of hydrated SF scaffolds. This would indicate that as the electrospun SF becomes hydrated, regardless of starting concentration, its mechanical properties stabilize at some base level.

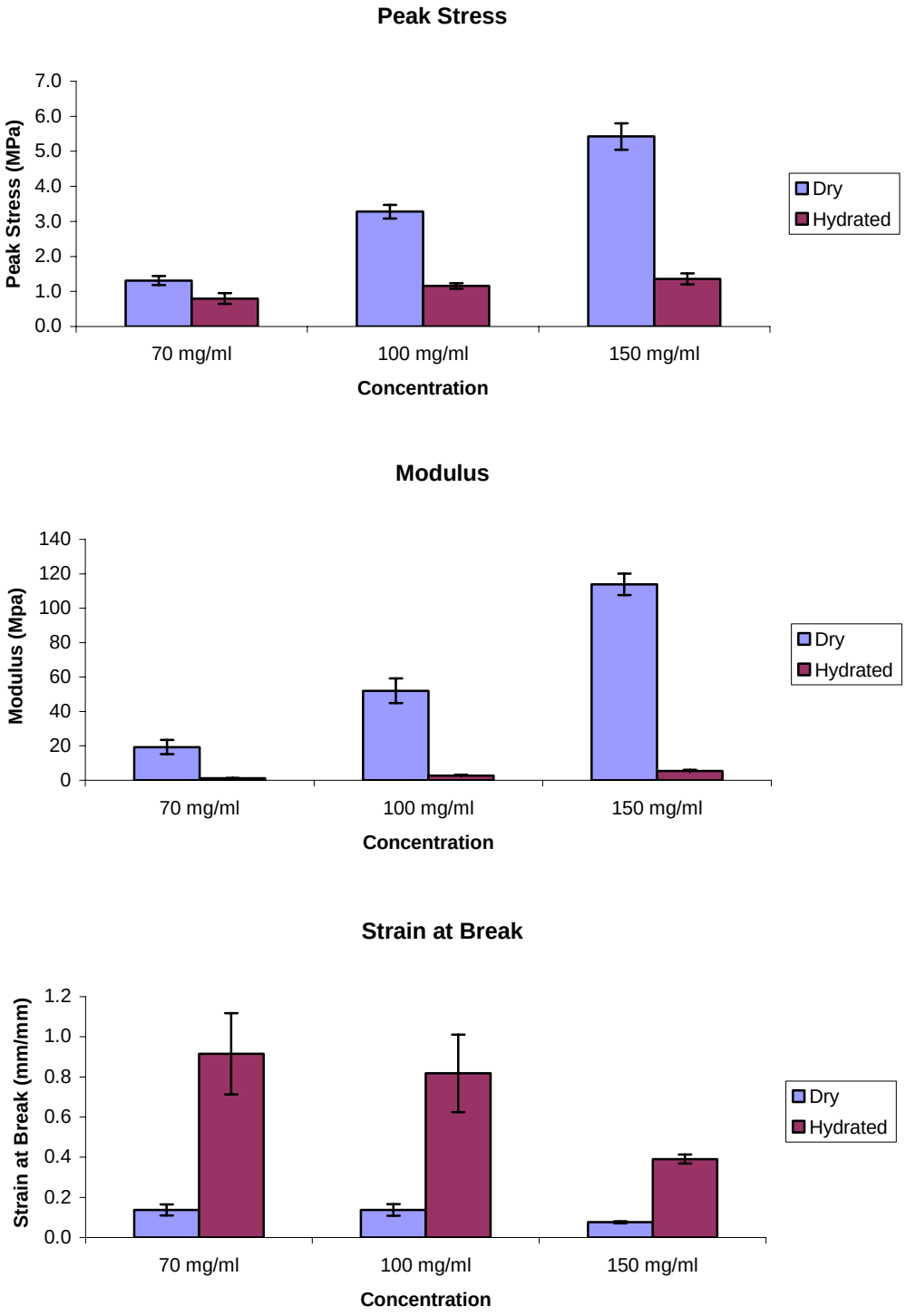

Figure A.3. Peak stress, modulus, and strain at break values achieved for uniaxial tensile testing of preliminary electrospun SF scaffolds.

VITA

Scott Allen Sell was born in LaCrosse, Wisconsin on April 8, 1981. He was raised in Chesterfield, Virginia and graduated from Manchester High School in 1999. He attended Virginia Commonwealth University from August 1999 to May 2003 and was awarded a Bachelor of Science in Biomedical Engineering. He continued his education at Virginia Commonwealth University, earning his Masters of Science in Biomedical Engineering in August 2006, and transitioned to the doctoral program immediately after. He currently resides in Midlothian, Virginia with his wife, Tracy Sell, and their dogs, Roxie and Clay.